KIT SCIENTIFIC REPORTS 7596

Post irradiation examination of RAFM steels after fast reactor irradiation up to 71 dpa and < 340 °C (ARBOR 2)

RAFM Steels: Metallurgical and Mechanical Characterisation

Final Report for TW5-TTMS-001, D 10

Ermile Gaganidze, Claus Petersen

Institut für Angewandte Materialien
Programm Kernfusion
Association Karlsruher Institut für Technologie / EURATOM

KIT Scientific Publishing

Ermile Gaganidze, Claus Petersen

Post irradiation examination of RAFM steels after fast reactor irradiation up to 71 dpa and < 340 °C (ARBOR 2)

RAFM Steels: Metallurgical and Mechanical Characterisation

Karlsruhe Institute of Technology
KIT SCIENTIFIC REPORTS 7596

Post irradiation examination of RAFM steels after fast reactor irradiation up to 71 dpa and < 340 °C (ARBOR 2)

RAFM Steels: Metallurgical and Mechanical Characterisation

Final Report for TW5-TTMS-001, D 10

by
Ermile Gaganidze
Claus Petersen

Institut für Angewandte Materialien
Programm Kernfusion
Association Karlsruher Institut für Technologie / EURATOM

KIT Scientific Publishing

Report-Nr. KIT-SR 7596

Impressum

Karlsruher Institut für Technologie (KIT)
KIT Scientific Publishing
Straße am Forum 2
D-76131 Karlsruhe
www.ksp.kit.edu

KIT – Universität des Landes Baden-Württemberg und nationales
Forschungszentrum in der Helmholtz-Gemeinschaft

KIT Scientific Publishing 2011
Print on Demand

ISSN 1869-9669
ISBN 978-3-86644-703-5

This work, supported by the European Communities under the contract of Association between EURATOM and Karlsruhe Institute of Technology, was carried out within the framework of the European Fusion Development Agreement. The views and opinions expressed herein do not necessarily reflect those of the European Commission.

REPORT for TASK of the EFDA Technology Programme	
Reference:	Field: Tritium Breeding and Materials Area: Materials Development Task: TW5-TTMS-001 Task Title: STRUCTURAL MATERIALS: Irradiation performance Subtask Title: Mechanical post irradiation examinations of KIT (former FZK) - specimens irradiated in the ARBOR 2 experiment in the BOR 60 reactor Deliverable No.: D10
Document:	Post irradiation examination of RAFM steels after fast reactor irradiation up to 71 dpa and < 340 °C (ARBOR 2)
Level of confidentiality	Free distribution ☐ Confidential ☐ Restricted distribution ☒
Author(s):	Ermile Gaganidze, Claus Petersen Karlsruhe Institute of Technology, Germany
Date:	5.04.2011
Distribution list:	Rainer Laesser (Field Co-ordinator) Eberhard Diegele (Responsible Officer) Enrico Lucon (Project Leader)
Abstract:	In an energy generating fusion reactor structural materials will be exposed to very high damage doses of about 150 dpa. The objective of the ARBOR 2 irradiation programme was to study the effects of low-temperature (330-340 °C) high dose (up to 70 dpa) neutron irradiation on the mechanical properties of the European reference structural material for the Demonstration Reactor (DEMO), EUROFER 97, its Oxide Dispersion Strengthened (ODS) variants, selected technological specimens and other international RAFM steels. The neutron irradiation of miniaturised impact, tensile and LCF specimens complying Small Specimen Testing Technology has been carried out in the fast experimental reactor BOR 60 at Joint Stock Company "State Scientific Centre Research Institute of Atomic Reactors" (SSC RIAR). Post Irradiation Examination of the specimens has been performed at the Materials Science Laboratory of SSC RIAR under the ISTC Partner Project #2781p. Neutron irradiation at 330-340 °C leads to a severe degradation of the impact and tensile properties of the RAFM steels. Neutron irradiation-induced hardening and embrittlement indicate saturating behaviour at the achieved damage doses for these low irradiation temperatures. The evolution of Yield Stress with dose is qualitatively understood within a Whapham and Makin model. Post-irradiation annealing of RAFM steels yields substantial recovery of the mechanical properties, indicating healing of most of the radiation defects. Helium contents already up to 120 appm lead to strong material em-

REPORT for TASK of the EFDA Technology Programme			
Reference:	Field: Tritium Breeding and Materials Area: Materials Development Task: TW5-TTMS-001 Task Title: STRUCTURAL MATERIALS: Irradiation performance Subtask Title: Mechanical post irradiation examinations of KIT (former FZK) - specimens irradiated in the ARBOR 2 experiment in the BOR 60 reactor Deliverable No.: D10		
	brittlement but have only minor influence on the tensile properties. The neutron irradiation induced hardening may differently affect the fatigue behaviour of the irradiated specimens. The increase of the elastic part of the cyclic deformation and the related reduction of the inelastic strain amplitude due to irradiation induced hardening lead to the increase of the fatigue lifetime especially at low strain ranges. The radiation hardening induced increase of the stress level might, however, lead to enhanced damage evolution and hence to lifetime reduction especially at high strain ranges. Electron beam welded EUROFER 97 technological specimens exhibited tensile and LCF properties that are comparable to those of irradiated base EUROFER 97 steels. The miniaturised EUROFER 97 specimens manufactured from a HIP welded First Wall mock-up showed large scatter of tensile properties both in unirradiated and irradiated conditions. The design relevant data obtained within the current work can be used for verification of the design rules and provides important input for modelling activities.		
Revision No: -	Changes: -		
	Written by:	Revised by:	Approved by:
	Ermile Gaganidze	Jarir Aktaa	Oliver Kraft

Abstract

In an energy generating fusion reactor structural materials will be exposed to very high damage doses of about 150 dpa. The objective of the ARBOR 2 irradiation programme was to study the effects of low-temperature (330-340 °C) high dose (up to 70 dpa) neutron irradiation on the mechanical properties of the European reference structural material for the Demonstration Reactor (DEMO), EUROFER 97, its Oxide Dispersion Strengthened (ODS) variants, selected technological specimens and other international RAFM steels. The neutron irradiation of miniaturised impact, tensile and LCF specimens complying Small Specimen Testing Technology has been carried out in the fast experimental reactor BOR 60 at Joint Stock Company "State Scientific Centre Research Institute of Atomic Reactors" (SSC RIAR). Post Irradiation Examination of the specimens has been performed at the Materials Science Laboratory of SSC RIAR under the ISTC Partner Project #2781p.

Neutron irradiation at 330-340 °C leads to a severe degradation of the impact and tensile properties of the RAFM steels. Neutron irradiation-induced hardening and embrittlement indicate saturating behaviour at the achieved damage doses for these low irradiation temperatures. The evolution of Yield Stress with dose is qualitatively understood within a Whapham and Makin model. Post-irradiation annealing of RAFM steels yields substantial recovery of the mechanical properties, indicating healing of most of the radiation defects. Helium contents already up to 120 appm lead to strong material embrittlement but have only minor influence on the tensile properties.

The neutron irradiation induced hardening may differently affect the fatigue behaviour of the irradiated specimens. The increase of the elastic part of the cyclic deformation and the related reduction of the inelastic strain amplitude due to irradiation induced hardening lead to the increase of the fatigue lifetime especially at low strain ranges. The radiation hardening induced increase of the stress level might, however, lead to enhanced damage evolution and hence to lifetime reduction especially at high strain ranges.

Electron beam welded EUROFER 97 technological specimens exhibited tensile and LCF properties that are comparable to those of irradiated base EUROFER 97 steels. The miniaturised EUROFER 97 specimens manufactured from a HIP welded First Wall mock-up showed large scatter of tensile properties both in unirradiated and irradiated conditions.

The design relevant data obtained within the current work can be used for verification of the design rules and provides important input for modelling activities.

Nachbestrahlungsuntersuchung von RAFM Stählen aus der Bestrahlung in einem Schnellen Reaktor bis zu 71 dpa und < 340 °C (ARBOR 2)

Zusammenfassung

In einem energieerzeugenden Fusionsreaktor werden Strukturmaterialien einer sehr hohen Bestrahlungsdosis ausgesetzt, welche bis zu 150 dpa betragen kann. Das Ziel des ARBOR 2 Bestrahlungsprogramms liegt in der Untersuchung der Effekte der Tieftemperatur (330-340 °C) Hochdosis (bis zu 70 dpa) Neutronenbestrahlung auf die mechanischen Eigenschaften von einem europäischen RAFM Referenzstahl für den Demonstrationsreaktor (DEMO), EUROFER 97, von dessen Oxiddispersionsgehärteter Varianten, ausgewählten technologischen Proben sowie anderen internationalen RAFM Stählen. Die Neutronenbestrahlung von miniaturisierten Kerbschlag-, Zug- und Ermüdungsproben erfolgte in dem schnellen experimentellen Reaktor BOR 60 am "State Scientific Centre Research Institute of Atomic Reactors" (SSC RIAR). Die Nachbestrahlungsuntersuchungen von Proben wurden unter dem ISTC Partner Projekt #2781p in den Heißen Zellen von SSC RIAR durchgeführt.

Die Neutronenbestrahlung führt zu einer starken Degradierung von Kerbschlag- und Zugeigenschaften bei tiefen Bestrahlungstemperaturen von 330-340 °C. Die bestrahlungsinduzierte Verfestigung und Versprödung deuten auf ein Sättigungsverhalten bei den erreichten Schädigungsdosen von 70 dpa hin. Die Dosisabhängigkeit der Streckgrenze bei diesen tiefen Bestrahlungstemperaturen kann im Rahmen des Whapham und Makin Models qualitativ beschrieben werden. Nachbestrahlungswärmebehandlung führt zu einer erheblichen Erholung der mechanischen Eigenschaften, was auf eine weitgehende Ausheilung von Strahlenschädigung hindeutet. Heliumgehalt bis zu 120 appm führt bereits zu einer starken Materialversprödung, hat allerdings nur einen geringen Effekt auf die Zugeigenschaften.

Die bestrahlungsinduzierte Verfestigung kann zu unterschiedlichen Einflüssen auf die Ermüdungseigenschaften führen. Die Zunahme des elastischen Anteils und die entsprechende Abnahme des inelastischen Anteils in der gesamten Verformung als Folge der Verfestigung führen zu einer Zunahme der Lebensdauer, insbesondere bei niedrigen Dehnamplituden. Die Zunahme der Spannungsamplitude kann andererseits die Beschleunigung der Ermüdungsschädigung and entsprechende Abnahme der Lebensdauer, insbesondere bei hohen Dehnamplituden, hervorrufen.

Die mittels Elektronenstrahl geschweißten technologischen EUROFER 97 Proben zeigen mit dem bestrahltem Basismaterial EUROFER 97 vergleichbare Zug- und Ermüdungseigenschaften. Die miniaturisierten, aus dem HIP geschweißten Ersten Wand Mock-Up hergestellten Proben zeigen große Streuung von Zugeigenschaften, sowohl in unbestrahlten als auch in bestrahlten Zuständen.

Die in dieser Arbeit generierten auslegungsrelevanten Daten können zur Verifizierung von Auslegungsregeln verwendet werden und liefern wichtigen Input für Modellierungsaktivitäten.

TABLE OF CONTENTS

LIST OF TABLES

LIST OF FIGURES

1 Introduction

The growing energy demand in the world along with the limited capacity of fossil energy sources makes the development of alternative energy sources indispensable. Fusion research aims at demonstrating that this energy source can be used to produce electricity in a safe and environmentally friendly way, with abundant fuel resources. The feasibility of energy generation by means of fusion has to be demonstrated in the Demonstration Power Plant (DEMO) which is intended to be built after the expected successful operation of ITER (International Thermonuclear Experimental Reactor). The development and validation of DEMO relevant structural materials and adequate joining technologies, therefore, belong to the key tasks within the European long term fusion R&D programme.

Structural Materials for the in-vessel components of a future energy generating Fusion Reactor (FR) will be exposed to high neutron and thermo-mechanical loads. Accumulated neutron displacement damage of up to 150 dpa along with transmutation helium and hydrogen generated in the structure materials due to 14.1 MeV fusion neutrons will strongly influence material embrittlement behaviour. Reduced Activation Ferritic/Martensitic (RAFM) steels are primary candidate structural materials for the First Wall (FW) and helium cooled Breeding Blanket (BB) with operating temperatures between 350 and 550 °C [1]. Since a facility providing a fusion reactor relevant neutron spectrum, like IFMIF, is not yet available, the irradiation performance of structural materials is often investigated in irradiation experiments performed in various Material Test Reactors [2],[3][4],[5],[6],[7],[8],[9]. Although the radiation damage resistance of RAFM steels is superior to that of conventional Ferritic/Martensitic steels, the low temperature (<350 °C) irradiation hardening, accompanied by embrittlement and reduced ductility, did not reach saturation up to 30 dpa and remains the limiting factor for material application, indicating further needs of material development as well as new approaches in BB design optimisation [3],[5],[10],[11],[12],[13],[14],[15],[16],[17].

2 ARBOR 2 Irradiation Programme

2.1 Overview

A cooperation between Karlsruher Institut für Technologie (formerly Forschungszentrum Karlsruhe, FZK) and Joint Stock Company “State Scientific Centre Research Institute of Atomic Reactors” (SSC RIAR) was implemented for investigation and analysis of the mechanical properties and microstructure of the European reference structural material EUROFER 97, its Oxide Dispersion Strengthened (ODS) variants, selected technological specimens and other international RAFM steels after irradiation up to 70 dpa in a temperature range between 332 and 338 °C. The irradiation project “Associated Reactor Irradiation in BOR 60” is named “ARBOR“ (Latin for tree). Within the framework of the ARBOR 1 irradiation programme the mechanical properties and microstructure of RAFM steels were investigated after irradiation up to a damage dose of 33 dpa [9]. In the subsequent ARBOR 2 irradiation programme the structural materials were irradiated up to a damage dose of 71 dpa, which is a further step towards fusion relevant damage doses.

2.2 Irradiated materials

EUROFER 97

An industrial batch of the European RAFM steel EUROFER 97 was produced by Böhler Austria GmbH. The chemical compositions of the steels along with the heat denomination are indicated in Table 7-1. Part of the specimens (labelled EUROF 1 = EUROFER 97) has been machined from 25 mm thick EUROFER 97 plates in the as-delivered state (i.e. austenitizing at 980 °C followed by tempering at 760 °C). In order to study the influence of a higher austenitizing temperature on a laboratory scale, other part of specimens (labelled EUROF 2 = EUROFER 97 HT) has been machined from EUROFER 97 plates subjected to a heat treatment at an austenitizing temperature of 1040 °C. Table 7-2 lists the heat treatment conditions along with selected properties of the investigated materials.

Reference RAFM steels

The Japanese RAFM steel F82H mod. is implemented as international reference steel (as received: 1040 °C 38 min/air cooled + 750 °C 2 h/air cooled), see Table 7-1 for steel's chemical composition. The German development OPTIFER IVc (labelled OPT IVc) (950 °C 30 min/air cooled + 750 °C 2 h/air cooled) is included as reference material to be compared to results from the HFR-irradiations. The recent developments of OPTIFER series alloys, *i.e.* OPTIFER XI (labelled OPT XI) (950 °C 30 min/air cooled+ 750 °C 120 min/air cooled) and OPTIFER XII (labelled OPT XII) (950 °C 30 min/air cooled + 750 °C 120 min/air cooled) have also been included in the irradiated matrix. The Nuclear Research and consultancy Group (NRG), Petten, contributed with a British Steel batch of EUROFER 97 (labelled BS-EUROF) (as received: 1050 °C 60 min/air cooled + 760 °C 120 min/air cooled).

ODS steels

The European RAFM steel EUROFER 97 was chosen for the production of two variants of ODS steels with different Y_2O_3 contents (0.3 and 0.5 wt%) [18]. The production process included inert gas atomisation of EUROFER and subsequent mechanical alloying in industrial ball mills. Hot Isostatic Pressing (HIP) was chosen as the appropriate consolidation process. The material denominations are (i) EODShip 3 for 0.3 wt% Y_2O_3 content (980 °C 31 min/air cooled+ 760 °C 90 min/air cooled) and (ii) EURODShip for 0.5 wt% Y_2O_3 content (980 °C 31 min/air cooled + 760°C 90 min/air cooled).

Technological specimens

In addition to base materials two EUROFER 97 weld joints were included in the ARBOR 2 irradiation programme.

The NRG, Petten, provided electron beam welded EUROFER 97 (labelled EUROF-EB). The Post Weld Heat Treatment (PWHT) was done at 730 °C for 120 min and was followed by air cooling.

KIT contributed to technological studies by investigating diffusion welded EUROFER 97 (labelled FZK DW). The impact and miniaturised tensile specimens were machined from the First Wall and Cooling Plates (CP) component mock-ups produced in diffusion welding ex-

periments using HIP. The components were welded in one (1xhip) or two (2xhip) successive HIP welding steps. Finally, all components were subjected to PWHT at 750 °C for 120 min.

Boron doped steels

The experimental heats ADS 2 (OPTIFER-VIII), ADS 3 and ADS4 with the basic composition of EUROFER 97 doped with different contents of natural boron and the separated ^{10}B-isotope (0.008-0.112 wt.%) were produced by a material development group of KIT to study the effects of helium generation [19]. In order to exclude significant differences in the microstructure, ADS 2 and ADS 3 were doped nearly with the same amount (82 wppm) of natural boron and separated ^{10}B isotope, respectively. All three boron doped steels underwent the same heat treatment of 1040 °C 31 min/air cooled + 760 °C 90 min/air cooled.

2.3 Specimens

Based on the knowledge gained from earlier fatigue experiments a tensile/low cycle fatigue specimen geometry was developed and optimised by finite element calculations using different material models, see Fig. 2-1. A special emphasis was put on the radius of curvature at the end of the gauge length to achieve homogeneous stress-strain fields throughout the gauge volume under uniaxial push-pull fatigue testing conditions [6]. The surface quality after the radial grinding procedure is R_{max} = 2.5 µm.

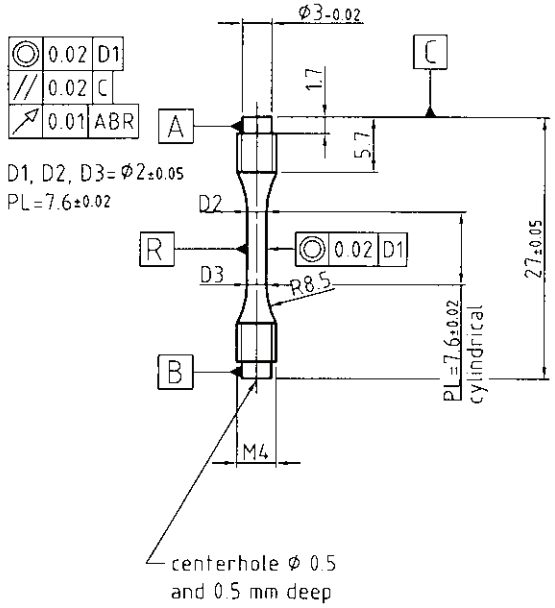

Fig. 2-1 Tensile/Low Cycle Fatigue specimen (all dimensions in mm).

The KLST miniaturised impact specimen geometry is according to DIN 50115: 27 x 3 x 4 mm³ with 1 mm notch depth and has a weight of: 2.4744 g. It was already used in former irradiation programmes (MANITU, HFR Ia, HFR Ib, SPICE). The KLST-specimens have two mechanically made engravings on left and right sides. They are labelled by a four-sign code, consisting of one or two letters for the material and two or three digits for the serial number.

For reliable determination of the Ductile to Brittle Transition Temperature (DBTT), a set of at least 6 specimens is necessary [6]. The KLST impact specimen is depicted in Fig. 2-2.

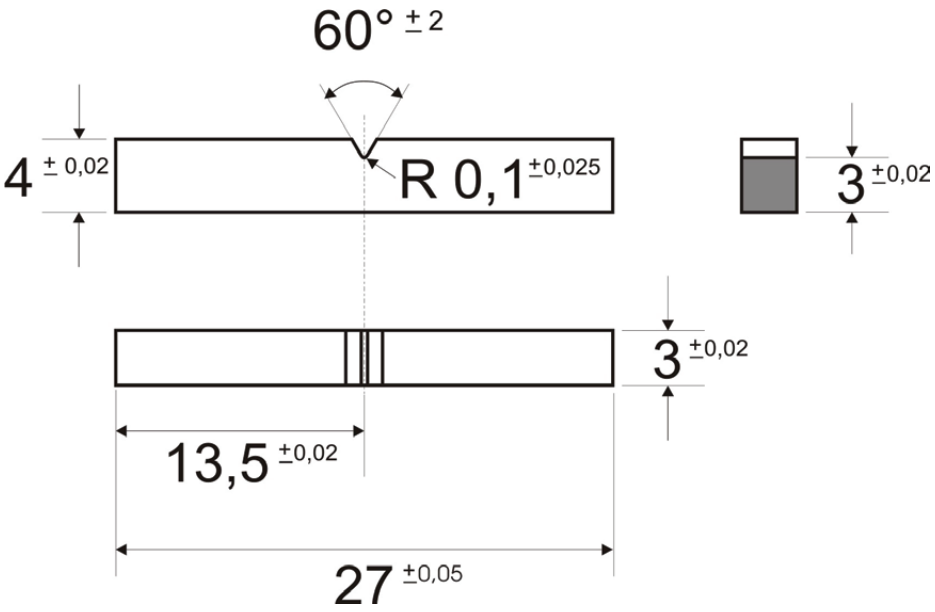

Fig. 2-2 KLST impact specimen (all dimensions in mm); Detail the specimen notch.

Double-T shaped specimens were used for the investigation of the tensile properties of FZK diffusion welds. Welding seams are transverse to the specimen longitudinal direction and are positioned in the middle of the specimens.

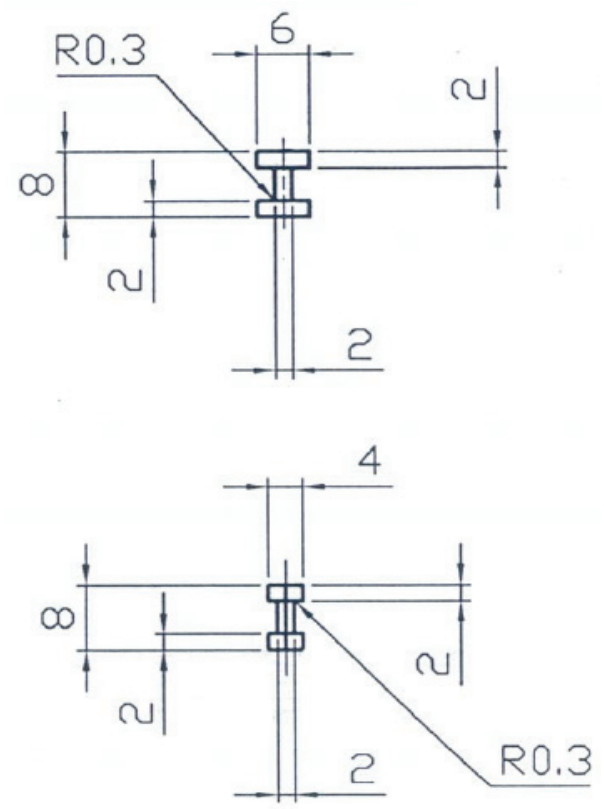

Fig. 2-3 Double-T shaped specimen for the tensile testing of diffusion welds.

2.4 Specimen preparation and delivery

The specimens for the ARBOR irradiation programme were fabricated at FZK's central workshop. All specimens were measured and comply with the tolerance dimensions indicated in the drawings.

All KLST-specimens and LCF/Tensile-specimens were cleaned in the following way:

- 10 minutes in ultrasonic bath with acetone and dried.
- cleaned with isopropyl alcohol.
- 5 minutes in ultrasonic bath with isopropyl alcohol and dried with hot air from fan.

This procedure was performed on 20.9.2000 by D. Rodrian. All KLST-specimens and LCF/Tensile-specimens were packed in packages of 10 in 3 segments of a plastic box in the right sequence of numbering to be implemented in one capsule of the BOR 60 irradiation rig. This procedure was performed on 22.9.2000 by D. Rodrian and C. Petersen.

The specimens were handed over to SSC RIAR on 17. October 2000. An associated technical documentation was delivered as well.

2.5 BOR 60

The BOR 60 experimental fast reactor, Fig. 2-4, started operation in December 1969. Initially designed for solving physical and technical problems of fast power reactors with sodium coolant, it is nowadays also widely used as irradiation facility for material science purposes. With a reactor core dimension of 450 mm height and 550 mm in equivalent diameter, different irradiation positions are available. The cell D-23 was selected for the first campaign, because in this position a direct temperature measurement by thermocouple during irradiation is possible.

Fig. 2-4 Reactor building of BOR 60.

2.6 Irradiation assembly

The ARBOR 2 irradiation experiment was performed with an irradiation rig already used in the ARBOR 1 programme shown in Fig. 2-5. The device of outer hexagon size of 45 mm, and specimen capsule diameter of 39 mm is based on a previously used design with heat insulation against the surrounding fuel assemblies to provide relatively low irradiation temperatures. The irradiation device is cooled by liquid sodium from the reactor high-pressure chamber, which allows a sufficiently large coolant flow rate (of the order of 7 m^3/ h) and a relatively low gamma heating rate of approximately 5 watts/g (leading to an increase of temperature by about 10-15 °C over the assembly length).

The irradiation device can carry 10 to 11 capsules each of 30 mm in height. Each capsule can contain either 30 LCF/Tensile or impact specimens. Within the ARBOR 2 irradiation programme KIT irradiated 144 LCF/Tensile- and 124 Charpy impact specimens.

2.7 Dosimetry

The irradiation rig is instrumented with neutron monitors, as indicated in Fig. 2-6 schematically; they are arranged in the central tube and on three of ten levels of specimen positions as well as with three temperature detectors also on three of ten levels.

During special reactor spectrometry experiments a large number of different material foils (about 50) were irradiated, their activity was measured and the spectrum was unfolded by using MIXER computer code [20].

The calculation of the damage dose values for ferritic steel specimens was conducted using SPECTER code [21]. In this case a neutron energy spectrum in cell D-23 was used that was measured in the previously performed dosimetry experiments and normalised for measured neutron fluence values with energies higher than 3, 4.6 and 7 MeV.

Metal foils with 0.1 mm thickness were used for the neutron monitor production. They were cut into discs having 1.0 mm diameter. All detectors were washed in a weak solution of nitric acid, in alcohol and then they were weighted with a “Sartorius” balance. The monitor sets were placed into labelled quartz ampoules having 3 mm diameter and 13 mm height. After irradiation the absolute measurement of γ-ray activity was performed.

During material science experiments only few different material foils (usually natural iron, niobium and titanium as well as of enriched copper: ^{63}Cu – 99.6%,) were irradiated and measured. The details of damage dose calculation for EUROFER 97 steel are given in [9].

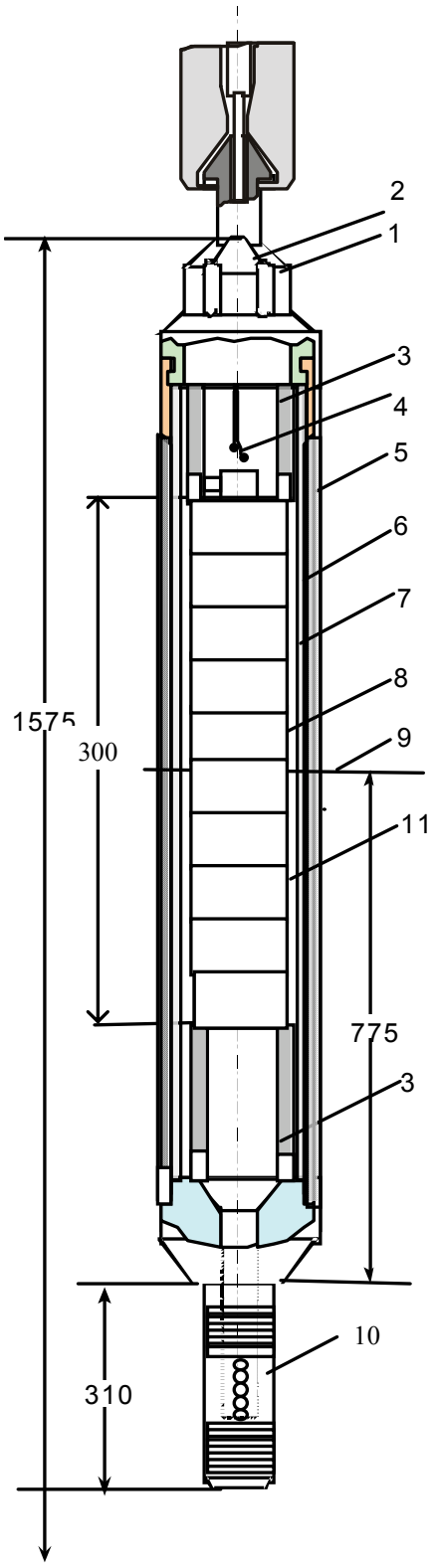

1- thermometric probe;
2- detachable head;
3- spacer tubes;
4- probe thermocouples;
5- wrapper;
6- gas gap;
7- internal tube;
8- ampoule assembly;
9- core center;
10- tail;
11- annular gap

Fig. 2-5 Dismountable assembly with a thermocouple. (Detail: Capsule filled with KLST mini impact specimens).

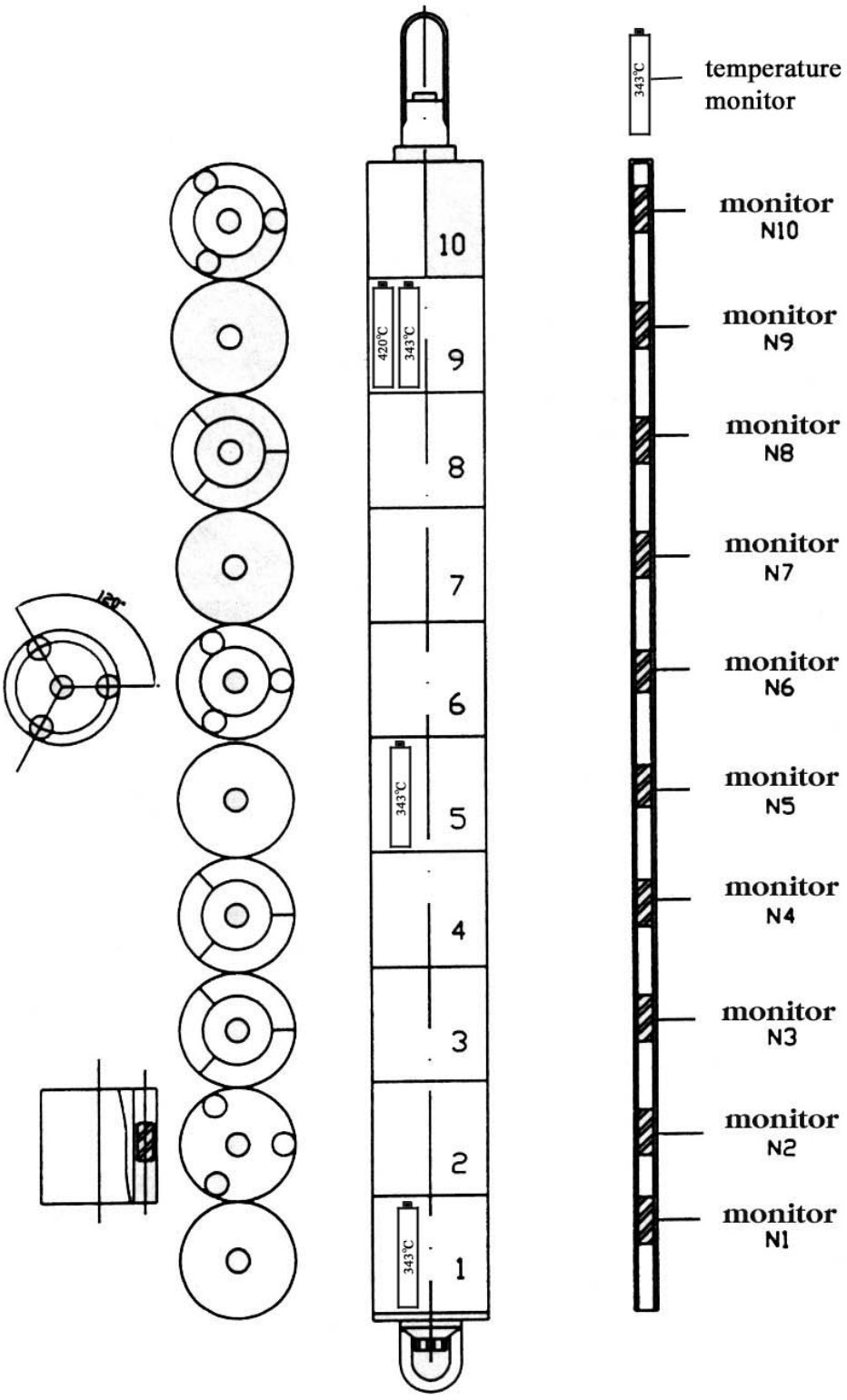

Fig. 2-6 Scheme of the neutron and temperature monitors location in the suspensor.

For the ARBOR 2 experiment the fluence was evaluated by means of dosimetric measurements and calculations. The controlled neutron fluence values (E_n>0.1 and 0.5 MeV), averaged ones, recalculated by four threshold reactions, as well as damage dose values (average, fluence E_n > 3 and 1 MeV) for the ARBOR 2 Irradiation Rig (IR) are presented in Table 2-1. For the 9th level the dose indicated in brackets is the dose received by the specimens loaded in a late stage.

Level	Distance from IR central plane (mm)	Neutron fluence (10^{22} cm^{-2})		Damage Dose (dpa)
		E_n> 0.1 MeV	E_n> 0.5 MeV	
11	150	4.91	2.64	27.0
10	120	5.63	3.02	31.0
9	90	6.10	3.27	33.1 (~12.0)
8	60	6.59	3.54	36.2
7	30	6.75	3.62	37.3
6	“0”	6.90	3.70	38.3
5	-30	7.11	3.82	38.7
4	-63	6.93	3.72	38.3
3	-96	6.86	3.68	37.6
2	-126	6.50	3.49	35.9
1	-158.5	6.11	3.28	33.6
	Monitor No.			Damage Dose (dpa)
11	18	5.44	2.92	30.1
	19	5.00	2.68	27.5
	20	5.00	2.69	27.5
6	15	6.73	3.61	37.2
	16	7.47	4.01	41.4
	17	7.03	3.78	38.8
3	12	7.28	3.91	40.1
	13	6.72	3.61	37.1
	14	6.96	3.74	37.9

Table 2-1: Controlled neutron fluence and damage dose of ARBOR 2 IR (SSC RIAR). Within this report the calculated dpa values were used for levels 1,2,4,5 and 7-10, whereas for levels 3, 6 and 11 the dpa values averaged over three neutron monitors’ data were applied.

Based on the measurements of neutron monitors located on the 11th, 6th an 3rd levels of the rig periphery at an azimuthal angle of 120 °C to each other, it is seen that the averaged damage dose is higher than the calculated dose by 1.4 dpa at 11th level, by 0.8 dpa at 6th level and by 0.7 dpa at 3rd level.

2.8 Irradiation conditions

Table 2-2 shows the material loading matrix for the ARBOR 2 irradiation programme. The capsule identification numbers as well as specimen type identification notations (i.e. Tensile, LCF, Impact, Mixed) are indicated in a table head. The capsules already irradiated within the ARBOR 1 irradiation are marked. The identification of material heats and thermal treatments are outlined in Table 7-2. The OPTIMAX alloys were delivered by CRPP-EPFL.

FZK Pre-irr.	FZK Pre-irr.	FZK Pre-irr.	FZK Pre-irr.	FZK new	FZK Pre-irr.	FZK new	FZK new	FZK new
capsule 3	capsule 5	capsule 6	capsule 7	capsule 8	capsule 9	capsule 9a	capsule 10	capsule 11
Tensile	LCF	Impact	Impact	Mixed	LCF	Mixed	Mixed	Impact
EUROF 1	EUROF 1	EUROF 1	EUROF 1	FZK DW H1	EUROF 1	OPT XI	EUROF 1	FZK DW H1
EUROF 1	EUROF 1	EUROF 1	EUROF 1	FZK DW H1	EUROF 1	OPT XI	EUROF 1	FZK DW H1
EUROF 1	EUROF 1	EUROF 1	EUROF 1	FZK DW H1	EUROF 1	OPT XI	EUROF 1	FZK DW H1
EUROF 1	EUROF 1	EUROF 1	EUROF 1	FZK DW H1	EUROF 1	OPT XI	EUROF 1	FZK DW H1
EUROF 2	EUROF 1	EUROF 1	EUROF 1	FZK DW H1	EUROF 1	OPT XI	EUROF 1	FZK DW H2
EUROF 2	EUROF 2	EUROF 1	EUROF 1	FZK DW H1	EUROF 2	OPT XI	EUROF 1	FZK DW H2
EUROF 2	EUROF 2	EUROF 1	EUROF 1	FZK DW H1	EUROF 2	OPT XI	EUROF 1	FZK DW H2
EUROF 2	EUROF 2	EUROF 1	EUROF 2	FZK DW H1	EUROF 2	OPT XI	EUROF 1	FZK DW H2
F82H-mod.	EUROF 2	EUROF 2	EUROF 2	FZK DW H1	EUROF 2	OPT XI	OPT XI	OPTIMAX
F82H-mod.	EUROF 2	EUROF 2	EUROF 2	FZK DW H1	EUROF 2	OPT XI	OPT XI	OPTIMAX
F82H-mod.	ADS 2	EUROF 2	EUROF 2	FZK DW H1	F82H-mod.	OPT XII	OPT XI	OPTIMAX
F82H-mod.	ADS 2	EUROF 2	EUROF 2	FZK DW H1	F82H-mod.	OPT XII	OPT XI	OPTIMAX
EURODShip	ADS 2	EUROF 2	EUROF 2	FZK DW H1	F82H-mod.	OPT XII	OPT XI	OPTIMAX
EURODShip	ADS 2	EUROF 2	EUROF 2	FZK DW H1	F82H-mod.	OPT XII	OPT XI	OPTIMAX
EURODShip	ADS 2	EUROF 2	EUROF 2	FZK DW H1	F82H-mod.	OPT XII	OPT XI	OPTIMAX
EURODShip	ADS 3	EUROF 2	F82H-mod.	FZK DW H2	ADS 4	OPT XII	OPT XI	OPTIMAX
ADS 2	ADS 3	ADS 2	F82H-mod.	FZK DW H2	ADS 4	OPT XII	EUROF 1	OPTIMAX
ADS 2	ADS 3	ADS 2	F82H-mod.	FZK DW H2	ADS 4	OPT XII	EUROF 1	OPTIMAX
ADS 2	ADS 3	ADS 2	F82H-mod.	FZK DW H2	ADS 4	OPT XII	EUROF 1	EODShip 3
ADS 3	ADS 3	ADS 2	F82H-mod.	FZK DW H2	ADS 4	OPT XII	EUROF 1	EODShip 3
ADS 3	OPT IVc	ADS 2	F82H-mod.	FZK DW H2	BS-EUROF	EURODShip	EUROF 1	EODShip 3
ADS 3	OPT IVc	ADS 2	F82H-mod.	FZK DW H2	BS-EUROF	EURODShip	OPT XI	EODShip 3
EUROF-EB	OPT IVc	ADS 2	EURODShip	FZK DW H2	BS-EUROF	EURODShip	OPT XI	EODShip 3
EUROF-EB	OPT IVc	ADS 3	EURODShip	FZK DW H2	BS-EUROF	EURODShip	OPT XI	EODShip 3
EUROF-EB	OPT IVc	ADS 3	EURODShip	FZK DW H2	BS-EUROF	EURODShip	OPT XI	EODShip 3
EUROF-EB	BS-EUROF	ADS 3	EURODShip	FZK DW H2	EURODShip	EURODShip	OPT XI	EODShip 3
EUROF-EB	BS-EUROF	ADS 3	EURODShip	FZK DW H2	EURODShip	EURODShip	EODShip 3	EODShip 3
EUROF-EB	BS-EUROF	ADS 3	EURODShip	FZK DW H2	EURODShip	EURODShip	EODShip 3	EODShip 3
EUROF-EB	BS-EUROF	ADS 3	EURODShip	FZK DW H2	EURODShip	EURODShip	EODShip 3	EODShip 3
EUROF-EB	BS-EUROF	ADS 3	EURODShip	FZK DW H2	EURODShip	EURODShip	EODShip 3	EODShip 3
				EUROF 1		EURODShip	EODShip 3	
				EUROF 1				
				EUROF 1				
				EUROF 1				
				EUROF 1				
				EUROF 1				
				OPTIMAX				
				OPTIMAX				
				OPTIMAX				

Table 2-2: Material loading matrix for ARBOR 2 irradiation.

Table 2-3 shows the specimen loading matrix. The specimen type identification letters are indicated. In addition to specimens for mechanical characterization, capsule 8 included 3 mm Punch Discs for TEM investigations. Flat tensile specimens A1-A7, A9, A10, A13-A23 as well as Charpy impact specimens A1-A10 were delivered from CRPP-EPFL (The post irradiation mechanical testing of these specimens has not been performed within the current campaign).

FZK Pre-irr.	FZK Pre-irr.	FZK Pre-irr.	FZK Pre-irr.	FZK new	FZK Pre-irr.	FZK new	FZK new	FZK new
capsule 3	capsule 5	capsule 6	capsule 7	capsule 8	capsule 9	capsule 9a	capsule 10	capsule 11
Tensile	LCF	Impact	Impact	Mixed	LCF	Mixed	Mixed	Impact
E 1 06	E 1 10	E 1 08	E 1 16	T: EH1 01	E 1 19	Ch: 11 09	C: E 138	C: EF12 01
E 1 07	E 1 11	E 1 09	E 1 17	T: EH1 02	E 1 20	Ch: 11 10	C: E 139	C: EF12 02
E 1 08	E 1 12	E 1 10	E 1 18	T: EH1 03	E 1 21	Ch: 11 11	C: E 140	C: EF12 03
E 1 09	E 1 13	E 1 11	E 1 19	T: EH1 04	E 1 22	Ch: 11 12	C: E 141	C: EF12 04
E 2 06	E 1 14	E 1 12	E 1 20	T: EH1 05	E 1 23	Ch: 11 13	C: E 142	C: EF22 01
E 2 07	E 2 10	E 1 13	E 1 21	T: EH1 06	E 2 19	Ch: 11 14	C: E 143	C: EF22 02
E 2 08	E 2 11	E 1 14	E 1 22	T: EH1 07	E 2 20	Ch: 11 15	C: E 144	C: EF22 03
E 2 09	E 2 12	E 1 15	E 2 17	T: EH1 08	E 2 21	Ts: 11 06	C: E 145	C: EF22 04
F 06	E 2 13	E 2 09	E 2 18	T: EH1 00	E 2 22	Ts: 11 07	C: 11 01	C: A1
F 07	E 2 14	E 2 10	E 2 19	T: EH1 10	E 2 23	Ts: 11 08	C: 11 02	C: A2
F 08	A 2 04	E 2 11	E 2 20	T: EH1 11	F 13	Ch: 12 01	C: 11 03	C: A3
F 09	A 2 05	E 2 12	E 2 21	T: EH1 12	F 14	Ch: 12 02	C: 11 04	C: A4
E O 02	A 2 06	E 2 13	E 2 22	T: EH1 13	F 15	Ch: 12 03	C: 11 05	C: A5
E O 04	A 2 07	E 2 14	E 2 23	T: EH1 14	F 16	Ch: 12 04	C: 11 06	C: A6
E O 07	A 2 08	E 2 15	E 2 24	T: EH1 15	F 17	Ch: 12 05	C: 11 07	C: A7
E O 09	A 3 04	E 2 16	F 08	T: EH2 01	A 4 04	Ch: 12 06	C: 11 08	C: A8
A 2 01	A 3 05	A 2 01	F 09	T: EH2 02	A 4 05	Ch: 12 07	T: E 134	C: A9
A 2 02	A 3 06	A 2 02	F 10	T: EH2 03	A 4 06	Ts: 12 01	T: E 135	C: A10
A 2 03	A 3 07	A 2 03	F 11	T: EH2 04	A 4 07	Ts: 12 02	T: E 136	O3 01
A 3 01	A 3 08	A 2 04	F 12	T: EH2 05	A 4 08	Ts: 12 03	T: E 137	O3 02
A 3 02	OT 01	A 2 05	F 13	T: EH2 06	A 910	Ch: E O 31	T: E 138	O3 03
A 3 03	OT 02	A 2 06	F 14	T: EH2 07	A 911	Ch: E O 32	T: 11 01	O3 04
C 093	OT 03	A 2 07	E O 08	T: EH2 08	A 912	Ch: E O 33	T: 11 02	O3 05
C 094	OT 04	A 3 01	E O 09	T: EH2 09	A 913	Ch: E O 34	T: 11 03	O3 06
C 095	OT 05	A 3 02	E O 10	T: EH2 10	A 914	Ch: E O 35	T: 11 04	O3 07
C 096	A 905	A 3 03	E O 11	T: EH2 11	E O 11	Ch: E O 36	T: 11 05	O3 08
C 097	A 906	A 3 04	E O 12	T: EH2 12	E O 13	Ch: E O 37	T: O3 01	O3 09
C 098	A 907	A 3 05	E O 13	T: EH2 13	E O 14	Ch: E O 38	T: O3 02	O3 10
C 099	A 908	A 3 06	E O 14	T: EH2 14	E O 16	Ts: E O 29	T: O3 03	O3 11
C 100	A 909	A 3 07	E O 15	T: EH2 15	E O 18	Ts: E O 30	T: O3 04	O3 12
				C: E 146		Ts: E O 31	T: O3 05	
				C: E 147				
				C: E 148				
				C: E 149				
				C: E 150				
				C: E 151				
				T: A13-23				
				T: A1-7; A9-10				
				TEM AP				

Legend:
Ch:, C: = KLST impact specimens
T:, Ts: = Tensile & mini-LCF specimens
TEM AP = 3mm Punch Discs for TEM

Table 2-3: Specimen loading matrix for ARBOR 2 irradiation.

Capsule Nr.	capsule 3	capsule 5	capsule 6	capsule 7	capsule 8	capsule 9	capsule 9a	capsule 10	capsule 11
	Tensile	LCF	Charpy	Charpy	Mixed	LCF	Mixed	Mixed	Charpy
Position from center [mm]	-110…-80	-44…-14	-14…+16	+16…+46	+46…+76	+76…+106	+76…+106	+106…+136	+136…+166
Mean position [mm]	-95	-29	1	31	61	91	91	121	151
Mean temperature [°C]	331.50	334.00	334.90	336.80	336.80	337.50	337.50	338.40	338.40
Measured central values [dpa]	31.70	32.10	30.70	27.60		25.70			
Calculated/Measured values [dpa]	38.40	38.70	39.10	37.30	36.20	21.10	12.00	31.00	28.4
Cummulative damage dose [dpa]	70.10	70.80	69.80	64.90	36.20	46.80	12.00	31.00	28.40

Legend:		
ARBOR 1	ARBOR 2	ARBOR 1 + ARBOR 2

Table 2-4: Calculated/measured damage doses in ARBOR 1 and ARBOR 2 experiments and calculated temperature vs. capsule position.

Damage doses and calculated temperatures vs. capsule positions for ARBOR 1 and ARBOR 2 irradiations are given in Table 2-4. It is important to point out that fusible temperature monitors for 343 and 420 °C (capsule 9) have not been damaged during the whole irradiation.

2.9 Performance of the irradiation experiment

The irradiation experiment ARBOR 2 started in the fourth quarter of 2002. After thermal physical calculations, the manufacturing and implementation of neutron monitors as well as the loading of the samples, hydraulic testing of complete irradiation device was performed. After a short-term experiment performed in D-23 cell in March 2003 the main irradiation campaign was launched in an identical position G-23 in the 5th row of the core. The newly loaded specimens were irradiated to damage doses up to 36 dpa, whereas the specimens pre-irradiated in ARBOR 1 programme reached cumulative damage doses up to 71 dpa. The irradiation ended in May 2005. The final analysis of the neutron monitors was available in December 2005.

3 Post Irradiation Examination (PIE)

After decontamination of the specimens the post irradiation mechanical testing of the selected specimens of the ARBOR 2 irradiation, see Table 8-1, was performed at the material science laboratory of SSC RIAR under the ISTC Partner Project #2781p. The testing facilities were repaired and calibrated before starting the examination of the irradiated specimens. The mechanical testing of ARBOR 2 irradiated specimens started in the second quarter of 2007 and lasted till the second quarter of 2010.

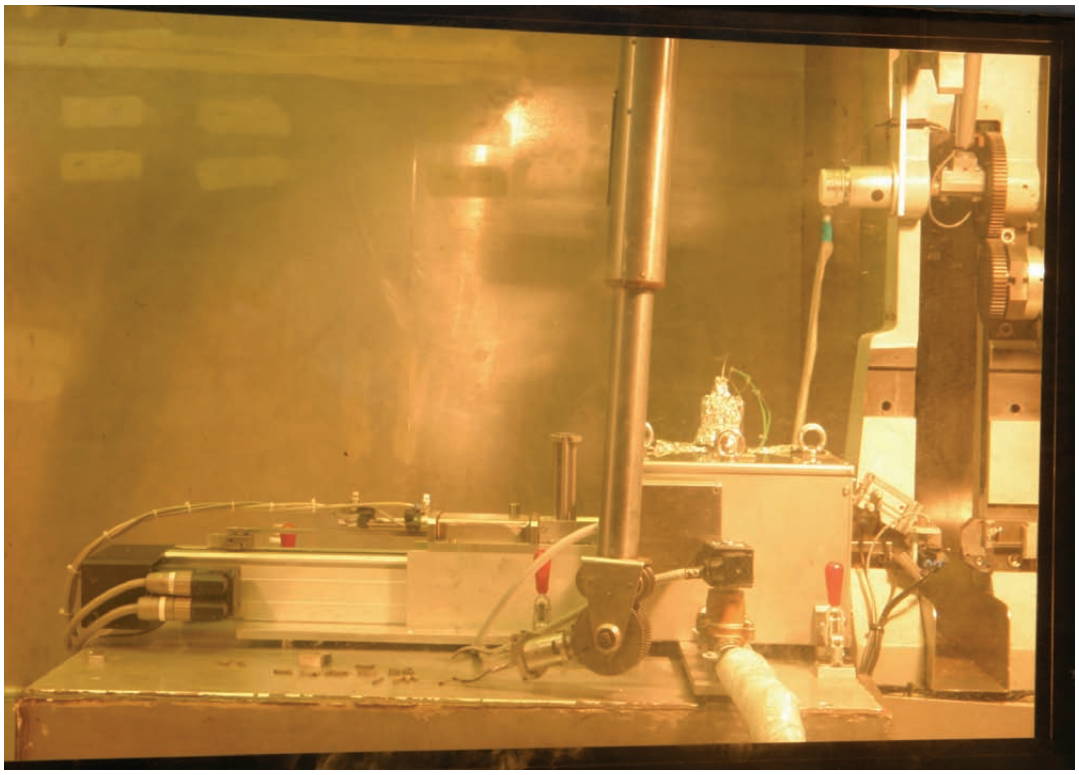

Fig. 3-1 Instrumented impact testing facility with specimen transporting system, cooling facility/furnace and specimen positioning system implemented in the hot cells of SSC RIAR.

The instrumented impact tests on irradiated KLST specimens were performed with an instrumented ZWICK 5113-HKE impact testing facility installed in the hot cell VK-39 of the materials department of SSC RIAR, see Fig. 3-1. This facility is identical with the one at KIT used for testing of the unirradiated reference specimens. Both facilities are equipped with 25 J pendulum impact hammers. The strikers of a radius of 2 mm are instrumented with strain gauges. The specimen support has a distance of 22 mm and the impact velocity is set to 3.85 m/s. The test execution with automatic cooling or heating of the specimen, between -180 °C and 600 °C, as well as transporting to the striking position is controlled by a PC. Data are recorded with a sampling rate of 1 MHz.

From the recorded force vs. time curve of each test the oscillatory part of the system was filtered out by a fast Fourier transformation. The deflection was calculated from the filtered force vs. time curves by solving the pendulum equation of motion and the impact velocity. After integration of the force vs. deflection curve, the impact energy, E, was obtained and plotted vs. test temperature, T, as shown in the following figures.

The impact energy vs. test temperature curves were analysed with respect to the characteristic values including the Upper Shelf Energy (USE, i.e. maximum in the energy versus temperature diagram) and the ductile-to-brittle transition temperature (DBTT). For the determination of the DBTT the temperature at USE/2 is used in the most cases.

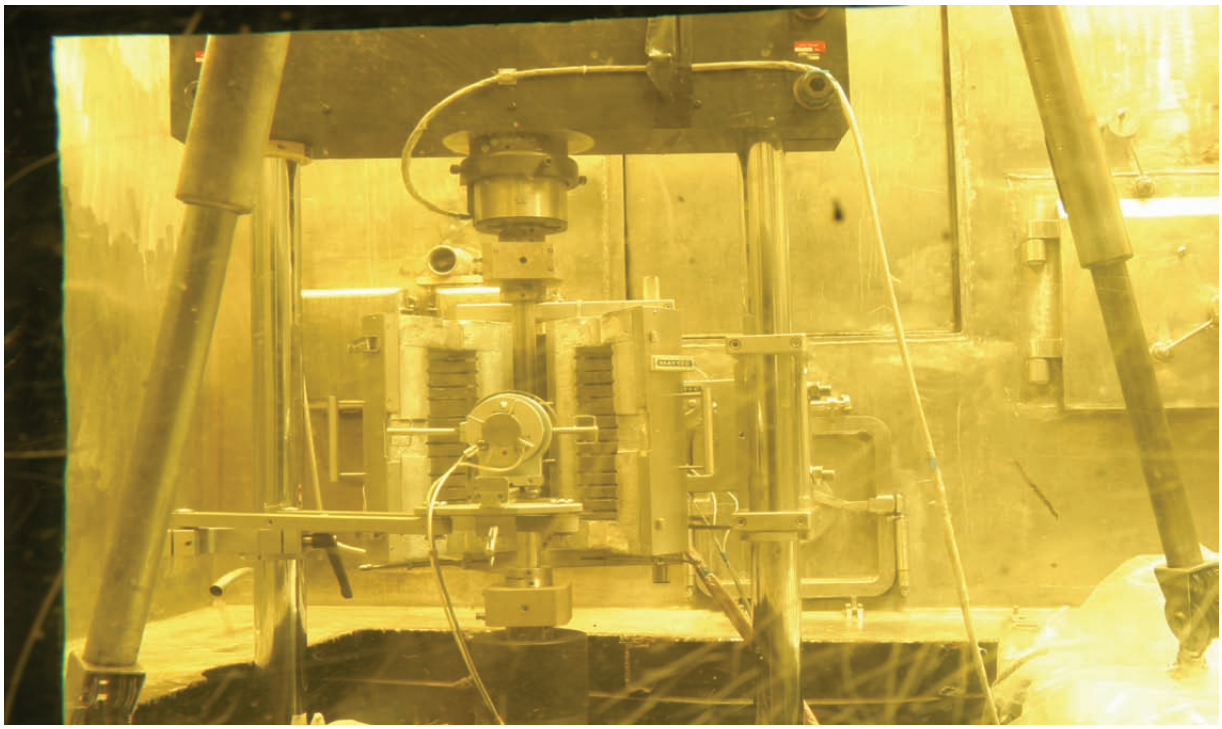

Fig. 3-2 Electro-mechanical testing machine with a three-zone furnace and a high temperature extensometer in the hot cells of SSC RIAR.

The tensile tests were performed with an electro-mechanical testing machine INSTRON 1362 DOLI, Fig. 3-2, which is equipped with a 100 KN load cell, a high temperature furnace and a strain measurement system. The machine is installed in the K-12 hot cell of SSC RIAR. Tensile specimens were tested under static (tensile) loading at different temperatures (RT, 250, 300 and 350 °C) at a strain rate of $3x10^{-3}$ s^{-1}. From the load-displacement curves,

strength and ductility properties including the 0.2% Yield Stress ($R_{p0.2}$), Ultimate Tensile Strength (R_m), Uniform Strain (A_g) and Total Strain (A) are calculated. Reduction of area (Z) was measured from photos of the broken specimens taken after testing.

The strain controlled push-pull (LCF) loading was performed at a constant temperature of 330 °C with different Total Strain ranges ($\Delta\varepsilon_{tot}$) between 0.8% and 1.2% at a common strain rate of $3x10^{-3}$ s^{-1}. The number of cycles to failure (N_f) was defined at a point where the peak tensile stress within a cycle decreased by 30% from its value at a point marking the termination of the linear dependence of peak tensile stress on the number of cycles (N). In addition, inelastic strain amplitudes ($\Delta\varepsilon_{inelastic}$) at $N_{f/2}$ were determined for given Total Strain amplitudes from the hysteresis loops.

The conditions for post irradiation mechanical testing of the specimens from the ARBOR 2 Irradiation are outlined in Table 8-1.

4 Testing Results

4.1 Impact testing

The impact properties of the investigated materials in the irradiated and reference unirradiated states are summarised in Table 4-1.

Materials & Irradiation conditions	DBTT unirr. (°C)	DBTT irr. (°C)	ΔDBTT (°C)	USE unirr. (J)	USE irr. (J)	ΔUSE (J)
EUROFER 97 as received, 336.8 °C, 64.9 dpa	-81.3	152.0	233.3	9.84	6.67	-3.17
EUROFER 97 as received, 334.9. °C, 69.8 dpa	-81.3	152.0	233.3	9.84	6.64	-3.20
EUROFER 97 heat treated, 336.8 °C, 64.9 dpa	-90.8	123.0	213.8	9.84	5.38	-4.46
EUROFER 97 heat treated, 334.9. °C, 69.8 dpa	-90.8	136.0	226.8	9.84	6.04	-3.80
F82H-mod., 336.8 °C, 64.9 dpa	-72.0	184.0	256.0	9.41	4.51	-4.90
OPTIFER XI, 337.5 °C, 12.0 dpa	-80.5	84.7	165.2	8.08	4.33	3.75
OPTIFER XI, 338.4 °C, 31.0 dpa	-80.5	123.3	203.8	8.08	4.05	4.03
OPTIFER XII, 337.5 °C, 12.0 dpa	-83.0	87.3	170.3	8.77	5.16	3.61
ADS 2 = EUROF 1 + 82 wppm natural B, 334.9°C, 69.8dpa	-74.0	238.0	312.0	8.81	3.39	-5.42

Materials & Irradiation conditions	DBTT unirr. (°C)	DBTT irr. (°C)	ΔDBTT (°C)	USE unirr. (J)	USE irr. (J)	ΔUSE (J)
ADS 3 = EUROF 1 + 83 wppm ^{10}B, 334.9 °C, 69.8 dpa	-100.0	260.0	360.0	8.92	3.81	-5.11
EURODShip = EUROF 1 + 0.5% Y_2O_3, 337.5 °C, 12.0 dpa	135.0	134.7*	-0.3	2.54	6.07	+3.53*
EODShip 3 = EUROF 1 + 0.3% Y_2O_3, 338.4 °C, 28.4 dpa	75.0	-	-	6.23	-	-
EUROFER 97 Diff. Welded, 338.4 °C, 28.4 dpa	-	133.9	-	-	4.0	-

Table 4-1: Impact properties of the materials investigated in ARBOR 2; Legend: "-" not determined; "*" apparent values, see text.

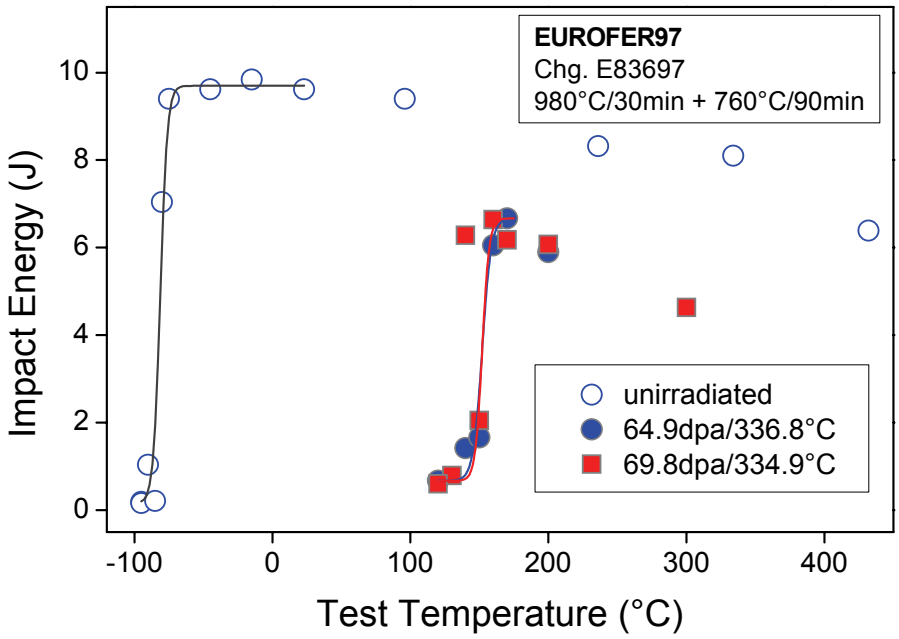

Fig. 4-1 Impact energy vs. test temperature curves of EUROFER 97 in the reference unirradiated condition and after irradiation to 64.9 dpa/336.8 °C and 69.8 dpa/334.9 °C.

The impact properties of the as-received EUROFER 97 in the reference unirradiated state and after irradiation up to a damage dose of 70 dpa are shown in Fig. 4-1. The load time diagrams of the irradiated EUROFER 97 specimens are shown in Fig. 9-1 and Fig. 9-2. The temperature dependence of the impact energy is summarised in Table 9-1 and Table 9-2. The neutron irradiation strongly degrades the impact properties leading to the shift of the DBTT towards higher temperatures and reduction of the USE. After irradiation to 64.9 dpa/336.8 °C the DBTT is found to be 152 °C yielding an irradiation-induced shift in DBTT (ΔDBTT) of 233 °C. Neutron irradiation to 69.8 dpa at 334.9 °C does not yield any further degradation of DBTT and USE indicating saturation of the impact properties at the achieved damage doses.

The impact properties of pre-irradiation heat treated EUROFER 97 HT in the reference unirradiated state, after irradiation to a damage dose of 70 dpa and after post-irradiation annealing (PIA) at 550 °C for 3 h are shown in Fig. 4-2. The load time diagrams of the irradiated EUROFER 97 HT specimens are shown in Fig. 9-3 and Fig. 9-4. The temperature dependence of the impact energy is summarised in Table 9-3 and Table 9-4. The neutron irradiation strongly degrades the impact properties leading to the shift of the DBTT towards higher temperatures and reduction of the USE. After irradiation to 64.9 dpa/336.8 °C the DBTT is found to be 123.0 °C, yielding an irradiation-induced shift in DBTT (ΔDBTT) of 213.8 °C. Neutron irradiation to 69.8 dpa at 334.9 °C leads to an additional increase in DBTT by 13 °C only. The influence of PIA on the impact properties was studied on the selected specimens, see Fig. 4-2. The PIA substantially improves the impact properties of the irradiated specimens. The post-irradiation annealing of e.g. 70 dpa irradiated EUROFER 97 HT leads to a reduction of the DBTT from 136 to -43 °C resulting a residual embrittlement of just ΔDBTT = 48 °C.

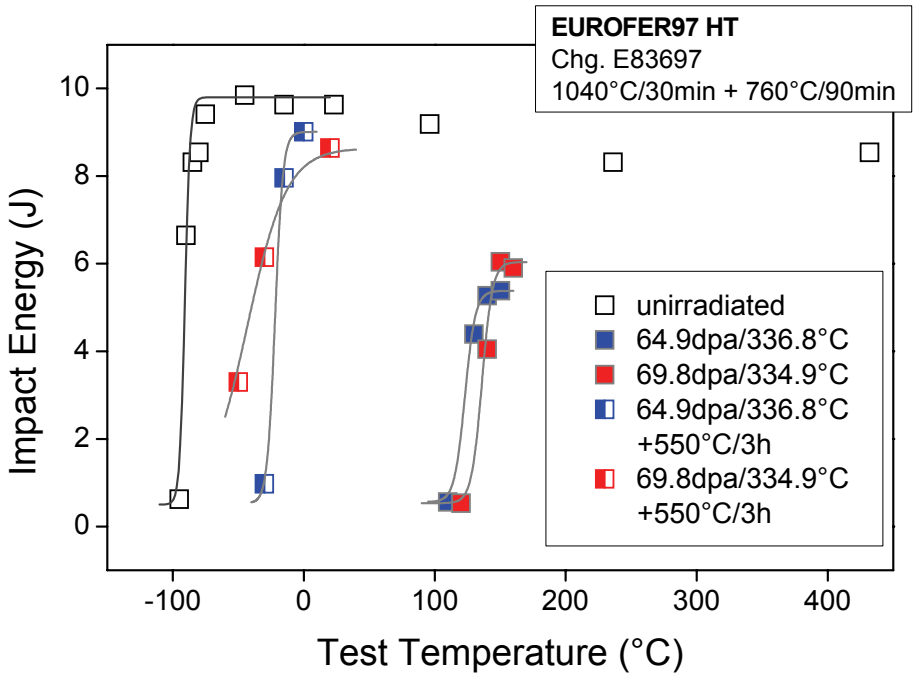

Fig. 4-2 Impact energy vs. test temperature curves of pre-irradiation heat treated EUROFER 97 HT in the reference unirradiated condition, after irradiation to 64.9 dpa/ 336.8 °C and 69.8 dpa/334.9 °C and after PIA at 550 °C/3 h.

The impact properties of F82H-mod. in the reference unirradiated state and after irradiation to 64.9 dpa at 336.8 °C are shown in Fig. 4-3. The load time diagrams of the irradiated specimens are shown in Fig. 9-5. The temperature dependence of the impact energy is summarised in Table 9-5. The neutron irradiation strongly degrades the impact properties leading to the shift of the DBTT towards higher temperatures and reduction of the USE. The irradiated F82H-mod. behaves somehow poorly compared to the EUROFER steels with respect to both DBTT and USE. After irradiation to 64.9 dpa/336.8 °C the DBTT shift is 256 °C. The post-irradiation annealing of F82H-mod. leads to substantial recovery of the impact properties in Fig. 4-2. The residual embrittlement of 106 °C is, however, larger than that of EUROFER 97 HT (48 °C).

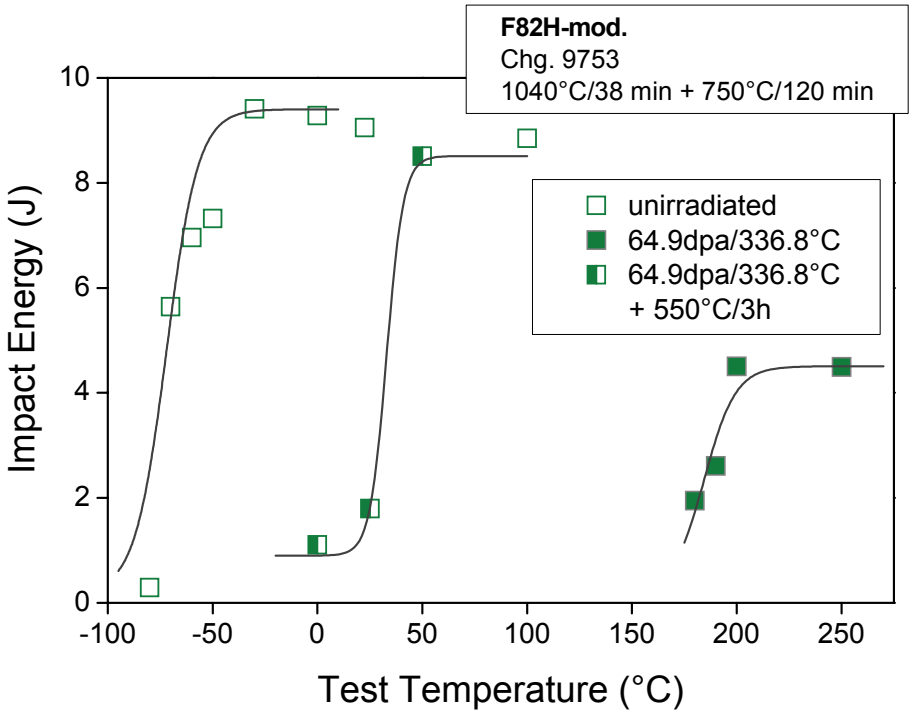

Fig. 4-3 Impact energy vs. test temperature curves of F82H-mod. in the reference unirradiated condition, after irradiation to 64.9 dpa/ 336.8 °C and after PIA at 550 °C/3 h.

The impact properties of OPTIFER XI in the reference unirradiated state and after irradiation to 12.0 dpa at 337.5 °C and to 31.0 dpa at 338.4 °C are shown in Fig. 4-4. The load time diagrams of the 12.0 dpa/337.5 °C and 31.0 dpa at 338.4 °C irradiated specimens are shown in Fig. 9-6 and in Fig. 9-7, respectively. The temperature dependences of the impact energies for the 12.0 dpa/337.5 °C and 31.0 dpa at 338.4 °C irradiated specimens are summarised in Table 9-6 and Table 9-7, respectively. The neutron irradiation strongly degrades the impact properties already after irradiation to 12 dpa at 337.5 °C leading to a DBTT shift of 165.2 °C towards higher temperatures and to a reduction of upper shelf toughness. The irradiation to 31 dpa leads to further material embrittlement yielding ΔDBTT of 203.8 °C. This value is comparable to the neutron irradiation induced DBTT shift of 218 °C observed for ERUFOER97 after irradiation to 31.8 dpa at 332 °C in the ARBOR 1 experiment [9]. The USE of 31 dpa irradiated OPTIFER XI is reduced by 4.03 J from the unirradiated reference value. This value is considerably larger than the USE reduction quantified for ERUFOER97 after irradiation to 31.8 dpa during the ARBOR 1 experiment [9].

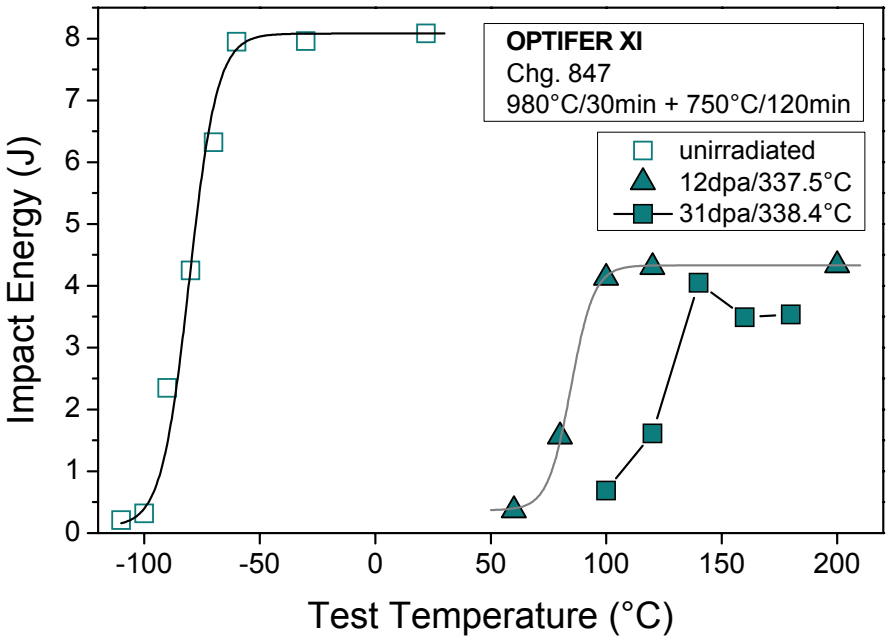

Fig. 4-4 The impact energy vs. test temperature curves of OPTIFER XI in the reference unirradiated state and after irradiation to 12.0 dpa at 337.5 °C and to 31.0 dpa at 338.4 °C.

The impact properties of OPTIFER XII in the reference unirradiated state and after irradiation to 12.0 dpa at 337.5 °C are shown in Fig. 4-5. The load time diagrams of the 12.0 dpa/337.5 °C irradiated specimens are shown in Fig. 9-8. The temperature dependences of the impact energies of the 12.0 dpa/337.5 °C irradiated specimens are summarised in Table 9-8. The neutron irradiation leads to a strong degradation of the impact properties compared to the unirradiated state as summarised in Table 4-1.

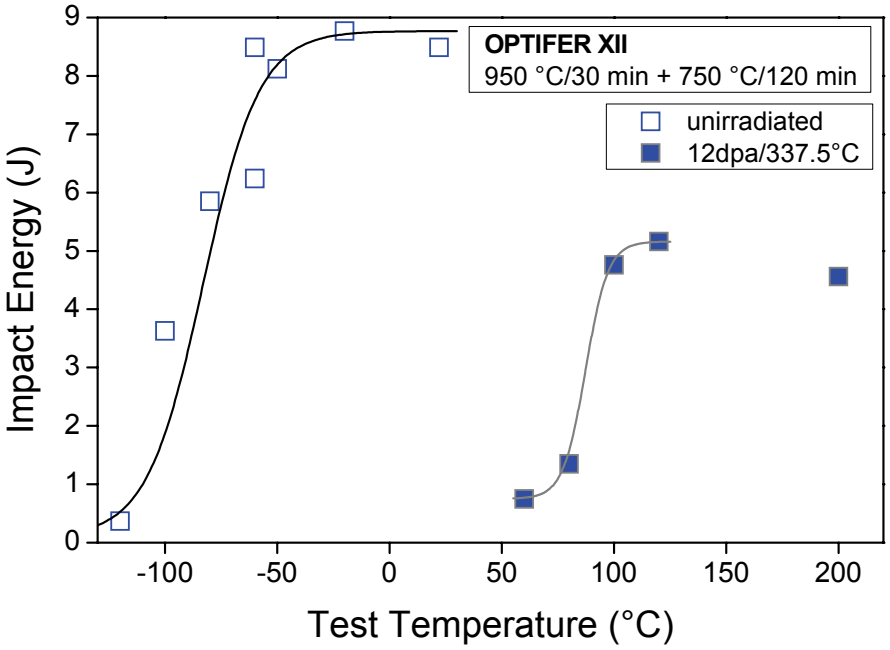

Fig. 4-5 The impact energy vs. test temperature curves of OPTIFER XII in the reference unirradiated state and after irradiation to 12.0 dpa at 337.5 °C.

The impact properties of 82 wppm natural boron doped steel ADS 2 in the reference unirradiated state, after neutron irradiation to 69.8 dpa at 334.9 °C and after post-irradiation annealing at 550 °C for 3 h are shown in Fig. 4-6. The load time diagrams of the irradiated specimens are shown in Fig. 9-9. The temperature dependences of the impact energies of the irradiated specimens are summarised in Table 9-9. The neutron irradiation strongly degrades the impact properties leading to a DBTT shift towards higher temperatures and reduction of the USE. After irradiation to 69.8 dpa at 334.9 °C the DBTT is 238 °C corresponding to an irradiation induced shift ΔDBTT of 312 °C. The irradiation induced embrittlement is thus by 85 °C larger than in 70 dpa irradiated EUROFER 97 HT, which is attributed to the boron-to-helium transformation under neutron irradiation [22],[17]. The post-irradiation annealing considerably improves the impact properties leading to the substantial recovery of the DBTT and to nearly complete recovery of the USE indicating substantial healing of the radiation defects. The residual embrittlement of 174 °C in ADS 2, however, is still considerably larger than the residual embrittlement of 48 °C in EUROFER 97 HT indicating strong influence of the synergy of helium and dpa effects on the evolution of the microstructure in RAFM steels. Helium bubbles are expected to be stable in the PIA experiments.

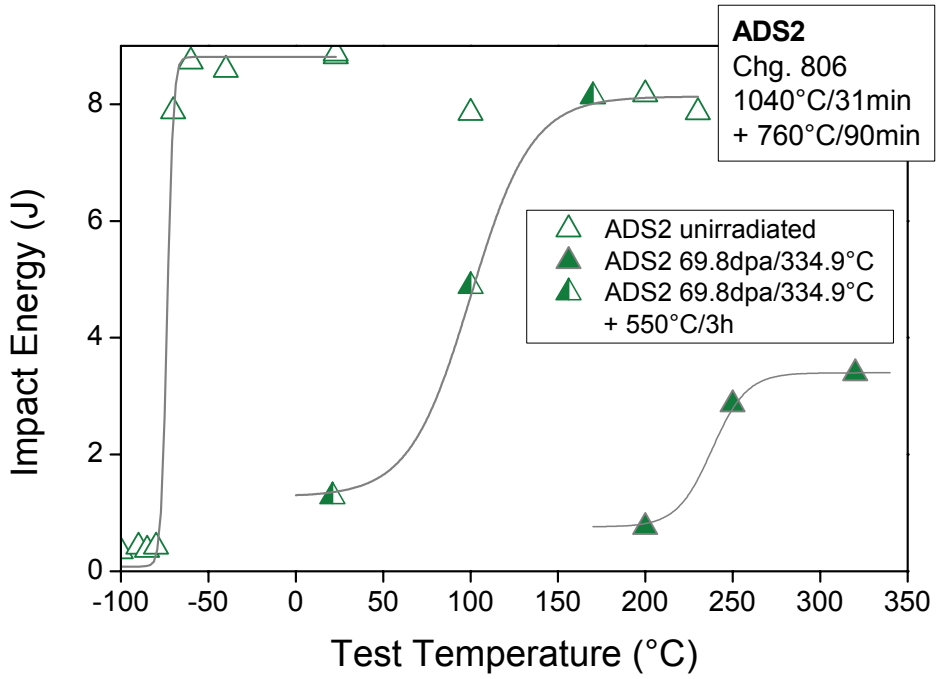

Fig. 4-6 Impact energy vs. test temperature curves of ADS 2 in the reference unirradiated condition, after irradiation to 69.8 dpa/ 334.9 °C and after PIA at 550 °C/3 h.

The impact properties of 82 wppm ^{10}B doped steel ADS 3 in the reference unirradiated state, after neutron irradiation to 69.8 dpa at 334.9 °C and after post-irradiation annealing at 550 °C for 3 h are shown in Fig. 4-7. The load time diagrams of the irradiated specimens are shown in Fig. 9-10. The temperature dependences of the impact energies of the irradiated specimens are summarised in Table 9-10. The neutron irradiation strongly degrades the impact properties leading to a shift of the DBTT towards higher temperatures and reduction of the USE. After irradiation to 69.8 dpa at 334.9 °C the DBTT is 260 °C corresponding to the irradiation induced DBTT shift ΔDBTT of 360 °C. Such a large irradiation induced embrittlement is a result of the synergy of the dpa and helium effects. About 120 appm helium is estimated

to be produced in ADS 3 after irradiation to 69.8 dpa as a result of ^{10}B to helium transformation [17]. The post-irradiation annealing considerably improves the impact properties leading to a substantial recovery of the DBTT and the USE indicating substantial healing of the radiation defects. The larger residual embrittlement of ADS 3 (210 °C) in comparison to EUROFER 97 HT (48 °C) again indicates a strong influence of the synergy of helium and dpa effects on the evolution of the microstructure under neutron irradiation.

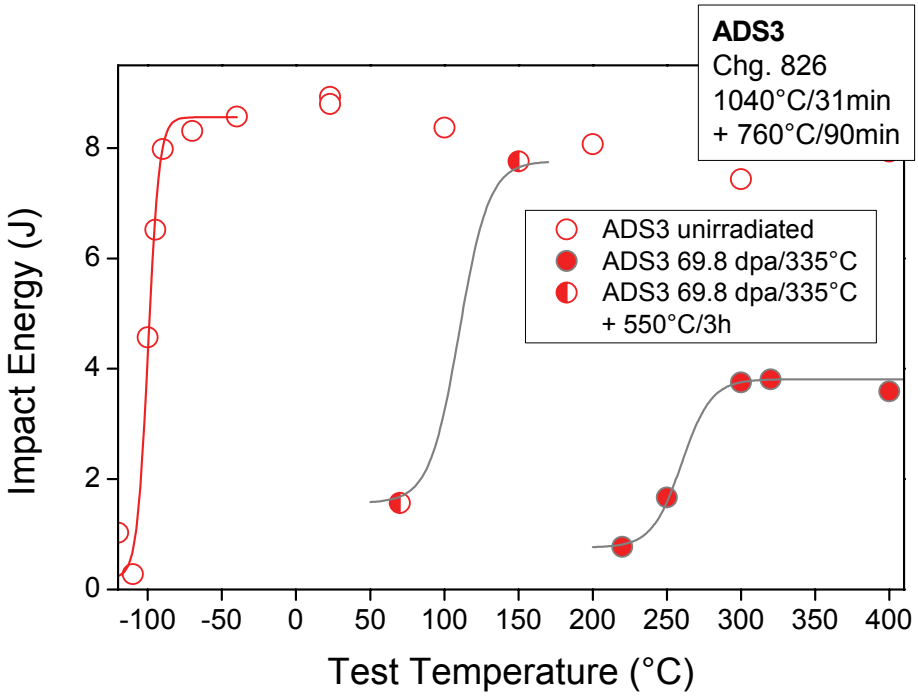

Fig. 4-7 Impact energy vs. test temperature curves of ADS 3 in the reference unirradiated condition, after irradiation to 69.8 dpa/ 334.9 °C and after PIA at 550 °C/3 h.

The impact properties of ODS EUROFER (EUROFER 97 with 0.5 wt.% Yttria) in the reference unirradiated condition and after neutron irradiation to 12.0 dpa at 337.5 °C and to 64.9 dpa at 336.8 °C are shown in Fig. 4-8. The load time diagrams of the specimens after irradiation to 12.0 dpa at 337.5 °C are shown in Fig. 9-11. The temperature dependence of the impact energies are summarised in Table 9-11. The load time diagrams of the specimens after irradiation to 64.9 dpa at 336.8 °C are shown in Fig. 9-12. The temperature dependence of the impact energies are summarised in Table 9-12. The neutron irradiation to 12 dpa at 337.5 °C leads to specimen failure by delamination at intermediate test temperatures which substantially increases impact toughness readings and hence results to apparent improvement of irradiation resistance. The corresponding load vs. time diagrams in Fig. 9-11 are characterized by multiple crack emission and arrest events. The maximum absorbed energy in the irradiated condition is 6.07 J, which is by 3.53 J larger than the USE in the unirradiated condition. The pseudo DBTT defined at a temperature where the impact energy reaches 50% value from its maximum level equals 134.7 °C. The impact energy was found to be very low after irradiation to 64.9 dpa at 336.8 °C even at a test temperature of 500 °C, see Fig. 4-8. The PIA at 550 °C for 3 h only slightly increased the impact energy at 500 °C and the specimen failed still in a brittle manner.

The impact tests on another ODS steel EODShip 3 (EUROFER 97 with 0.3 wt.% Yttria) after irradiation to 28.4 dpa at 338.4 °C yielded brittle fracture up to 250 °C test temperature. The DBTT and USE could not be determined. The load vs. time diagrams of the specimens after irradiation to 28.4 dpa at 338.4 °C are shown in Fig. 9-13. The temperature dependence of the impact energies are summarised in Table 9-13.

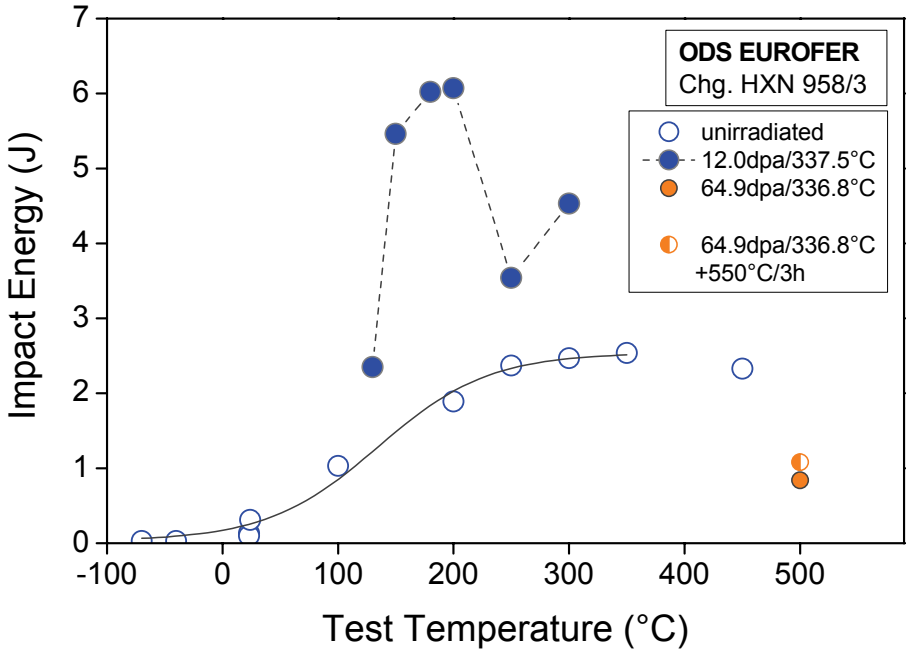

Fig. 4-8 Impact energy vs. test temperature curves of ODS EUROFER (EUROFER 97 with 0.5 wt.% Yttria) in the reference unirradiated condition, after neutron irradiation to 12.0 dpa/ 337.5 °C, to 64.9 dpa/ 336.8 °C and after PIA at 550 °C/3 h.

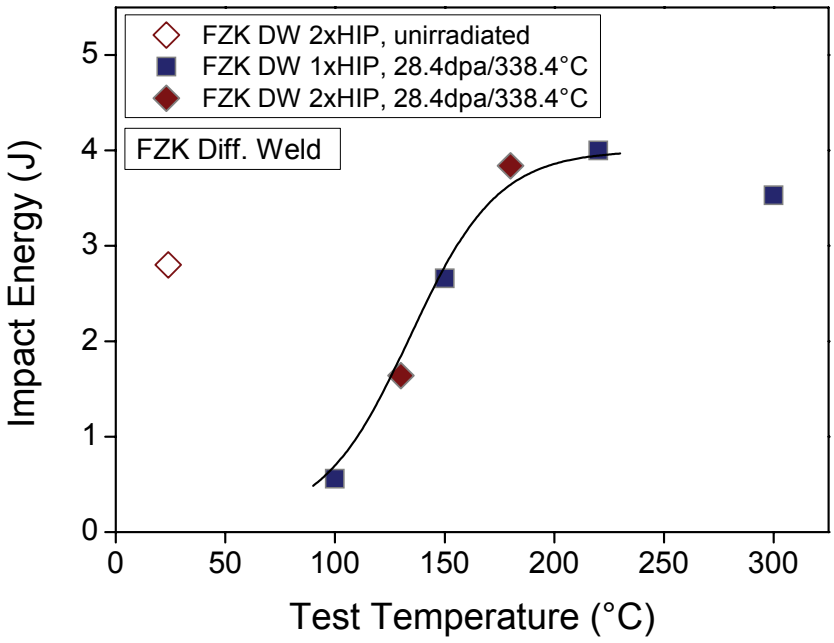

Fig. 4-9 Impact energy vs. test temperature curves of diffusion welded EUROFER 97 specimens in the reference unirradiated state and after irradiation to 28.4 dpa at 338.4 °C.

The impact tests results of diffusion welded EUROFER 97 specimens in the unirradiated state and after irradiation to 28.4 dpa at 338.4 °C are shown in Fig. 4-9. The load time diagrams of the irradiated specimens are shown in Fig. 9-14. The temperature dependence of the impact energies are summarised in Table 9-14. The welds produced in one (1xhip) or two (2xhip) successive HIP welding steps show comparable irradiation performance in Fig. 4-9. The DBTT in the irradiated state is 133.9 °C and the USE equals 4.0 J. Comparatively, the DBTT and USE values for the as delivered EUROFER 97 after irradiation to a slightly larger damage dose of 31.8 dpa at 332 °C [9] were 137 °C and 7.0 J, respectively.

4.1.1 Irradiation dose evolution of embrittlement

Fig. 4-10 shows the evolution of the neutron irradiation induced embrittlement (measured in impact tests) with dose for EUROFER 97 and F82H steels at irradiation temperatures between 300 and 337 °C. For comparison the literature results from [23],[15] as well as neutron irradiation induced embrittlement for OPTIFER steels are also included. In case of EUROFER 97, differentiation is made between specimens machined from as-delivered products and specimens machined from the plates subjected to pre-irradiation HT. The results on F82H and F82H-mod. are plotted together for different heat treatments and material compositions [15]. These circumstances partly explain the large data scatter observed for F82H. The pre-irradiation HT of EUROFER leads to considerable improvement of the irradiation resistance at doses up to 30 dpa. All three steels show steep increase in the ΔDBTT with dose below 10 dpa. This is in a good agreement with a strong embrittlement observed on F82H for different pre-irradiation heat treatment conditions after irradiation at 300 °C to 5 dpa [24]. At the achieved doses a clear tendency to saturation of embrittlement is identified. Indeed, for 70 dpa/335 °C irradiation the ΔDBTT of EUROFER 97 is found to be 233 °C. This value is only 15 °C higher than the ΔDBTT after 32 dpa/332 °C irradiation. F82H-mod. irradiated to 65 dpa/337 °C behaves somewhat poorly compared to the EUROFER steels with respect to embrittlement. The embrittlement of OPTIFER XI and OPTIFER XII steels after low temperature irradiation to 12 dpa (and 31 dpa in case of OPTIFER XI) confirms the embrittlement trend of EUROFER 97 steels.

Due to the close correlation between low temperature hardening and embrittlement [12], the evolution of embrittlement with irradiation dose can be qualitatively described by an equation of the type $\Delta DBTT=\Delta DBTT_s(1-\exp(-\Phi/\Phi_o))^{1/2}$ with $\Delta DBTT_s$ as the saturation value of the embrittlement [15],[17]. The solid lines in Fig. 4-10 are fit to the data with the above equation. A good qualitative description of the data is provided. The results for EUROFER 97 are best described with $\Delta DBTT_s$ =238 °C and Φ_o =16.7 dpa.

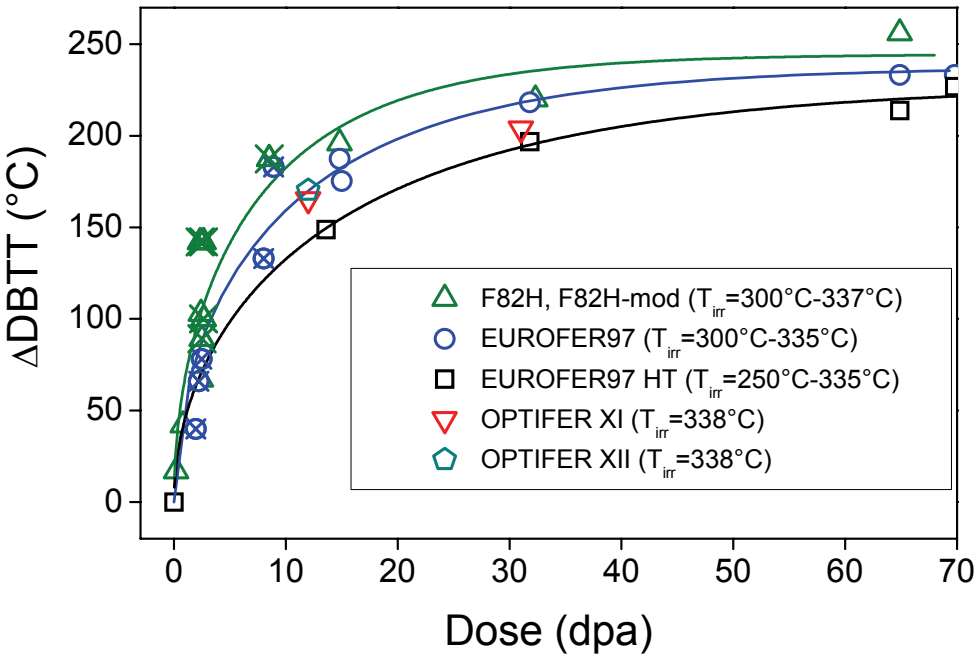

Fig. 4-10 Irradiation shifts of the DBTT vs. dose for EUROFER 97, EUROFER 97 HT, F82H and OPTIFER steels. The open symbols represent KIT results and the crossed symbols are from [23]. The solid lines are a model description of the data [15],[17].

4.2 Tensile testing

The main results of the tensile testing of the investigated specimens are discussed in this section. The recorded tensile curves of the investigated irradiated specimens as well as the quantified tensile properties in the irradiated and reference unirradiated conditions are given in Annex 10.

Fig. 4-11 shows Yield Stress (R_{p02}) and Ultimate Tensile Strength (R_m) of the steels and technological specimens irradiated to 70.1 dpa at 331.5 °C and tested at 350 °C. The investigated base RAFM steels show comparable Yield Stress and Ultimate Strength in the irradiated condition. The Ultimate Strength is if any only slightly larger than the Yield Stress values indicating strong suppression of the strain hardening capability of the irradiated RAFM steels. Boron doped steels ADS 2 and ADS 3 show tensile properties which are comparable to those of base EUROFER steels indicating only minor influence of the produced transmutation helium (up to 120 appm He in ADS 3) on the tensile properties. Tensile properties of the EB welded EUROFER 97 specimens are comparable to those of base EUROFER steels. Oxide Dispersion Strengthened EUROFER shows the largest tensile strength among the investigated materials. Tensile testing of the 70.1 dpa, 331.5 °C irradiated steels at 20 °C leads to qualitatively similar results in Fig. 4-12. The absolute values of the Yield Stress (R_{p02}) and Ultimate Tensile Strength (R_m) are however larger at 20 °C test temperature in comparison to 350 °C test temperature, partly due to the temperature dependence of the tensile properties of RAFM steels.

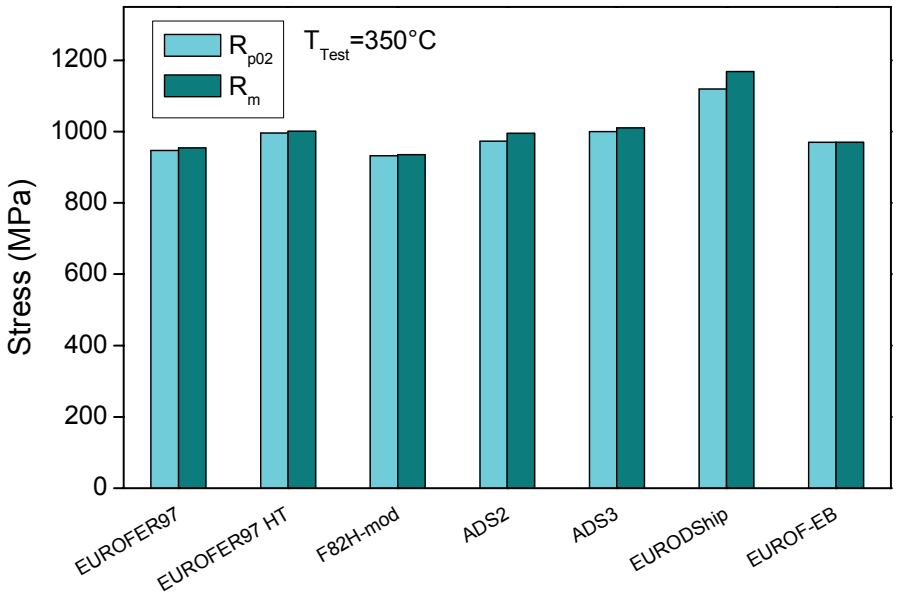

Fig. 4-11 Yield Stress (R_{p02}) and Ultimate Tensile Strength (R_m) of 70.1 dpa, 331.5 °C irradiated RAFM materials tested at 350 °C.

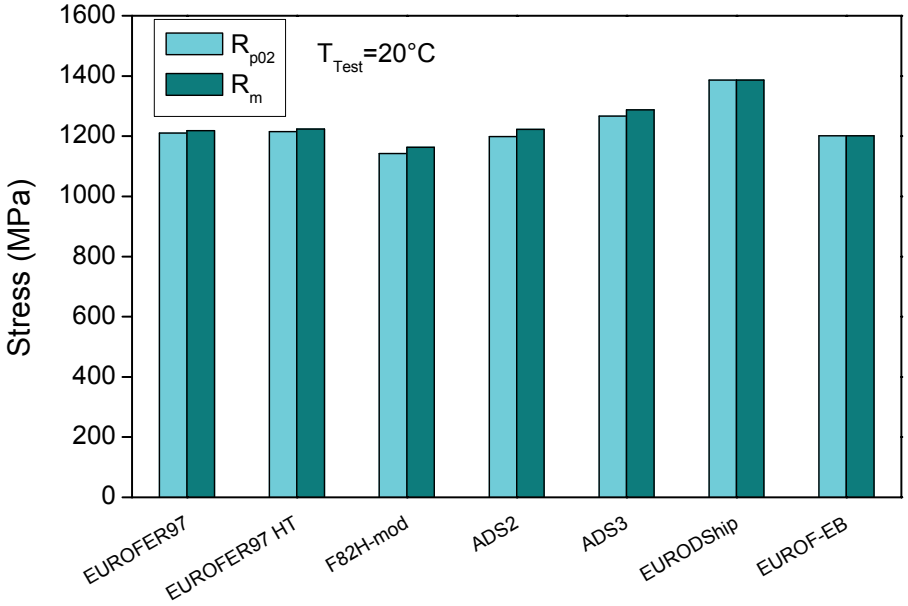

Fig. 4-12 Yield Stress (R_{p02}) and Ultimate Tensile Strength (R_m) of 70.1 dpa, 331.5 °C irradiated RAFM materials tested at 20 °C.

Fig. 4-13 shows Uniform Strain (A_g) and Total Strain (A) of the steels and technological specimens irradiated to 70.1 dpa at 331.5 °C and tested at 350 °C. Rather low values of the Uniform Strains below 1% are observed for all investigated base RAFM steels. The Total Strains, in contrast, remain at a high level above 9%-10%. The boron doped steels show larger Uniform and reduced Total Strains in comparison to base RAFM steels. Among all investigated steels the Oxide Dispersion Strengthened EUROFER shows the largest value of the Uniform Strain of 1.73%. The Total Strain at the same time is reduced down to 4.45%. The Total Strain of the EB welded EUROFER 97 specimens is comparable to those of base EUROFER 97 steels. The testing at 20 °C yielded slight improved Strain characteristics of

base RAFM and EB welded steels. The Total Strain of the boron doped steels was in contrast considerably reduced at a test temperature of 20 °C. Remarkable is also nearly vanished Total Strain of ODS EUROFER steels.

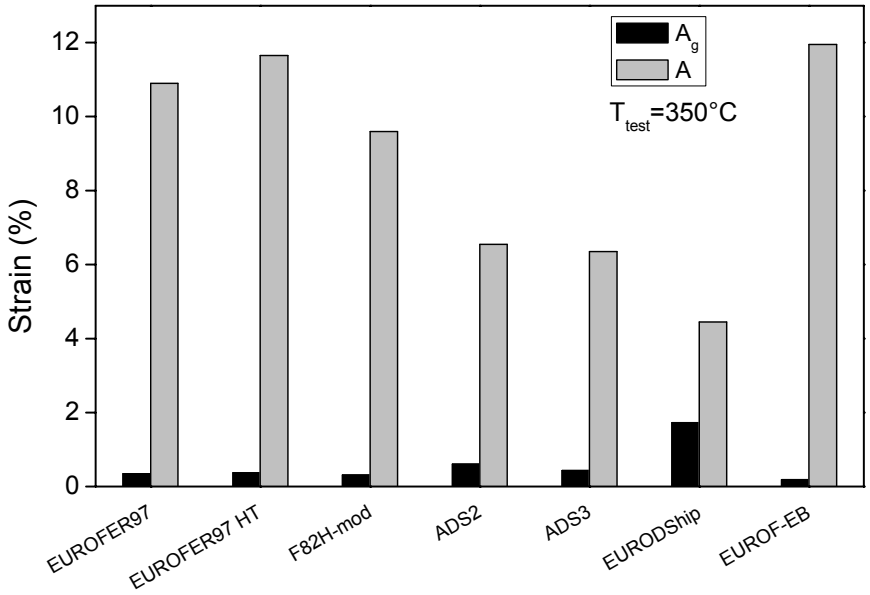

Fig. 4-13 Uniform Strain (A_g) and Total Strain (A) of 70.1 dpa, 331.5 °C irradiated RAFM materials tested at 350 °C.

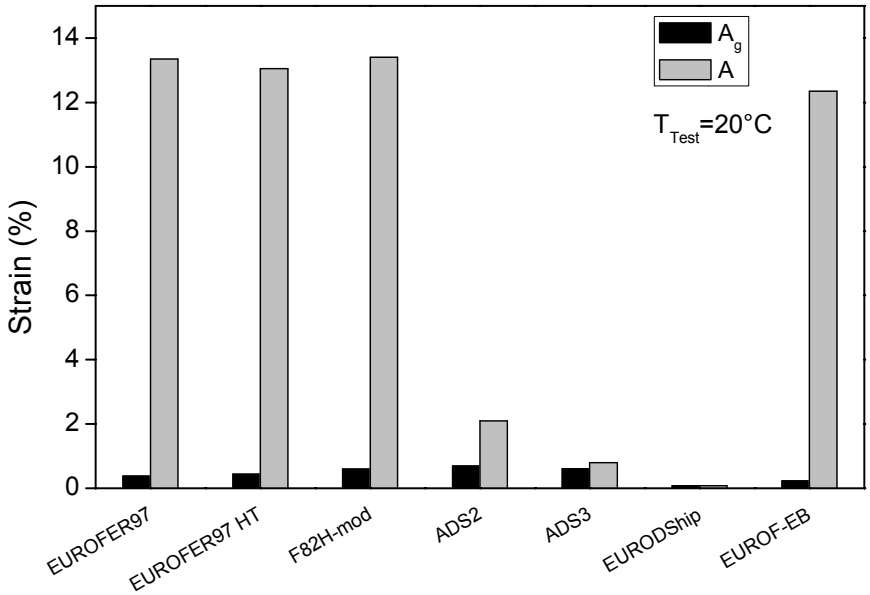

Fig. 4-14 Uniform Strain (A_g) and Total Strain (A) of 70.1 dpa, 331.5 °C irradiated RAFM materials tested at 20 °C.

Fig. 4-15 shows the Reduction of Area (Z) of the steels and technological specimens irradiated to 70.1 dpa at 331.5 °C and tested at 350 °C. Among the base RAFM steels EUROFAR97 HT shows the larges area reduction of 60%. F82H-mod. shows considerably lower area reduction in comparison to EUROFER steels. Low Z-values in the boron doped steels

can not be related to the helium contents as ADS 2 steel (containing less helium than ADS 3) shows lower area reduction than ADS 3. The lowest Z-value among the investigated steels is observed for Oxide Dispersion Strengthened EURFOFER with 0.5 wt.% Y_2O_3. Remarkably, Z-value of EB welded EUROFER 97 is larger than the base EUROFER steel. Reduction of Area increased for EUROFER 97 and F82H-mod. steels after testing at 20 °C as shown in Fig. 4-16. Z-values of boron doped steels in contrast have completely vanished at this test temperature.

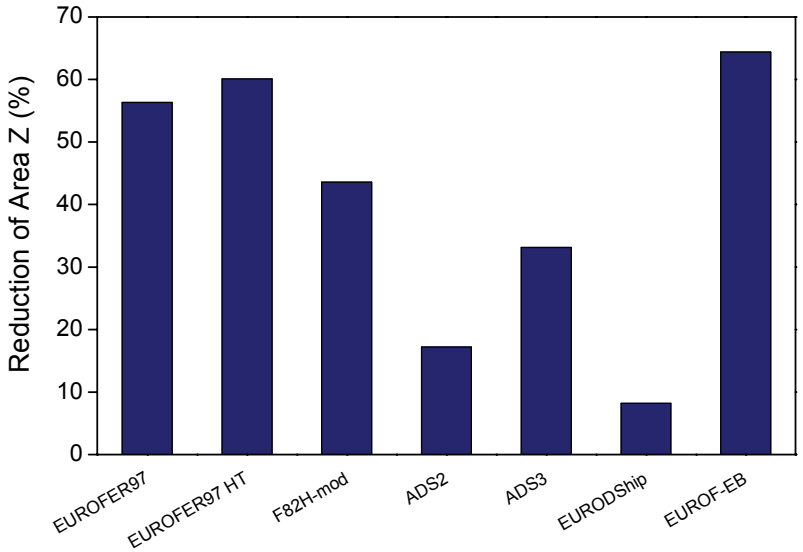

Fig. 4-15 Reduction of area of 70.1 dpa, 331.5 °C irradiated RAFM materials after testing at 350 °C.

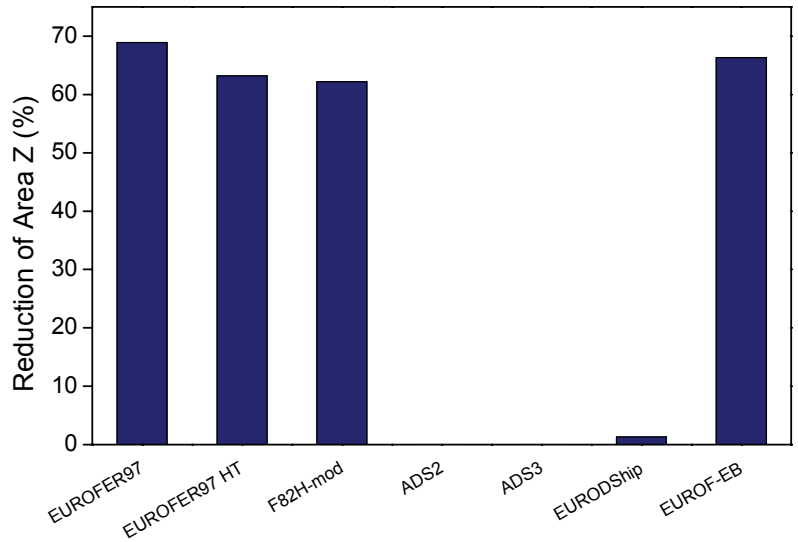

Fig. 4-16 Reduction of area of 70.1 dpa, 331.5 °C irradiated RAFM materials after testing at 20 °C.

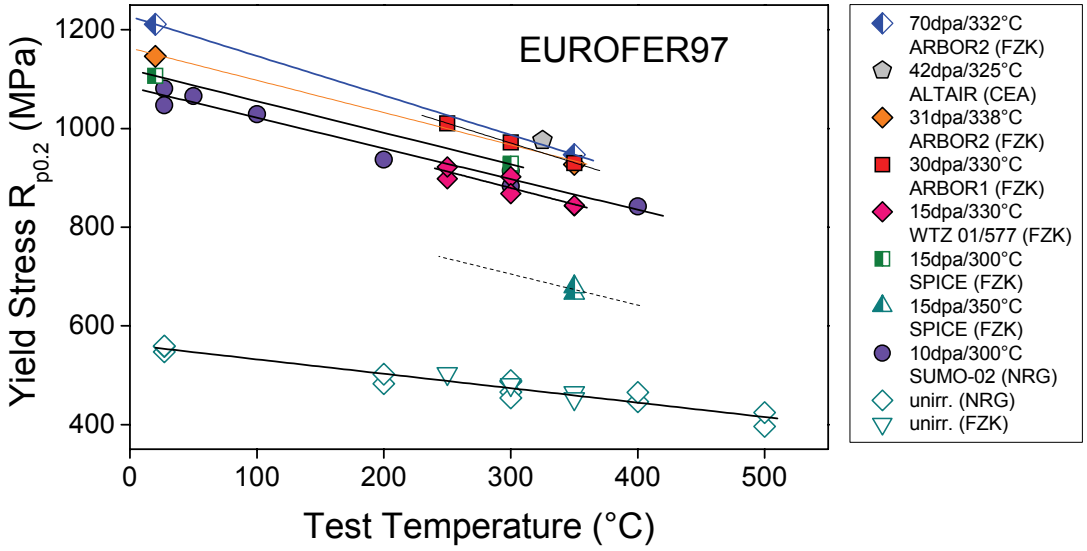

Fig. 4-17 Yield Stress vs. test temperature for EUROFER 97 in the unirradiated condition and after neutron irradiations in different European irradiation programmes (irradiation conditions and programmes are given in the figure legend). The lines are a guide for the eye.

Fig. 4-17 shows Yield Stress ($R_{p0.2}$) vs. test temperature (T_{test}) for EUROFER 97 in the unirradiated condition and after neutron irradiation in different medium and high dose European irradiation programmes at target irradiation temperatures (T_{irr}) between 300 and 350 °C [8],[9],[14],[23], [25]. Tensile tests were performed on four different kinds of specimen types utilized in the different irradiations. NRG irradiated cylindrical specimens of 20 mm gauge length and 4 mm diameter and performed the tests with a strain rate of $5x10^{-4}$ s^{-1}[23]. In the SPICE irradiation cylindrical specimens of 18 mm gauge length and 3 mm diameter are tensile tested under vacuum with a strain rate of $1x10^{-4}$ s^{-1}[8]. In the 15 dpa WTZ 01/577 irradiation cylindrical specimens of 15 mm gauge length and 3 mm diameter are tensile tested with a strain rate of $3x10^{-3}$ s^{-1} [14].

The reference tensile test performed at NRG and FZK concerning the stresses are in a narrow scatter band and give a good basis for the interpretation of the tensile results. Neutron irradiation leads to substantial increases in the Yield Stress which is sensitive to the irradiation parameters i.e. irradiation dose and temperature [15]. Furthermore, for given irradiation conditions the Yield Stress increase depends on the test temperature and is larger at low test temperatures. The specimens from ARBOR 2 irradiated to 70 dpa show the highest Yield Stress at test temperatures of 20 and 350 °C. Remarkably, the temperature dependence of the Yield Stress measured on the specimens irradiated in ARBOR 1 to 30 dpa nicely agrees with the temperature dependence trend of the Yield Stress measured on the specimens from ARBOR 2 after irradiation to 31 dpa. While the differences in the Yield Stress values at 300 and 330 °C irradiations to 15 dpa are still moderate and within data scatter, as can be seen from the comparison between WTZ [14] and SPICE [8] results, Yield Stress values after 15 dpa/350 °C irradiation are considerably lower indicating substantial thermal recovery at this irradiation temperature.

The temperature dependence of the ultimate tensile strength (R_m) for irradiated EUROFER 97 shown in Fig. 4-18 resembles to that of the Yield Stress shown in Fig. 4-17. Close values of the ultimate tensile strength (R_m) and Yield Stress ($R_{p0.2}$) in the irradiated conditions indicates a strong suppression of the strain hardening capability under neutron irradiation.

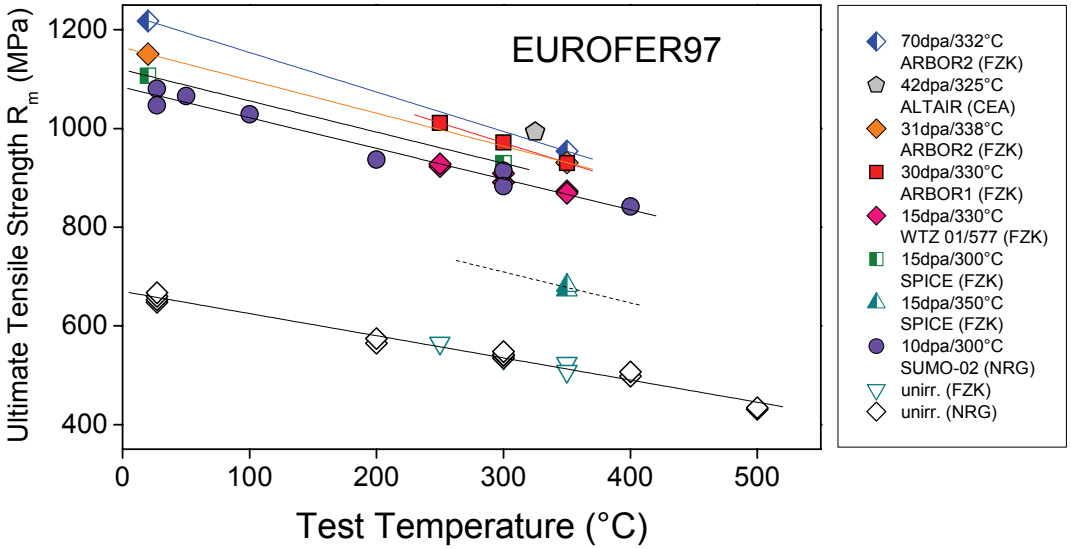

Fig. 4-18 Ultimate tensile strength vs. test temperature for EUROFER 97 in the unirradiated condition and after neutron irradiations in different European irradiation programmes. The lines are a guide for the eye.

The Uniform Strains quantified in the reference tensile test at NRG and FZK shown in Fig. 4-19 are in a certain scatter band but also give a good basis for the interpretation of the tensile results. Uniform Strain is strongly suppressed after low temperature irradiation and is scattered at values mostly below 0.5%.

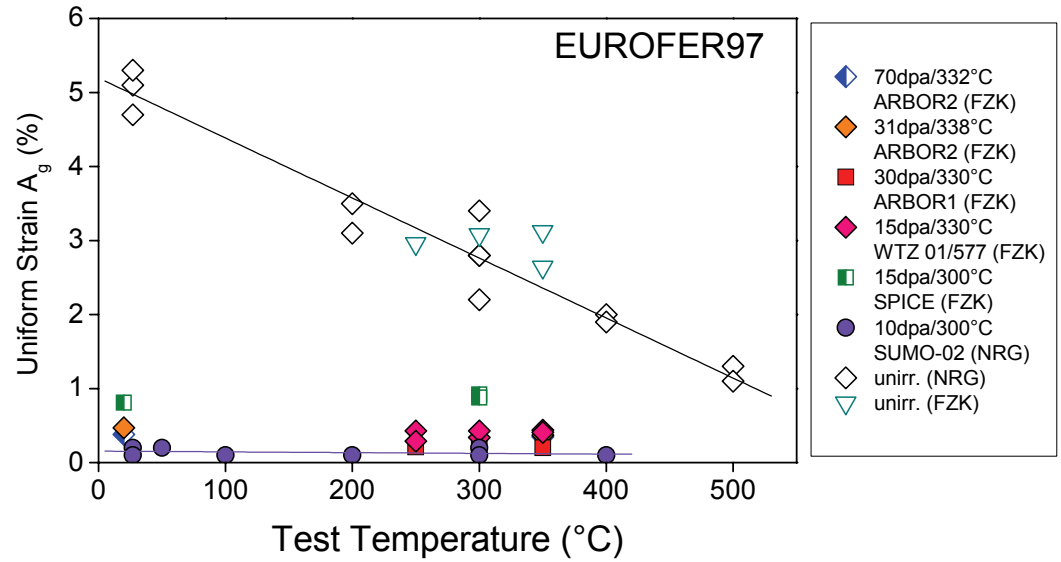

Fig. 4-19 Uniform Strain vs. test temperature for EUROFER 97 in the unirradiated condition and after neutron irradiations in different European irradiation programmes. The lines are a guide for the eye.

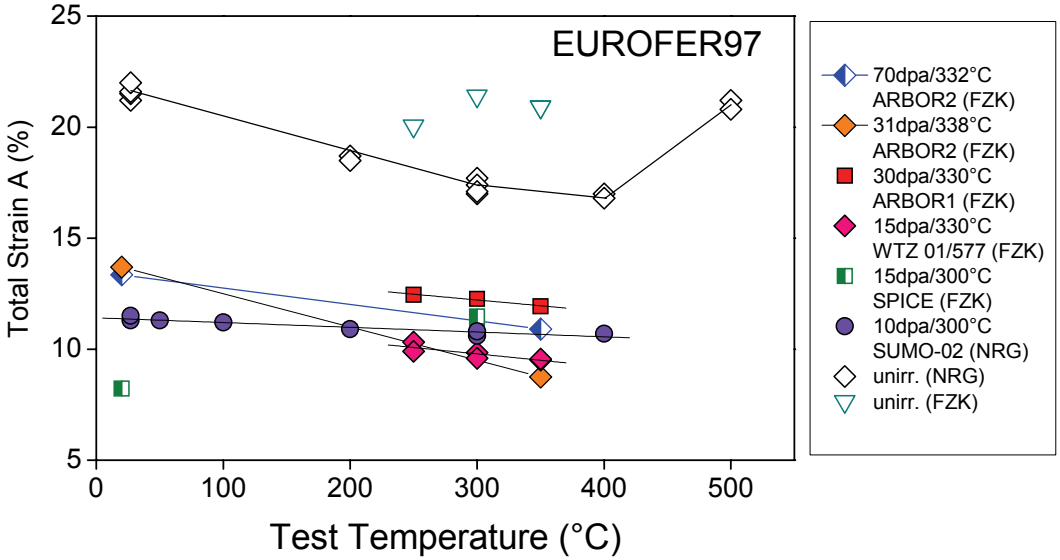

Fig. 4-20 Total Strain vs. test temperature for EUROFER 97 in the unirradiated condition and after neutron irradiations in different European irradiation programmes. The lines are a guide for the eye.

Though also strongly reduced in comparison to the unirradiated condition, the Total Strain retain considerable values in the irradiated state up to achieved damage doses as seen in Fig. 4-20. The observed Total Strains mostly above 10% are of great importance for structural material application.

4.2.1 Irradiation dose evolution of hardening

Fig. 4-21 presents the evolution of the hardening, as the increase in Yield Stress, with dose for EUROFER 97 and F82H-mod. for irradiation temperatures between 300 and 335 °C and for test temperatures between 300 and 350 °C. KIT results from ARBOR 2 as well as from the recent KIT irradiations programmes SPICE [8], WTZ 01/577 and ARBOR 1 [9] are presented by solid symbols. For comparison the literature results from [23],[25],[26],[15],[17] are also included in the diagram. Neutron irradiation leads to substantial increase in the Yield Stress with the dose. The Yield Stress increase is rather steep at doses below 10 dpa and in a good agreement with the observations on F82H after low temperature irradiation [27]. In spite of large data scatter, partly due to different irradiation temperatures, a clear tendency to saturation at the achieved doses is identified for both RAFM steels.

Severe degradation of the tensile properties of RAFM steels observed in Fig. 4-21 is a result of neutron irradiation induced severe changes in the microstructure. Dislocation loops and α′-precipitates nearly homogeneously distributed in RAFM steels are believed to be a main source of the irradiation hardening and embrittlement. The radiation defects acting as impeding obstacles to glide dislocations lead to strong material hardening which can be evaluated according to the following relationship

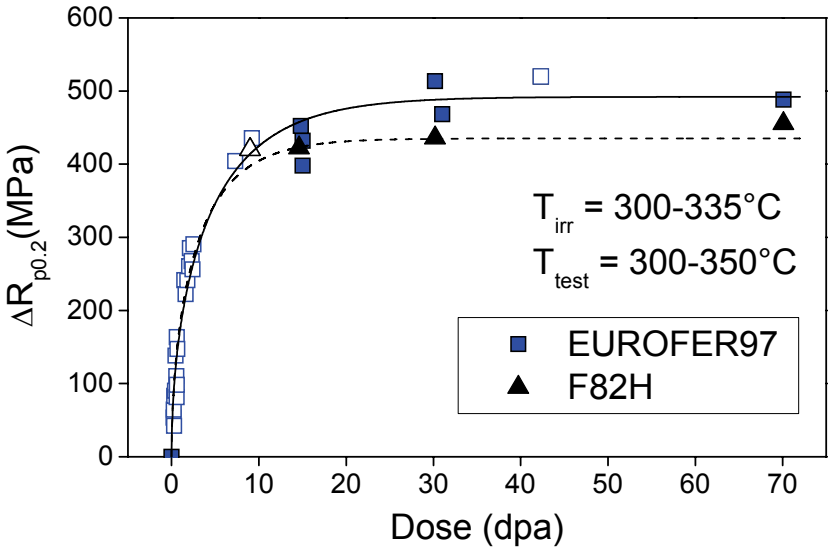

Fig. 4-21 Irradiation hardening vs. irradiation dose for EUROFER 97 and F82H steels for T_{irr} = 300-335 °C and T_{test} = 300-350 °C. The full symbols represent KIT results [8],[9]. The open symbols are from the literature [23],[25],[26],[15],[17]. The solid line is a least square fit to the EUROFER 97 data with Eq. (3). The dashed line is only a guide for the eye.

$$\Delta\sigma = M\alpha\mu b\sqrt{Nd} \tag{1}$$

with *M* being the Taylor factor, α – an average obstacle strength, μ – the shear modulus of the steel, *b* – the Burgers vector of the moving dislocation, *N* – the volume density of the obstacles and *d* – their average diameter.

A phenomenological approach to the evolution of the radiation defect density with irradiation dose was given by Whapham and Makin in [28]. In this model the defect density *N* increases with dose at the initial stage of irradiation, but as their concentration increases the newly formed defects become captured by the already existing ones leading to a decrease of the number of newly formed defects during a given increment of dose as the dose increases. Hence, the increase in *N* and the achievement of a saturation value N_s is expected:

$$N = N_s\left[1-\exp\left(-\frac{\Phi}{\Phi_0}\right)\right] \tag{2}$$

here Φ denotes the irradiation dose and Φ_0 is the scaling dose characterizing how fast the saturation of *N* sets in. For irradiation hardening dominated by a single obstacle type, combination of Eq. (2) with Eq. (1) yields the following relationship for the evolution of the irradiation hardening with dose:

$$\Delta\sigma = \Delta\sigma_s\sqrt{1-\exp\left(-\frac{\Phi}{\Phi_0}\right)} \tag{3}$$

where $\Delta\sigma_s$ is the saturation value of hardening.

The solid line in Fig. 4-21 is a description of the irradiation hardening according to Eq. (3) with $\Delta\sigma_s$ =492 MPa and Φ_0 =7.3 dpa. In spite of (i) differences in the irradiation conditions, *e.g.* the

irradiation temperature, the neutron flux, (ii) differences in test conditions *e.g.* specimen geometry, strain rate and (iii) scatter of experimental data, Eq. (3) describes qualitatively the evolution of hardening with dose. Furthermore, the hardening rate appears to be significantly decreased at the achieved damage doses. Planned quantitative analysis of the radiation defects and their evolution with damage dose will shed more light on the hardening mechanisms.

4.2.2 Post-irradiation annealing

Fig. 4-22 shows the influence of the post-irradiation annealing at 550 °C on the tensile properties of EUROFER 97 specimens irradiated to a damage dose of 70.1 dpa at 331.5 °C, see also Fig. 10-1 and Table 10-1. The applied PIA consisted of the following steps: i) heating the specimen from RT to 550 °C during 3 h, ii) annealing at 550 °C for a nominal annealing time and iii) cooling down the specimen from 550 °C to RT during 3 h. The neutron irradiation induced hardening, quantified as the increase of the Yield Stress and Ultimate Tensile Strength is substantially reduced after annealing already for 1 hour. Recovery in the hardening is accompanied with the recovery in the ductility properties, i.e. a complete recovery of the Uniform Strain and substantial recovery of the Total Strain is achieved already after one hour PIA. Nearly complete recovery of the tensile properties, both with respect to the strength and ductility indicates recovery of the microstructure to a large extend.

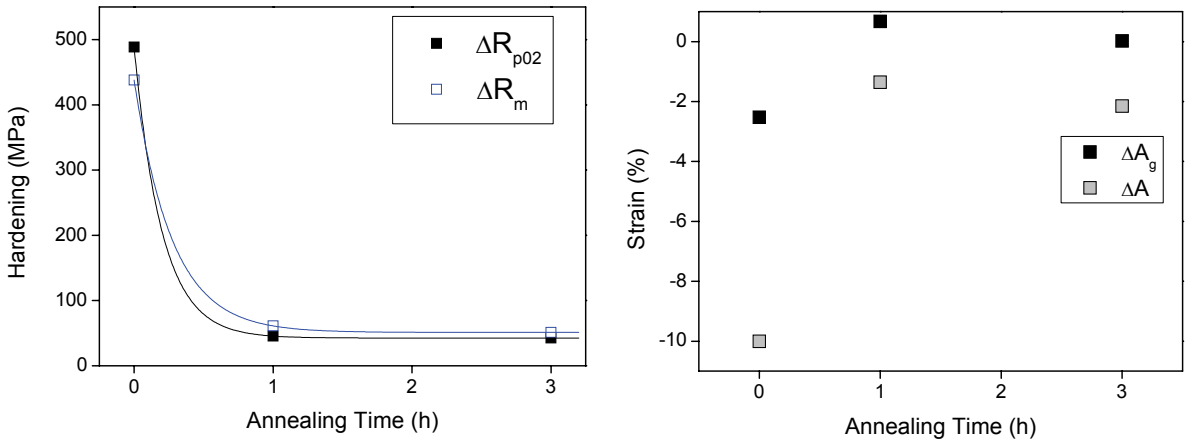

Fig. 4-22 Hardening, quantified as increase in the Yield Stress and Ultimate Tensile Strength (left) and ductility properties, quantified as changes in the Uniform and Total Strains (right) as a function of the post-irradiation annealing time at 550 °C. Annealing time "0" corresponds to the as irradiated state (70.1 dpa/ 331.5 °C). T_{test} = 350 °C; Strain rate =1x10^{-3} 1/s.

In order to study the kinetics of the radiation damage recovery the PIA experiment at 550 °C were performed on EUROFER 97 specimens irradiated to 31 dpa at 338.4 °C, see Fig. 10-2 and Table 10-2. PIA on one of the specimens was performed without dwell time, i.e. the heating up of the specimen to 550 °C was followed by its cooling down to RT. The neutron irradiation induced hardening, quantified as the increase of the Yield Stress and Ultimate Tensile Strength show nearly complete recovery already after heating the specimen to 550 °C, see Fig. 4-23, indicating very fast kinetics of the radiation damage annealing.

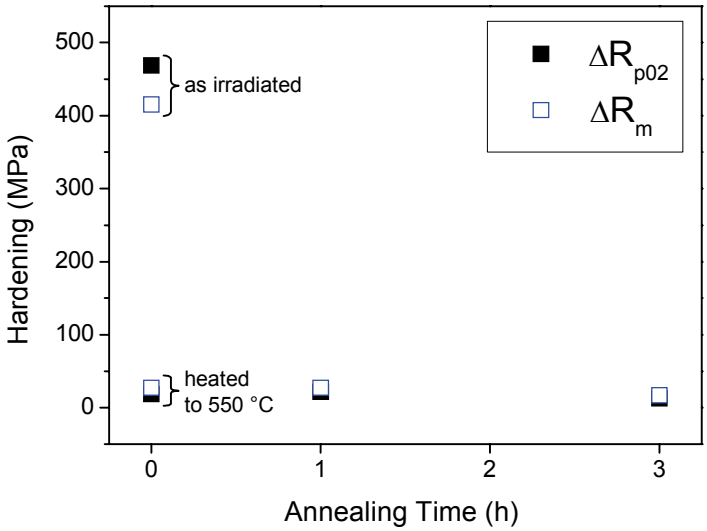

Fig. 4-23 Hardening, quantified as increase in the Yield Stress and Ultimate Tensile Strength as a function of the post-irradiation annealing time at 550 °C. As irradiated specimen (31 dpa/ 338.4 °C) and a specimen heated and immediately cooled up to/ from 550 °C are marked correspondingly. T_{test}= 350 °C; Strain rate =1x10^{-3} 1/s.

Similar to EUROFER 97 other RAFM steels also exhibited substantial recovery of the tensile properties in PIA experiments.

4.2.3 Miniaturised diffusion welded specimens

The tensile tests of miniaturised double-T shaped diffusion welded specimens were performed with an electro-mechanical testing machine of INSTRON-DOLI at two temperatures of 20 and 300 °C and at two crosshead speeds of 0.1 and 1.0 mm/min. Almost all specimens were broken within the gauge length.

Fig. 4-24 shows the $R_{p0.2}$ Yield Stress of 1xHIP and 2xHIP welded specimens in the unirradiated condition and after neutron irradiation to 36.2 dpa at 336.8 °C. For comparison the results obtained with double-T shaped specimens on the unirradiated base EUROFER 97 subjected to a similar HIPping process are also included. The Yield Stress values of unirradiated and 1 and 2 times HIPped base EUROFER 97 are comparable to those of as delivered EUROFER 97. The $R_{p0.2}$ Yield Stress of HIP welded specimens shows scatter in the unirradiated condition in Fig. 4-24. Furthermore, in the unirradiated condition 2xHIP welded specimens show $R_{p0.2}$ values well above the Yield Stress values for base material. The neutron irradiation leads to a strong hardening of welds. Exact assessment of the hardening is not possible due to scattering of the tensile results. The post-irradiation annealing at 550 °C for 3 h lead to substantial recovery of the tensile properties both for 1xHIP and 2xHIP welded specimens.

Fig. 4-25 shows the Yield Stress as a function of crosshead speed at two different test temperatures. Due to a large data scatter no clear effect of the crosshead speed on the Yield Stress can be identified both in the unirradiated and irradiated conditions. Also for the base material no strong effect of the deformation rate on the Yield Stress is observable.

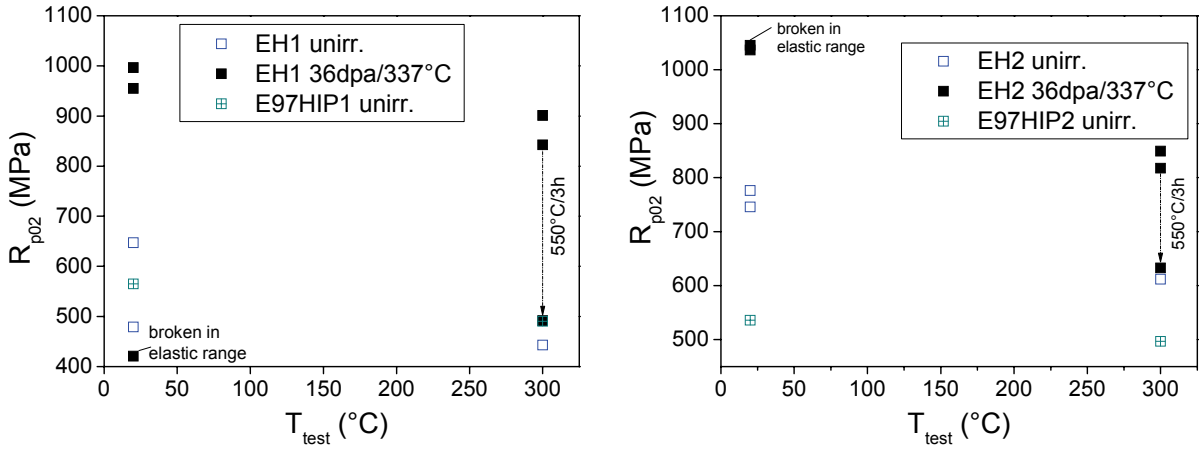

Fig. 4-24 Yield Stress vs. test temperature for 1xHIP (EH1) and 2xHIP (EH2) welded specimens in the unirradiated condition and after neutron irradiation to 36.2 dpa at 336.8 °C. The results on 1x HIPped (E97HIP1) and 2x HIPped (E97HIP2) base EUROFER 97 in the unirradiated condition are included. Crosshead speed of 1.0 mm/min corresponds to 4.8×10^{-3} 1/s strain rate. Dashed arrows indicate recovery of the Yield Stress after post irradiation annealing at 550 °C for 3 h.

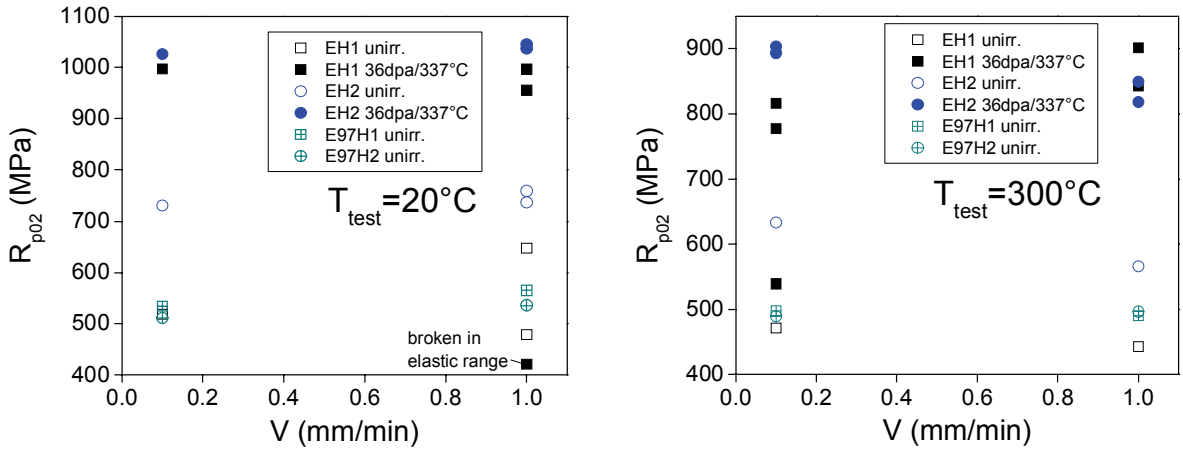

Fig. 4-25 Yield Stress vs. crosshead speed for 1xHIP (EH1) and 2xHIP (EH2) welded specimens in the unirradiated condition and after neutron irradiation to 36.2dpa at 336.8 °C. The results on 1x HIPped (E97HIP1) and 2x HIPped (E97HIP2) base EUROFER 97 in the unirradiated condition are included. Crosshead speeds of 0.1 and 1.0 mm/min correspond to a strain rate of 4.8×10^{-4} and 4.8×10^{-3} 1/s, respectively.

Uniform Strain values obtained with miniaturised double-T shaped specimens are shown in Fig. 4-26. Neutron irradiation leads to a strong reduction of the Uniform Strain in comparison to the reference unirradiated state both for 1xHIP and 2xHIP welded specimens. An exception was one 2xHIP welded specimen which at a test temperature of 300 °C yielded a Uniform Strain comparable to that of unirradiated state. Post irradiation annealing at 550 °C for 3 h yielded recovery of the Uniform Strain at a test temperature of 300 °C. The Total Strain values quantified with miniaturised double-T shaped specimens were well above the corresponding values quantified with mini-tensile specimens indicating non optimized geometry of double-T shaped specimens.

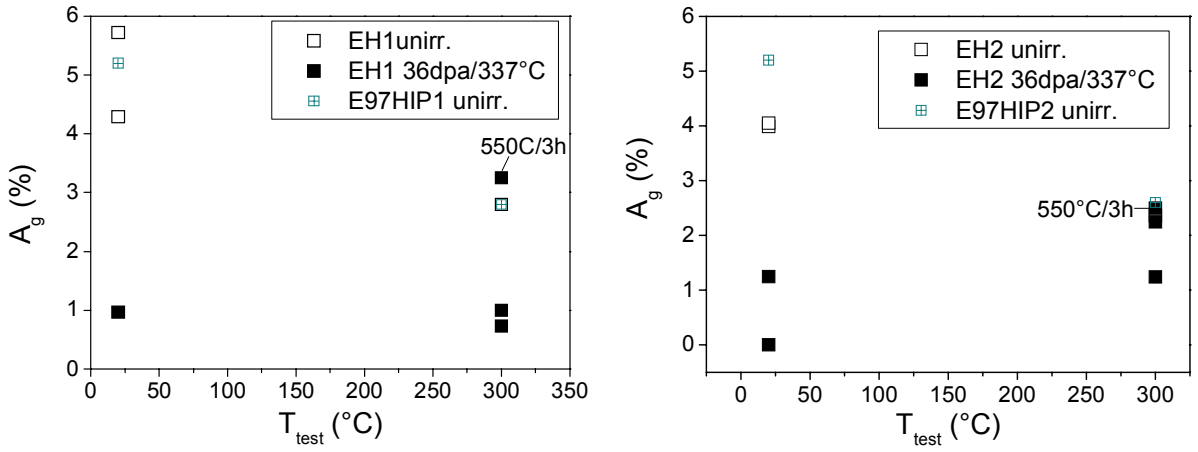

Fig. 4-26 Uniform Strain vs. test temperature for 1xHIP (EH1) and 2xHIP (EH2) welded specimens in the unirradiated condition and after neutron irradiation to 36.2dpa at 336.8 °C. The results on 1x HIPped (E97HIP1) and 2x HIPped (E97HIP2) base EUROFER 97 in the unirradiated condition are included. Crosshead speed of 1.0 mm/min corresponds to $4.8x10^{-3}$ 1/s strain rate.

4.3 Low cycle fatigue testing

The Influence of the high dose up to 70 dpa neutron irradiation on the isothermal, strain controlled LCF properties of RAFM steels is reported in the current section. The comparison with the corresponding results in the reference unirradiated state was performed both for the adequate total and inelastic strain amplitudes. In addition the comparison with the literature data will be given on availability. The Peak Stress vs. Number of Cycle diagrams for each investigated steel along with selected hysteresis loops can be found in Annex 11.

Fig. 4-27 shows total ($\Delta\varepsilon_{tot}$) strain range vs. the number of cycles to failure (N_f) in double logarithmic scale for EUROFER 97 in the unirradiated condition and after neutron irradiation in ARBOR 2 irradiation up to 71 dpa at 330-337 °C. For comparison the LCF properties from ARBOR 1 irradiation [9] are also included. The results in the reference unirradiated state are summarised in Table 4-2. The results after neutron irradiation in ARBOR 2 up to 47 and 71 dpa are given in Table 4-3 and Table 4-4, respectively. For the majority of the investigated EUROFER 97 specimens and for the total strain amplitudes between 0.8% and 1.1% the neutron irradiation has only a minor influence on the fatigue behaviour. In some cases a slight enhancement of the fatigue lifetime in comparison to the unirradiated state is observed. An exception is a specimen (E1 12) irradiated to 70.8 dpa at 334 °C and fatigue tested at $\Delta\varepsilon_{tot}$= 1.1% which shows a strongly reduced lifetime in comparison to the unirradiated state. The Peak Tensile and Peak Compression stresses for E1 12 were found to show non-monotonous evolution with a Number of Cycles (N), see Fig. 11-6, thus yielding strong variation of parameter R, defined as a ratio of Peak compression and Peak Tensile stresses within a cycle, during the measurement. Due to this reason the results on E1 12 as well as on the specimens exhibiting a nonmonotonous evolution of the peak stresses with a number of cycles should be taken into account with precautions during the analysis of the fatigue behaviour.

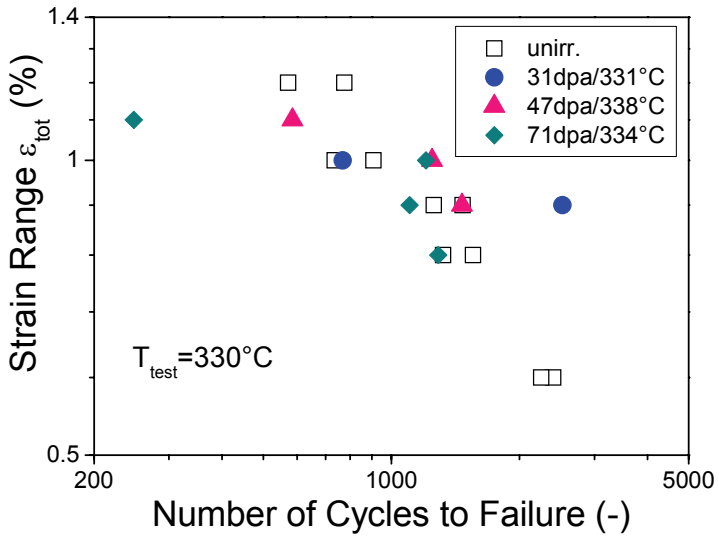

Fig. 4-27 Fatigue lifetime vs. total strain range for unirradiated and up to 71 dpa irradiated (T_{irr} = 331-338 °C) EUROFER 97 (980 °C/0.5 h + 760 °C/1.5 h).

Specimen	T_{test} (°C)	N_f (-)	ε_{tot} (%)	$\varepsilon_{inelastic}$ (%)
10	330	2400	0.6	0.27
11	330	2250	0.6	0.26
1	330	1556	0.8	0.42
5	330	1324	0.8	0.42
2	330	1470	0.9	0.54
6	330	1258	0.9	0.53
3	330	736	1.0	0.61
7	330	907	1.0	0.61
4	330	572	1.2	0.79
8	330	775	1.2	0.82

Table 4-2: LCF data on unirradiated EUROFER 97.

Specimen	T_{test} (°C)	N_f (-)	ε_{tot} (%)	$\varepsilon_{inelastic}$ (%)
E1 19	330	1247	1.0	0.48
E1 20	330	1467	0.9	0.44
E1 21	330	586	1.1	0.55

Table 4-3: LCF data on EUROFER 97 irradiated to 46.8 dpa at 337.5 °C.

Specimen	T_{test} (°C)	N_f (-)	ε_{tot} (%)	$\varepsilon_{inelastic}$ (%)
E1 10	330	1206	1	0.51
E1 11	330	1103	0.9	0.48
E1 12	330	248	1.1	0.57
E1 13	330	1289	0.8	0.32

Table 4-4: LCF data on EUROFER 97 irradiated to 70.8 dpa at 334.0 °C.

Fig. 11-107 and Fig. 11-108 show SEM micrographs of fracture surface of LCF tested E1 21 and E1 10 specimens. Specimen irradiation and LCF tested conditions are indicated in the corresponding figure legends. Remarkable is an appearance of course, three dimensional fracture surface morphology which is more pronounced at high irradiation dose. The fracture surface morphology reveals a terrace-like pattern due to multiple deflections of the fatigue crack along its propagation path. Formation of a thin, few µm thick modified surface layer which is supposed to develop in a corrosion process of a specimen being in contact with coolant during irradiation is recognizable for the both irradiation conditions. Noticeably such a layer was already observable after irradiation to 31 dpa in ARBOR 1 experiment [9]. The role of the detected few µm thick modified surface layer which can act as a preferable crack emitter should be analysed in more detail during microstructural analysis at KIT.

LCF properties of EUROFER 97 HT in the unirradiated condition and after neutron irradiation to a damage dose of 71 dpa are shown in Fig. 4-28. For comparison the results from ARBOR 1 irradiation are also included. The data in the reference unirradiated state are summarised in Table 4-5. The results after neutron irradiation in ARBOR 2 to 47 and 71 dpa are given in Table 4-6 and Table 4-7, respectively. The neutron irradiation has qualitatively different influence trends for 47 and 71 dpa irradiated EUROFER 97 HT for total strain amplitudes between 0.8% and 1.1%. The 47 dpa irradiated specimens show if any only slight decrease of the lifetime in comparison to the unirradiated state. The 71 dpa irradiated specimens show in contrast an increase of the lifetime for adequate total strain amplitudes.

Fig. 11-109 shows SEM micrographs of fracture surface of E2 12 (71 dpa/334 °C) after LCF test at $\Delta\varepsilon_{tot}$ = 0.9% at 330 °C. In addition to the features already observed for irradiated ERUOFER97 specimens, deep secondary cracks propagating into the axial directions can be identified. It has to be noted that such a pronounced modification of the fatigue fracture surface morphology does not show a clear effect on the fatigue lifetime. Indeed, 71 dpa irradiated E1 10 and E2 12 specimens showed fatigue lifetimes that are comparable to those of in the unirradiated state for the adequate inelastic strains, see Fig. 4-38.

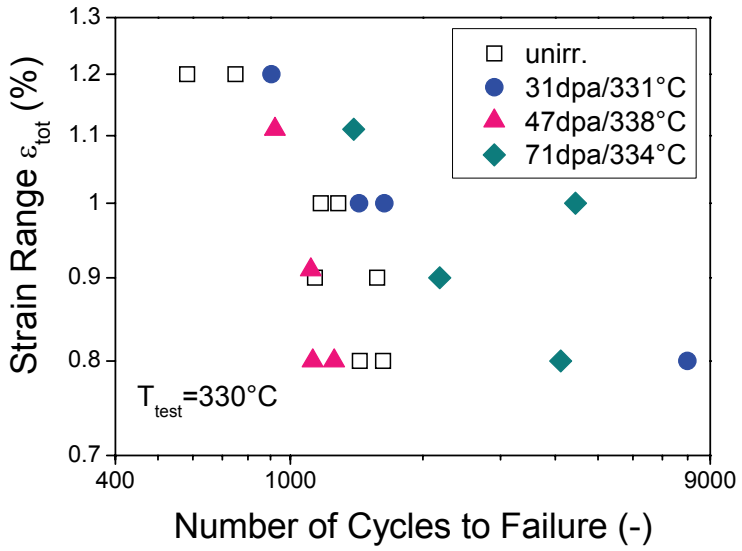

Fig. 4-28 Fatigue lifetime vs. total strain range for unirradiated and up to 71 dpa irradiated (T_{irr} = 331-338 °C) EUROFER 97 HT (1040 °C/38 min + 750 °C/2 h).

Specimen	T_{test} (°C)	N_f (-)	ε_{tot} (%)	$\varepsilon_{inelastic}$ (%)
1	330	1623	0.8	0.47
5	330	1438	0.8	0.46
6	330	1574	0.9	0.56
2	330	1137	0.9	-
7	330	1172	1.0	0.66
3	330	1285	1.0	0.66
4	330	582	1.2	0.84
8	330	750	1.2	0.86

Table 4-5: LCF data on unirradiated EUROFER 97 HT.

Specimen	T_{test} (°C)	N_f (-)	ε_{tot} (%)	$\varepsilon_{inelastic}$ (%)
E2 19	330	922	1.1	0.58
E2 20	330	1123	0.8	0.39
E2 21	330	1112	0.9	0.43
E2 22	330	1257	0.8	0.32

Table 4-6: LCF data on EUROFER 97 HT irradiated to 46.8 dpa at 337.5 °C.

Specimen	T_{test} (°C)	N_f (-)	ε_{tot} (%)	$\varepsilon_{inelastic}$ (%)
E2 10	330	1392	1.1	0.58
E2 11	330	4112	0.8	0.32
E2 12	330	2184	0.9	0.40
E2 13	330	4444	1.0	0.52

Table 4-7: LCF data on EUROFER 97 HT irradiated to 70.8 dpa at 334.0 °C.

Fig. 4-29 shows total strain range ($\Delta\varepsilon_{tot}$) vs. the number of cycles to failure (N_f) in double logarithmic scale for F82H-mod. in the unirradiated condition and after neutron irradiation in ARBOR 2 irradiation to 47 dpa at 337 °C. For comparison the LCF properties from ARBOR 1 irradiation [9] are also included. The data in the reference unirradiated state are summarised in Table 4-8. The results after neutron irradiation in ARBOR 2 to 46.8 dpa at 337.5 °C are shown in Table 4-9. The neutron irradiation of F82H-mod. to 47 dpa leads to the increase of the lifetime in comparison with unirradiated state for adequate total strain amplitudes. The SEM micrographs of the fatigue fracture surface of selected F82H-mod. specimens are summarised in Fig. 11-110, Fig. 11-111 and Fig. 11-112. A coarse terrace like fracture surface morphology is observed especially pronounced for F 13 specimen. Fatigue lifetime of F 13, however, fell in the lifetime scattering band for the unirradiated state thus indicating no clear effect of the fracture surface morphology on the lifetime.

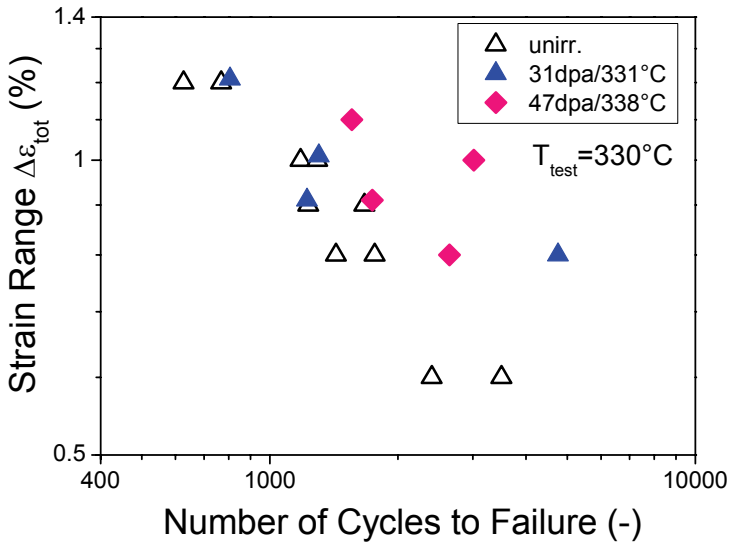

Fig. 4-29 Fatigue lifetime vs. total strain range for unirradiated and up to 47 dpa irradiated F82H-mod.

Specimen	T_{test} (°C)	N_f (-)	ε_{tot} (%)	$\varepsilon_{inelastic}$ (%)
11	330	2400	0.6	0.25
10	330	3500	0.6	0.27
1	330	1763	0.8	0.44
6	330	1430	0.8	0.45
7	330	1232	0.9	0.54
3	330	1668	0.9	0.52
4	330	1181	1.0	0.62
8	330	1293	1.0	0.62
5	330	627	1.2	0.83
9	330	768	1.2	0.80

Table 4-8: LCF data on unirradiated F82H-mod.

Specimen	T_{test} (°C)	N_f (-)	ε_{tot} (%)	$\varepsilon_{inelastic}$ (%)
F13	330	1740	0.9	0.43
F14	330	2643	0.8	0.37
F15	330	3013	1.0	0.57
F16	330	1558	1.1	0.63

Table 4-9: LCF data on F82H-mod. irradiated to 46.8 dpa at 337.5 °C.

LCF properties of OPTIFER IVc in the unirradiated condition and after neutron irradiation to 70.8 dpa at 334.0 °C are shown in Fig. 4-30. The results in the reference unirradiated and irradiated states are summarised in Table 4-10 and Table 4-11, respectively. With exception of one result the neutron irradiation leads to a considerable enhancement of lifetime which is more pronounced for the low total strain ranges. An outlier point was classified as invalid because the corresponding specimen was broken outside of a gauge length. Fig. 11-113 shows SEM micrographs of an irradiated specimen tested at $\Delta\varepsilon_{tot}$ =0.8%. A strongly inclined propagation of the fatigue crack as well as deep fatigue lines is identified.

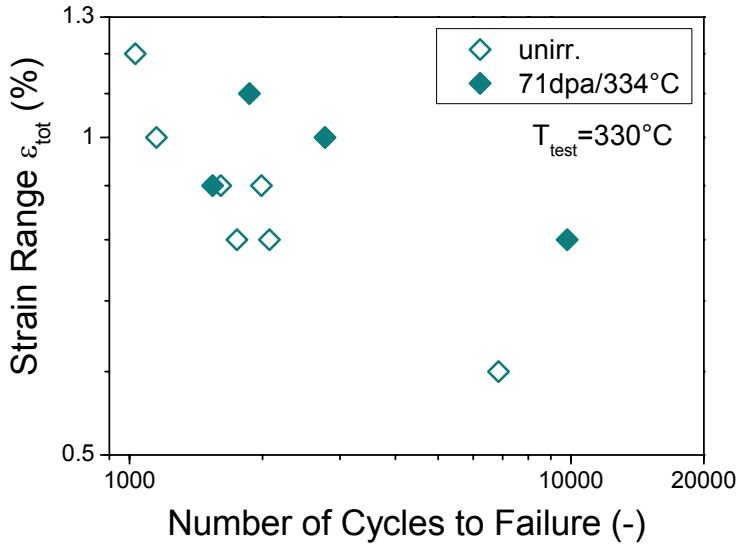

Fig. 4-30 Fatigue lifetime vs. total strain range for unirradiated and up to 71 dpa irradiated OPTIFER IVc.

Specimen	T_{test} (°C)	N_f (-)	ε_{tot} (%)	$\varepsilon_{inelastic}$ (%)
P1	300	6850	0.6	0.24
P2	330	1750	0.8	0.42
P3	330	1990	0.9	0.53
P4	330	1150	1	0.61
P5	330	1030	1.2	0.81
P6	330	2075	0.8	0.43
P7	330	1610	0.9	0.52

Table 4-10: LCF data on unirradiated OPTIFER IVc.

Specimen	T_{test} (°C)	N_f (-)	ε_{tot} (%)	$\varepsilon_{inelastic}$ (%)	
OT01	330	1542	0.9	0.36	invalid
OT02	330	9801	0.8	0.38	
OT03	330	2770	1.0	0.46	
OT04	330	1869	1.1	0.53	

Table 4-11: LCF data on OPTIFER IVc irradiated to 70.8 dpa at 334.0 °C.

Fig. 4-31 shows total ($\Delta\varepsilon_{tot}$) strain range vs. the number of cycles to failure (N_f) in double logarithmic scale for a British Steel batch of EUROFER 97 (BS-EUROF) after neutron irradiation to 46.8 dpa at 337.5 °C and to 70.8 at 334 °C. For comparison the results on the unirradiated EUROFER 97 are also presented. The results for irradiated BS-EUROF specimens are summarised in Table 4-12 and Table 4-13. For the most investigated specimens the neutron irradiation leads to the enhancement of the lifetime in comparison with the unirradiated EUROFER 97. This is especially pronounced for total strain amplitudes below 1.1% and 0.9% for 71 and 47 dpa irradiated states, respectively.

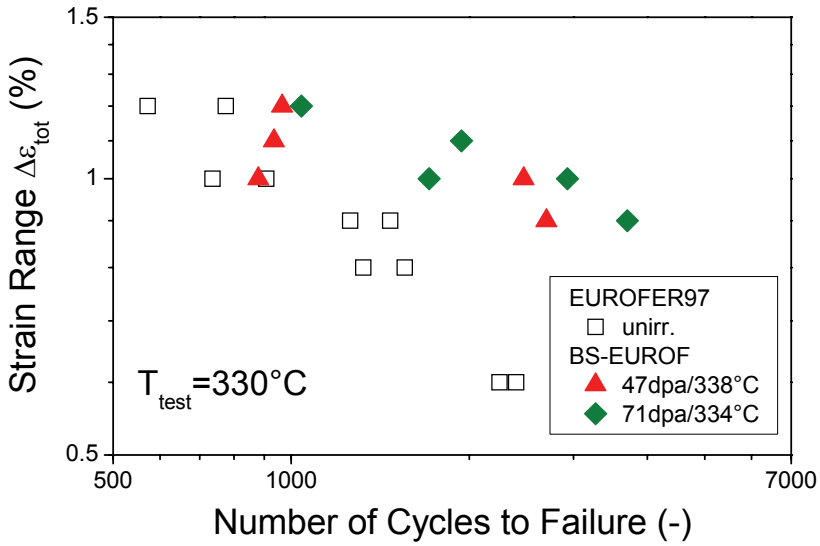

Fig. 4-31 Fatigue lifetime vs. total strain range for BS-EUROF after irradiation to damage doses of 47 and 71 dpa as well as for EUROFER 97 in the reference unirradiated state.

Specimen	T_{test} (°C)	N_f (-)	ε_{tot} (%)	$\varepsilon_{inelastic}$ (%)
A910	330	2470	1.0	0.52
A911	330	2700	0.9	0.5
A912	330	880	1.0	0.46
A913	330	935	1.1	0.64
A914	330	965	1.2	0.76

Table 4-12: LCF data on BS-EUROF irradiated to 46.8 dpa at 337.5 °C.

Specimen	T_{test} (°C)	N_f (-)	ε_{tot} (%)	$\varepsilon_{inelastic}$ (%)
A905	330	1710	1.0	0.48
A906	330	3700	0.9	0.39
A907	330	1940	1.1	0.59
A908	330	1040	1.2	0.66
A909	330	2930	1.0	0.51

Table 4-13: LCF data on BS-EUROF irradiated to 70.8 dpa at 334 °C.

Fatigue properties of EURODShip (EUROFER 97 with 0.5 wt.% Yttria) in the unirradiated state and after neutron irradiation to 46.8 dpa at 337.5 °C are presented in Fig. 4-32. The results for the unirradiated and irradiated conditions are summarised in Table 4-14 and Table 4-15. Neutron irradiation leads to a considerable lifetime enhancement for $\Delta\varepsilon_{tot}$ = 1.0%, so that one specimen even exhibited an endurance behaviour. A post irradiation annealing of one specimen at 550 °C for 3 hours lead to a substantially reduced lifetime being now slightly above the lifetime in the unirradiated state. The pronounced lifetime enhancement for $\Delta\varepsilon_{tot}$ = 1.0% is thus mainly related to the neutron irradiation induced material hardening. SEM micrographs of the fracture surface of EO 13 are shown in Fig. 11-114. The fracture surface appears relatively flat in comparison to non ODS RAFM steels indicating influence of the

ODS particles on the fatigue crack evolution. Fatigue striations bounded by fatigue lines observed in EUROFER 97 are no more recognizable in ODS steel.

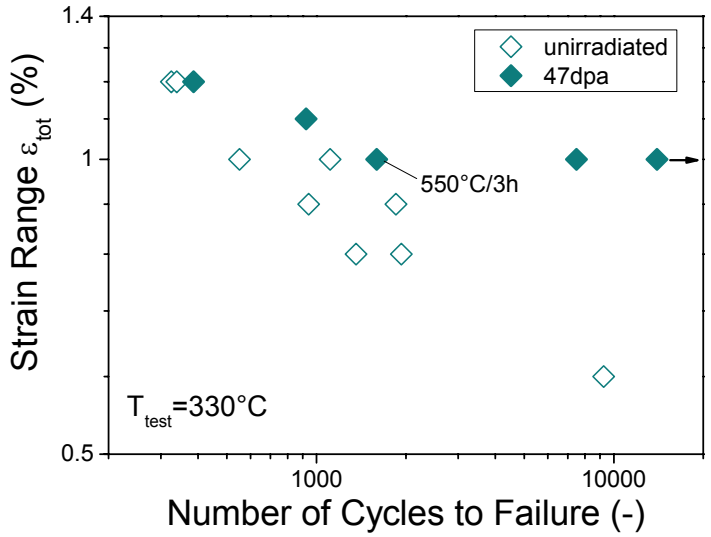

Fig. 4-32 Fatigue lifetime vs. total strain range for unirradiated and up to 46.8 dpa irradiated EURODSHIP (EUROFER 97 with 0.5 wt.% Yttria).

Specimen	T_{test} (°C)	N_f (-)	ε_{tot} (%)	$\varepsilon_{inelastic}$ (%)
1	330	1931	0.8	0.18
2	330	1850	0.9	0.21
3	330	551	1.0	0.28
4	330	325	1.2	0.42
5	330	1358	0.8	0.19
6	330	941	0.9	0.24
7	330	1112	1.0	0.26
8	330	339	1.2	0.45
9	330	9250	0.6	
12	330	9250	0.6	

Table 4-14: LCF data on unirradiated EURODSHIP (EUROFER 97 with 0.5wt.% Yttria).

Specimen	T_{test} (°C)	N_f (-)	ε_{tot} (%)	$\varepsilon_{inelastic}$ (%)	
EO11	330	13969	1.0	0.11	endurance
EO16	330	922	1.1	0.14	
EO13	330	386	1.2	0.25	
EO14	330	1595	1.0	0.20	PIA 550°C/3h
EO18	330	7490	1.0	0.19	

Table 4-15: LCF data on EURODSHIP (EUROFER 97 with 0.5 wt.% Yttria) irradiated to 46.8 dpa at 337.5 °C.

Fig. 4-33 shows total ($\Delta\varepsilon_{tot}$) strain range vs. the number of cycles to failure (N_f) in double logarithmic scale for ADS 2 in the unirradiated condition and after neutron irradiation to 70.8

dpa at 334 °C. The LCF test results are summarised in Table 4-16 and Table 4-17. The result obtained on A204 was interpreted as invalid as the specimen was broken outside the gauge length. Neutron irradiation leads to a considerable enhancement of the lifetime in comparison with the unirradiated state which is especially pronounced at low total strain ranges. So, for $\Delta\varepsilon_{tot}$ = 1.0% the Number of Cycles to Failure is about 10500 which is about ten-fold of lifetime in the reference unirradiated state. The reason for such a large lifetime is unknown. The role of approximately 24 appm extra helium in comparison to 71 dpa irradiated EUROFER 97 HT produced as a result of ^{10}B burn-up should be investigated in the future. Remarkably, similar to the observations for ADS 2 the lifetime of to 71 dpa irradiated EUROFER 97 HT was also quite large for a total strain rate of 1.0%. Some of the ADS 2 specimens exhibited non monotonous evolution of the peak stress with the Number of Cycles, see Annex 11. Whether such behaviour reflects intrinsic material response to cycling loading, is not clear. Due to variation of the parameter R from its target values, however, the experiments with a non- monotonous evolution of the peak stresses with the Number of Cycles have to be treated with precautions during the analysis of the material irradiation response.

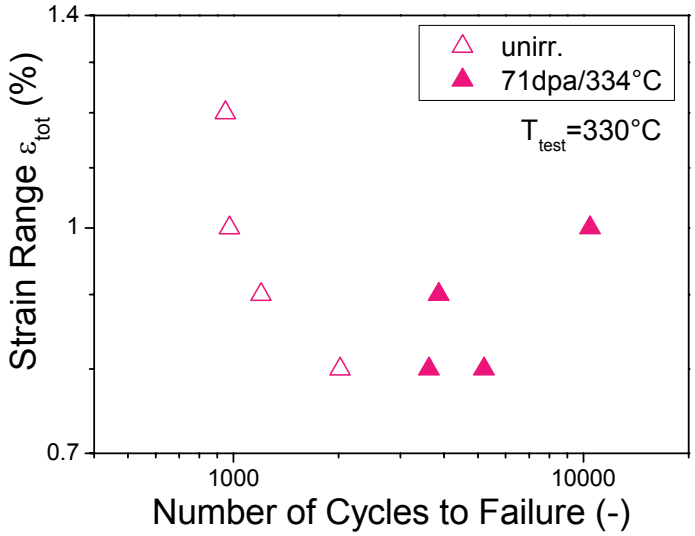

Fig. 4-33 Fatigue lifetime vs. total strain range for unirradiated and to 71dpa irradiated ADS2.

Specimen	T_{test} (°C)	N_f (-)	ε_{tot} (%)	$\varepsilon_{inelastic}$ (%)
P1	330	950	1.2	0.82
P2	330	975	1.0	0.65
P3	330	1200	0.9	0.54
P4	330	2020	0.8	0.42

Table 4-16: LCF data on unirradiated ADS 2.

Specimen	T_{test} (°C)	N_f (-)	ε_{tot} (%)	$\varepsilon_{inelastic}$ (%)	
A204	330	5202	0.8	0.26	invalid
A205	330	10459	1.0	0.46	
A206	330	3621	0.8	0.26	
A207	330	3863	0.9	0.40	

Table 4-17: LCF data on ADS 2 irradiated to 70.8 dpa at 334 °C.

Fatigue properties of ADS 3 in the unirradiated state and after neutron irradiation to 70.8 dpa at 334 °C are presented in Fig. 4-34 and in Table 4-18 and Table 4-19. Neutron irradiation leads to a strong lifetime increase in comparison with the unirradiated state being pronounced for the low total strain ranges. It has to be noted that at $\Delta\varepsilon_{tot}$ =0.9% tested specimens showed non monotonous evolution of the peak stresses with the Number of Cycles.

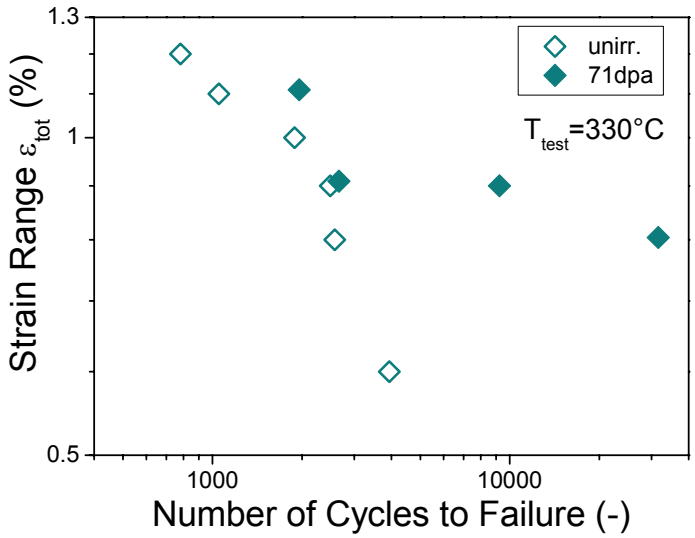

Fig. 4-34 Fatigue lifetime vs. total strain range for unirradiated and to 71 dpa irradiated ADS 3.

Specimen	T_{test} (°C)	N_f (-)	ε_{tot} (%)	$\varepsilon_{inelastic}$ (%)
P1	330	780	1.2	0.83
P2	330	1890	1.0	0.62
P3	330	2490	0.9	0.52
P4	330	2580	0.8	0.45
P5	330	3940	0.6	0.45
P6	330	1050	1.1	0.72

Table 4-18: LCF data on unirradiated ADS 3.

Specimen	T_{test} (°C)	N_f (-)	ε_{tot} (%)	$\varepsilon_{inelastic}$ (%)
A304	330	31610	0.8	0.35
A305	330	1957	1.1	0.59
A306	330	2665	0.9	0.46
A307	330	9234	0.9	0.41

Table 4-19: LCF data on ADS 3 irradiated to 70.8 dpa at 334 °C.

Fig. 4-35 shows total ($\Delta\varepsilon_{tot}$) strain range vs. the number of cycles to failure (N_f) in double logarithmic scale for ADS 4 in the unirradiated condition and after neutron irradiation to 46.8 dpa at 337.5 °C. The LCF test results are summarised in Table 4-20 and Table 4-21. The investigation of the effect of the 1120 wppm bor on the microstructure of ADS 4 performed in [19] revealed strong degradation of the microstructure, characterized by a presence of high

density of coarse Fe, Cr and B rich inclusions. This might be an explanation of rather unusual LCF behaviour of ADS 4 already in the unirradiated condition, namely for all investigated specimens the initial softening phase was followed by pronounced continuous hardening phase in contrast to the observations for martensitic steels where a continuous softening phase is identified. Remarkably, the continuous hardening phase was not observed for the irradiated specimens. The irradiated specimens showed, with exception of one specimen, pronounced lifetime increase in comparison to the unirradiated state. A specimen tested at 0.8% exhibited even endurance behaviour.

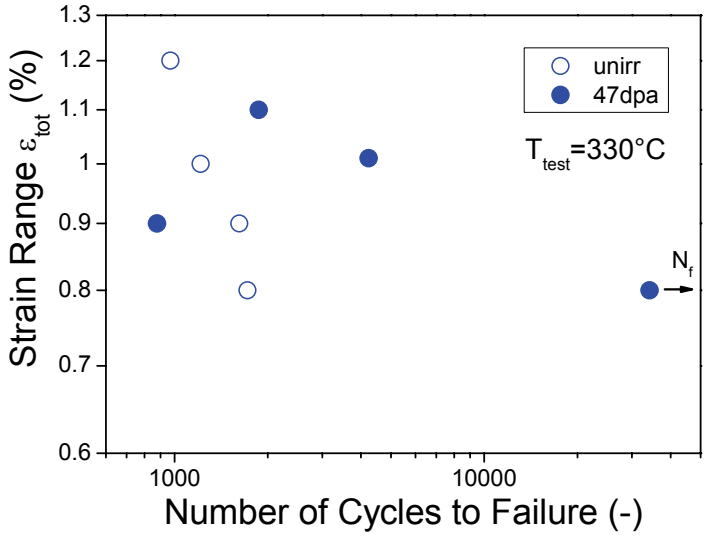

Fig. 4-35 Fatigue lifetime vs. total strain range for unirradiated and to 47 dpa irradiated ADS 4.

Specimen	T_{test} (°C)	N_f (-)	ε_{tot} (%)	$\varepsilon_{inelastic}$ (%)
P1	330	970	1.2	0.75
P2	330	1215	1.0	0.56
P3	330	1620	0.9	0.46
P4	330	1720	0.8	0.34

Table 4-20: LCF data on unirradiated ADS4.

Specimen	T_{test} (°C)	N_f (-)	ε_{tot} (%)	$\varepsilon_{inelastic}$ (%)
A404	330	34199	0.8	0.34
A405	330	4239	1.0	0.41
A406	330	879	0.9	0.31
A407	330	1869	1.1	0.43

Table 4-21: LCF data on ADS4 irradiated to 46.8 dpa at 337.5 °C.

Fatigue properties of EB welded EUROFER 97 after irradiation to a damage dose of 70.1 dpa at 331.5 °C are shown in Fig. 4-36. For comparison the lifetime data obtained on base EUROFER 97 steel in unirradiated condition is also included. The LCF test results on EUROF-EB are summarised in Table 4-22. Irradiated EUROF-EB specimens show fatigue life-

times that are comparable with those of base EURFER97 steel in the reference unirradiated state.

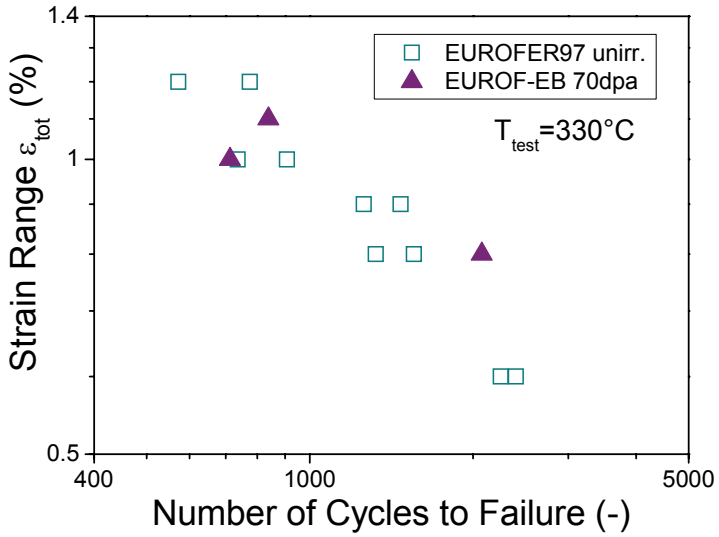

Fig. 4-36 Fatigue lifetime vs. total strain range for 70 dpa irradiated EB welded EUROFER 97 (EUROF-EB) and for unirradiated reference ERUOFER97.

Specimen	T_{test} (°C)	N_f (-)	ε_{tot} (%)	$\varepsilon_{inelastic}$ (%)
C098	330	713	1.0	0.41
C099	330	2077	0.8	0.20
C100	330	839	1.1	0.53

Table 4-22: LCF data on EUROF-EB irradiated to 70.1 dpa at 331.5 °C.

4.3.1 Discussion of LCF behaviour

Prior to discussion of the influence of the neutron irradiation on the LCF properties the effect of application of Small Specimen Testing Technology (SSTT) should be addressed. Fig. 4-37 shows total ($\Delta\varepsilon_{tot}$) strain range vs. the number of cycles to failure (N_f) in double logarithmic scale for EUROFER 97 in the unirradiated condition and after neutron irradiation in ARBOR 2 programme up to 71 dpa at 330-337 °C [29]. For comparison 31 dpa data from ARBOR 1 [9] as well as 2 dpa data from SOSIA-02 (NRG) [23] are also included. In SOSIA-02 programme LCF specimens of 3 mm diameter and 7.5 mm gauge length were irradiated at 300 °C. Afterwards, those specimens were tested at 300 °C. Comparison of the results obtained in the reference unirradiated state by using SSTT (KIT) and larger (NRG) specimens indicates considerable underestimation of the fatigue lifetime by SSTT. The state of the surface finish quality and its possibly different influence on the fatigue lifetime of the SSTT specimens in the unirradiated and irradiated conditions need to be investigated in more details for the unambiguous interpretation of the irradiation influence on the fatigue behaviour. The dashed dotted line in Fig. 4-37 is reproduced from [30] and represents model prediction of lifetime in the reference unirradiated state at a test temperature of 330 °C. The model gives a right bound of the lifetime obtained in the unirradiated state on 3 mm specimens in [23].

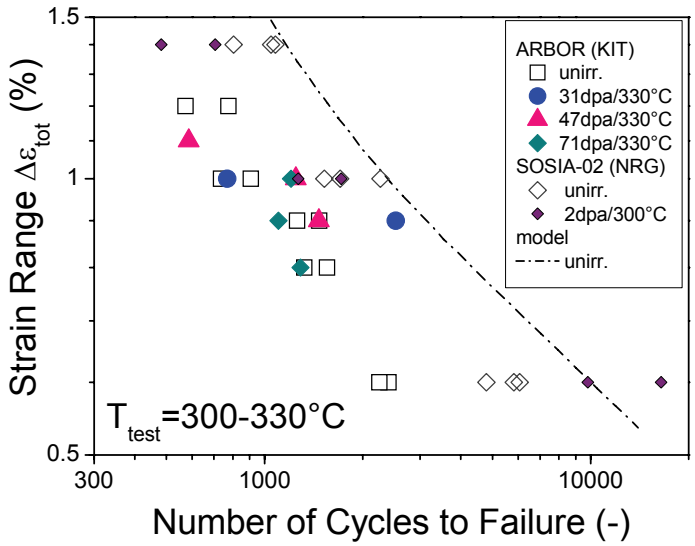

Fig. 4-37 Fatigue lifetime for unirradiated and up to 71 dpa irradiated (T_{irr} = 300-337 °C) EUROFER 97 vs. total strain range [29]. 2 dpa data stems from SOSIA-02 (NRG) irradiation [23]. The dashed line represents the model description of the unirradiated data [30].

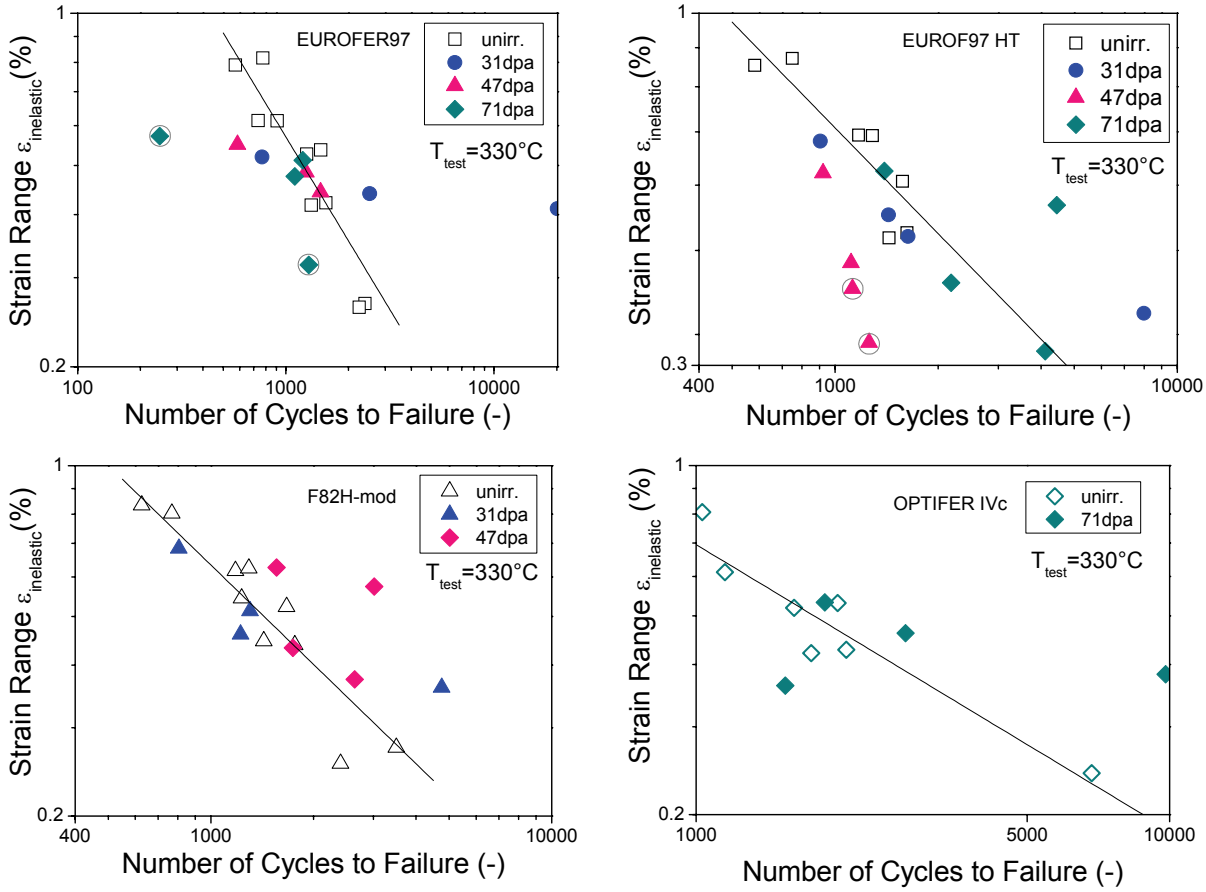

Fig. 4-38 Fatigue lifetime vs. inelastic strain range for selected unirradiated and irradiated RAFM steels. The circled points are obtained on the specimens exhibiting strongly non-monotonous evolution of peak tensile and compression stresses with Number of Cycles. The solid lines represent the description of the unirradiated data by a Manson-Coffin relation.

The neutron irradiation leads to the increase of fatigue lifetime for the majority of the investigated SSTT type RAFM specimens in comparison to the reference unirradiated state for comparable total strain amplitudes especially pronounced at low total strains. For quantification of the role of the neutron irradiation induced hardening and resulted increase of the elastic strain amplitude for given total strains, the inelastic strain amplitudes were quantified near a cycle $N_f/2$. Fig. 4-38 shows fatigue lifetime vs. inelastic strain range for selected RAFM steels. The data points obtained on the specimens exhibiting strongly non-monotonous evolution of peak tensile and compression stresses with Number of Cycles and hence strongly varying parameter $R = \sigma_{min}/\sigma_{max}$ are circled and will not be taken into account during the following discussions.

In the low cycle fatigue regime the evolution of the fatigue life with inelastic strain can be described by the Manson-Coffin relationship

$$\Delta\varepsilon_{inelastic} = CN_f^m \qquad (4)$$

with *m* and *C* as material and temperature dependent parameters. The solid lines in Fig. 4-38 represent the description of the unirradiated data with the above equation. The best fits were obtained with *m* = -0.68, -0.52, -0.66 and -0.57 for EUROFER 97, EUROFER 97 HT, F82H-mod. and OPTIFER IVc steels, respectively. For adequate inelastic strain amplitudes and for the SSTT used in the current work part of the irradiated data are scattered around the unirradiated ones. Considering the large inherent scattering of fatigue lifetime this indicates little or no influence of the neutron irradiation on the fatigue damage evolution. The apparent increase of the fatigue lifetime observed in corresponding $\Delta\varepsilon_{tot}(N_f)$ representation is thus mainly related to the irradiation hardening revealed in monotonic tensile experiments. Comparatively, in [31] the influence of the low temperature neutron irradiation (3.8 dpa at 250 °C) on the fatigue behaviour of F82H was found to be sensitive to the test temperature. The fatigue tests at 250 °C yielded comparable results for the unirradiated and irradiated specimens for adequate inelastic strain amplitudes, whereas a strong reduction of the lifetime in the irradiated condition was found in a RT test at a low total strain range (of 0.4%) attributed to the occurrence of a channel fracture.

Noticeable reduction of the fatigue lifetime of some EUROFER 97 and EUROFER 97 HT specimens after irradiation to 47 dpa more pronounced at high (and sometimes intermediate) strain ranges in comparison to the unirradiated state indicates, however, that the inelastic strain amplitude is not the only controlling parameter for the fatigue damage accumulation. The neutron irradiation induced stress increase in comparison to the unirradiated state for adequate inelastic strain amplitudes [29], might also accelerate the fatigue damage evolution [30],[32].

Though lifetime enhancement in the irradiated state at low total strain ranges is attributed to strongly reduced inelastic strain amplitude, the reason for lifetime enhancement observed for some specimens at relatively high inelastic strain ranges, see e.g. F82H-mod., is not fully understood.

Accumulated helium contents up to 1135 appm (1142 appm total) seems to have no negative effect on the specimen lifetime. Indeed, part of helium containing specimens exhibits lifetimes far above the lifetimes observed for irradiated base EUROFER 97 steel.

Fractographic investigations of the fatigue tested irradiated specimens do not yield clear correlation between the fracture surface morphology and mechanical properties. Though irradiation damage remarkably modifies the fracture surface morphology, appearance of a complex, three dimensional fracture surfaces, initiation of the secondary cracks propagating into axial direction, considerable coarsening of the fracture surface morphology with increasing the irradiation dose, do not show clear effects on the fatigue lifetime. Which role the detected few µm thick modified surface layer that is supposed to be generated during the sodium contact of the specimen during irradiation campaign, is playing should be analysed in more detail during microstructural analysis at KIT.

5 Conclusion

Impact, tensile and LCF properties were studied for eleven RAFM steels and two technological specimens after neutron irradiation to displacement damage doses up to 71 dpa at 330-337 °C by using SSTT.

Neutron irradiation leads to severe degradation of the impact and tensile properties of the RAFM steels at irradiation temperatures below $T_{irr} \leq$300-340 °C. Neutron irradiation-induced hardening and embrittlement indicate saturating behaviour at the achieved damage doses for these low irradiation temperatures. The evolution of hardening with irradiation dose can be qualitatively described by using Whapham and Makin's model. Ongoing and planned quantitative microstructural investigations are mandatory to get deeper insight in the radiation damage mechanisms and for a quantitative description of the neutron irradiation induced hardening and embrittlement within appropriate models.

The neutron irradiation induced hardening may differently affect the fatigue behaviour of the irradiated specimens. The increase of the elastic part of the cyclic deformation and related reduction of the inelastic strain amplitude due to irradiation induced hardening lead to the increase of the fatigue lifetime especially at low strain ranges. The radiation hardening induced increase of the stress level might, however, lead to enhanced damage evolution and hence to lifetime reduction especially at high strain ranges. The limited number of available irradiated specimens does not allow detailed statistical analysis of the LCF results emphasizing a need for further investigations.

Due to absence of fusion relevant neutron spectrum the effects of Helium could not be appropriately studied in fission reactor experiments. The boron doping technique used in the current irradiation programme provides, however, valuable insight into helium effects for low helium contents. Helium contents of about 120 appm have already strong effect on the material embrittlement but only minor effect on the material hardening and LCF behaviour.

The state-of-the-art structural materials are highly suited for the special fusion reactor design with the operating temperature range for the FW and BB being between 350 and 550 °C. The

thermal recovery experiments yielded very promising results. After possible validation of this method through the study of the repeatability of these experiments, recovery heat-treatments can also be utilized for extension of the operating temperature range down to RT.

Acknowledgement

The authors thank A. Povstyanko, V. Prokhorov, A. Fedoseev, O Makarov and all other staff members of RIAR, who were involved in the ISTC Partner Project #2781p, for the highly qualified performance of the PIE at the hot laboratory of RIAR.

M. Walter, B. Dafferner, U. Bürkle and M. Klotz are acknowledged for performing the cold reference experiments.

6 References

[1] A. Möslang, E. Diegele, M. Klimiankou, R. Lässer, R. Lindau, E. Lucon, E. Materna-Morris, C. Petersen, R. Pippan, J.W. Rensman, M. Rieth, B. van der Schaaf, H.-C. Schneider and F. Tavassoli, Towards reduced activation structural materials data for fusion DEMO reactors, Nucl. Fusion 45 (2005) 649-655.

[2] M. Rieth, B. Dafferner, H. Ries, O. Romer, Bestrahlungsprogramm MANITU: Ergebnisse der Kerbschlagbiegeversuche mit den bis 0,8 dpa bestrahlten Werkstoffen der ersten Bestrahlungsphase, Forschungszentrum Karlsruhe, FZKA 5619, September 1995.

[3] M. Rieth, B. Dafferner, H.-D. Röhrig, Charpy impact properties of low activation alloys for fusion applications after neutron irradiation, Journal of Nuclear Materials 233-237 (1996) 351-355.

[4] M. Rieth, B. Dafferner, H. Ries, O. Romer, Bestrahlungsprogramm MANITU: Ergebnisse der Kerbschlagbiegeversuche mit den bis 0,2 dpa bestrahlten Werkstoffen, Forschungszentrum Karlsruhe, FZKA 5750, April 1997.

[5] M. Rieth, B. Dafferner, H.-D. Röhrig, Embrittlement behaviour of different international low activation alloys after neutron irradiation, J. Nucl. Mater. 258-263 (1998) 1147-1152.

[6] H.-C. Schneider, M. Rieth, B. Dafferner, H. Ries, O. Romer, Bestrahlungsprogramm MANITU: Ergebnisse der Kerbschlagversuche mit den bis 0,8 dpa bestrahlten Werkstoffen der zweiten Bestrahlungsphase, Forschungszentrum Karlsruhe, FZKA 6519, September 2000.

[7] E. Gaganidze, B. Dafferner, H. Ries, R. Rolli, H.-C. Schneider, J. Aktaa, Irradiation Programme HFR Phase IIb (SPICE), Impact testing on up to 16.3 dpa irradiated

RAFM steels, Forschungszentrum Karlsruhe, FZKA 7371, April 2008.

[8] E. Materna-Morris, A. Möslang, S. Baumgärtner, B. Dafferner, J. Ehrmann, E. Gaganidze, M. Holzer, S. Lautensack, H. Ries, R. Rolli, H.-C. Schneider, and H. Zimmermann, Irradiation Programme HFR IIb (SPICE-T), Post-Irradiation Examinations after 16.3 dpa, Tensile Properties, Fatigue Properties, Fractography and Structure Analysis after Charpy and Tensile Tests, Internal FZKA Report FUSION 323, Dec. 2008.

[9] C. Petersen, Post irradiation examination of RAFM steels after fast reactor irradiation up to 33 dpa and < 340°C (ARBOR 1), Karlsruher Institut für Technologie, FZKA 7517, 2010.

[10] H.-C. Schneider, B. Dafferner, J. Aktaa, Embrittlement behaviour of different international low activation alloys after neutron irradiation, J. Nucl. Mater. 295 (2001) 16-20.

[11] H.-C. Schneider, B. Dafferner, J. Aktaa, Embrittlement behaviour of low-activation alloys with reduced boron content after neutron irradiation, J. Nucl. Mater. 321 (2003) 135-140.

[12] E. Gaganidze, H.-C. Schneider, B. Dafferner, J. Aktaa, J. Nucl. Mater. 355 (2006) 83.

[13] C. Petersen, A. Povstyanko, V. Prokhorov, A. Fedoseev, O. Makarov, B. Dafferner, Impact property degradation of ferritic/martensitic steels after the fast reactor irradiation ‘ARBOR 1’, J. Nucl. Mater. 367–370 (2007) 544–549.

[14] C. Petersen, A. Povstyanko, V. Prokhorov, A. Fedoseev, O. Makarov, M. Walter, Tensile and low cycle fatigue properties of different ferritic/martensitic steels after the fast reactor irradiation ‘ARBOR 1’, J. Nucl. Mater. 386-388 (2009) 299-302.

[15] E. Gaganidze, H.-C. Schneider, C. Petersen, J. Aktaa, A. Povstyanko, V. Prokhorov, R. Lindau, E. Materna-Morris, A. Möslang, E. Diegele, R. Lässer, B. van der Schaaf, E. Lucon, Proc. of 22st IAEA Fusion Energy Conference, 13-18 October 2008 Geneva, Switzerland; Paper FT/P2-1.

[16] E. Gaganidze, H.-C. Schneider, B. Dafferner, J. Aktaa, J. Nucl. Mater. 367-370 (2007) 81.

[17] E. Gaganidze, C. Petersen, E. Materna-Morris, C. Dethloff, O. J. Weiß, J. Aktaa, A. Povstyanko, A. Fedoseev, O. Makarov, V. Prokhorov, Mechanical properties and TEM examination of RAFM steels irradiated up to 70 dpa in BOR-60, to be published in J. Nucl. Mater. 2011

[18] R. Lindau, A. Moeslang, M. Schirra, P. Schlossmacher, M. Klimenkov, Mechanical and microstructural properties of a hipped RAFM ODS-steel, Journal of Nuclear Materials 307-311 (2002) 769-772.

[19] P. Graf et al., Der Einfluss von Bor auf die Gefügeeigenschaften von martensitischen 9%-Chromstählen, P. Portella [Hrsg.], Fortschritte in der Metallographie: Vortragstexte der 37.Metallographie-Tagung, Berlin, 17.-19. September 2003; Sonderbände der Metallographie 35, 2004, S71-76.

[20] A.I.Tellin, D.K.Ryazanov, N.V. Markina, G.I. Gadzhiev, Experimental Study of Space-Energy Neutron Distribution in the BOR-60 Reactor, Preprint RIAR-1(853), Dimitrovgrad, 1996 (in Russian).

[21] Greenwood and R. K. Smither, SPECTER: Neutron Damage Calculations for Materials Irradiations, ANL/FPP/TM-197, 1985.

[22] E. Gaganidze, J. Aktaa, Fusion Engineering and Design 83 (2008) 1498-1502.

[23] J. Rensman, NRG Irradiation Testing: Report on 300 °C and 60 °C Irradiated RAFM Steels, Petten 2005, 20023/05.68497/P.

[24] H. Tanigawa et al., J. Nucl. Mater. 367-370 (2007) 42-47.

[25] A. Alamo et al., Mechanical properties of 9Cr martensitic steels and ODS-FeCr alloys after neutron irradiation at 325 °C up to 42 dpa, J. Nucl. Mater. 367-370 (2007) 54-59.

[26] E. Lucon, W. Vandermeulen, Overview of the tensile properties of EUROFER in the unirradiated and irradiated conditions, J. Nucl. Mater. 386-388 (2009) 254-256.

[27] H. Tanigawa et al., J. Nucl. Mater. 386-388 (2009) 231-235.

[28] A. D. Whapham, M. J. Makin, Phil. Mag. 5, 51 (1960) 237-250.

[29] E. Gaganidze, C. Petersen, J. Aktaa, A. Povstyanko, V. Prokhorov, E. Diegele, R. Lässer, Low Cycle Fatigue Properties of Reduced Activation Ferritic/Martensitic Steels after High Dose Neutron Irradiation, Proc. of 23rd IAEA Fusion Energy Conference, 11-16 October 2010, Daejeon, Korea; Paper FTP/3-4Rb.

[30] J. Aktaa, C. Petersen, ICFRM 14, Sapporo, Japan, 2009, accepted for publication in J. Nucl. Mater. (2010).

[31] Y. Miwa, S. Jitsukawa, M. Yonekawa, J. Nucl. Mater. 329-333 (2004) 1098-1102.

[32] J. Aktaa, R. Schmitt, Fus. Eng. Des. 81 (2006) 2221-2231.

7 Annex: Material Chemical Composition and Thermal Treatment

Material	Heat	Cr	C	Si	Mn	P	S	Mo	Ni	Al	B	Cu	N	Nb	Ti	V	W	Ta
EUROF 1 (=EUROFER 97)	E83697	8.93	0.12	0.06	0.47	<0.005	0.004	0.0015	0.022	0.008	<0.001	0.0036	0.018	0.0022	0.009	0.2	1.07	0.14
EUROF 2 (=EUROFER 97 HT)	E83697	8.93	0.12	0.06	0.47	<0.005	0.004	0.0015	0.022	0.008	<0.001	0.0036	0.018	0.0022	0.009	0.2	1.07	0.14
F82H mod.	9753	7.89	0.09	0.08	0.1	0.003	0.001	0.003	0.02	0.001	0.0002	0.01	0.006	0.0002	0.004	0.19	1.99	0.02
OPTiFER IVc	986779	9.35	0.12	0.022	0.54	0.004	0.003	<0.002	0.0073	<0.0005	<0.004	0.0019	0.05	<0.0006	<0.0004	0.26	1.03	0.07
OPTIFER XI	847	10.1	0.1	0.035	0.532	0.001	0.0015	0.005	0.005	-	0.0008	-	0.0405	0.001	0.001	0.200	1.11	0.055
OPTIFER XII	848	10.65	0.11	0.153	0.464	0.0012	0.0015	-	-	-	0.0008	-	0.051	-	-	0.195	1.13	0.070
BS-EUROF	VS3102	9.03	0.094	0.05	0.42	<0.005	0.005	<0.02	<0.02	0.009	<0.001	<0.02	0.027	<0.02	<0.02	0.19	1.14	0.08
ADS 2	806	9.31	0.109	0.02	0.602	0.0035	0.003	0.002	0.005	0.001	0.0082	0.005	0.021	0.005	0.001	0.19	1.27	0.055
ADS 3	826	8.8	0.095	0.031	0.395	0.0024	0.003	0.046	0.008	0.004	0.0083	0.006	0.028	0.005	0.001	0.193	1.125	0.088
ADS 4	825	9.0	0.1	0.03	0.38	0.001	0.0025	0.028	0.006	0.004	0.112	0.005	0.0255	0.002	0.001	0.197	1.06	0.08
EURODShip = EUROFER 97 + 0.5% Y_2O_3	HXN 958/3	8.94	0.11	0.08	0.37	0.007	0.004	0.007	0.03	0.01	<0.001	0.018	0.027	0.001	0.006	0.19	1.07	0.87
ODShip 3 = EUROFER 97 + 0.3 wt.% Y_2O_3	HXN 954/4-3	8.94	0.11	0.08	0.37	0.007	0.004	0.007	0.03	0.01	<0.001	0.018	0.027	0.001	0.006	0.19	1.07	0.87
EUROF-EB	E83697	8.93	0.12	0.06	0.47	<0.005	0.004	0.0015	0.022	0.008	<0.001	0.0036	0.018	0.0022	0.009	0.2	1.07	0.14
FZK D.W.	E83697	8.93	0.12	0.06	0.47	<0.005	0.004	0.0015	0.022	0.008	<0.001	0.0036	0.018	0.0022	0.009	0.2	1.07	0.14

Table 7-1: Material chemical composition in wt.% (Fe balance).

E83697	EUROF 1 = EUROFER 97 (980°C 31 min/air + 760°C 90 min/air)
E83697	EUROF 2 = EUROFER 97 HT (1040°C 31 min/air + 760°C 90 min/air)
9753	F82H mod. = F82H mod. (1040°C 38 min/air + 750°C 120 min/air)
986779	OPT IVc = OPTIFER IVc (950°C 30 min/air + 750°C 120 min/air)
806	ADS 2 = EUROFER 97-Steel with 82 wppm nat. B (1040°C 31 min/air + 760°C 90 min/air)
826	ADS 3 = EUROFER 97-Steel with 83 wppm B10 (1040°C 31 min/air + 760°C 90 min/air)
825	ADS 4 = EUROFER 97-Steel with 1160 wppm B10 (1040°C 31 min/air + 760°C 90 min/air)
HXN 958/3	EURODShip = EUROFER 97 with 0.5wt.% Yttria ODS (980°C 31 min/air + 760°C 90 min/air)
VS3102	BS-EUROF = EUROFER 97 (1050°C 60 min/air + 750°C 120 min/air)
E83697	EUROF-EB = EUROFER 97, EB welded (post weld heat treatment 730°C 120 min/air)
847	OPT XI = OPTIFER XI (980°C 30 min/air + 750°C 120 min/air)
HXN 954/4-3	EODShip 3 = EUROFER 97 with 0.3wt% Yttria ODS (980°C 31 min/air + 760°C 90 min/air)
E83697	FZK DW = FZK Diffusion Welded EUROF 1 (post weld heat treated: 750°C 120 min/air)
848	OPT XII = OPTIFER XII (950°C 30 min/air + 750°C 120 min/air)

Table 7-2: Heat identification and thermal treatment.

8 Annex: Test Conditions for PIE of ARBOR 2

FZK Pre-irr.	Test Temp.	FZK Pre-irr.	Test Cond.	FZK Pre-irr.	Test Temp.	FZK Pre-irr.	Test Temp.	FZK new	Test Temp.	FZK Pre-irr.	Test Cond.	FZK new	Test Temp.	FZK new	Test Temp.	FZK new	Test Temp.
capsule 3	°C	capsule 5	°C / %	capsule 6	°C	capsule 7	°C	capsule 8	°C	capsule 9	°C / %	capsule 9a	°C	capsule 10	°C	capsule 11	°C
Tensile		LCF		Impact		Impact		Mixed		LCF		Mixed		Mixed		Impact	
E 1 06	350	E 1 10	330 / 1.0	E 1 08	300	E 1 16	120	T: EH1 01	300	E 1 19	330 / 1.0	Ch: 11 09	100	C: E 138	no test	C: EF12 01	150
E 1 07	/ 350	E 1 11	330 / 0.9	E 1 09	200	E 1 17	140	T: EH1 02	300	E 1 20	330 / 0.9	Ch: 11 10	80	C: E 139	no test	C: EF12 02	300
E 1 08	20	E 1 12	330 / 1.1	E 1 10	170	E 1 18	170	T: EH1 03	20	E 1 21	330 / 1.1	Ch: 11 11	120	C: E 140	no test	C: EF12 03	100
E 1 09	// 350	E 1 13	330 / 0.8	E 1 11	140	E 1 19	150	T: EH1 04	/300	E 1 22	330 / 0.8	Ch: 11 12	60	C: E 141	no test	C: EF12 04	220
E 2 06	350	E 1 14	no test	E 1 12	120	E 1 20	160	T: EH1 05	20	E 1 23	no test	Ch: 11 13	200	C: E 142	no test	C: EF22 01	130
E 2 07	/ 350	E 2 10	330 / 1.1	E 1 13	130	E 1 21	200	T: EH1 06	300	E 2 19	330 / 1.1	Ch: 11 14	no test	C: E 143	no test	C: EF22 02	180
E 2 08	20	E 2 11	330 / 0.8	E 1 14	150	E 1 22	no test	T: EH1 07	20	E 2 20	330 / 0.8	Ch: 11 15	no test	C: E 144	no test	C: EF22 03	no test
E 2 09	no test	E 2 12	330 / 0.9	E 1 15	160	E 2 17	140	T: EH1 08	20	E 2 21	330 / 0.9	Ts: 11 06	20	C: E 145	no test	C: EF22 04	no test
F 06	350	E 2 13	330 / 1.0	E 2 09	120	E 2 18	130	T: EH1 00	300	E 2 22	330 / 0.8	Ts: 11 07	350	C: 11 01	120	C: A1	no test
F 07	/ 350	E 2 14	no test	E 2 10	140	E 2 19	110	T: EH1 10	300	E 2 23	no test	Ts: 11 08	/ 350	C: 11 02	140	C: A2	no test
F 08	20	A 2 04	330 / 0.8	E 2 11	160	E 2 20	150	T: EH1 11	20	F 13	330 / 0.9	Ch: 12 01	100	C: 11 03	160	C: A3	no test
F 09	no test	A 2 05	330 / 1.0	E 2 12	150	E 2 21	/ -30	T: EH1 12	no test	F 14	330 / 0.8	Ch: 12 02	80	C: 11 04	no test	C: A4	no test
E O 02	350	A 2 06	330 / 0.8	E 2 13	/ 20	E 2 22	no test	T: EH1 13	no test	F 15	330 / 1.0	Ch: 12 03	120	C: 11 05	180	C: A5	no test
E O 04	/ 350	A 2 07	330 / 0.9	E 2 14	/ -20	E 2 23	/ 0	T: EH1 14	no test	F 16	330 / 1.1	Ch: 12 04	60	C: 11 06	no test	C: A6	no test
E O 07	20	A 2 08	no test	E 2 15	/ -50	E 2 24	/ -15	T: EH1 15	no test	F 17	no test	Ch: 12 05	200	C: 11 07	100	C: A7	no test
E O 09	no test	A 3 04	330 / 0.8	E 2 16	/ -30	F 08	200	T: EH2 01	300	A 4 04	330 / 0.8	Ch: 12 06	no test	C: 11 08	no test	C: A8	no test
A 2 01	20	A 3 05	330 / 1.1	A 2 01	250	F 09	180	T: EH2 02	300	A 4 05	330 / 1.0	Ch: 12 07	no test	T: E 134	20	C: A9	no test
A 2 02	350	A 3 06	330 / 0.9	A 2 02	/ 20	F 10	250	T: EH2 03	/300	A 4 06	330 / 0.9	Ts: 12 01	20	T: E 135	350	C: A10	no test
A 2 03	/ 350	A 3 07	330 / 0.9	A 2 03	320	F 11	190	T: EH2 04	20	A 4 07	330 / 1.1	Ts: 12 02	350	T: E 136	/ 350	O3 01	150
A 3 01	20	A 3 08	no test	A 2 04	200	F 12	/ 0	T: EH2 05	20	A 4 08	no test	Ts: 12 03	/ 350	T: E 137	// 350	O3 02	250
A 3 02	350	OT 01	330 / 0.9	A 2 05	/ 100	F 13	/ 50	T: EH2 06	300	A 910	330 / 1.0	Ch: E O 31	200	T: E 138	/// 350	O3 03	no test
A 3 03	/ 350	OT 02	330 / 0.8	A 2 06	/ 170	F 14	/ 25	T: EH2 07	20	A 911	330 / 0.9	Ch: E O 32	150	T: 11 01	20	O3 04	no test
C 093	250	OT 03	330 / 1.0	A 2 07	no test	E O 08	500	T: EH2 08	300	A 912	330 / 1.0	Ch: E O 33	250	T: 11 02	350	O3 05	no test
C 094	300	OT 04	330 / 1.1	A 3 01	250	E O 09	/500	T: EH2 09	300	A 913	330 / 1.1	Ch: E O 34	130	T: 11 03	/ 350	O3 06	no test
C 095	350	OT 05	no test	A 3 02	320	E O 10	no test	T: EH2 10	20	A 914	330 / 1.2	Ch: E O 35	180	T: 11 04	no test	O3 07	no test
C 096	/ 350	A 905	330 / 1.0	A 3 03	400	E O 11	no test	T: EH2 11	no test	E O 11	330 / 1.0	Ch: E O 36	300	T: 11 05	no test	O3 08	no test
C 097	20	A 906	330 / 0.9	A 3 04	/ 70	E O 12	no test	T: EH2 12	no test	E O 13	330 / 1.2	Ch: E O 37	no test	T: O3 01	20	O3 09	no test
C 098	330 / 1.0	A 907	330 / 1.1	A 3 05	/ 150	E O 13	no test	T: EH2 13	no test	E O 14	/ 330 / 1.0	Ch: E O 38	no test	T: O3 02	350	O3 10	no test
C 099	330 / 0.8	A 908	330 / 1.2	A 3 06	220	E O 14	no test	T: EH2 14	no test	E O 16	330 / 1.1	Ts: E O 29	20	T: O3 03	/ 350	O3 11	no test
C 100	330 / 1.1	A 909	330 / 1.0	A 3 07	300	E O 15	no test	T: EH2 15	no test	E O 18	330 / 1.0	Ts: E O 30	350	T: O3 04	no test	O3 12	no test
								C: E 146	no test			Ts: E O 31	no test	T: O3 05	no test		
331.5 °C		334.0 °C		334.9 °C		336.8 °C		C: E 147	no test	337.5 °C		337.5 °C		338.4 °C		338.4 °C	
70.10 dpa		70.8 dpa		69.8 dpa		64.9 dpa		C: E 148	no test	46.8 dpa		12.0 dpa		31.0 dpa		28.4 dpa	
								C: E 149	no test								
								C: E 150	no test								
								C: E 151	no test								
								T: A13-A23	no test								
								T: A1-7; A9-1	no test								
								TEM AP	no test								
								336.8 °C									
								36.2 dpa									

Legend
Tensile and Impact specimens
/ = Post-irradiation annealed 550°C, 3h
// = Post-irradiation annealed 550°C, 1h
/// = Post-irradiation annealed 550°C, 0h

Table 8-1: Test conditions for PIE of ARBOR 2.

9 Annex: Impact Tests

9.1 EUROFER 97

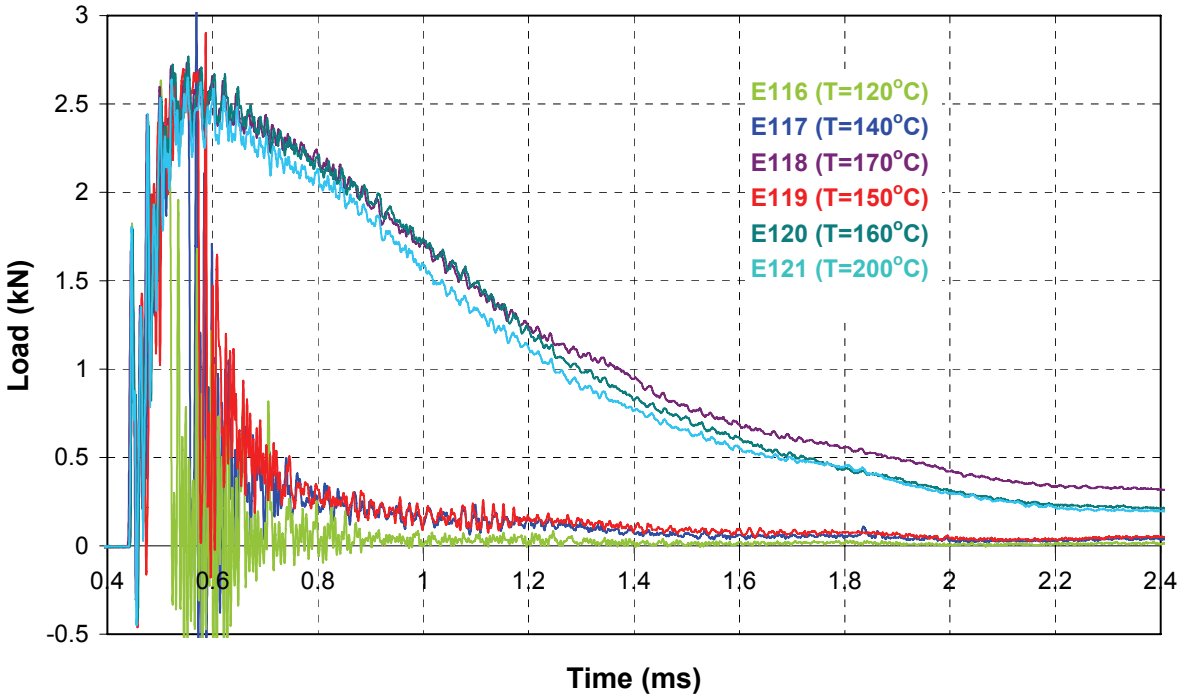

Fig. 9-1 Load-time diagrams of impact testing of EUROFER 97 after irradiation to 64.9 dpa at 336.8 °C (specimens: E1 16 to E1 21).

Specimen	T_{Test} (°C)	Av (J)
E1 16	120	0.67
E1 17	140	1.42
E1 18	170	6.67
E1 19	150	1.66
E1 20	160	6.05
E1 21	200	5.90

Table 9-1: Temperature dependence of impact toughness of EUROFER 97 after irradiation to 64.9 dpa at 336.8 °C.

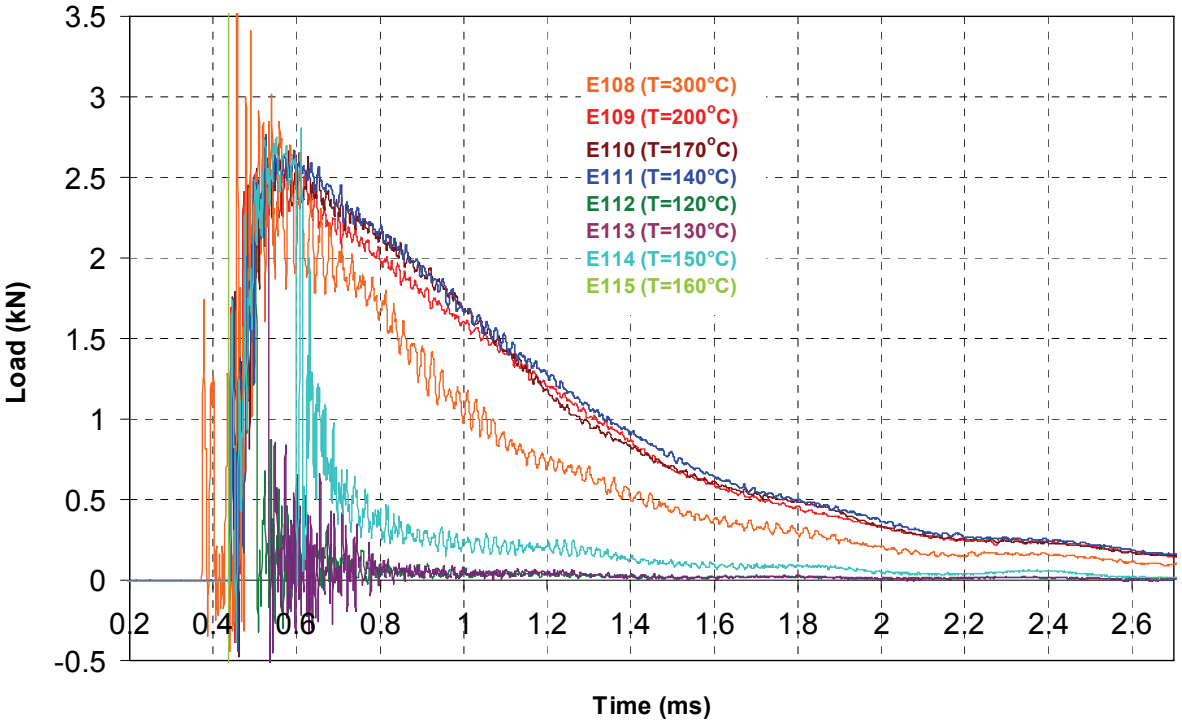

Fig. 9-2 Load vs. time diagrams of impact testing of EUROFER 97 after irradiation to 69.8 dpa at 334.9 °C.

Specimen	T_{Test} (°C)	Av (J)
E1 08	300	4.63
E1 09	200	6.07
E1 10	170	6.18
E1 11	140	6.28
E1 12	120	0.6
E1 13	130	0.79
E1 14	150	2.05
E1 15	160	6.64

Table 9-2: Temperature dependence of impact toughness of EUROFER 97 after irradiation to 69.8 dpa at 334.9 °C.

9.2 EUROFER 97 HT

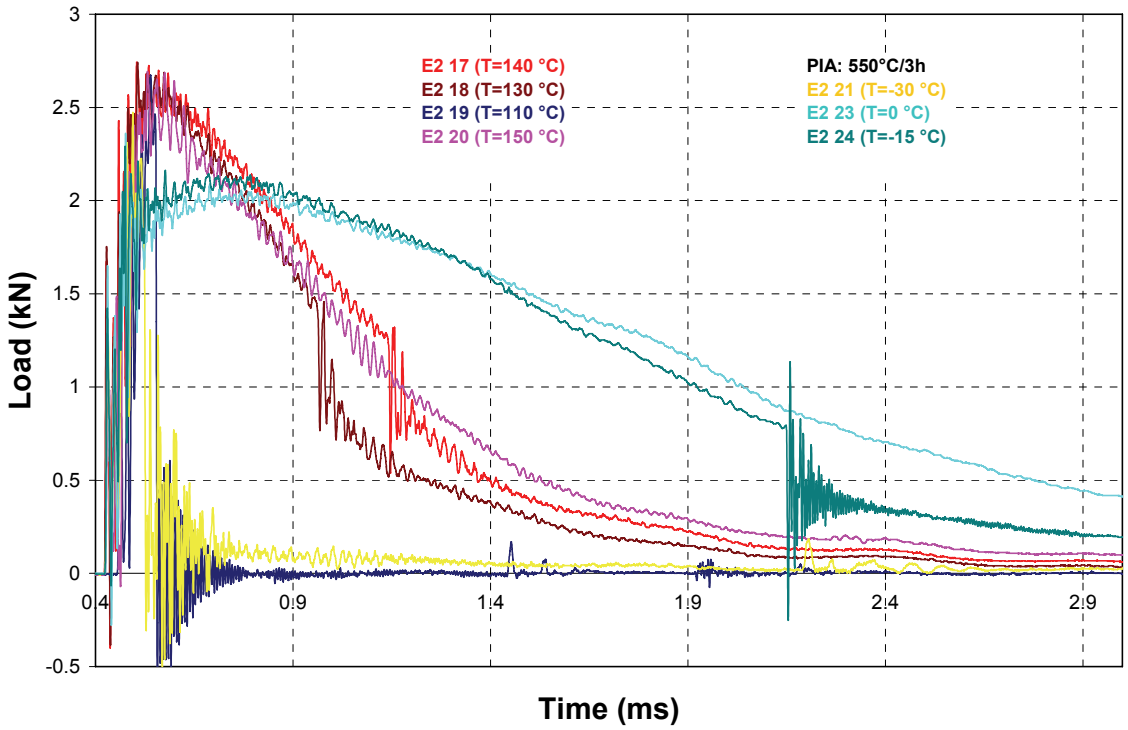

Fig. 9-3 Load vs. time diagrams of impact testing of EUROFER 97 HT after irradiation to 64.9 dpa at 336.8 °C. Specimens E2 21, E2 23, E2 24 are tested after post-irradiation annealing (PIA) at 550 °C/3 h.

Specimen	T_{Test} (°C)	Av (J)	PIA
E2 17	140	5.27	
E2 18	130	4.39	
E2 19	110	0.56	
E2 20	150	5.38	
E2 21	-30	0.97	550 °C/3 h
E2 23	0	9.01	550 °C/3 h
E2 24	-15	7.96	550 °C/3 h

Table 9-3: Temperature dependence of impact toughness of EUROFER 97 HT after irradiation to 64.9 dpa at 336.8 °C. Selected specimens are tested after PIA at 550 °C/3 h.

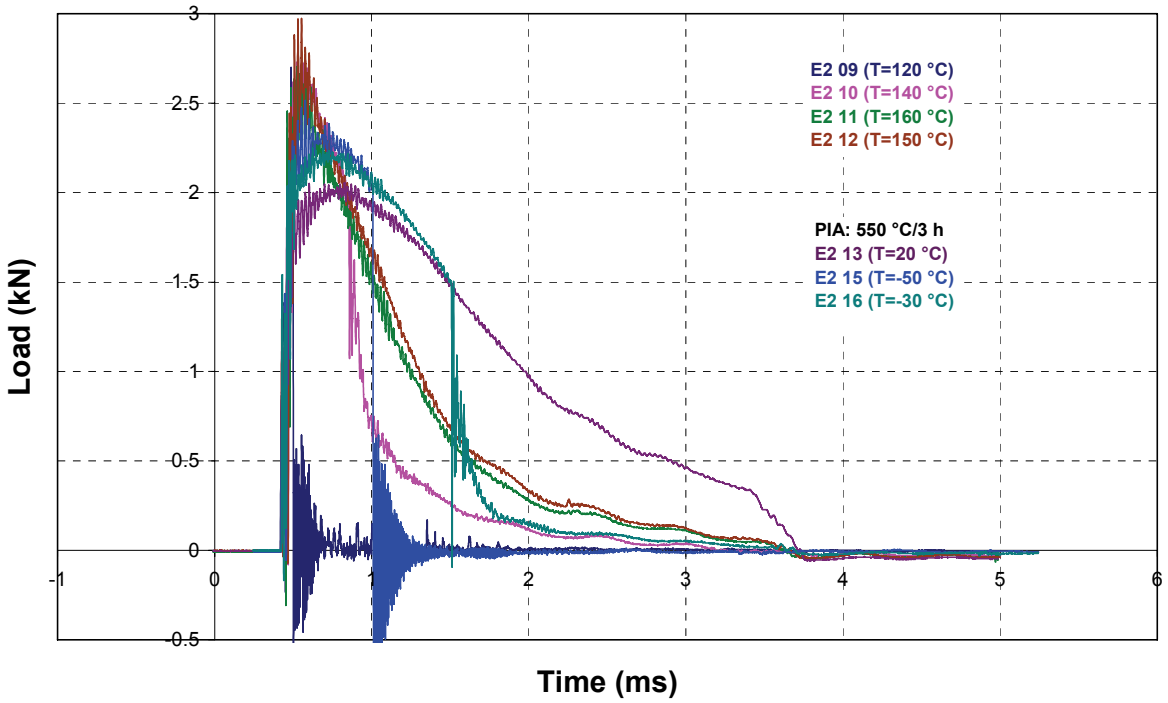

Fig. 9-4 Load vs. time diagrams of impact testing of EUROFER 97 HT after irradiation to 69.8 dpa at 334.9 °C. Specimens E2 13, E2 15, E2 16 are tested after PIA at 550 °C/3 h.

Specimen	T_{Test} (°C)	Av (J)	PIA
E2 09	120	0.53	
E2 10	140	4.05	
E2 11	160	5.9	
E2 12	150	6.04	
E2 13	20	8.64	550 °C/3 h
E2 15	-50	3.3	550 °C/3 h
E2 16	-30	6.15	550 °C/3 h

Table 9-4: Temperature dependence of impact toughness of EUROFER 97 HT after irradiation to 69.8 dpa at 334.9 °C. Selected specimens are tested after PIA at 550 °C/3 h.

9.3 F82H-mod.

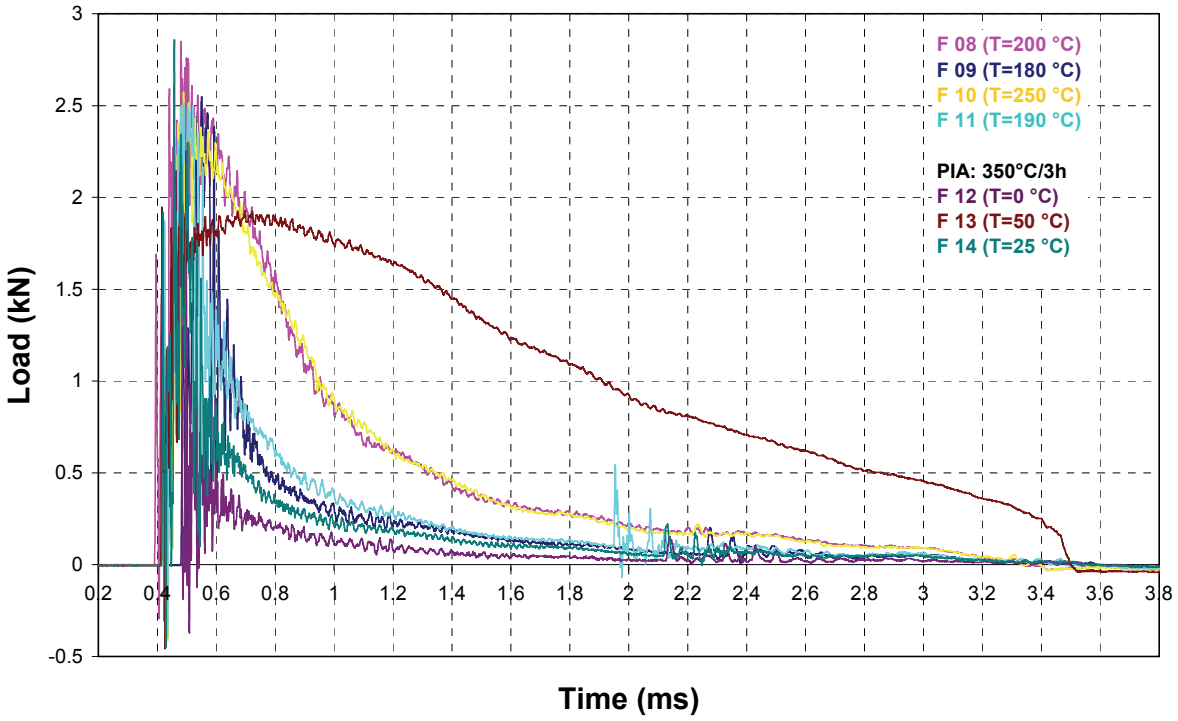

Fig. 9-5 Load vs. time diagrams of impact testing of F82H-mod. after irradiation to 64.9 dpa at 336.8 °C. Specimens F 12, F 13, F 14 are tested after PIA at 550 °C/3 h.

Specimen	T_{Test} (°C)	Av (J)	PIA
F 08	200	4.51	
F 09	180	1.95	
F 10	250	4.49	
F 11	190	2.61	
F 12	0	1.10	550 °C/3 h
F 13	50	8.51	550 °C/3 h
F 14	25	1.80	550 °C/3 h

Table 9-5: Temperature dependence of impact toughness of F82H-mod. after irradiation to 64.9 dpa at 336.8 °C. Selected specimens are tested after PIA at 550 °C/3 h.

9.4 OPTIFER XI

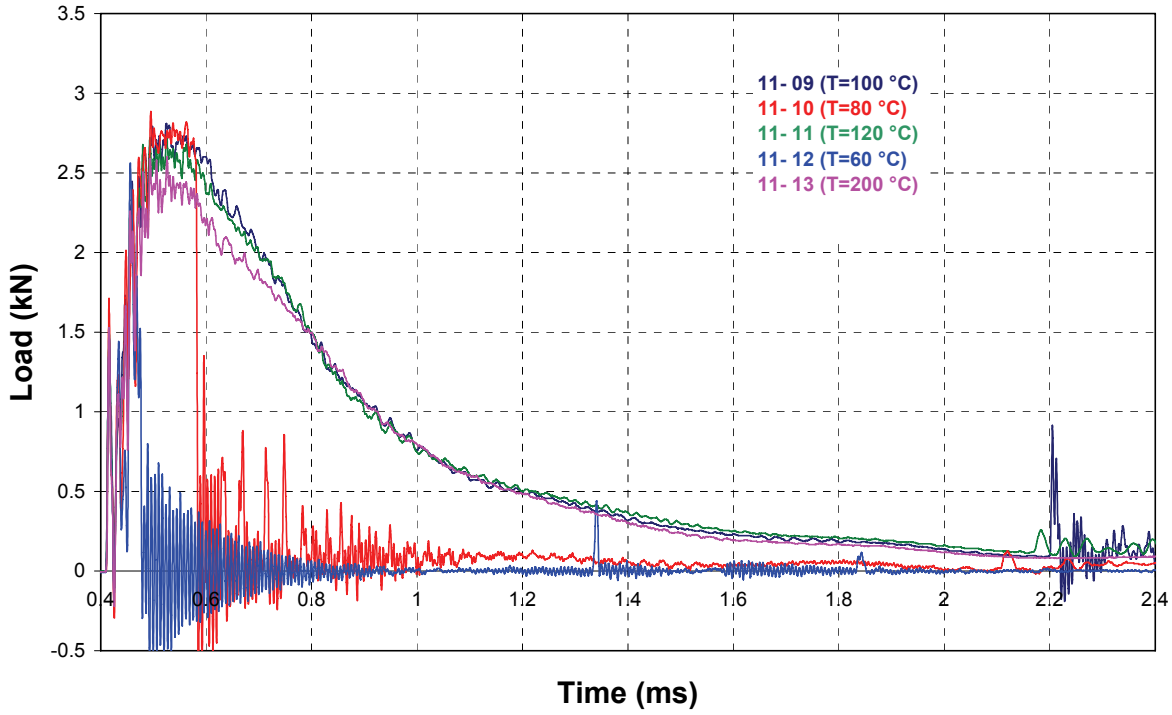

Fig. 9-6 Load vs. time diagrams of impact testing of OPTIFER XI after irradiation to 12.0 dpa at 337.5 °C.

Specimen	T_{Test} (°C)	Av (J)
11 09	100	4.13
11 10	80	1.56
11 11	120	4.3
11 12	60	0.37
11 13	200	4.33

Table 9-6: Temperature dependence of impact toughness of OPTIFER XI after irradiation to 12.0 dpa at 337.5 °C.

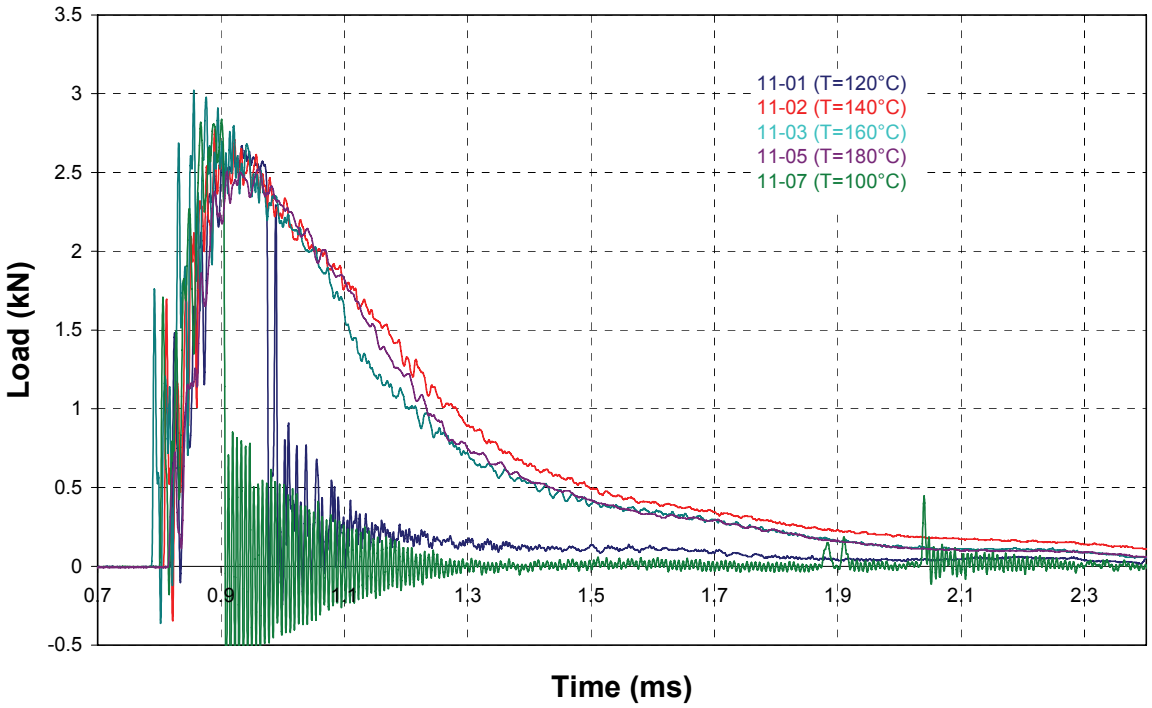

Fig. 9-7 Load vs. time diagrams of impact testing of OPTIFER XI after irradiation to 31 dpa at 338.4 °C.

Specimen	T_{Test} (°C)	Av (J)
11 01	120	1.61
11 02	140	4.05
11 03	160	3.49
11 05	180	3.54
11 07	100	0.69

Table 9-7: Temperature dependence of impact toughness of OPTIFER XI after irradiation to 31 dpa at 338.4 °C.

9.5 OPTIFER XII

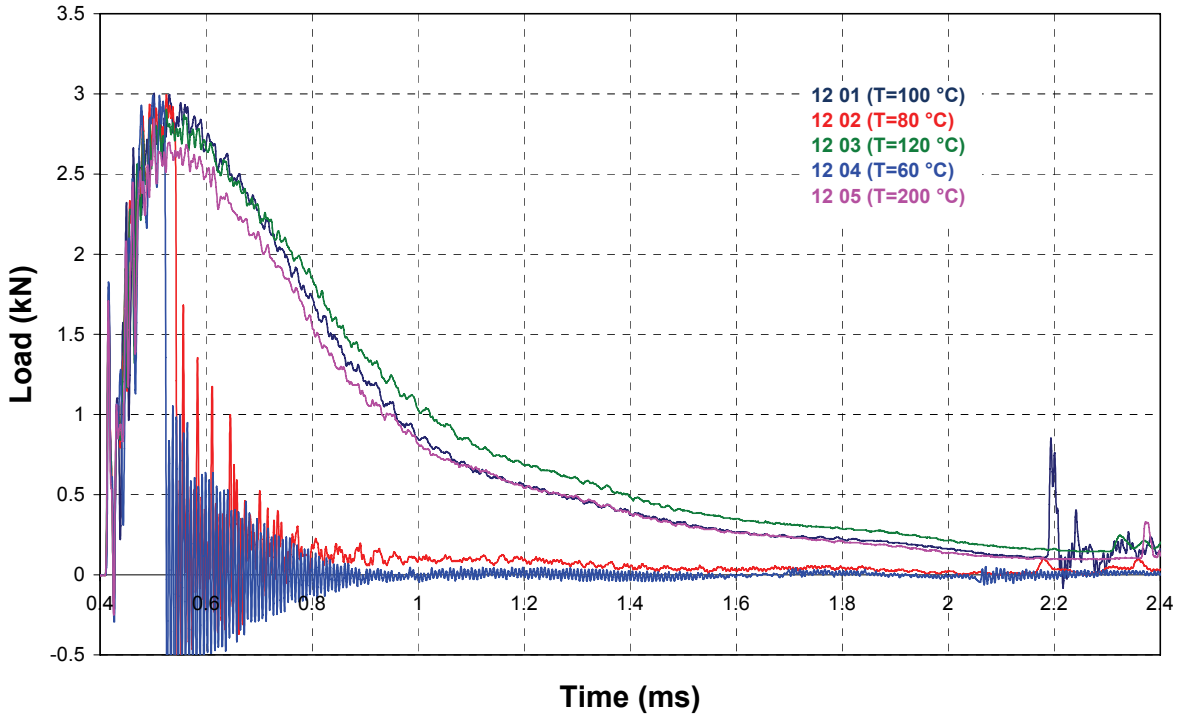

Fig. 9-8 Load vs. time diagrams of impact testing of OPTIFER XII after irradiation to 12.0 dpa at 337.5 °C.

Specimen	T_{Test} (°C)	Av (J)
12 01	100	4.76
12 02	80	1.35
12 03	120	5.16
12 04	60	0.75
12 05	200	4.56

Table 9-8: Temperature dependence of impact toughness of OPTIFER XII after irradiation to 12.0 dpa at 337.5 °C.

9.6 ADS 2

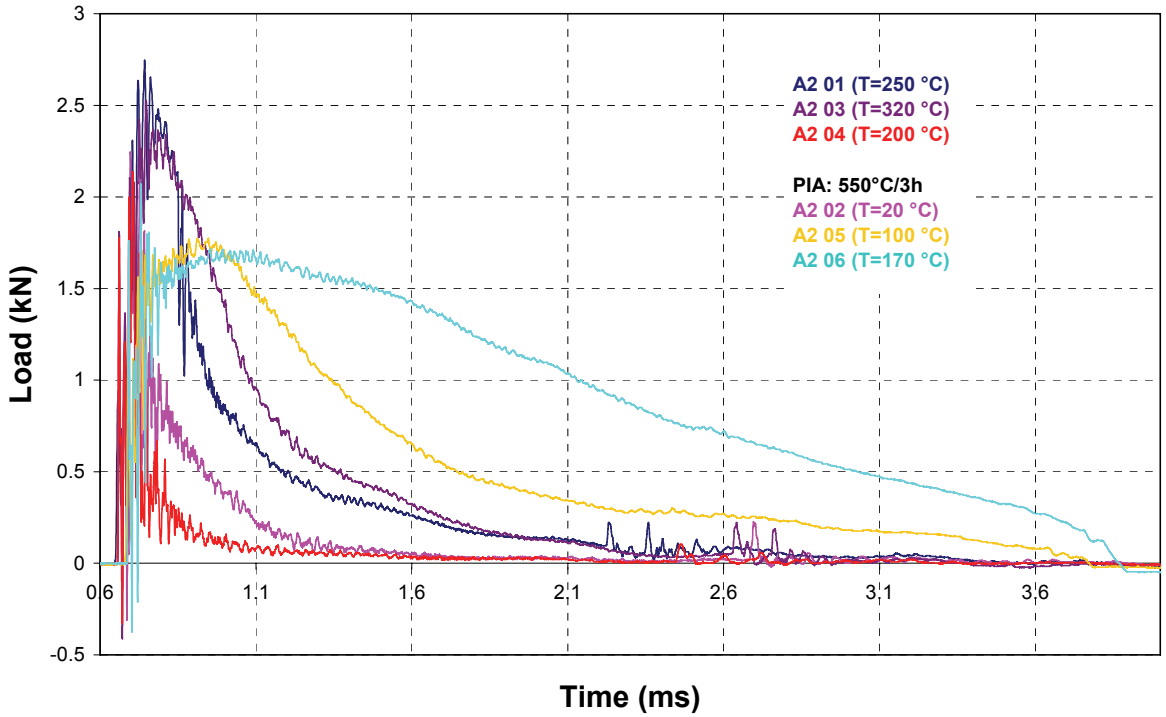

Fig. 9-9 Load vs. time diagrams of impact testing of ADS 2 after irradiation to 69.8 dpa at 334.9 °C. Specimens A2 02, A2 05, A2 06 are tested after PIA at 550 °C/3 h.

Specimen	T_{Test} (°C)	Av (J)	PIA
A2 01	250	2.86	
A2 02	20	1.28	550 °C/3 h
A2 03	320	3.39	
A2 04	200	0.76	
A2 05	100	4.88	550 °C/3 h
A2 06	170	8.13	550 °C/3 h

Table 9-9: Temperature dependence of impact toughness of ADS 2 after irradiation to 69.8 dpa at 334.9 °C.

9.7 ADS 3

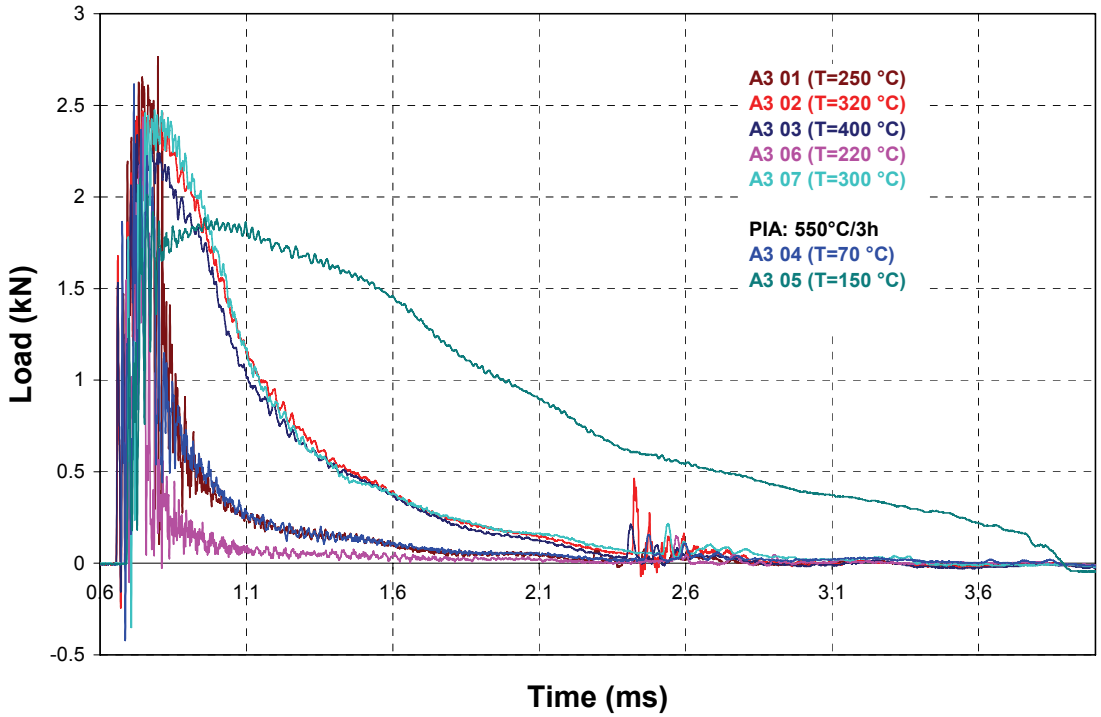

Fig. 9-10 Load vs. time diagrams of impact testing of ADS 3 after irradiation to 69.8 dpa at 334.9 °C. Specimens A3 04, A3 05 are tested after PIA at 550 °C/3 h.

Specimen	T_{Test} (°C)	Av (J)	PIA
A3 01	250	1.67	
A3 02	320	3.81	
A3 03	400	3.59	
A3 04	70	1.57	550 °C/3 h
A3 05	150	7.76	550 °C/3 h
A3 06	220	0.77	
A3 07	300	3.75	

Table 9-10: Temperature dependence of impact toughness of ADS 3 after irradiation to 69.8 dpa at 334.9 °C.

9.8 EURODShip with 0.5 wt.% Y_2O_3

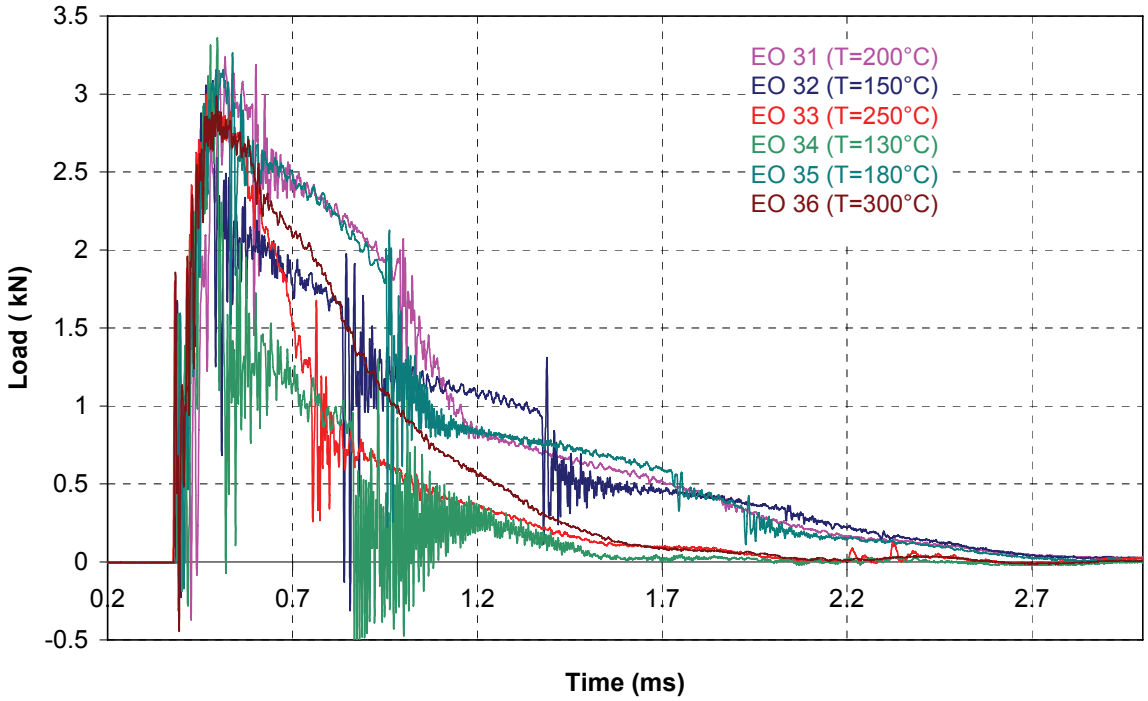

Fig. 9-11 Load vs. time diagrams of impact testing of EURODShip after irradiation to 12.0 dpa at 337.5 °C.

Specimen	T_{Test} (°C)	Av (J)
EO 31	200	6.07
EO 32	150	5.46
EO 33	250	3.54
EO 34	130	2.35
EO 35	180	6.02
EO 36	300	4.53

Table 9-11: Temperature dependence of impact toughness of EURODShip after irradiation to 12.0 dpa at 337.5 °C.

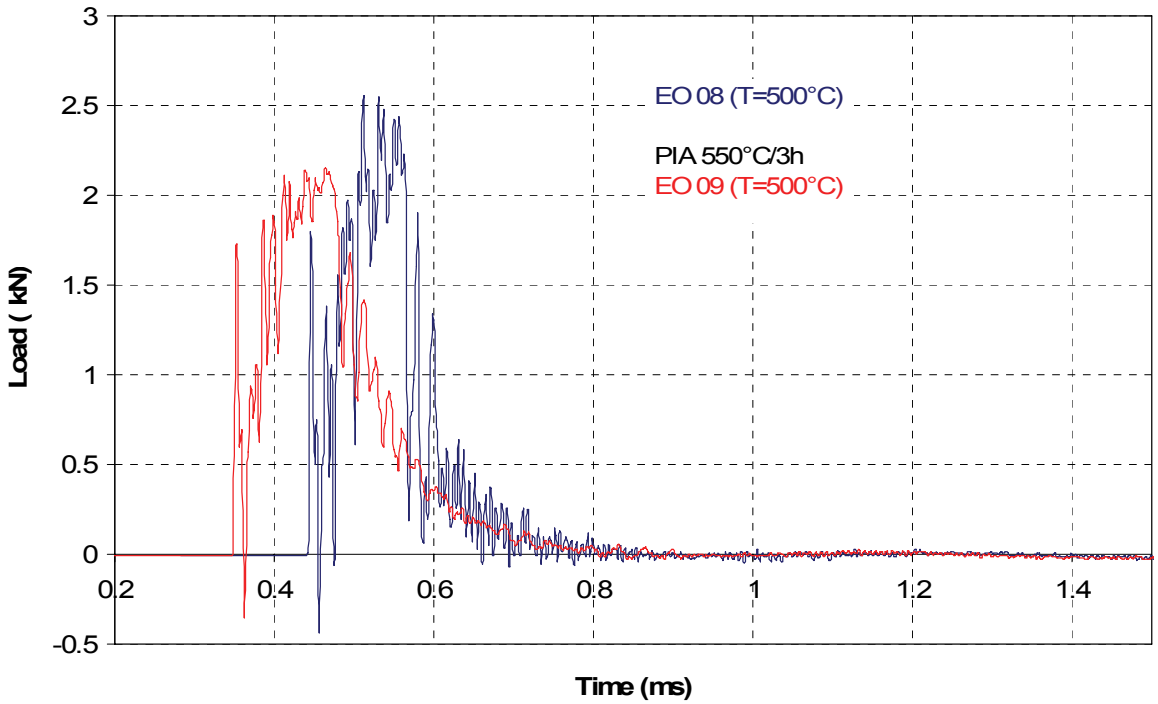

Fig. 9-12 Load vs. time diagrams of impact testing of EURODShip after irradiation to 64.9 dpa at 336.8 °C. Specimen EO 09 is tested after PIA at 550 °C/3 h.

Specimen	T_{Test} (°C)	Av (J)	PIA
EO 08	500	0.84	
EO 09	500	1.08	550 °C/3 h

Table 9-12: Temperature dependence of impact toughness of EURODShip after irradiation to 64.9 dpa at 336.8 °C.

9.9 EODShip3 with 0.3 wt.% Y_2O_3

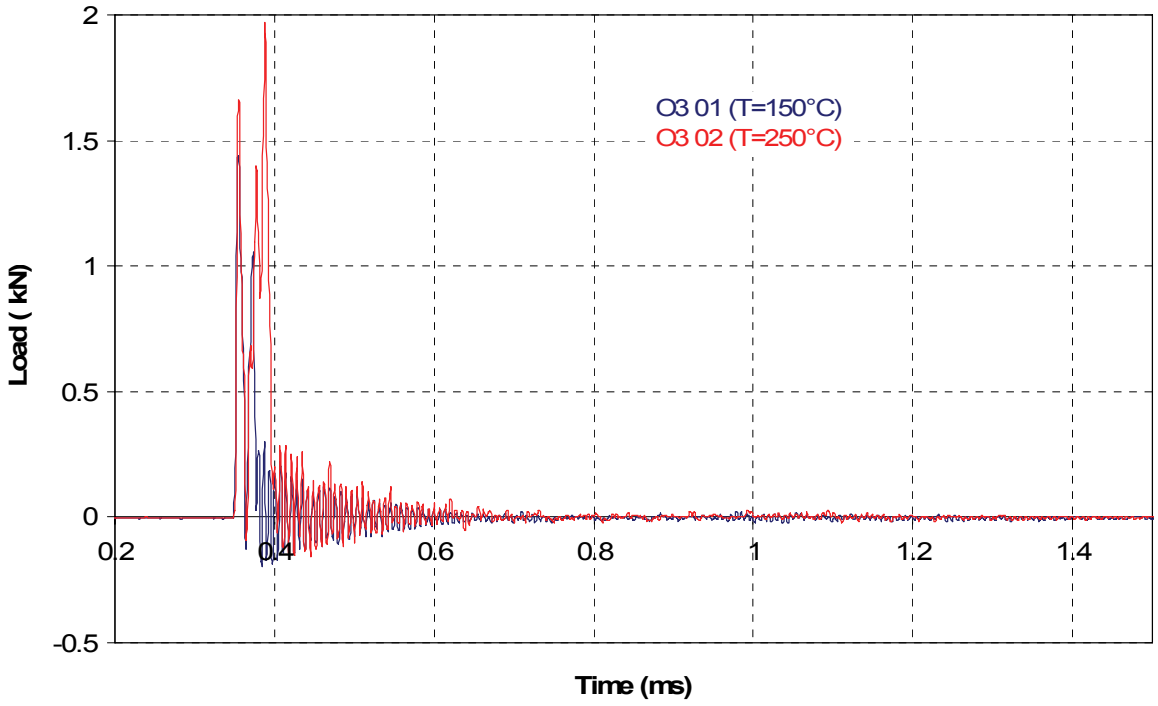

Fig. 9-13 Load vs. time diagrams of impact testing of EODShip 3 after irradiation to 28.4 dpa at 338.4 °C.

Specimen	T_{Test} (°C)	Av (J)
O3 01	150	0.22
O3 02	250	0.30

Table 9-13: Temperature dependence of impact toughness of EODShip 3 after irradiation to 28.4 dpa at 338.4 °C.

9.10 Diffusion welded EUROFER 97

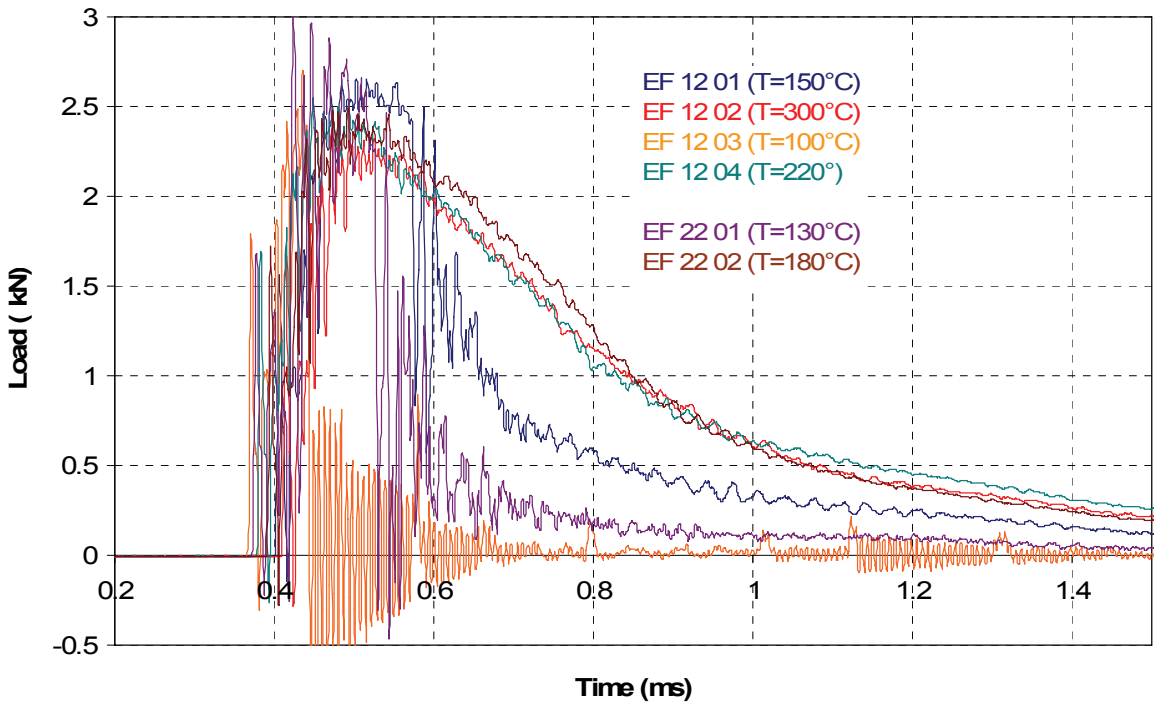

Fig. 9-14 Load vs. time diagram of impact testing of diffusion welded EUROFER 97 after irradiation to 28.4 dpa at 338.4 °C.

Specimen	T_{Test} (°C)	Av (J)
EF 12 01	150	2.66
EF 12 02	300	3.53
EF 12 03	100	0.56
EF 12 04	220	4.00
EF 22 01	130	1.64
EF 22 02	180	3.84

Table 9-14: Temperature dependence of impact toughness of diffusion welded EUROFER 97 after irradiation to 28.4 dpa at 338.4 °C.

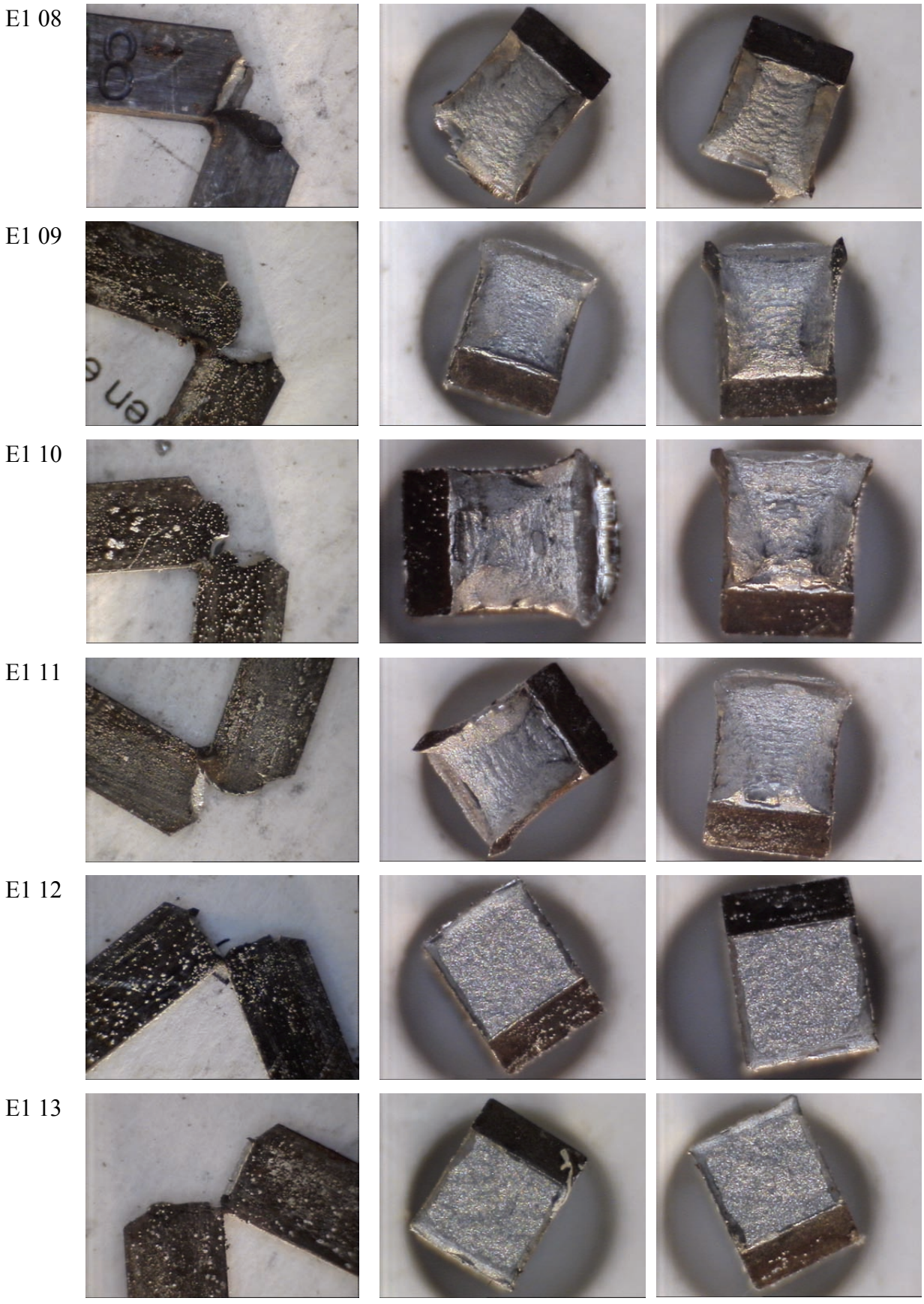

Fig. 9-15 Charpy specimens E1 08, E1 09, E1 10, E1 11, E1 12, E1 13 after impact testing and after complete separation.

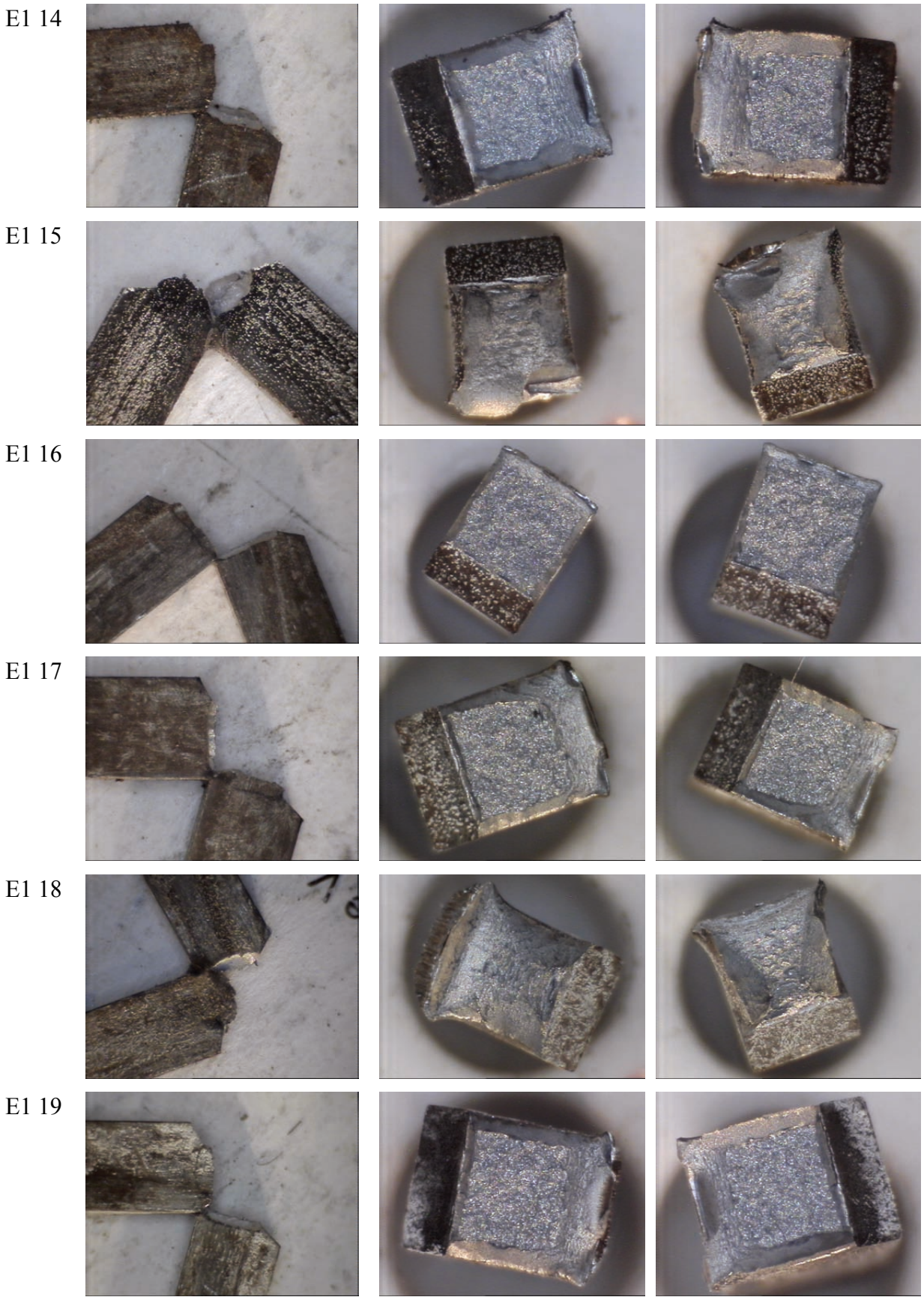

Fig. 9-16 Charpy specimens E1 14, E1 15, E1 16, E1 17, E1 18, E1 19 after impact testing and after complete separation.

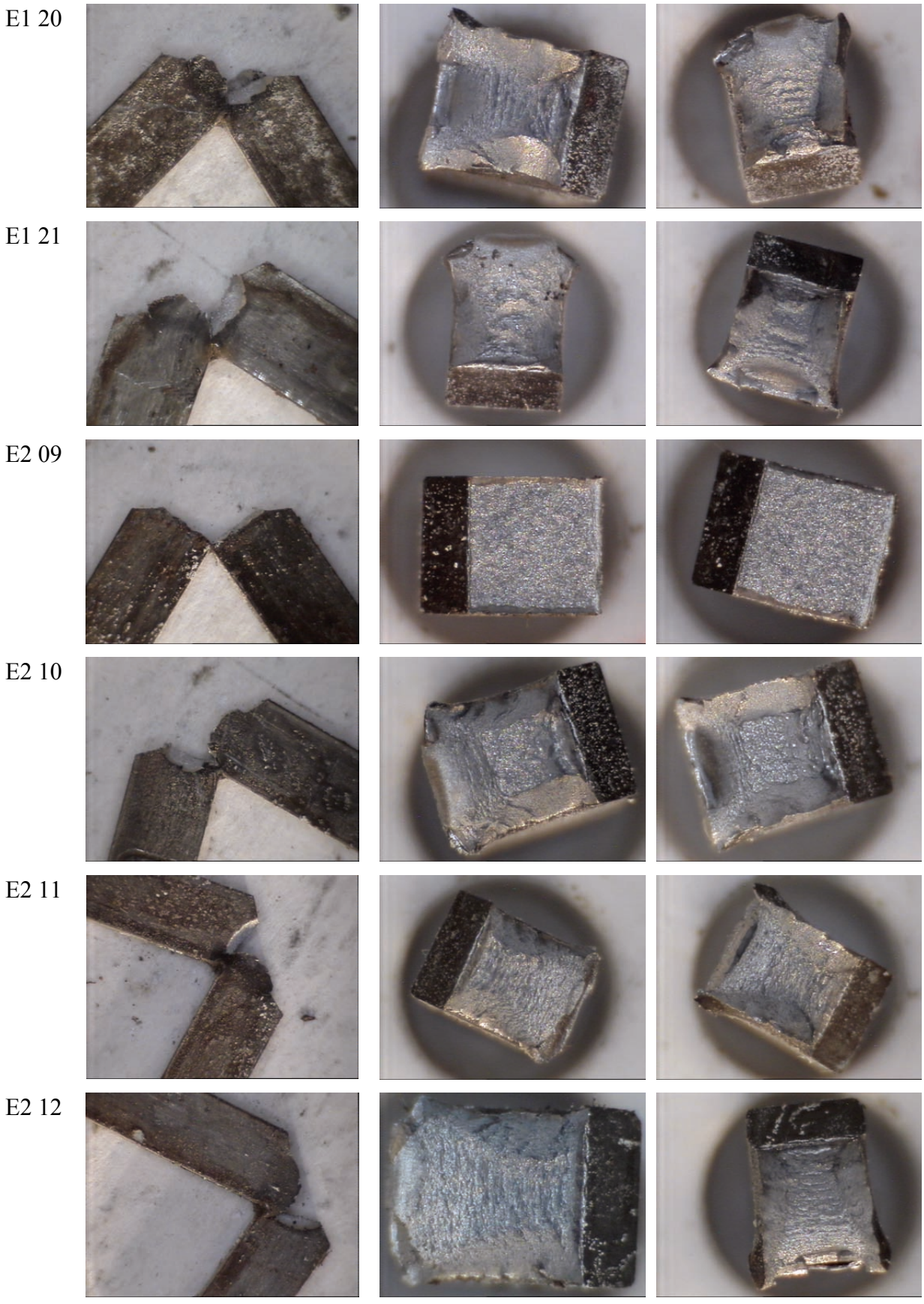

Fig. 9-17 Charpy specimens E1 20, E1 21, E2 09, E2 10, E2 11, E2 12 after impact testing and after complete separation.

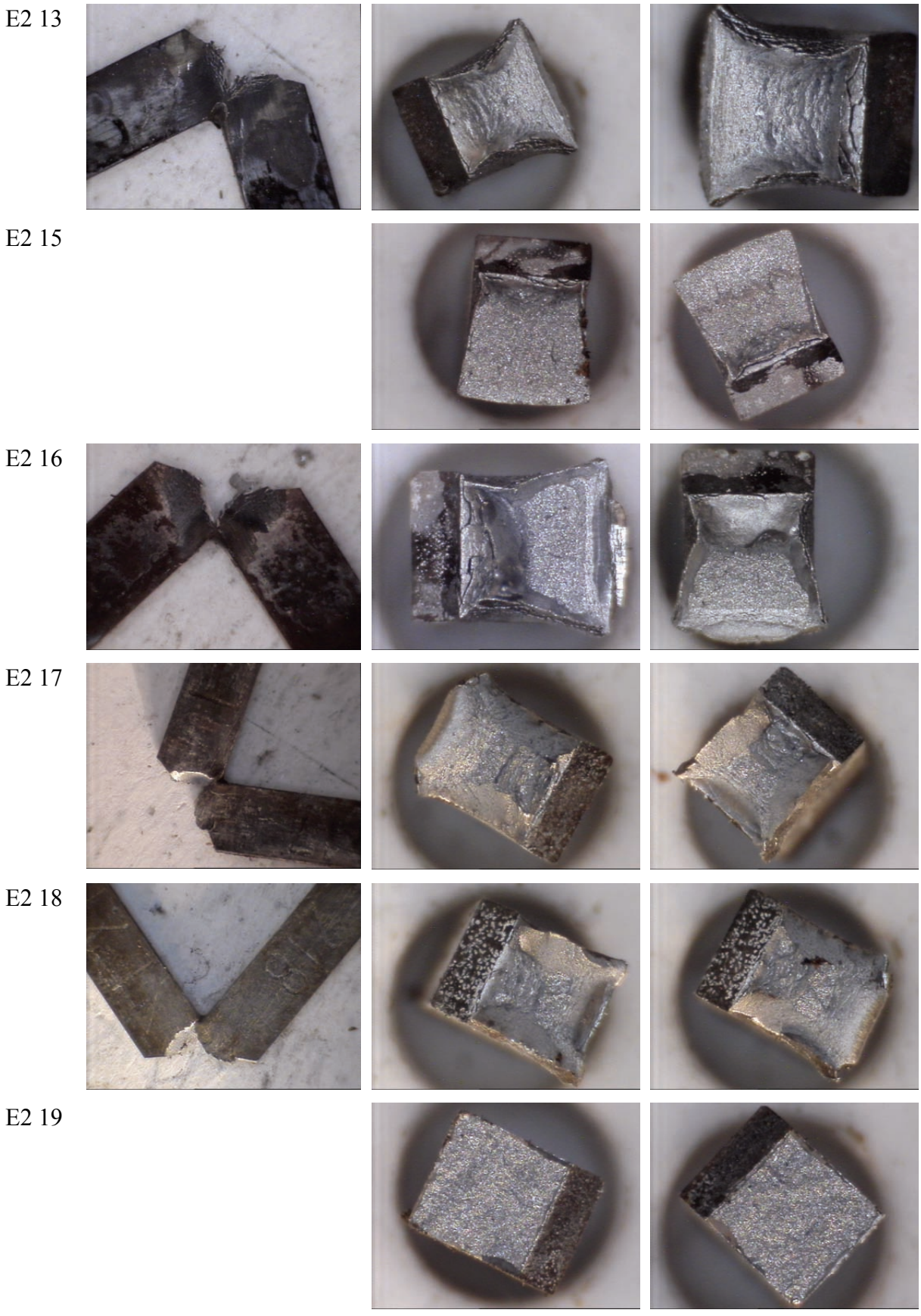

Fig. 9-18 Charpy specimens E2 13, E2 15, E2 16, E2 17, E2 18, E2 19 after impact testing and after complete separation.

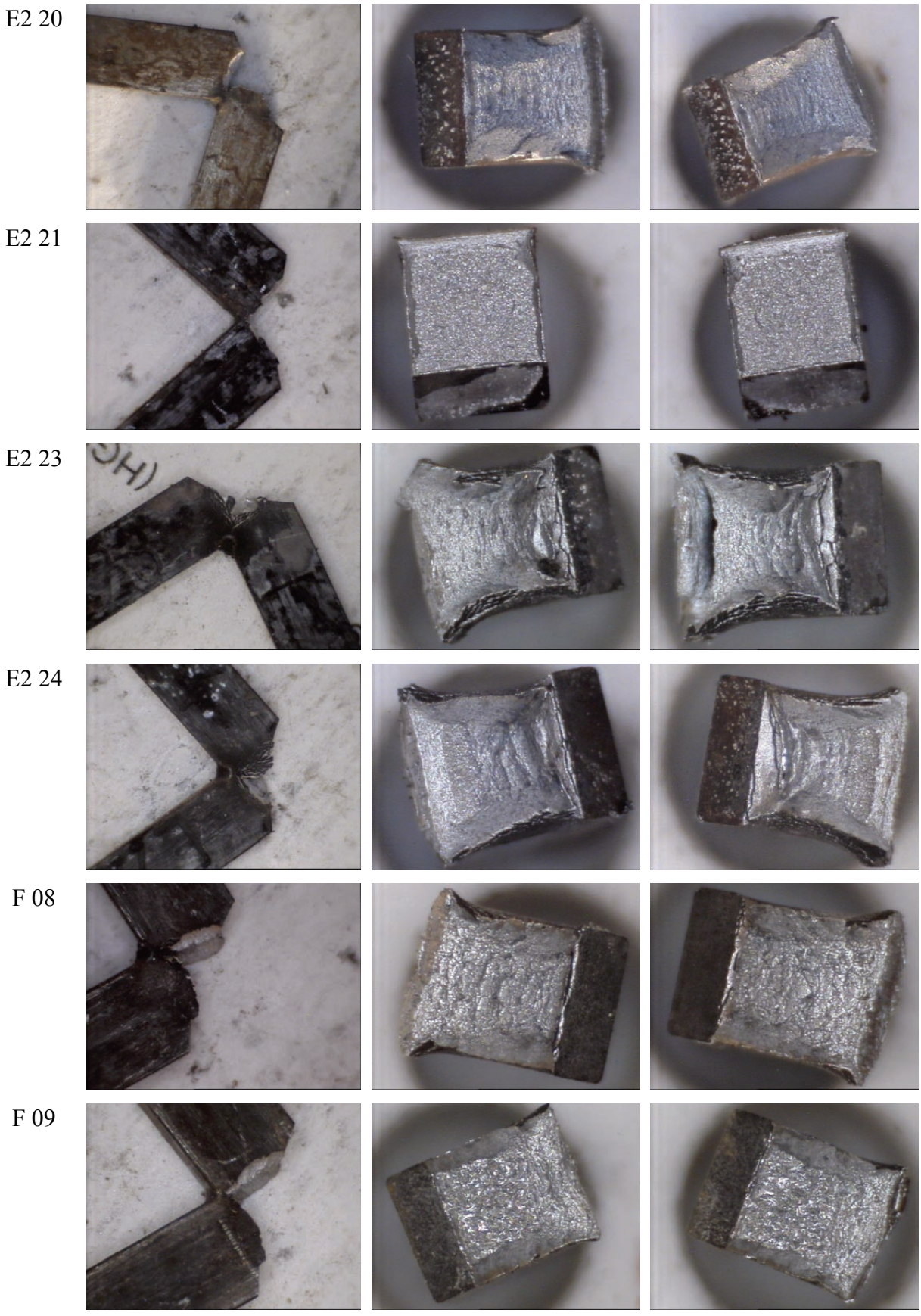

Fig. 9-19 Charpy specimens E2 20, E2 21, E2 23, E2 24, F 08, F 09 after impact testing and after complete separation.

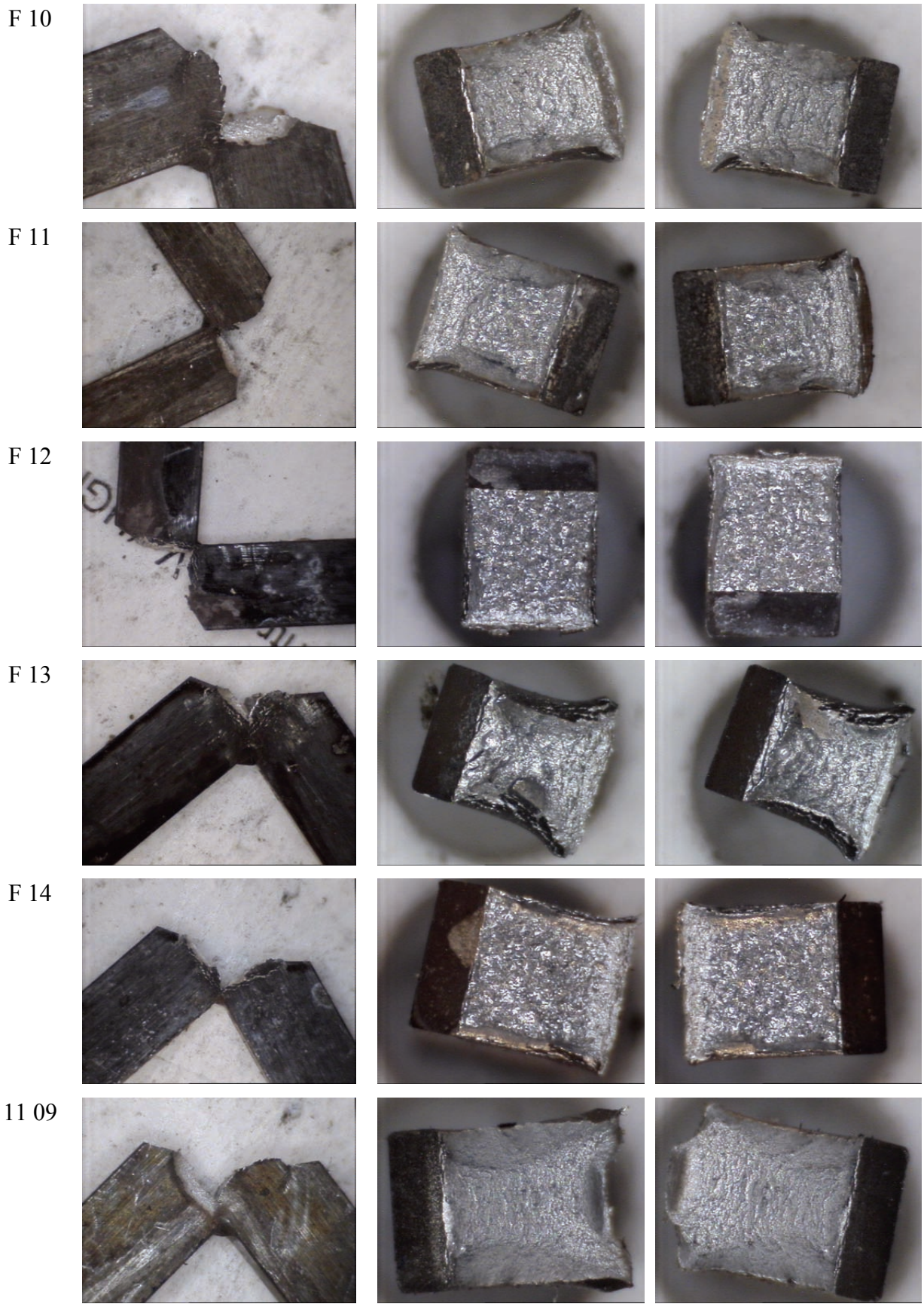

Fig. 9-20 Charpy specimens F 10, F 11, F 12, F 13, F 14, 11 09 after impact testing and after complete separation.

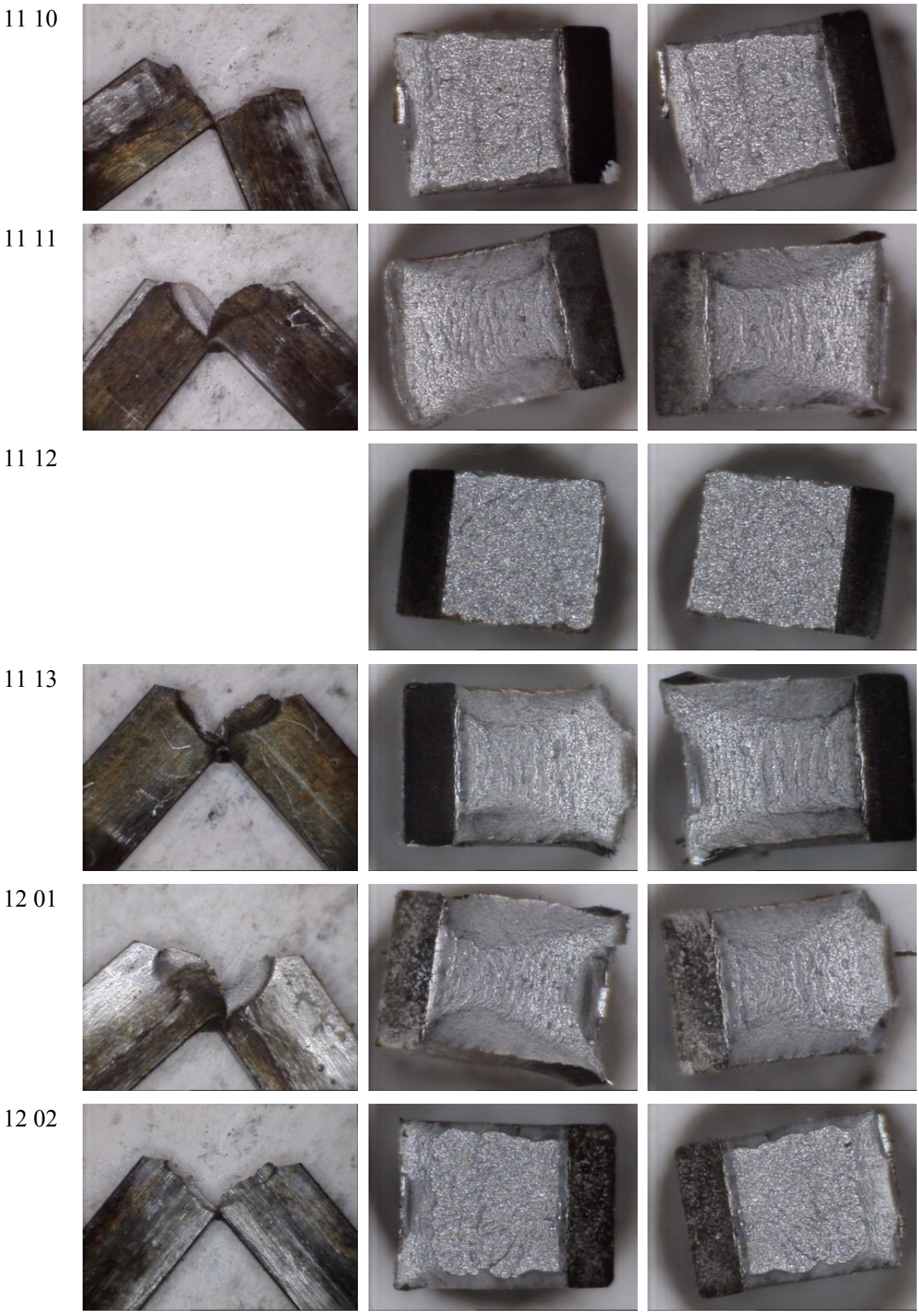

Fig. 9-21 Charpy specimens 11 10, 11 11, 11 12, 11 13, 12 01, 12 02 after impact testing and after complete separation.

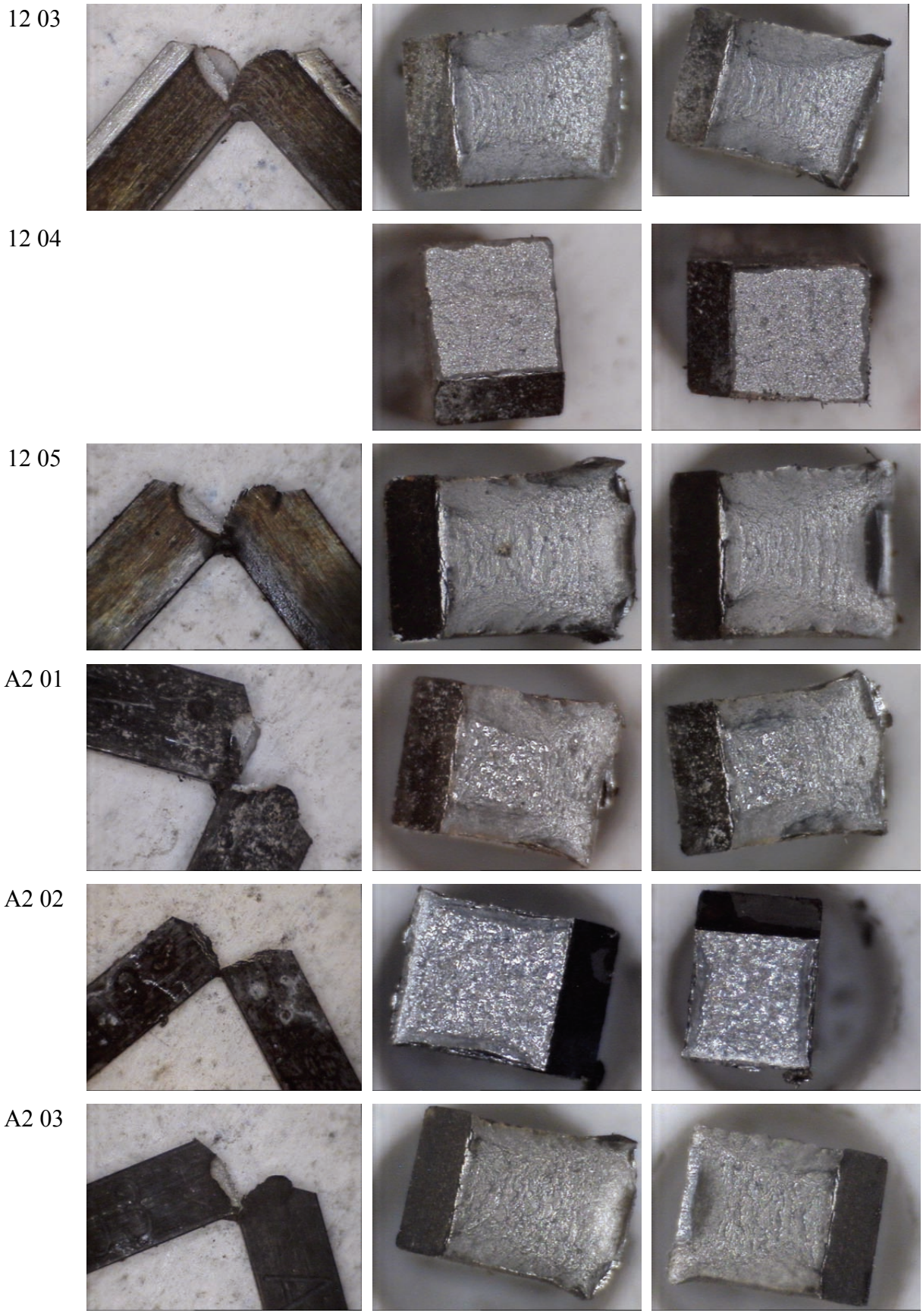

Fig. 9-22 Charpy specimens 12 03, 12 04, 12 05, A2 01, A2 02, A2 03 after impact testing and after complete separation.

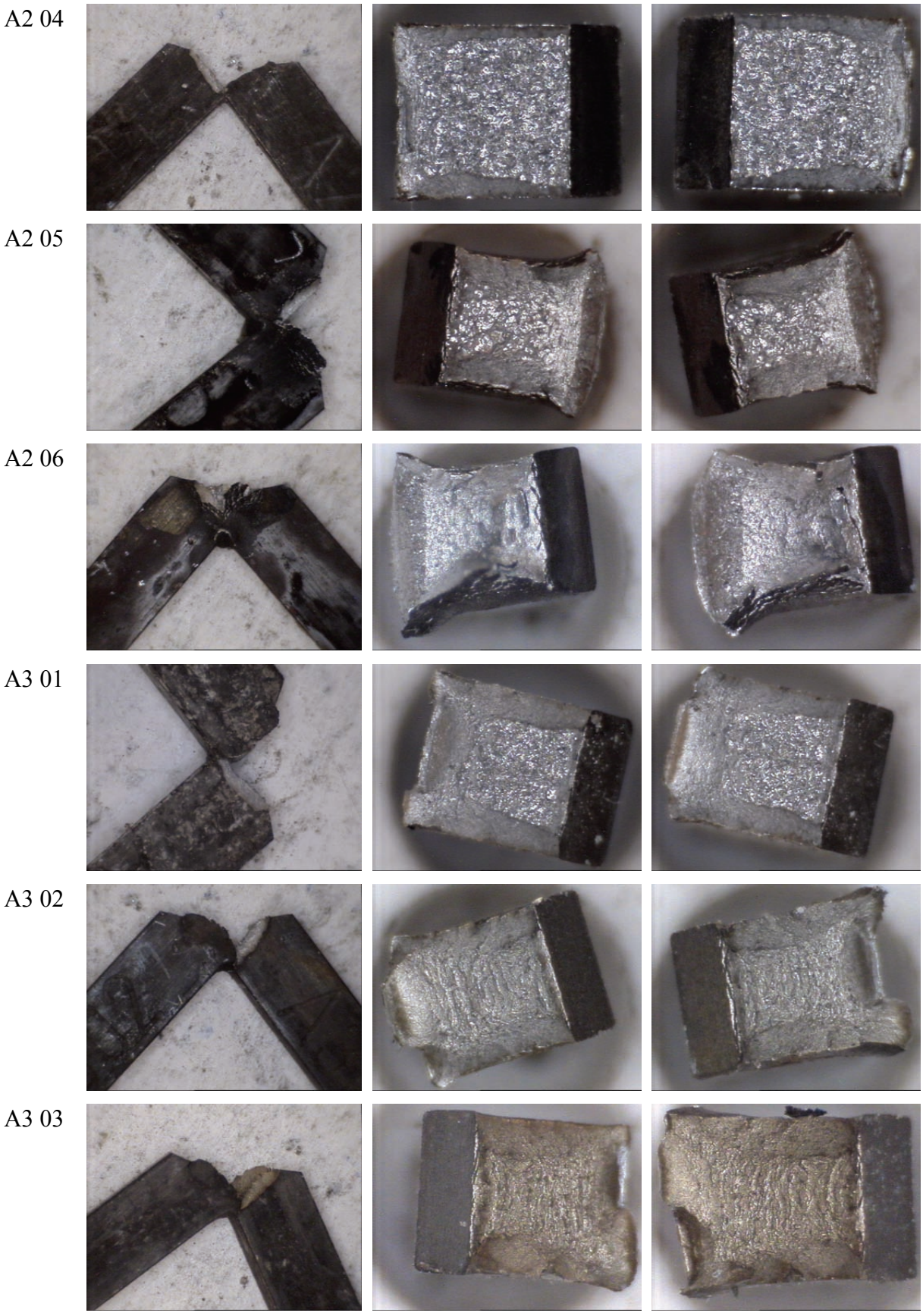

Fig. 9-23 Charpy specimens A2 04, A2 05, A2 06, A3 01, A3 02, A3 03 after impact testing and after complete separation.

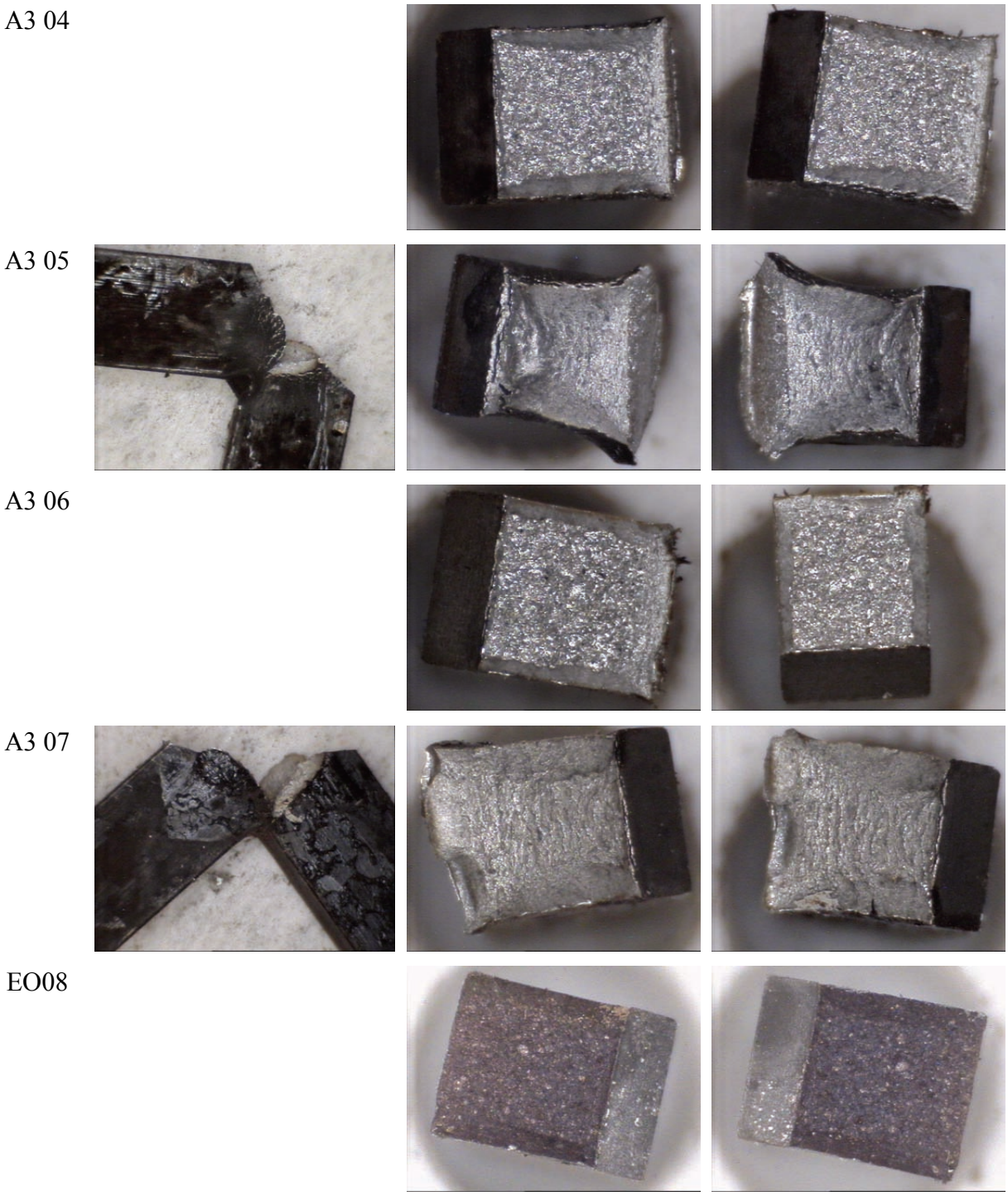

Fig. 9-24 Charpy specimens A3 04, A3 05, A3 06, A3 07, EO 08 after impact testing and after complete separation.

Fig. 9-25 Charpy specimens EO 31, EO 32, EO 33, EO 34, EO 34, EO 36 after impact testing and after complete separation.

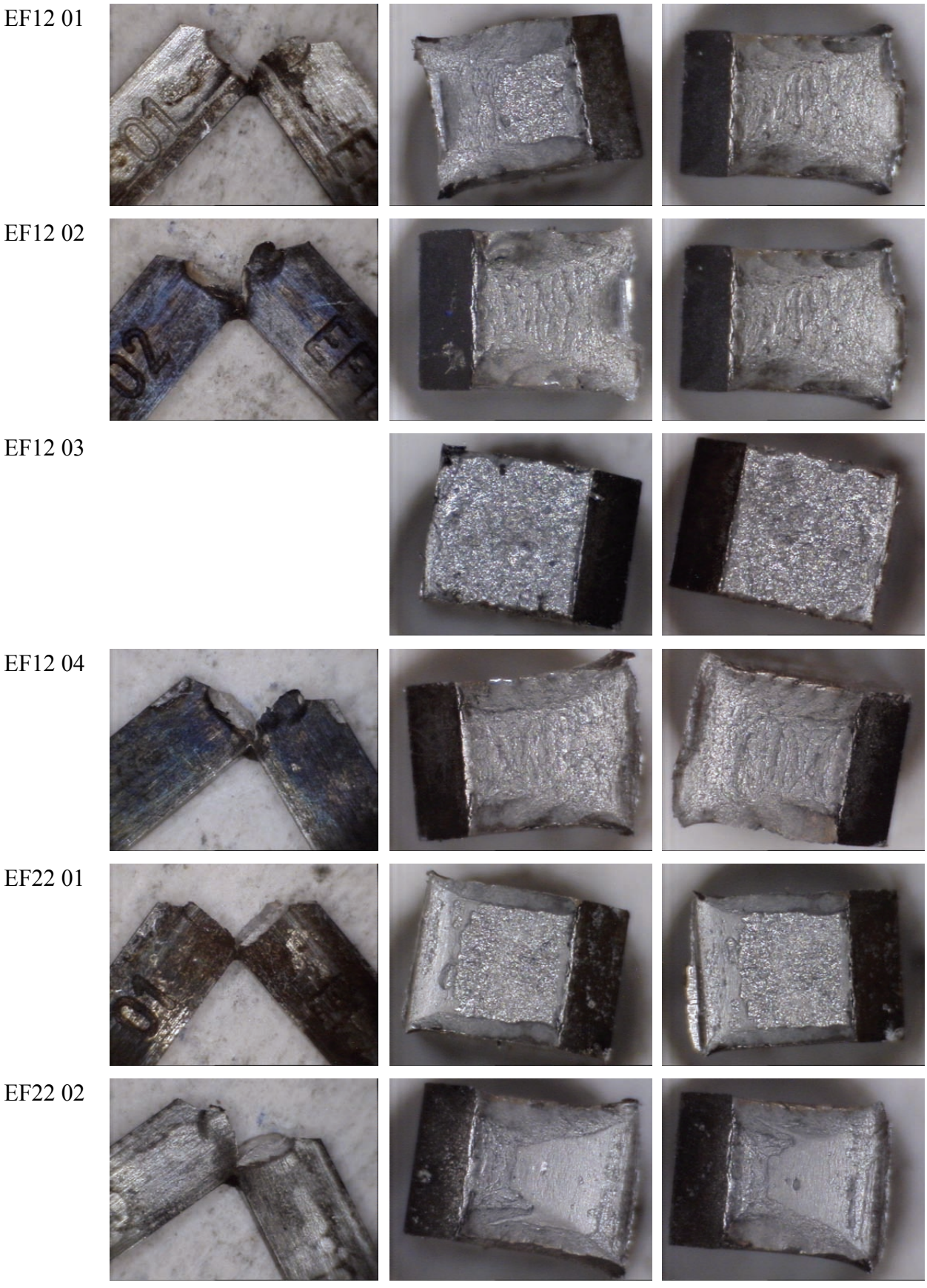

Fig. 9-26 Charpy specimens EF12 01, EF12 02, EF12 03, EF12 04, EF22 01, EF22 02 after impact testing and after complete separation.

O3 01

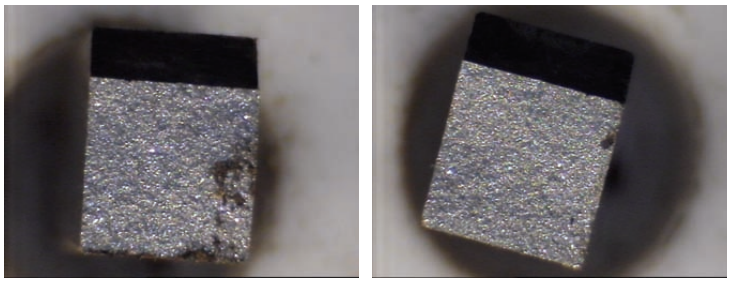

O3 02

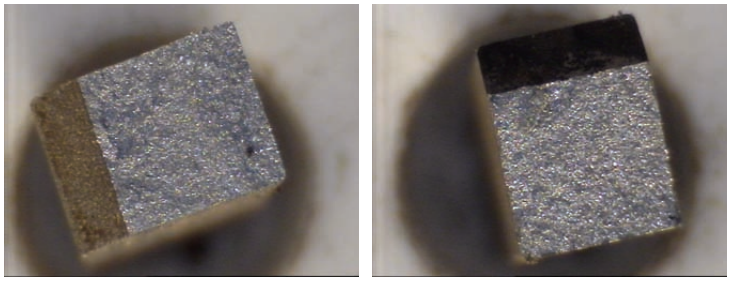

Fig. 9-27 Charpy specimens O3 01, O3 02 after impact testing and after complete separation.

10 Annex: Tensile Tests

10.1 EUROFER 97

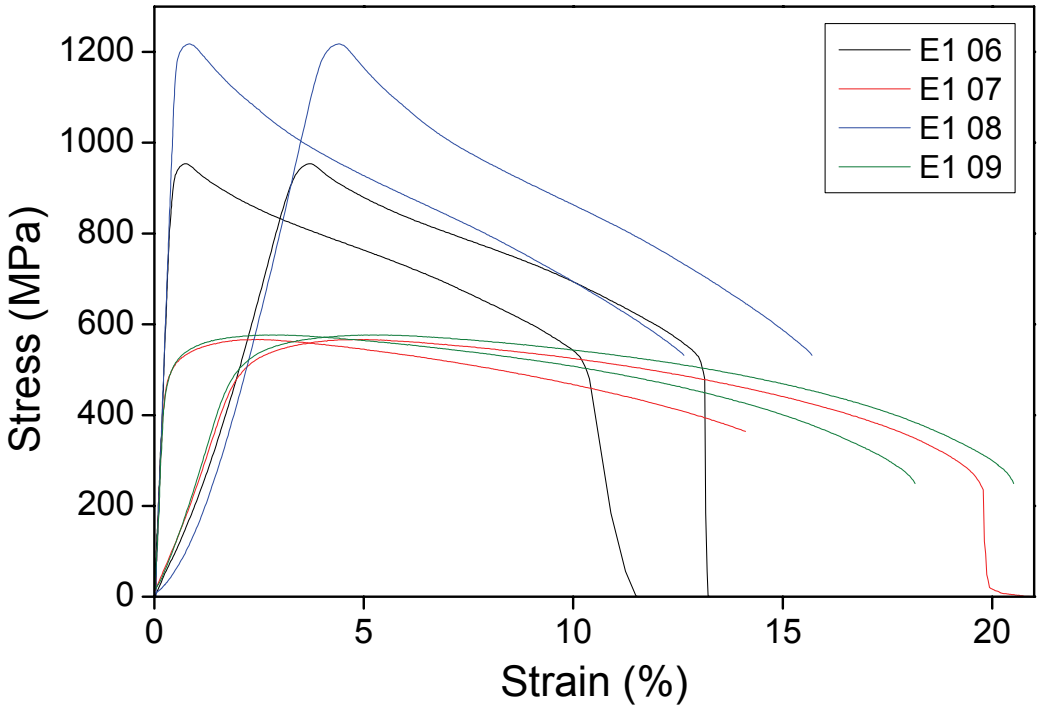

Fig. 10-1 Tensile stress vs. strain diagrams (displacement recording of extensometer and crosshead) of EUROFER 97 after irradiation to 70.1 dpa at 331.5 °C, the test conditions and the assessment results are summarised in Table 10-1.

File Name	T (°C)	R_{p02} (MPa)	R_m (MPa)	A_g (%)	A (%)	PIA
E1 06 -e	350	949	954	0.32	10.15	
E1 06 -t	350	947	954	0.35	10.90	
E1 07 -e	350	504	567	2.15	------	550 °C/3 h
E1 07 -t	350	501	567	2.90	18.75	550 °C/3 h
E1 09 -e	350	510	577	2.67	18.05	550 °C/1 h
E1 09 -t	350	504	577	3.55	19.55	550 °C/1 h
E1 08 -e	20	1211	1218	0.37	12.40	
E1 08 -t	20	1211	1218	0.38	13.35	

Table 10-1: Analysis of the tensile diagrams of EUROFER 97 after irradiation to 70.1 dpa at 331.5 °C (-e: extensometer, -t: crosshead).

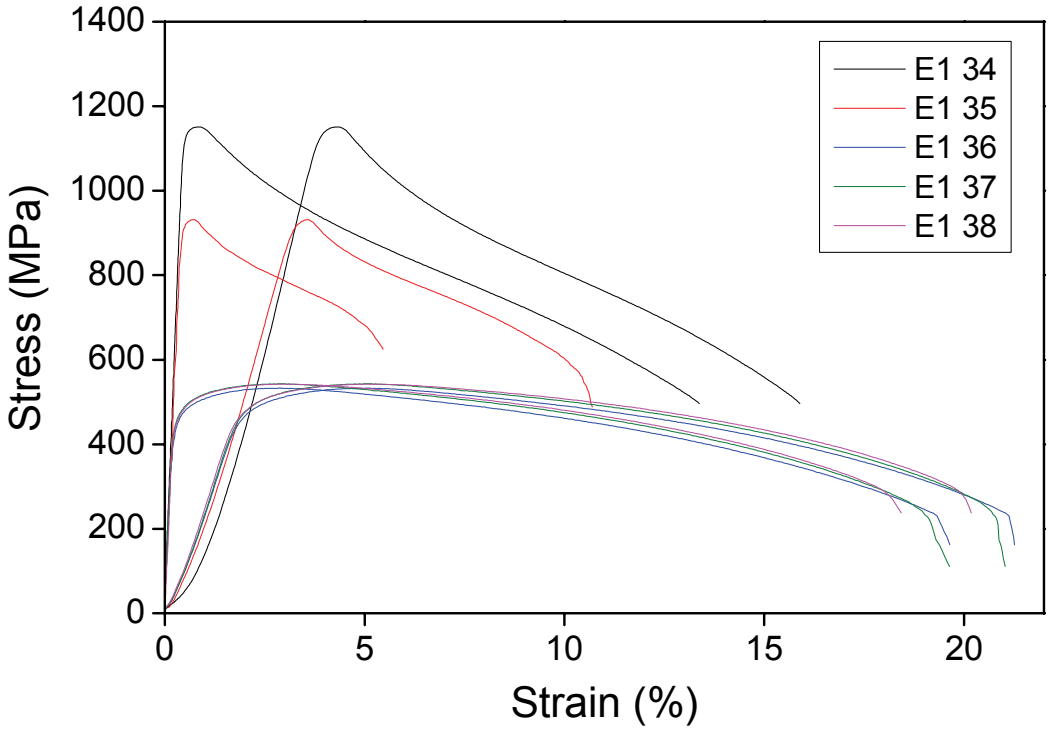

Fig. 10-2 Tensile stress vs. strain diagrams (displacement recording of extensometer and crosshead) of EUROFER 97 after irradiation to 31.0 dpa at 338.4 °C, the test conditions and the assessment results are summarised in Table 10-2.

File Name	T (°C)	R_{p02} (MPa)	R_m (MPa)	A_g (%)	A (%)	PIA
E1 34 -e	20	1146	1151	0.42	13.15	
E1 34 -t	20	1146	1151	0.47	13.70	
E1 35 -e	350	928	931	0.33	5.20	
E1 35 -t	350	927	931	0.37	8.75	
E1 36 -e	350	470	533	2.86	19.25	550 °C/3 h
E1 36 -t	350	471	533	3.05	20.15	550 °C/3 h
E1 37 -e	350	478	543	2.75	19.50	550 °C/1 h
E1 37 -t	350	480	543	3.20	20.50	550 °C/1 h
E1 38 -e	350	477	543	3.12	18.30	550 °C/0 h
E1 38 -t	350	477	543	3.35	18.40	550 °C/0 h

Table 10-2: Analysis of the tensile diagrams of EUROFER 97 after irradiation to 31.0 dpa at 338.4 °C (-e: extensometer, -t: crosshead).

10.2 EUROFER 97 HT

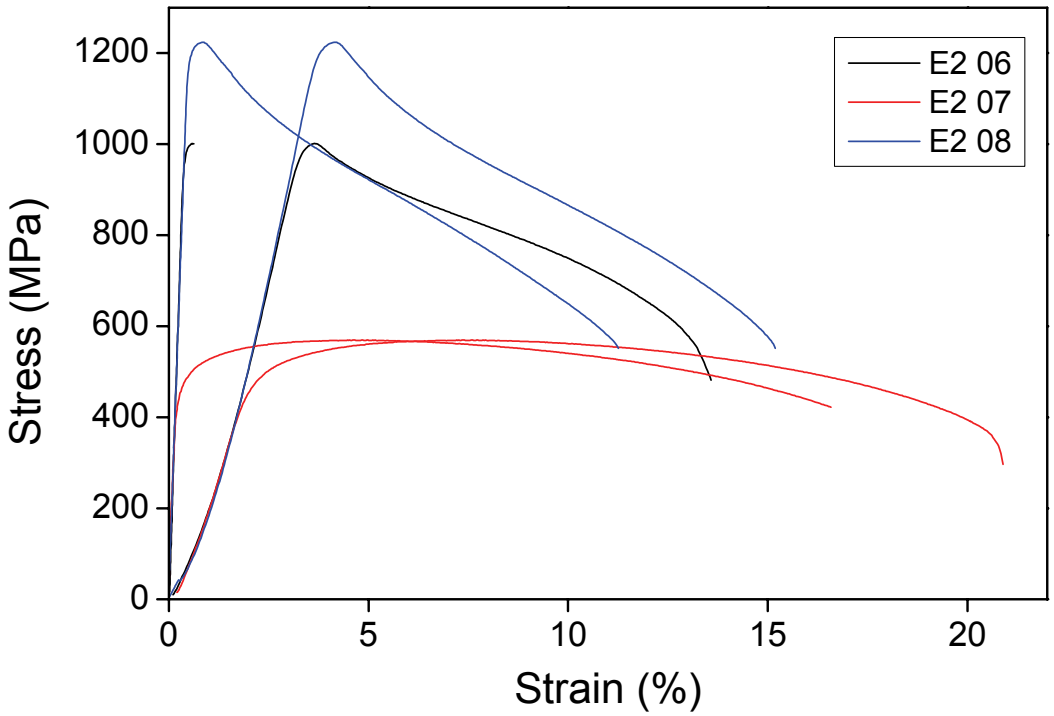

Fig. 10-3 Tensile stress vs. strain diagrams (displacement recording of extensometer and crosshead) of EUROFER 97 HT after irradiation to 70.1 dpa at 331.5 °C, the test conditions and the assessment results are summarised in Table 10-3.

File Name	T (°C)	R_{p02} (MPa)	R_m (MPa)	A_g (%)	A (%)	PIA
E2 06 -e	350	-----	1001	-----	-----	
E2 06 -t	350	996	1001	0.37	11.65	
E2 07 -e	350	478	570	5.00	-----	550 °C/3 h
E2 07 -t	350	477	570	5.85	19.50	550 °C/3 h
E2 08 -e	20	1217	1224	0.40	11.05	
E2 08 -t	20	1215	1224	0.44	13.05	

Table 10-3: Analysis of the tensile diagrams of EUROFER 97 HT after irradiation to 70.1 dpa at 331.5 °C (-e: extensometer, -t: crosshead).

10.3 F82H-mod.

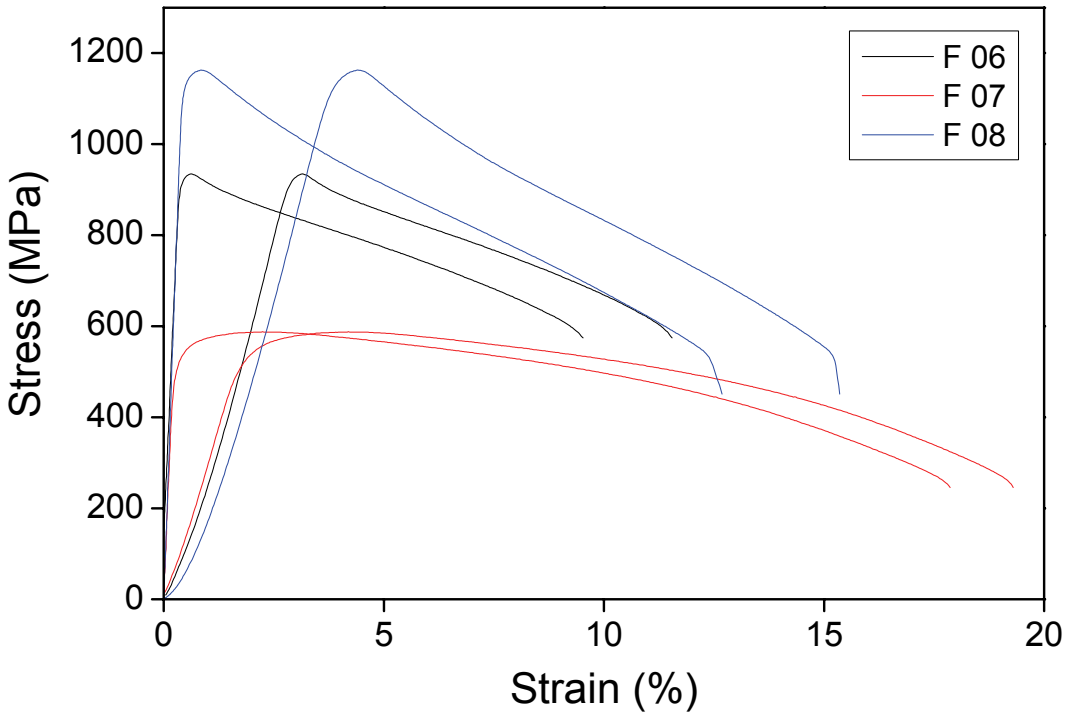

Fig. 10-4 Tensile stress vs. strain diagrams (displacement recording of extensometer and crosshead) of F82H-mod. after irradiation to 70.1 dpa at 331.5 °C, the test conditions and the assessment results are summarised in Table 10-4.

File Name	T (°C)	R_{p02} (MPa)	R_m (MPa)	A_g (%)	A (%)	PIA
F 06 -e	350	933	935	0.28	9.10	
F 06 -t	350	932	935	0.31	9.60	
F 07 -e	350	537	588	2.17	17.75	550 °C/3 h
F 07 -t	350	533	588	2.46	18.45	550 °C/3 h
F 08 -e	20	1151	1163	0.48	12.50	
F 08 -t	20	1142	1163	0.60	13.40	

Table 10-4: Analysis of the tensile diagrams of F82H-mod. after irradiation to 70.1 dpa at 331.5 °C (-e: extensometer, -t: crosshead).

10.4 ADS 2

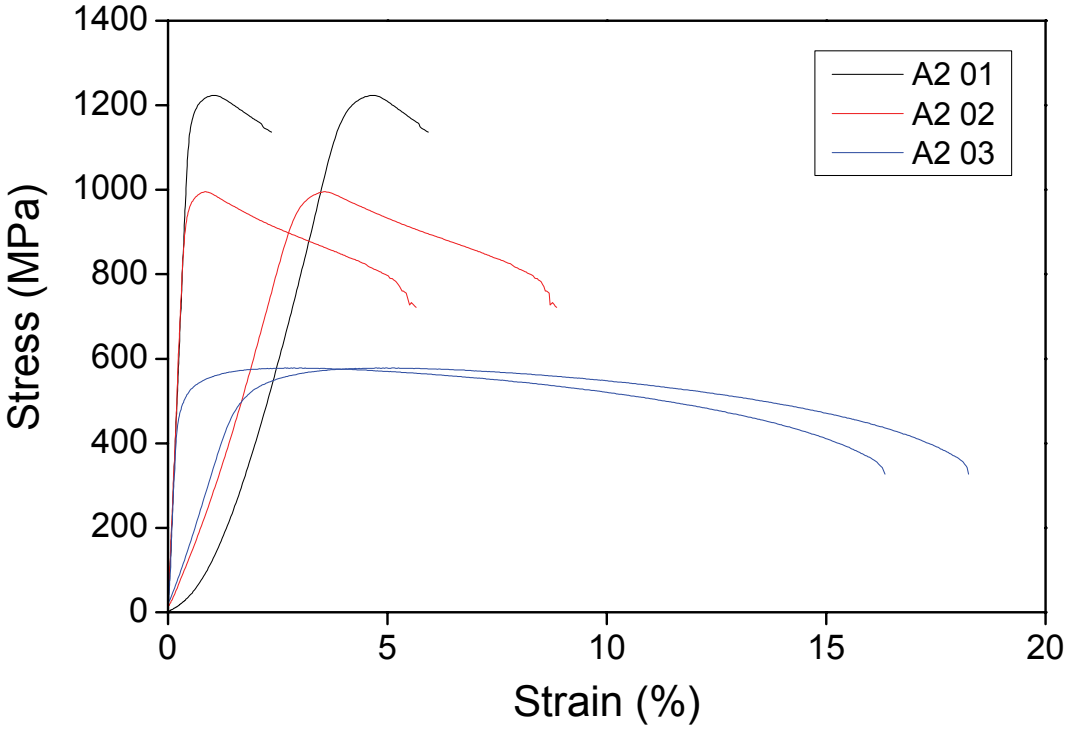

Fig. 10-5 Tensile stress vs. strain diagrams (displacement recording of extensometer and crosshead) of ADS 2 after irradiation to 70.1 dpa at 331.5 °C, the test conditions and the assessment results are summarised in Table 10-5.

File Name	T (°C)	R_{p02} (MPa)	R_m (MPa)	A_g (%)	A (%)	PIA
A2 01 -e	20	1199	1223	0.65	1.90	
A2 01 -t	20	1198	1223	0.69	2.10	
A2 02 -e	350	977	995	0.48	5.35	
A2 02 -t	350	973	995	0.61	6.55	
A2 03 -e	350	514	578	2.85	16.20	550 °C/3 h
A2 03 -t	350	504	578	3.62	17.25	550 °C/3 h

Table 10-5: Analysis of the tensile diagrams of ADS 2 after irradiation to 70.1 dpa at 331.5 °C (-e: extensometer, -t: crosshead).

10.5 ADS 3

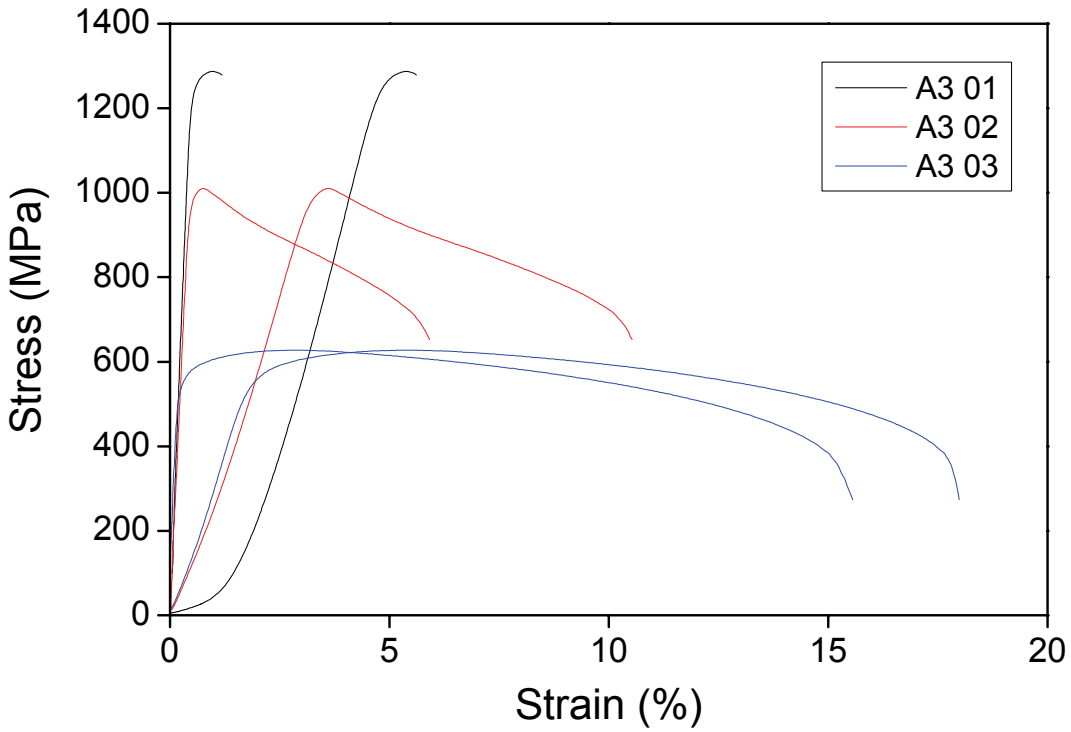

Fig. 10-6 Tensile stress vs. strain diagrams (displacement recording of extensometer and crosshead) of ADS 3 after irradiation to 70.1 dpa at 331.5 °C, the test conditions and the assessment results are summarised in Table 10-6.

File Name	T (°C)	R_{p02} (MPa)	R_m (MPa)	A_g (%)	A (%)	PIA
A3 01 -e	20	1268	1287	0.53	0.70	
A3 01 -t	20	1267	1287	0.61	0.80	
A3 02 -e	350	1004	1010	0.32	5.62	
A3 02 -t	350	1000	1010	0.43	6.35	
A3 03 -e	350	568	628	2.67	15.50	550 °C/3 h
A3 03 -t	350	556	628	3.60	17.05	550 °C/3 h

Table 10-6: Analysis of the tensile diagrams of ADS 3 after irradiation to 70.1 dpa at 331.5 °C (-e: extensometer, -t: crosshead).

10.6 OPTIFER XI

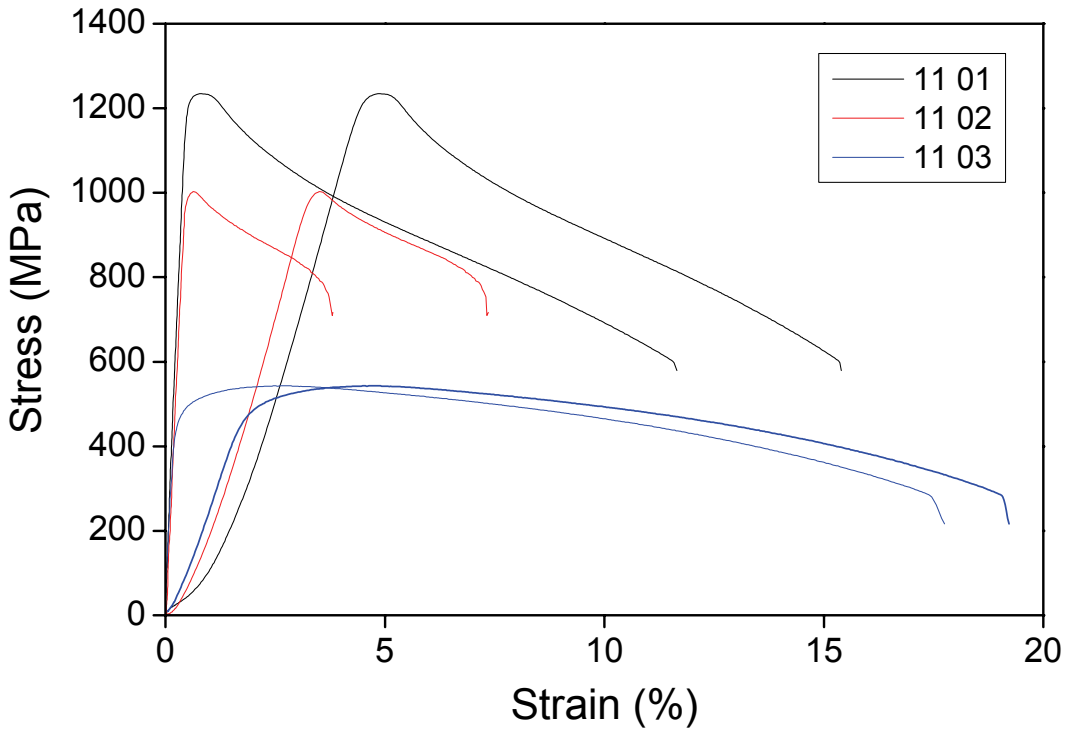

Fig. 10-7 Tensile stress vs. strain diagrams (displacement recording of extensometer and crosshead) of OPTIFER XI after irradiation to 31.0 dpa at 338.4 °C, the test conditions and the assessment results are summarised in Table 10-7.

File Name	T (°C)	R_{p02} (MPa)	R_m (MPa)	A_g (%)	A (%)	PIA
11 01 -e	20	1229	1235	0.36	11.35	
11 01 -t	20	1229	1235	0.41	12.60	
11 02 -e	350	1003	1003	0.20	3.47	
11 02 -t	350	1002	1003	0.23	4.70	
11 03 -e	350	483	543	2.40	17.30	550 °C/3 h
11 03 -t	350	483	543	2.80	17.90	550 °C/3 h

Table 10-7: Analysis of the tensile diagrams of OPTIFER XI after irradiation to 31 dpa at 338.4 °C (-e: extensometer, -t: crosshead).

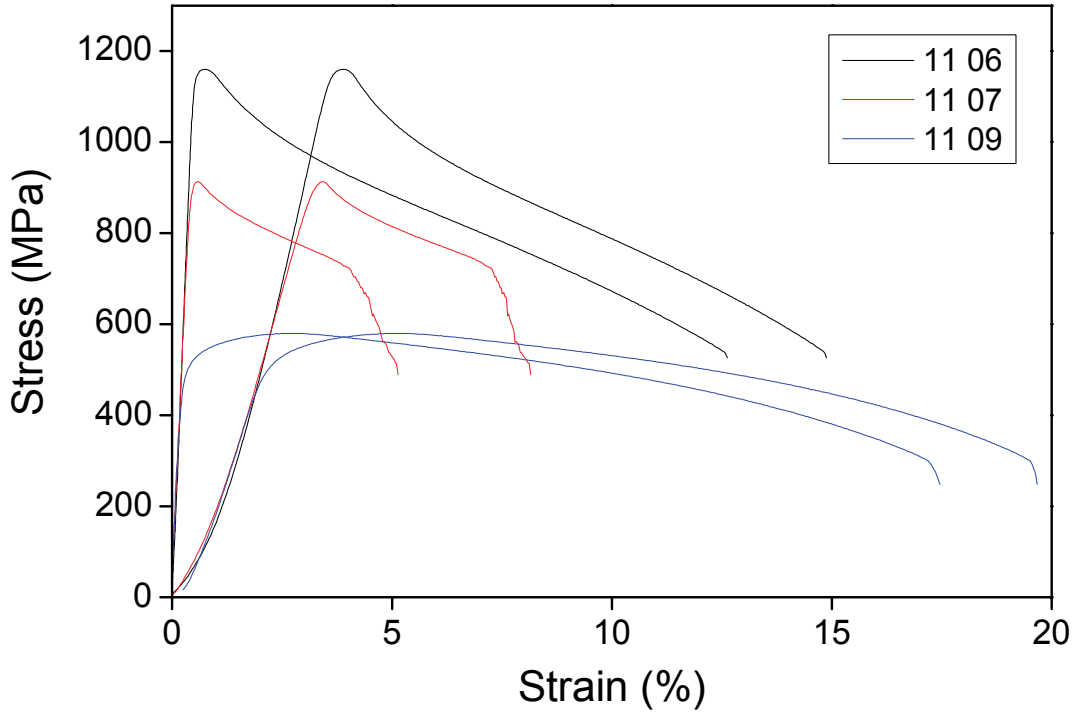

Fig. 10-8 Tensile stress vs. strain diagrams (displacement recording of extensometer and crosshead) of OPTIFER XI after irradiation to 12 dpa at 337.5 °C, the test conditions and the assessment results are summarised in Table 10-8.

File Name	T (°C)	R_{p02} (MPa)	R_m (MPa)	A_g (%)	A (%)	PIA
11 06 -e	20	1160	1160	0.27	12.40	
11 06 -t	20	1159	1160	0.31	12.75	
11 07 -e	350	913	914	0.18	4.90	
11 07 -t	350	913	914	0.25	6.15	
11 09 -e	350	517	580	2.76	17.40	550 °C/3 h
11 09 -t	350	515	580	3.10	18.45	550 °C/3 h

Table 10-8: Analysis of the tensile diagrams of OPTIFER XI after irradiation to 12 dpa at 337.5 °C (-e: extensometer, -t: crosshead).

10.7 OPTIFER XII

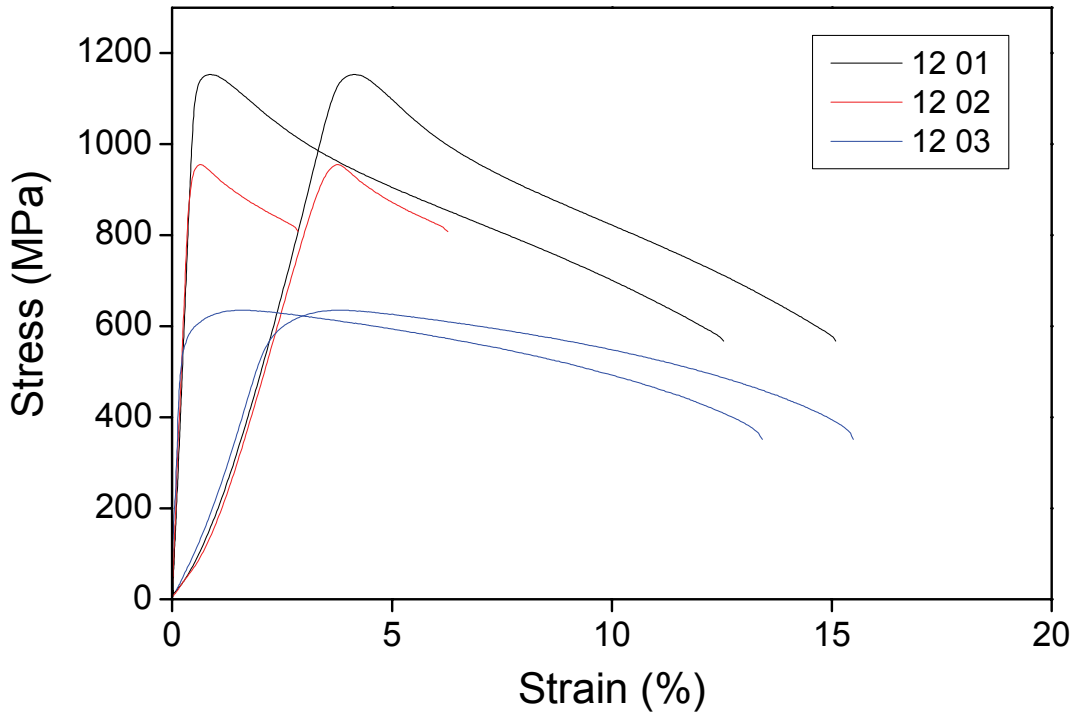

Fig. 10-9 Tensile stress vs. strain diagrams (displacement recording of extensometer and crosshead) of OPTIFER XII after irradiation to 12 dpa at 337.5 °C, the test conditions and the assessment results are summarised in Table 10-9.

File Name	T (°C)	R_{p02} (MPa)	R_m (MPa)	A_g (%)	A (%)	PIA
12 01 -e	20	1148	1153	0.38	12.25	
12 01 -t	20	1148	1153	0.42	12.85	
12 02 -e	350	954	956	0.25	2.52	
12 02 -t	350	949	956	0.33	3.25	
12 03 -e	350	588	635	1.52	13.30	550 °C/3 h
12 03 -t	350	589	635	1.73	14.05	550 °C/3 h

Table 10-9: Analysis of the tensile diagrams of OPTIFER XII after irradiation to 12 dpa at 337.5 °C (-e: extensometer, -t: crosshead).

10.8 EURODShip with 0.5 wt.% Y_2O_3

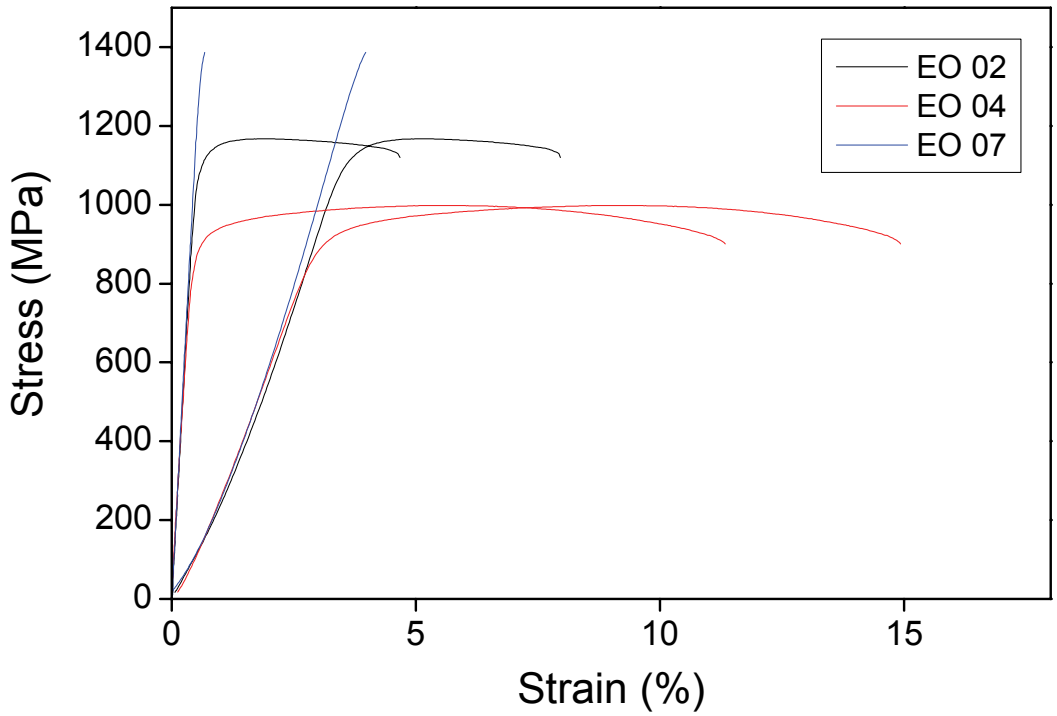

Fig. 10-10 Tensile stress vs. strain diagrams (displacement recording of extensometer and crosshead) of EURODShip with 0.5 wt.% Y_2O_3 after irradiation to 70.1 dpa at 331.5 °C, the test conditions and the assessment results are summarised in Table 10-10.

File Name	T (°C)	R_{p02} (MPa)	R_m (MPa)	A_g (%)	A (%)	PIA
EO 02 -e	350	1122	1168	1.58	4.17	
EO 02 -t	350	1119	1168	1.73	4.45	
EO 04 -e	350	904	998	5.51	10.90	550 °C/3 h
EO 04 -t	350	900	998	6.42	12.00	550 °C/3 h
EO 07 -e	20	1387	1387	0.09	0.09	
EO 07 -t	20	1387	1387	0.08	0.08	

Table 10-10: Analysis of the tensile diagrams of EURODShip with 0.5 wt.% Y_2O_3 after irradiation to 70.1 dpa at 331.5 °C (-e: extensometer, -t: crosshead).

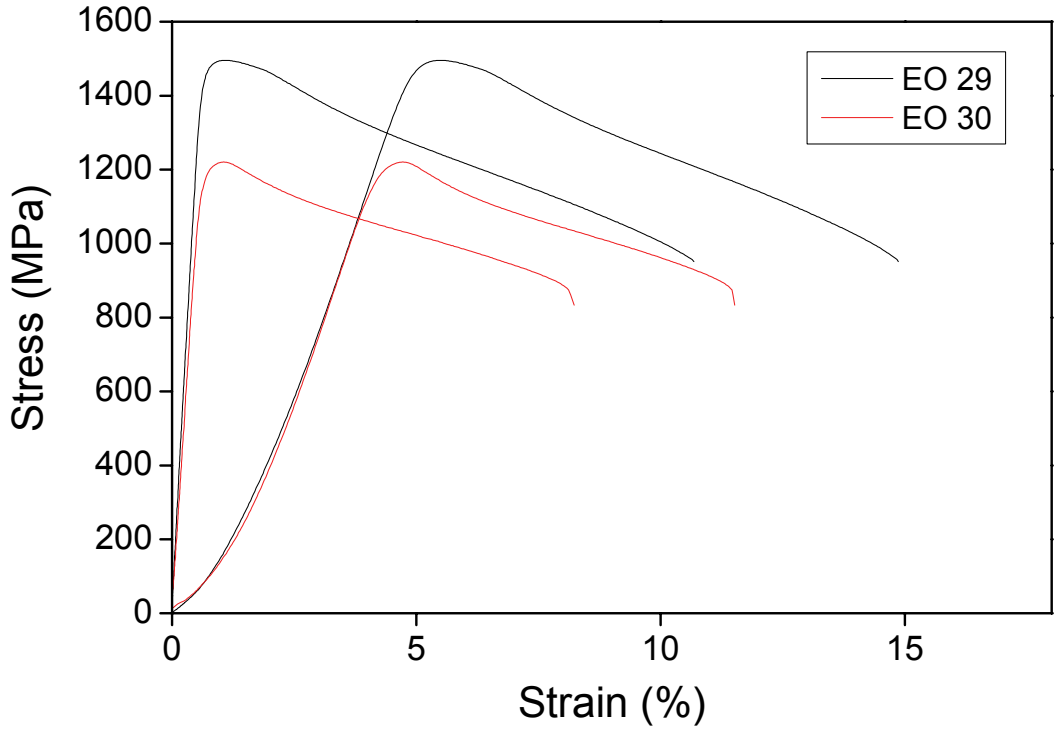

Fig. 10-11 Tensile stress vs. strain diagrams (displacement recording of extensometer and crosshead) of EURODShip with 0.5 wt.% Y_2O_3 after irradiation to 12 dpa at 337.5 °C, the test conditions and the assessment results are summarised in Table 10-11.

File Name	T (°C)	R_{p02} (MPa)	R_m (MPa)	A_g (%)	A (%)
EO 29 -e	20	1480	1496	0.48	10.25
EO 29 -t	20	1479	1496	0.55	11.35
EO 30 -e	350	1201	1221	0.52	7.82
EO 30 -t	350	1202	1221	0.54	8.30

Table 10-11: Analysis of the tensile diagrams of EURODShip with 0.5 wt.% Y_2O_3 after irradiation to 12 dpa at 337.5 °C (-e: extensometer, -t: crosshead).

10.9 EODShip3 with 0.3 wt.% Y_2O_3

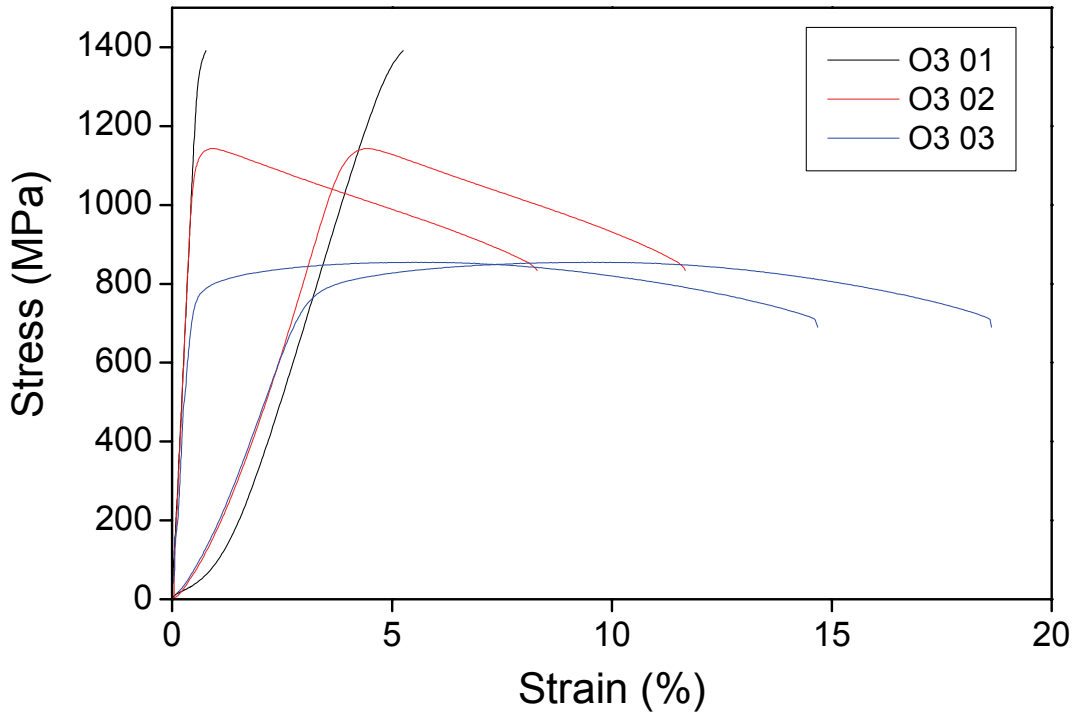

Fig. 10-12 Tensile stress vs. strain diagrams (displacement recording of extensometer and crosshead) of EURODShip with 0.3 wt.% Y_2O_3 after irradiation to 12 dpa at 337.5 °C, the test conditions and the assessment results are summarised in Table 10-12.

File Name	T (°C)	R_{p02} (MPa)	R_m (MPa)	A_g (%)	A (%)	PIA
O3 01 -e	20	1391	1391	0.17	0.17	
O3 01 -t	20	1361	1391	0.33	0.33	
O3 02 -e	350	1130	1143	0.53	7.95	
O3 02 -t	350	1125	1143	0.64	8.55	
O3 03 -e	350	777	855	5.39	14.30	550 °C/3 h
O3 03 -t	350	760	855	6.69	15.90	550 °C/3 h

Table 10-12: Analysis of the tensile diagrams of EODShip3 with 0.3 wt.% Y_2O_3 after irradiation to 31 dpa at 338.4 °C (-e: extensometer, -t: crosshead).

10.10 EUROF-EB

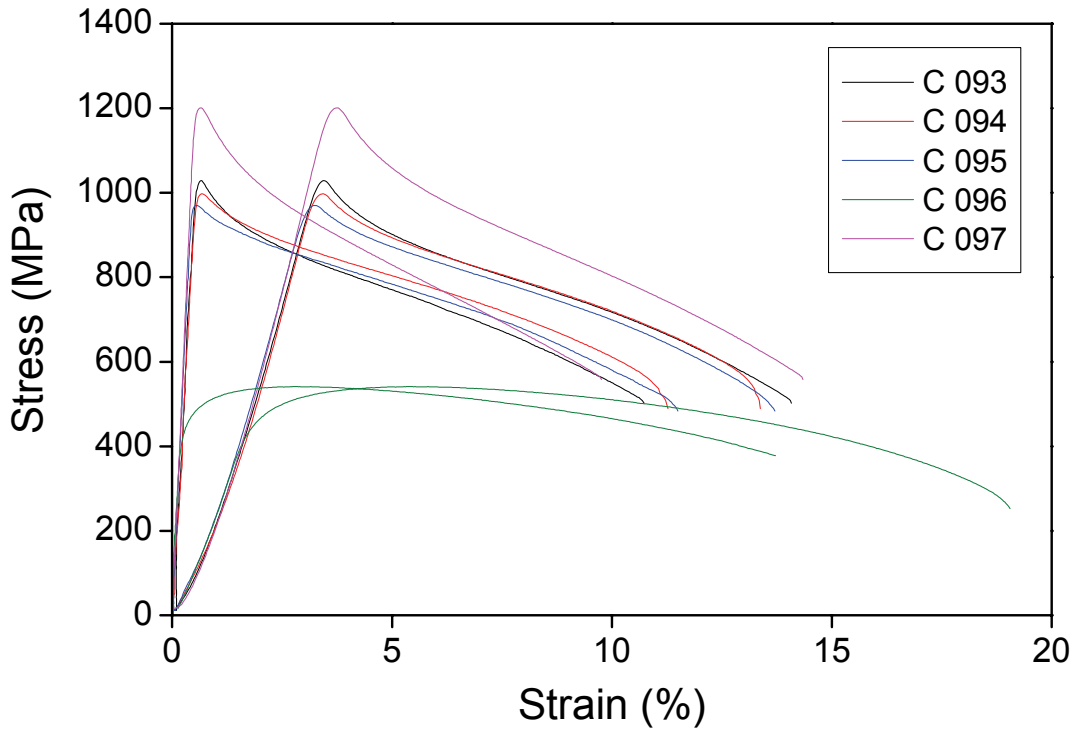

Fig. 10-13 Tensile stress vs. strain diagrams (displacement recording of extensometer and crosshead) of EUROF-EB after irradiation to 70.1 dpa at 331.5 °C, the test conditions and the assessment results are summarised in Table 10-13.

File Name	T (°C)	R_{p02} (MPa)	R_m (MPa)	A_g (%)	A (%)	PIA
C 093 -e	250	1022	1029	0.15	10.45	
C 093 -t	250	1027	1029	0.18	12.20	
C 094 -e	300	997	997	0.16	11.00	
C 094 -t	300	997	997	0.22	11.45	
C 095 -e	350	970	970	0.16	11.25	
C 095 -t	350	970	970	0.19	11.95	
C 096 -e	350	467	541	2.78	------	550 °C/3 h
C 096 -t	350	460	541	3.62	18.00	550 °C/3 h
C 097 -e	20	1201	1201	0.16	10.33	
C 097 -t	20	1201	1201	0.23	12.35	

Table 10-13: Analysis of the tensile diagrams of EUROF-EB after irradiation to 70.1 dpa at 331.5 °C (-e: extensometer, -t: crosshead).

10.11 Tensile properties in the reference unirradiated state

Material	Specimen	Condition	T_{test} (°C)	$R_{p0.2}$ (MPa)	Rm (MPa)	A_g (%)	A (%)
EUROFER 97	Probe01	unirradiated	350	464.64	524	3.12	20.92
EUROFER 97	Probe02	unirradiated	350	452.29	507.85	2.64	20.9
EUROFER 97 HT	Probe01	unirradiated	350	444.99	502.55	2.41	20.18
EUROFER 97 HT	Probe02	unirradiated	350	427.75	496.78	3.24	21.02
ADS 2	Probe01	unirradiated	350	418.70	472.50	3.20	20.50
ADS 2	Probe02	unirradiated	350	408.92	464.78	2.83	19.70
ADS 3	Probe01	unirradiated	350	407.82	470.00	3.50	20.75
ADS 3	Probe02	unirradiated	350	405.37	465.00	2.95	20.48
F82H-mod.	Probe01	unirradiated	350	478.65	531.15	2.37	19.29
F82H-mod.	Probe02	unirradiated	350	475.91	-	-	-
OPTIFER XI	Probe01	unirradiated	350	485.36	550.40	3.40	19.20
OPTIFER XI	Probe02	unirradiated	350	486.85	547.74	3.30	19.20
OPTIFER XII	Probe01	unirradiated	350	483.24	566.18	3.70	19.00
OPTIFER XII	Probe02	unirradiated	350	490.80	577.82	3.85	19.70
EODShip3	Probe01	unirradiated	350	587.24	779.82	8.20	17.75

Table 10-14: Analysis of the tensile diagrams of the investigated steels in the reference unirradiated condition.

10.12 Diffusion welded EUROFER 97 (1xHIP)

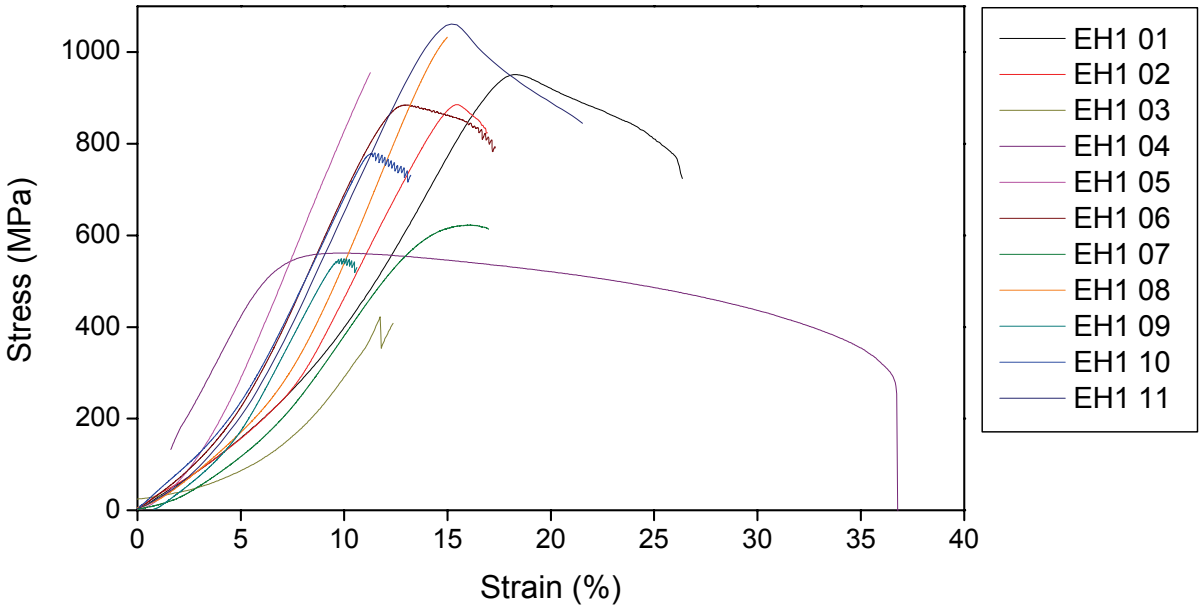

Fig. 10-14 Tensile stress vs. displacement diagrams (displacement recording of crosshead) of 1xHIP diffusion welded EUROFER 97 after irradiation to 36.2 dpa at 336.8 °C. The test conditions and the assessment results are summarised in Table 10-15.

Specimen	T_{test} (°C)	V (mm/min)	$R_{p0.2}$ (MPa)	R_m (MPa)	A_g (%)	A (%)	File Name	comment
EH1 01	300	1.0	901.0	950.4	1.00	11.47	2_340	
EH1 02	300	1.0	842.5	885.3	0.73	2.41	2_346	
EH1 03	20	1.0	-	421.0	-	5.07	2_348	
EH1 04	300	1.0	491.8	561.2	3.25	33.50	2_354	PIA 550°C/3h
EH1 05	20	1.0	955.2	955.2	-	0.00	2_380	broken at the head
EH1 06	300	0.1	815.9	884.3	1.04	6.30	2_382	
EH1 07	20	0.1	548.3	622.2	2.40	3.30	2_377	broken at the head
EH1 08	20	0.1	997.0	1032.4	0.45	0.45	2_385	
EH1 09	300	0.1	539.0	549.1	0.40	1.30	2_387	
EH1 10	300	0.1	777.4	777.4	0.35	2.70	2_398	
EH1 11	20	1.0	996.5	1061.6	0.97	10.00	2_394	

Table 10-15: Analysis of the tensile diagrams of 1xHIP diffusion welded EUROFER 97 after irradiation to 36.2 dpa at 336.8 °C.

Specimen/ Test	T_{test} (°C)	V (mm/min)	$R_{p0.2}$ (MPa)	R_m (MPa)	A_g (%)	A (%)	File Name
Test-1	20	0.1	524.2	596.6	4.32	39.60	2_324
Test-1, KIT	20	0.1	518.6	654.0	4.62	39.50	Gaga01_1xhip_01
Test-3	20	1	647.4	743.0	4.29	41.06	2_327
1xhip(2)	20	1	478.8	673.3	5.72	35.28	2_331
1xhip 300	300	1	442.8	541.2	2.80	34.50	2_338
x1-300	300	0.1	471.3	524.8	2.50	38.70	2_407

Table 10-16: Analysis of the tensile diagrams of diffusion 1xHIP welded EUROFER 97 in the reference unirradiated state.

10.13 Diffusion welded EUROFER 97 (2xHIP)

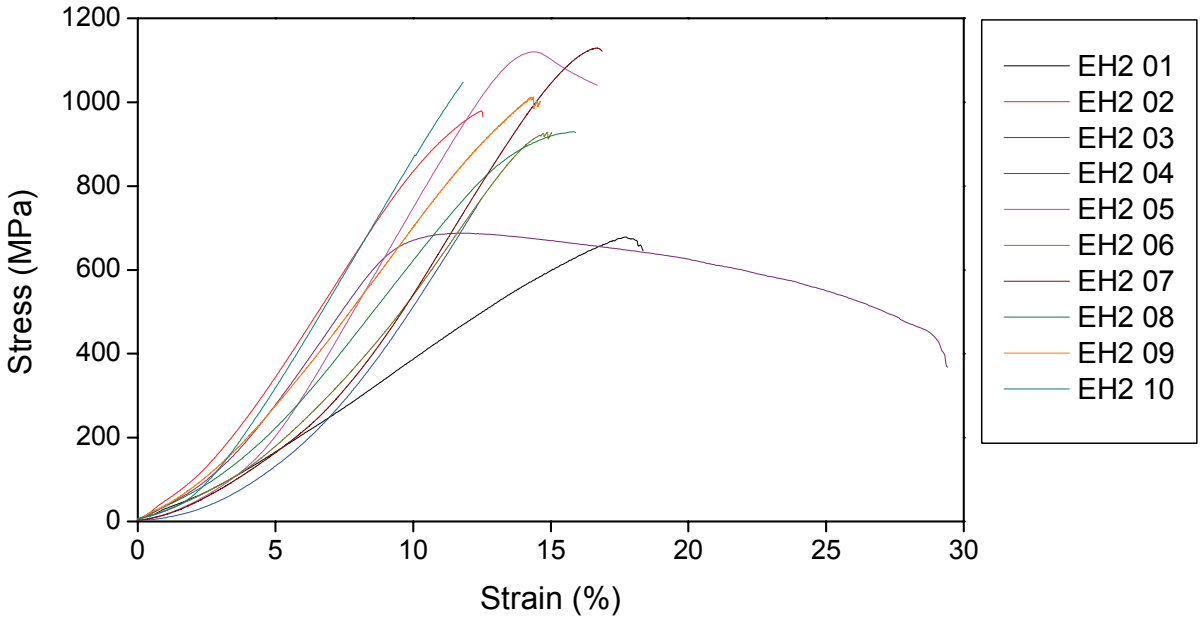

Fig. 10-15 Tensile stress vs. displacement diagrams (displacement recording of crosshead) of 2xHIP diffusion welded EUROFER 97 after irradiation to 36.2 dpa at 336.8 °C. The test conditions and the assessment results are summarised in Table 10-17.

Specimen	T_{test} (°C)	V (mm/min)	$R_{p0.2}$ (MPa)	R_m (MPa)	A_g (%)	A (%)	File Name	comment
EH2 01	300	1.0	560.0	678.4	1.40	2.66	2_342	
EH2 02	300	1.0	849.0	978.7	1.24	1.24	2_344	
EH2 04	20	1.0	-	772.9	0.00	0.00	2_347	
EH2 03	300	1.0	632.9	687.6	2.50	22.00	2_358	PIA 550°C/ 3 h
EH2 05	20	1.0	1036.7	1120.2	1.25	4.10	2_378	
EH2 06	300	0.1	893.2	928.0	0.80	1.20	2_384	
EH2 07	20	0.1	1026.4	1129.0	1.20	1.35	2_379	
EH2 08	300	1.0	817.7	929.4	2.25	2.25	2_389	
EH2 09	300	0.1	903.0	1011.8	0.80	1.15	2_391	
EH2 10	20	1.0	1045.2	1045.2	-	-	2_395	

Table 10-17: Analysis of the tensile diagrams of 2xHIP diffusion welded EUROFER 97 after irradiation to 36.2 dpa at 336.8 °C.

Specimen	T_{test} (°C)	V (mm/min)	$R_{p0.2}$ (Mpa)	Rm (Mpa)	A_g (%)	A (%)	File Name
Test-2	20	0.1	731.0	912.5	5.00	29.70	2_325
Test-4	20	1.0	759.0	836.4	3.50	36.26	2_328
2xhip(2)	20	1.0	736.3	869.9	4.05	29.00	2_330
2xhip 300	300	1.0	565.7	676.7	1.40	2.30	2_336
X2-300	300	0.1	633.0	701.7	2.90	26.40	2_402

Table 10-18: Analysis of the tensile diagrams of diffusion 2xHIP welded EUROFER 97 in the reference unirradiated state.

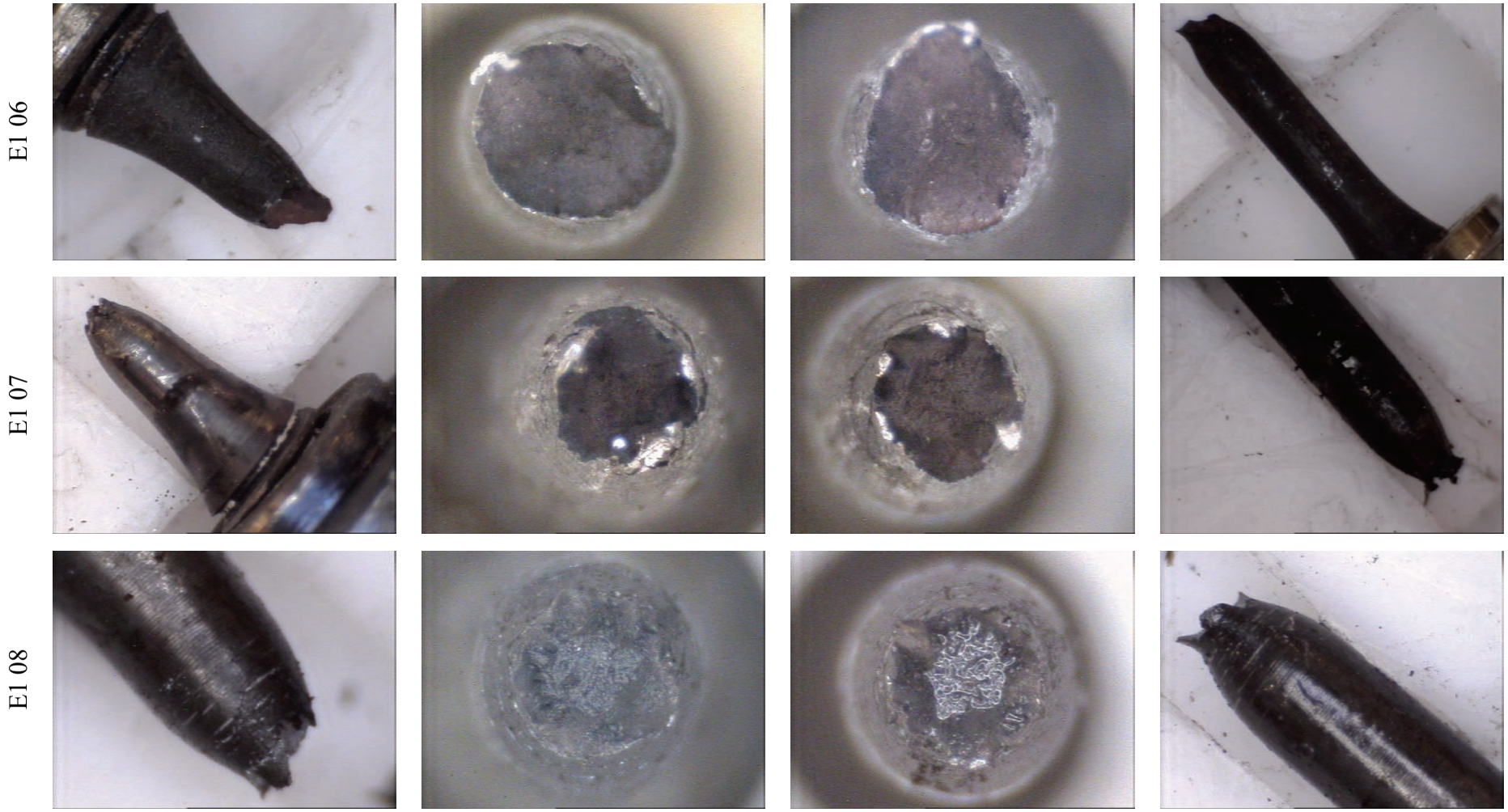

Fig. 10-16 Photographs (macro) of the tensile tested EUROFER 97 specimens: E1 06 (T_{test}=350 °C), E1 07 (T_{test}=350 °C after annealing at 550 °C/3 h), E1 08 (T_{test}=20 °C).

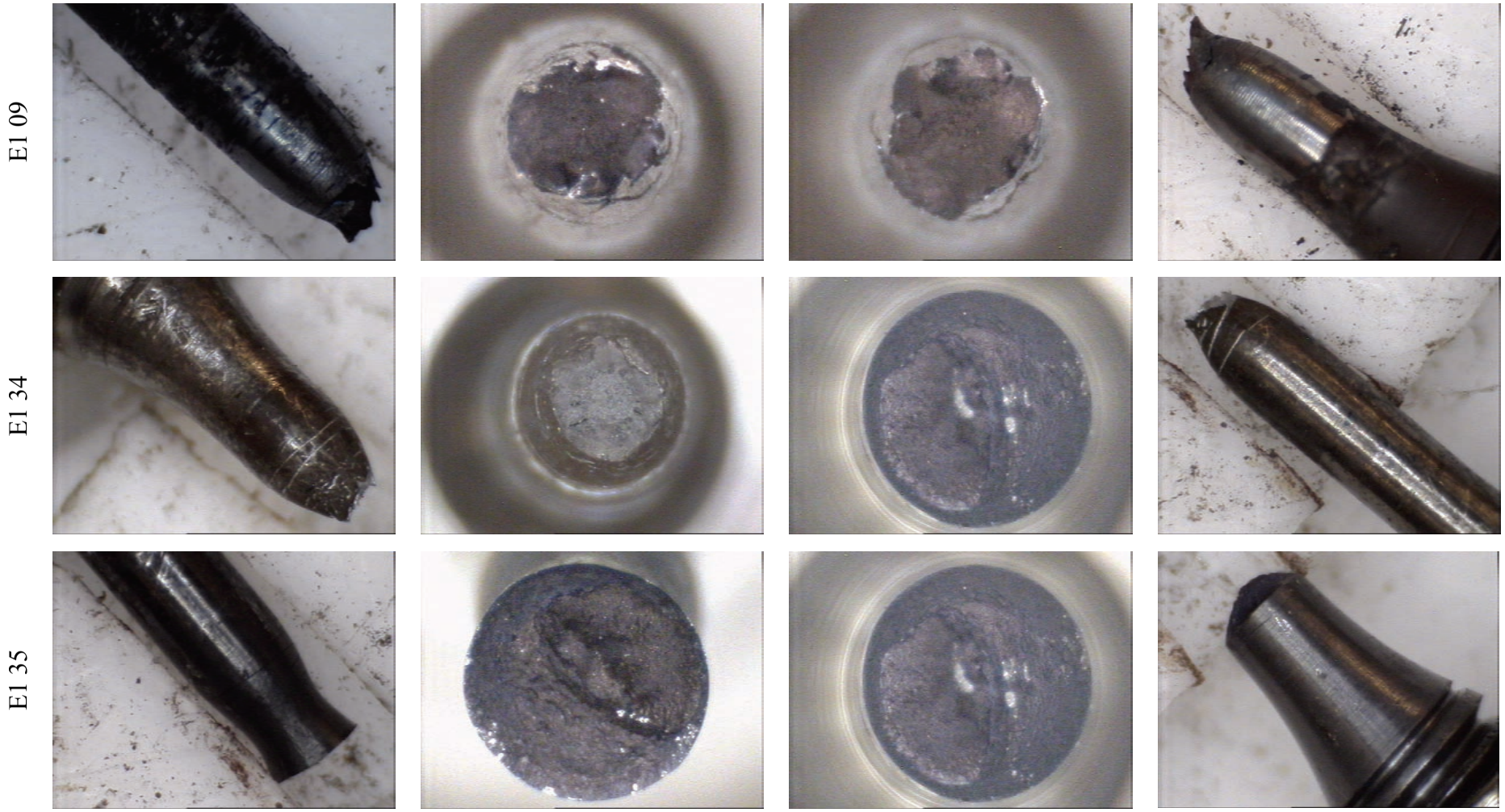

Fig. 10-17 Photographs (macro) of the tensile tested EUROFER 97 specimens: E1 09 (T_{test}=350 °C after annealing at 550 °C/1 h), E1 34 (T_{test}=20 °C), E1 35 (T_{test}=350 °C).

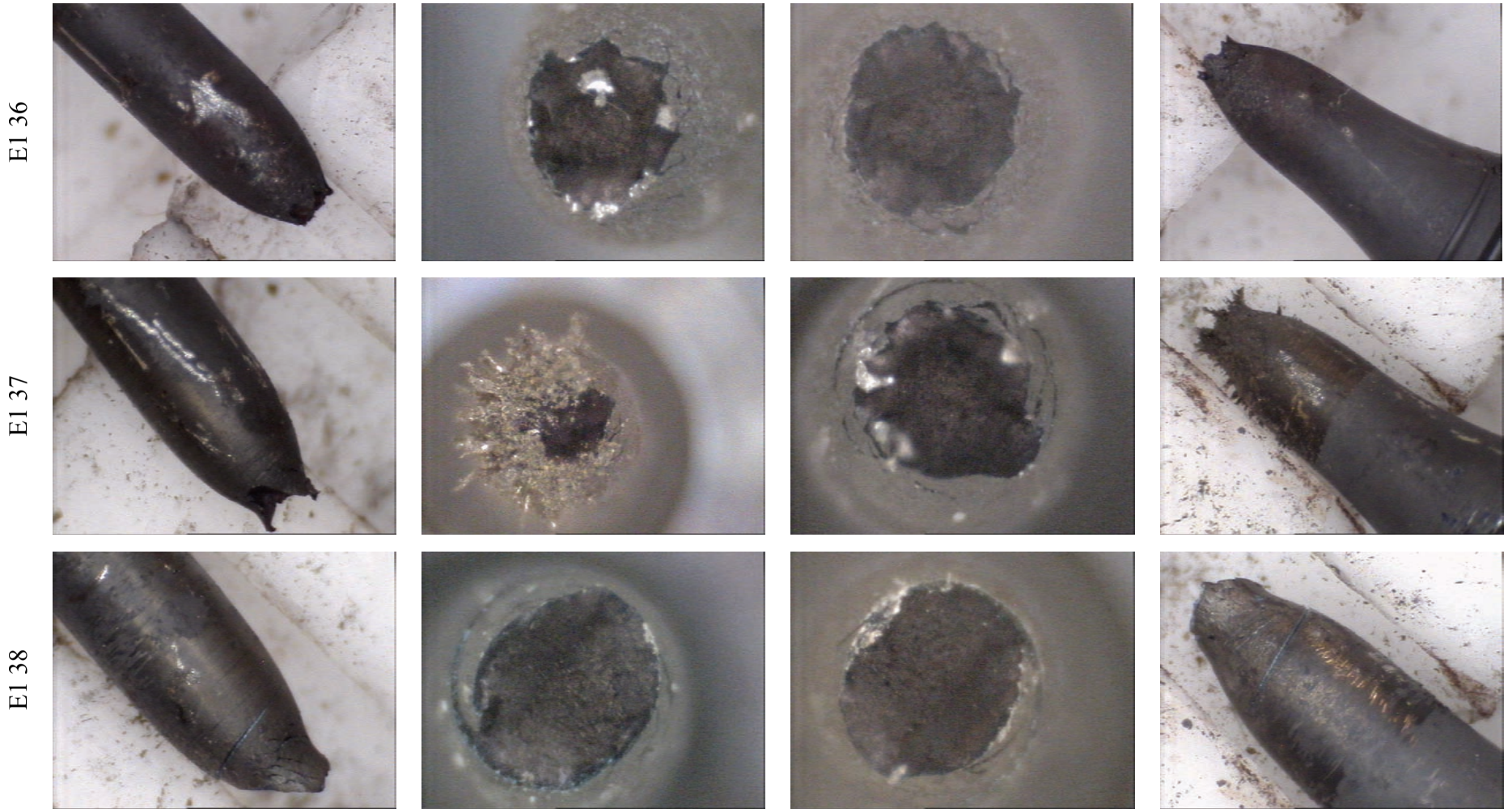

Fig. 10-18 Photographs (macro) of the tensile tested EUROFER 97 specimens: E1 36 (T_{test}=350 °C after annealing at 550 °C/3 h), E1 37 (T_{test}=350 °C after annealing at 550 °C/1 h), E1 38 (T_{test}=350 °C after annealing at 550 °C/”0” h).

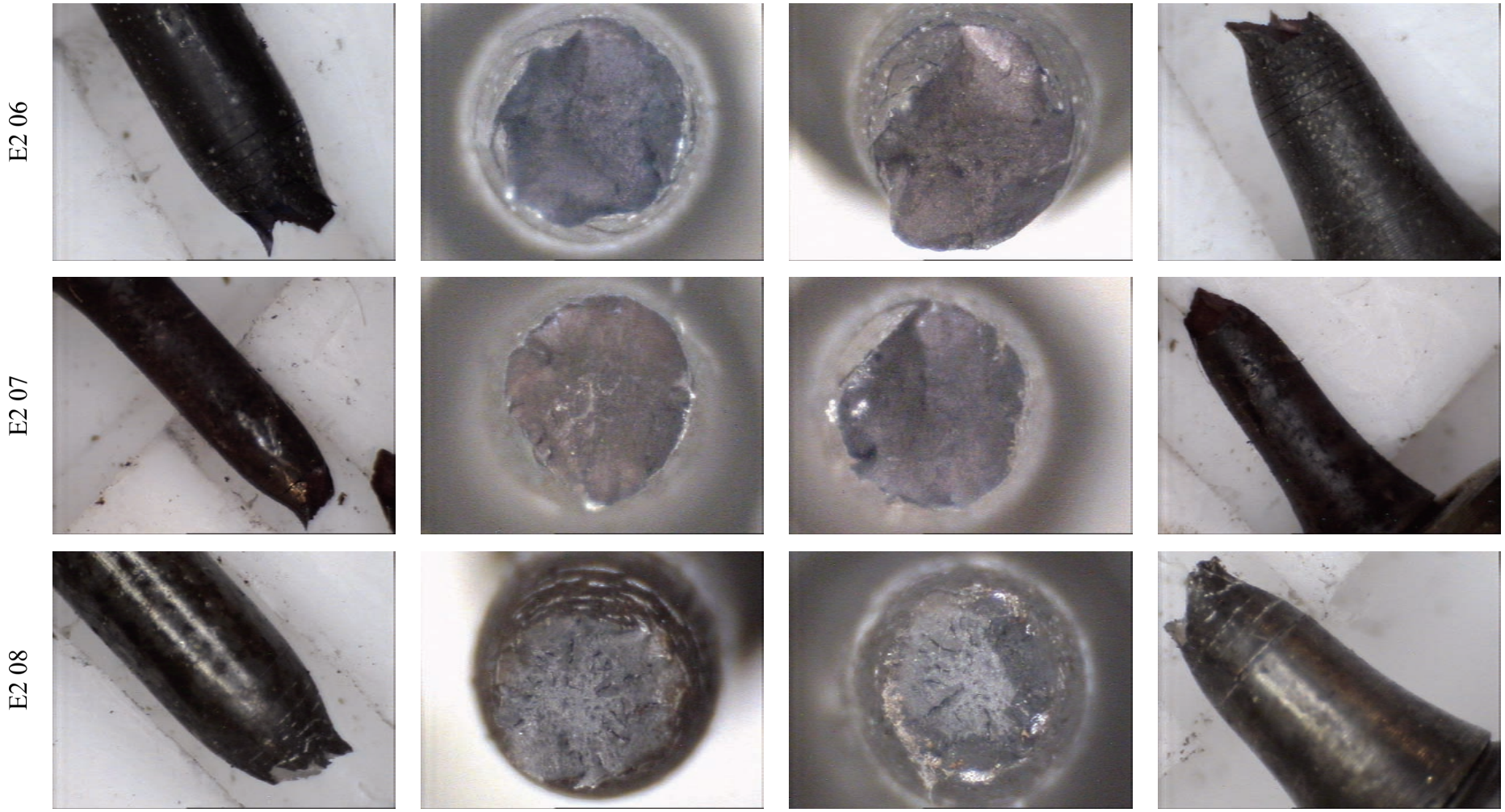

Fig. 10-19 Photographs (macro) of the tensile tested EUROFER 97 HT specimens: E2 06 (T_{test}=350 °C), E2 07 (T_{test}=350 °C after annealing at 550 °C/3 h), E2 08 (T_{test}=20 °C).

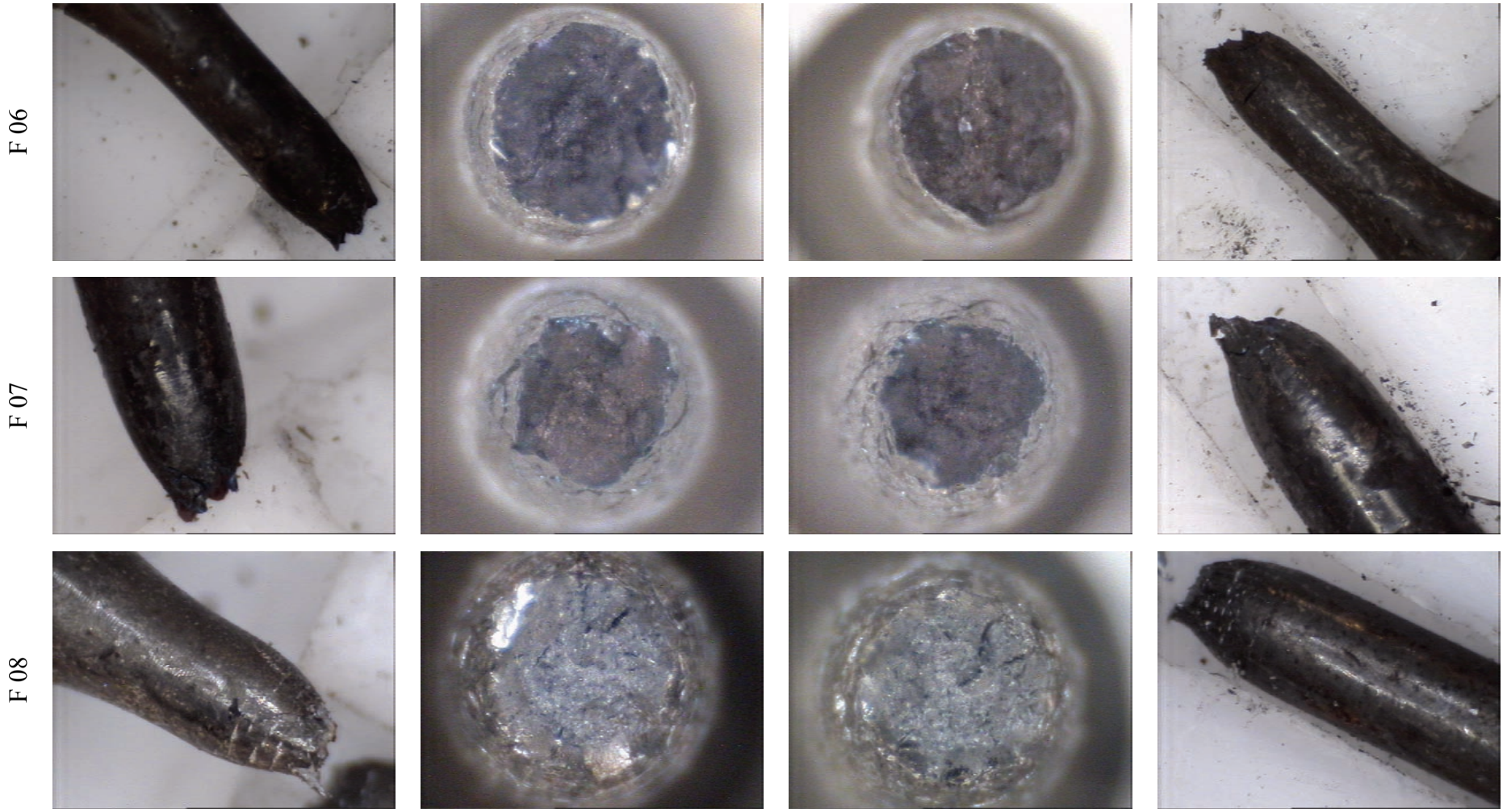

Fig. 10-20 Photographs (macro) of the tensile tested F82H-mod. specimens: F 06 (T_{test}=350 °C), F 07 (T_{test}=350 °C after annealing at 550 °C/3 h), F 08 (T_{test}=20 °C).

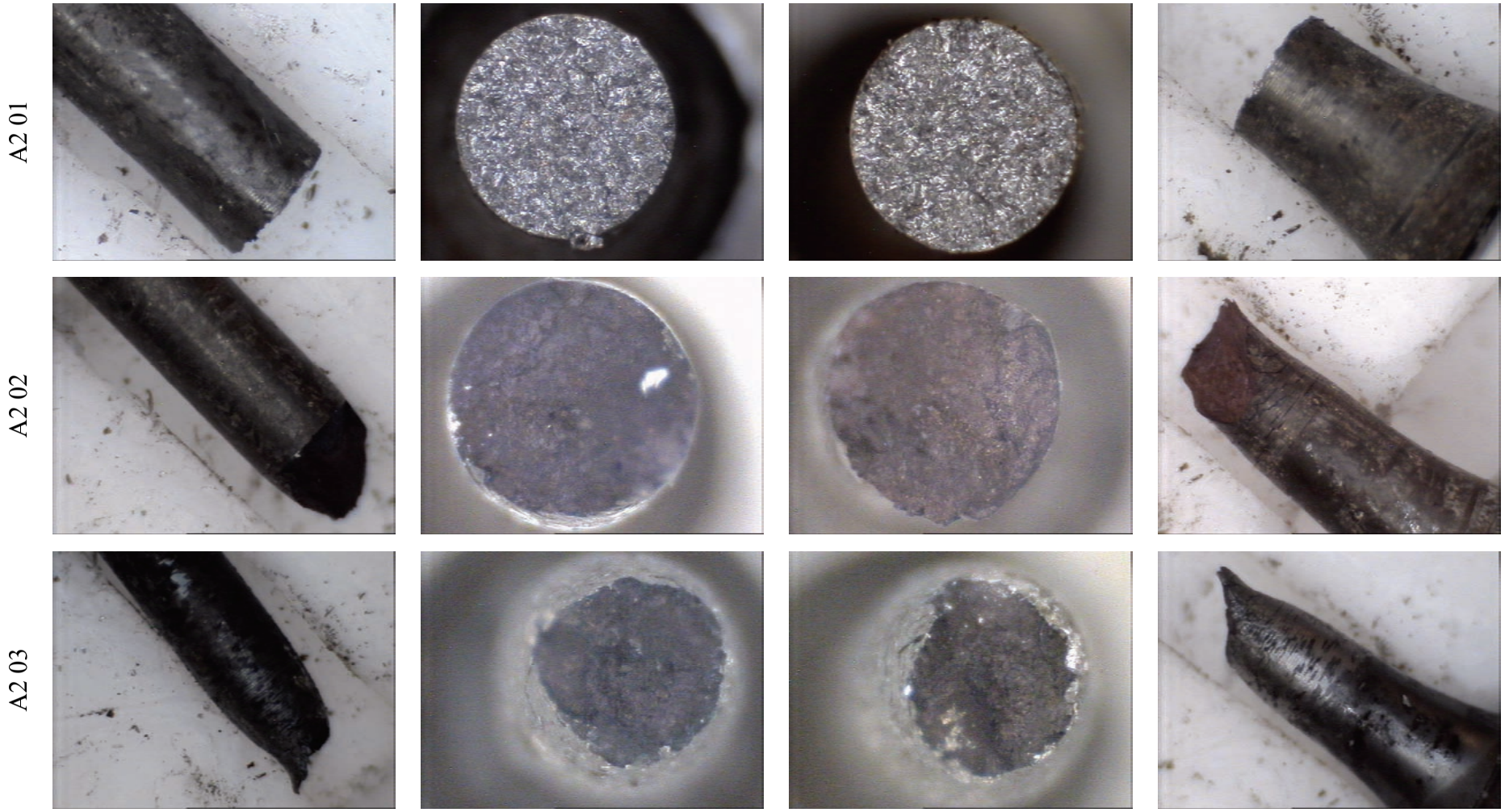

Fig. 10-21 Photographs (macro) of the tensile tested ADS 2 specimens: A2 01 (T_{test}=20 °C), A2 02 (T_{test}=350 °C), A2 03 (T_{test}=350 °C after annealing at 550 °C/3 h).

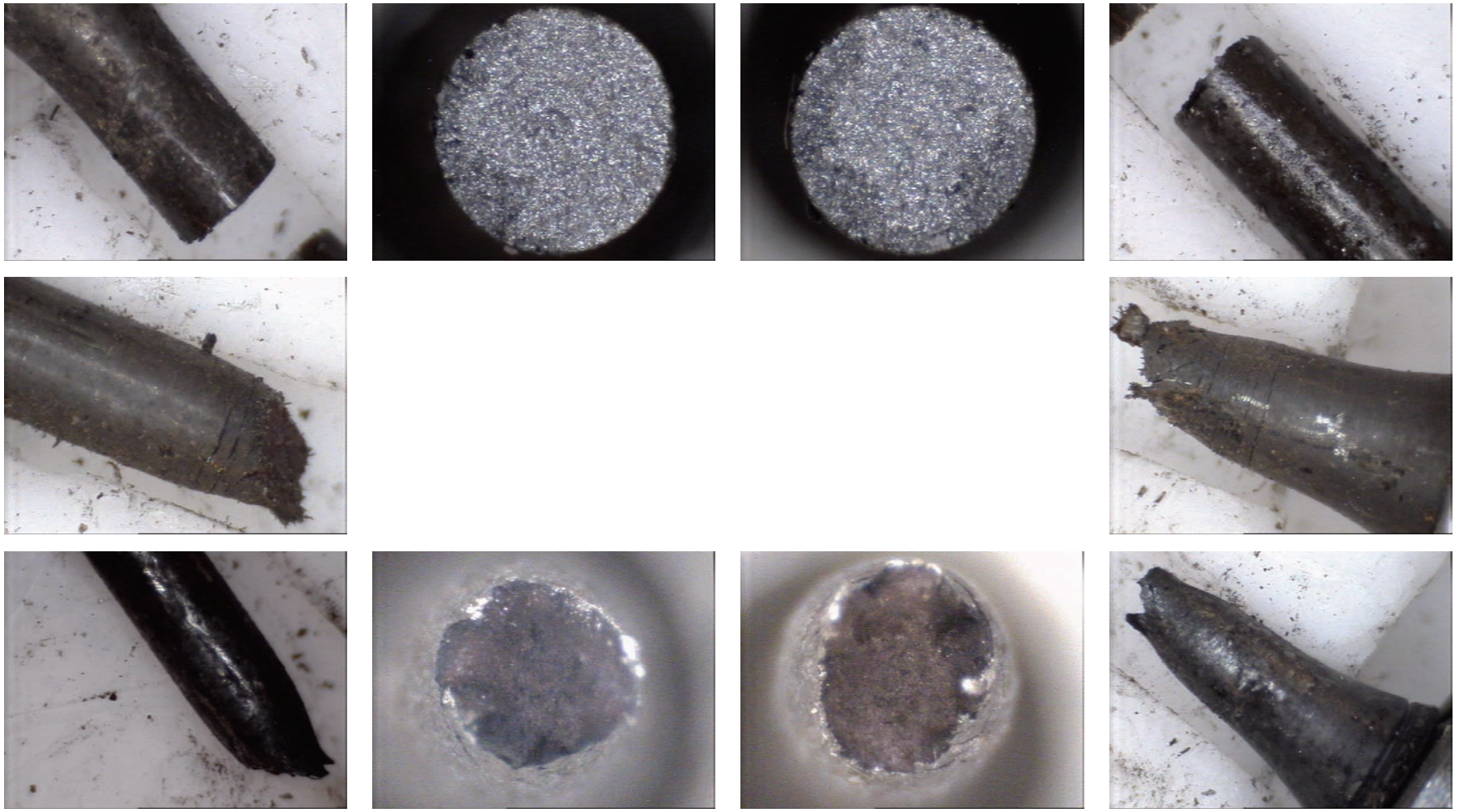

Fig. 10-22 Photographs (macro) of the tensile tested ADS 3 specimens: A3 01 (T_{test}=20 °C), A3 02 (T_{test}=350 °C), A3 03 (T_{test}=350 °C after annealing at 550 °C/3 h).

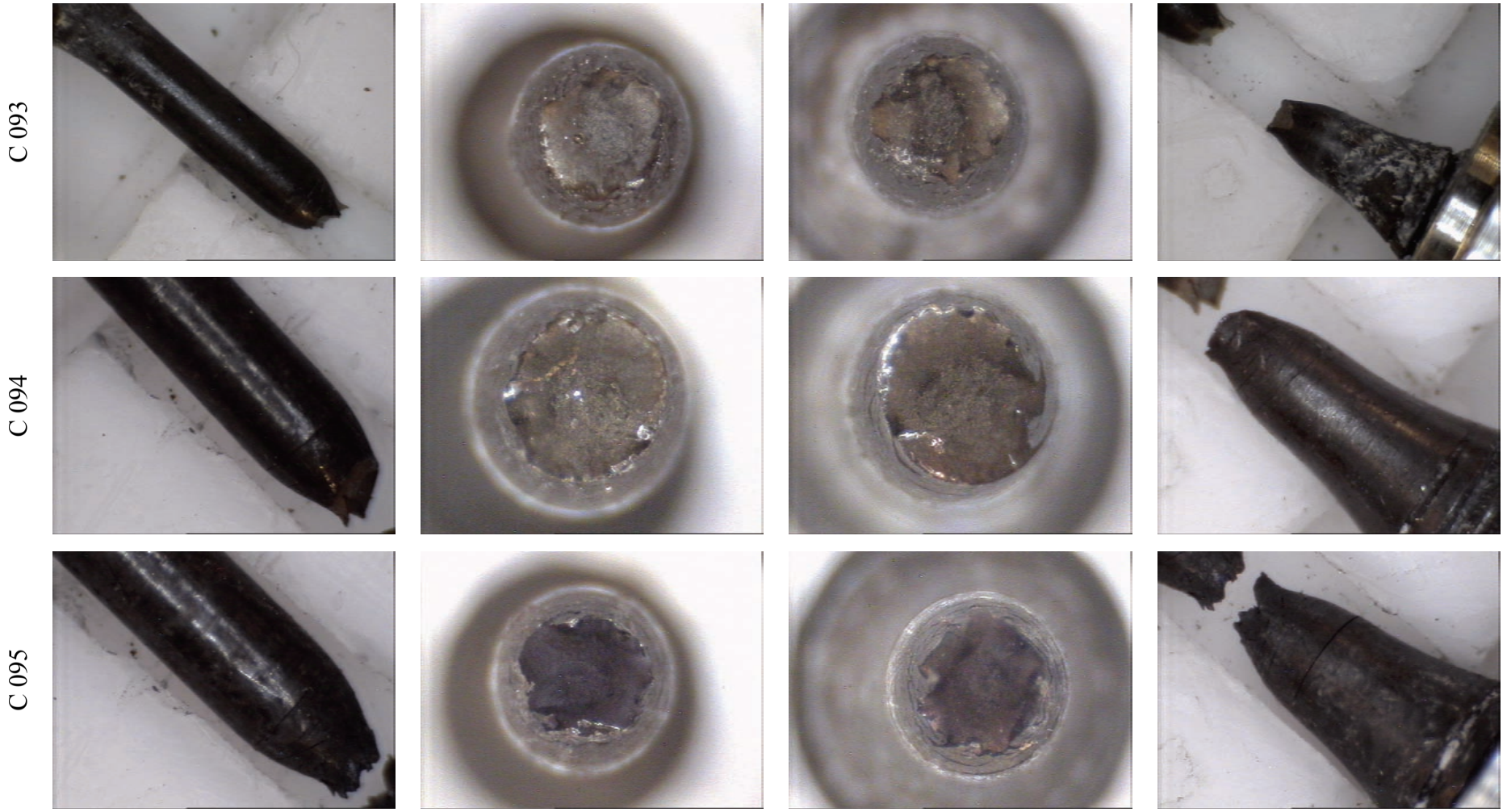

Fig. 10-23 Photographs (macro) of the tensile tested EB welded EUROFER specimens: C 093 (T_{test}=250 °C), C 094 (T_{test}=300 °C), C 095 (T_{test}=350 °C).

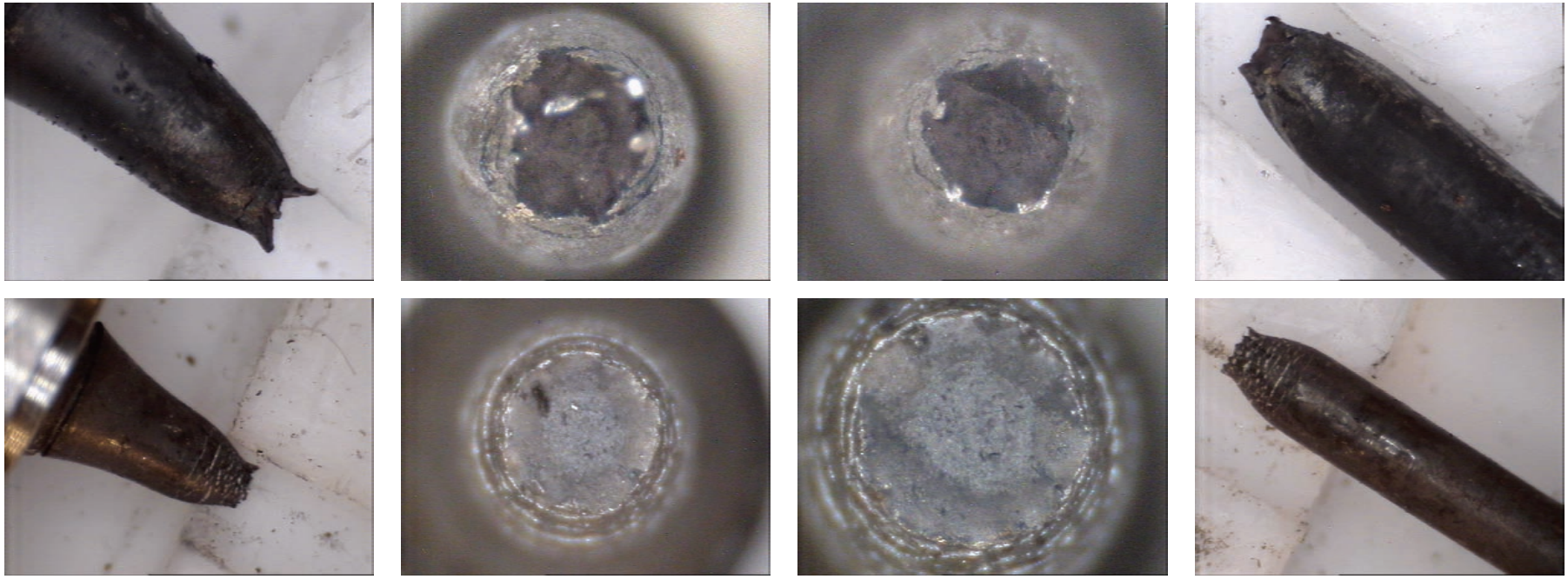

Fig. 10-24 Photographs (macro) of the tensile tested EB welded EUROFER specimens: C 096 (T_{test}=350 °C after annealing at 550 °C/3 h), C 097 (T_{test}=20 °C).

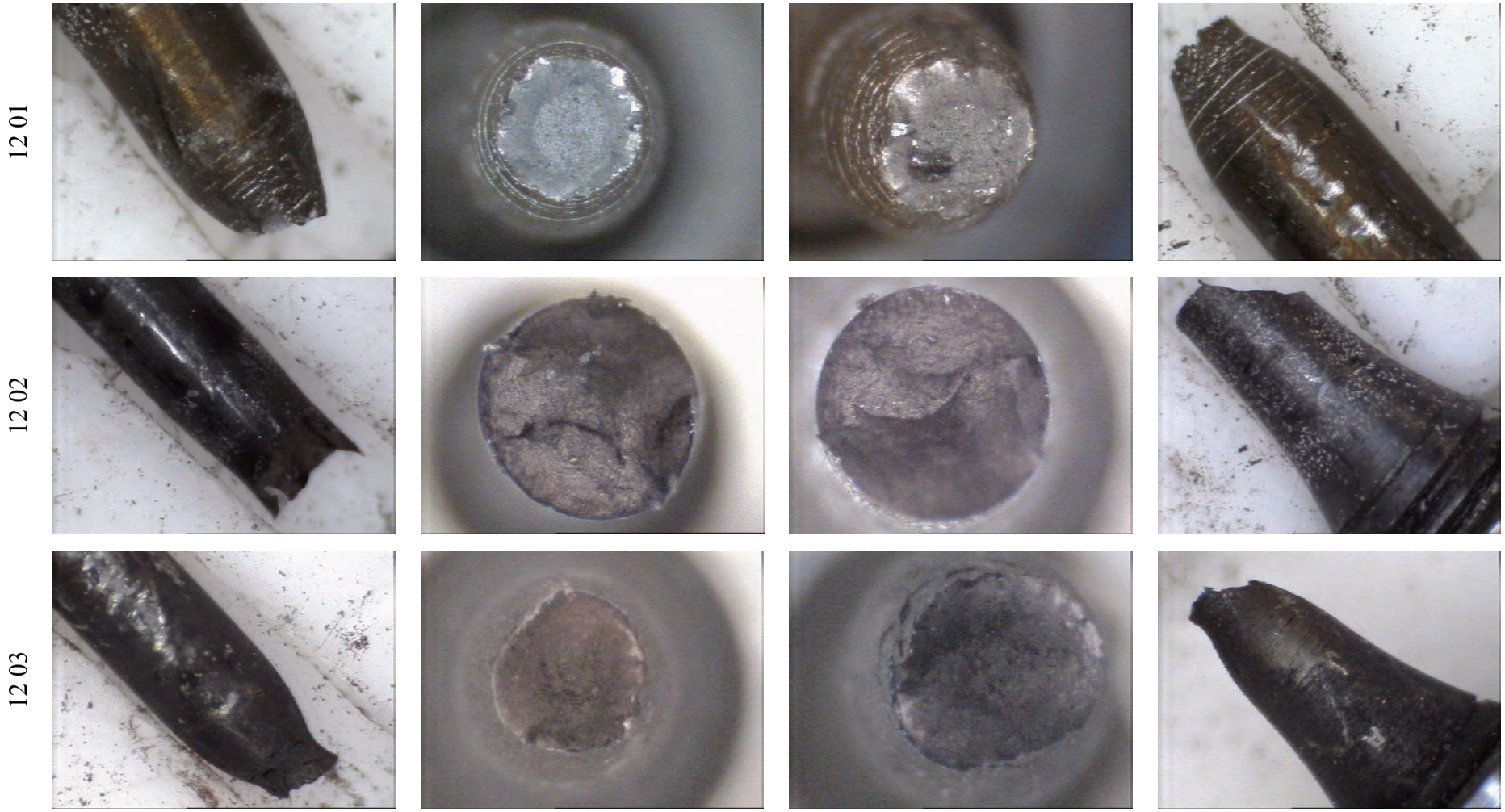

Fig. 10-25 Photographs (macro) of the tensile tested OPTIFER XII specimens: 12 01 (T_{test}=20 °C), 12 02 (T_{test}=350 °C), 12 03 (T_{test}=350 °C after annealing at 550 °C/3 h).

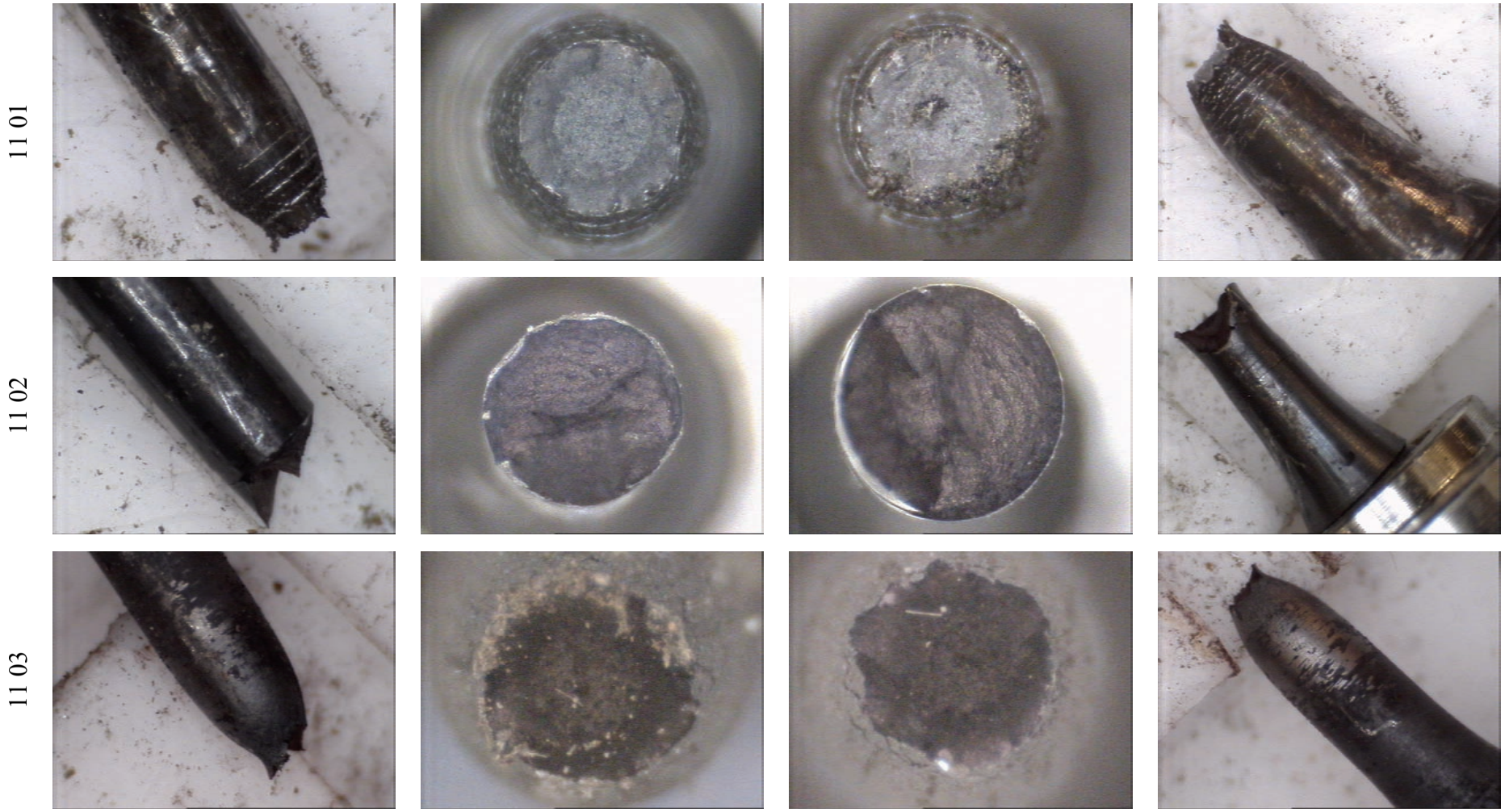

Fig. 10-26 Photographs (macro) of the tensile tested OPTIFER XI specimens: 11 01 (T_{test}=20 °C), 11 02 (T_{test}=350 °C), 11 03 (T_{test}=350 °C after annealing at 550 °C/3 h).

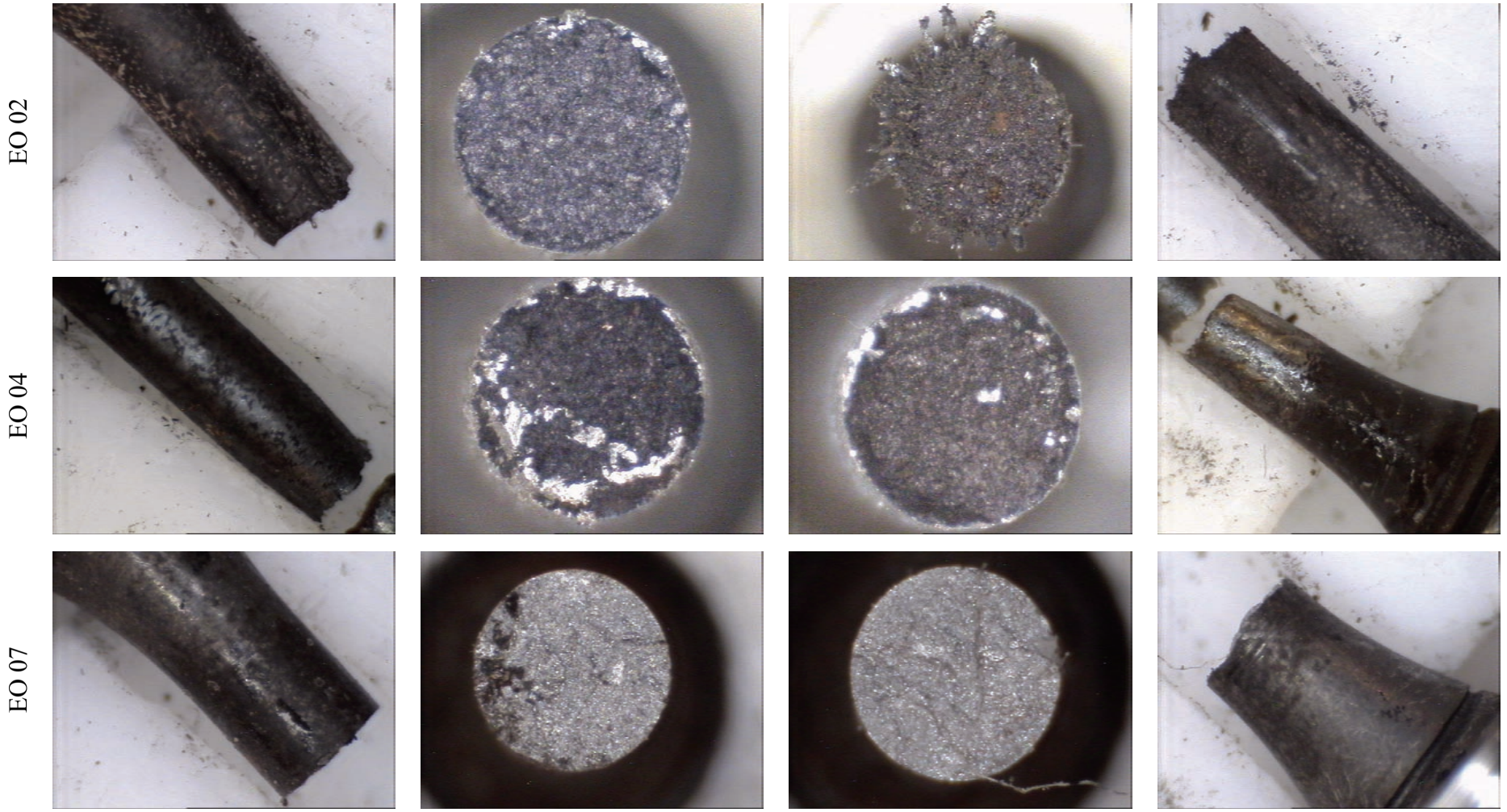

Fig. 10-27 Photographs (macro) of the tensile tested EURODShip (EUROFER ODS with 0.5 wt.% Y_2O_3) specimens: EO 02 (T_{test}=350 °C), EO 04 (T_{test}=350 °C after annealing at 550 °C/3 h), EO 07 (T_{test}=20 °C).

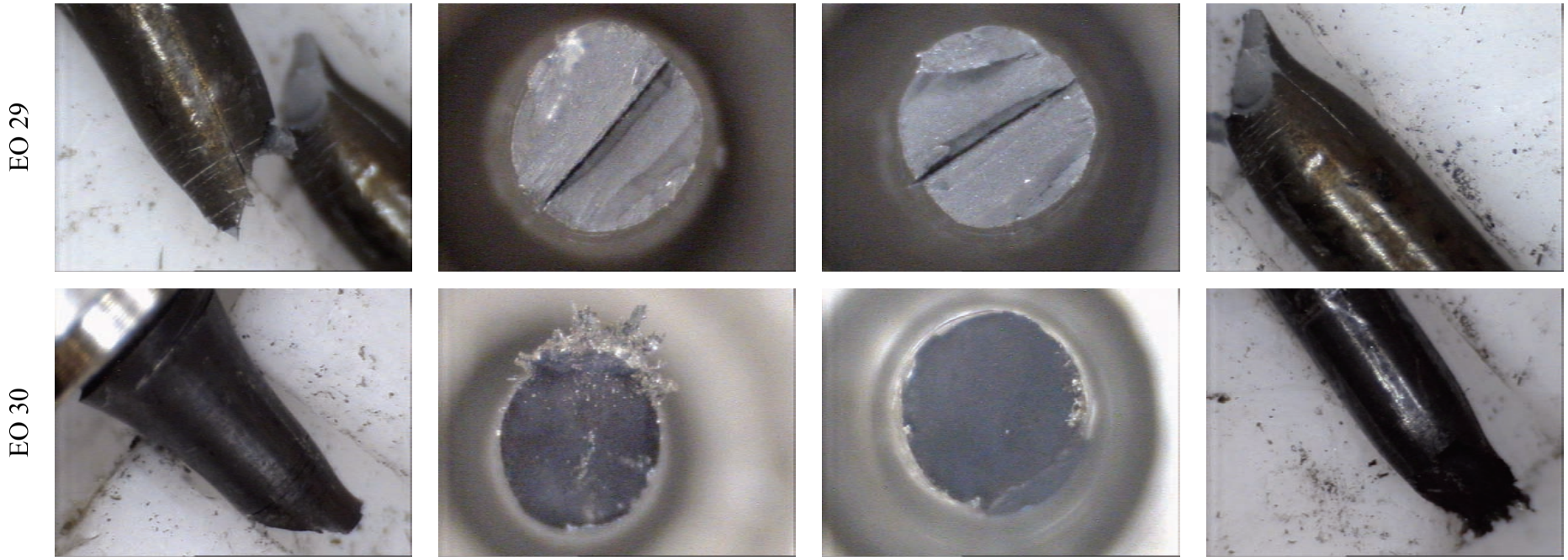

Fig. 10-28 Photographs (macro) of the tensile tested EURODShip (EUROFER ODS with 0.5 wt.% Y_2O_3) specimens: EO 29 (T_{test}=20 °C), EO 30 (T_{test}=350 °C).

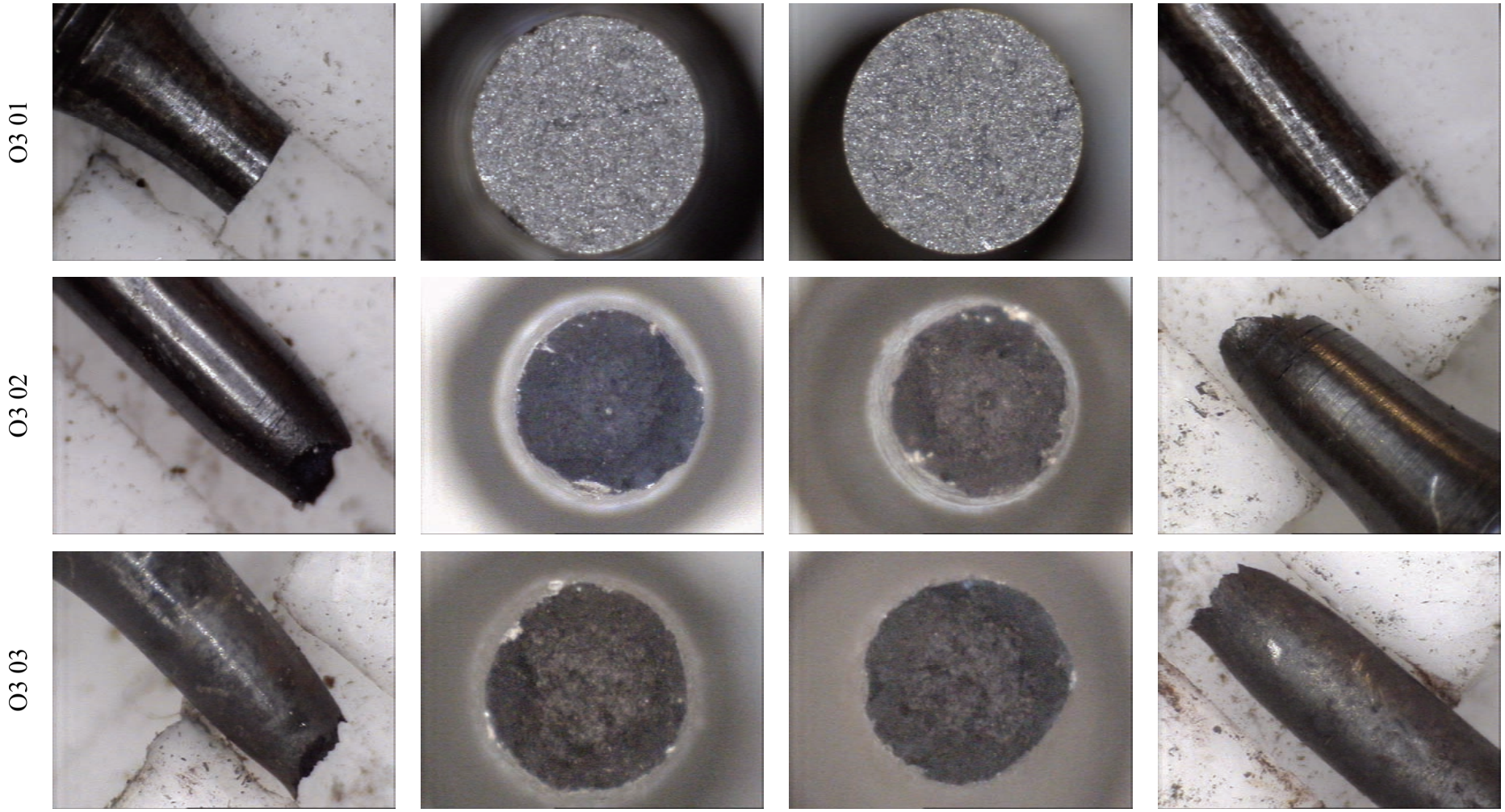

Fig. 10-29 Photographs (macro) of the tensile tested EODShip3 (EUROFER ODS with 0.3 wt.% Y_2O_3) specimens: O3 01 (T_{test}=20 °C), O3 02 (T_{test}=350 °C), O3 03 (T_{test}=350 °C after annealing at 550 °C/3 h).

11 Annex: Low Cycle Fatigue Tests

11.1 EUROFER 97

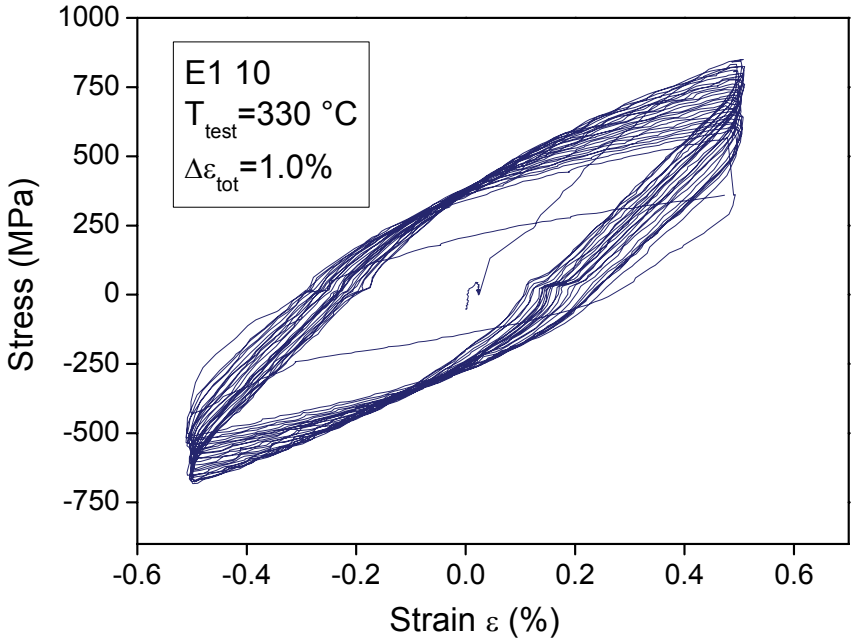

Fig. 11-1 Stress vs. strain for E1 10 (70.8 dpa/334 °C).

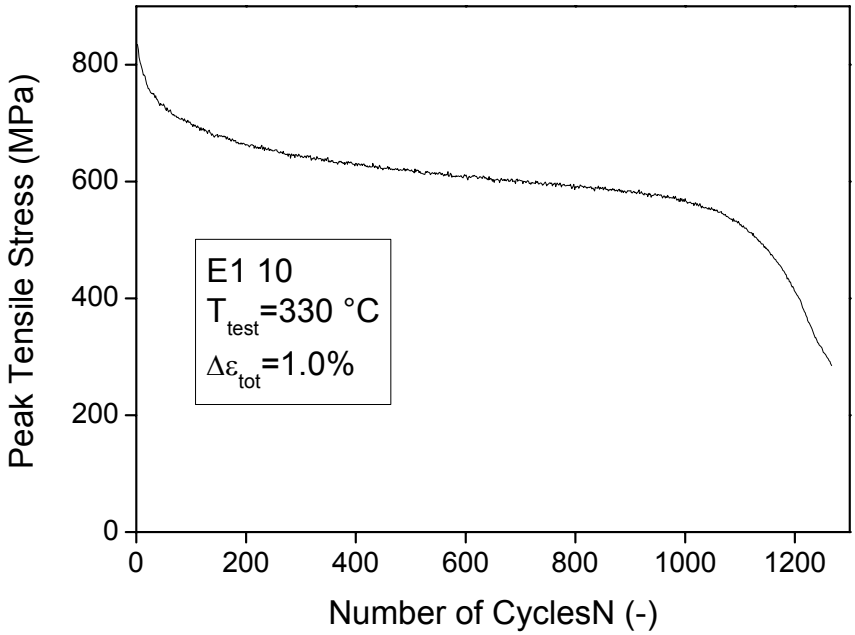

Fig. 11-2 Peak tensile stress vs. number of cycles for E1 10 (70.8 dpa/334 °C).

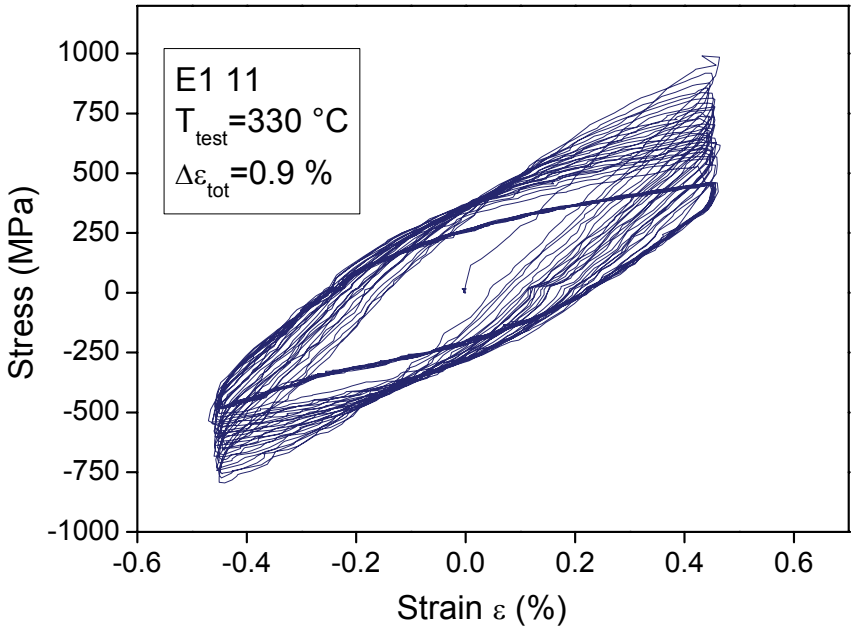

Fig. 11-3 Stress vs. strain for E1 11 (70.8 dpa/334 °C).

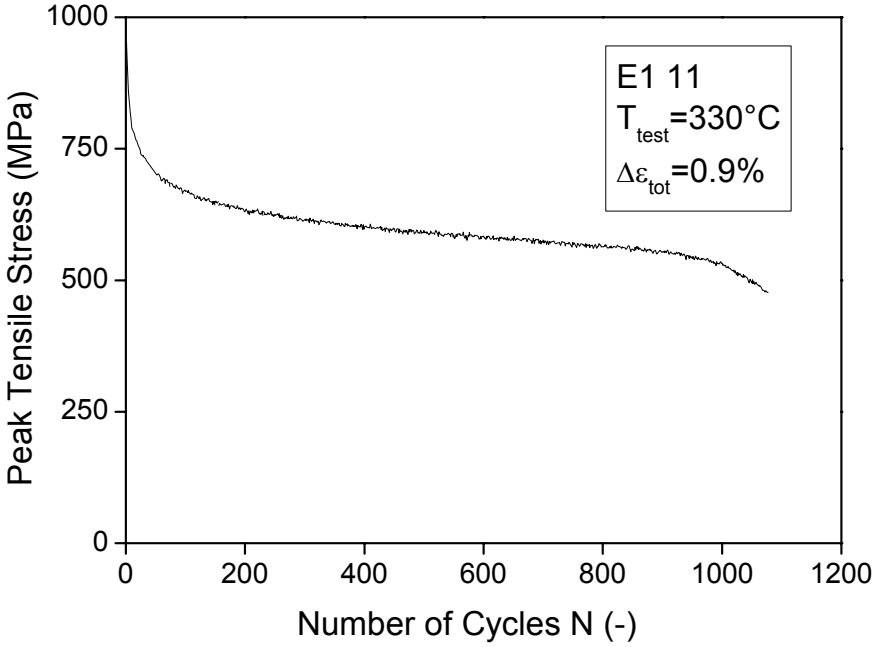

Fig. 11-4 Peak tensile stress vs. number of cycles for E1 11 (70.8 dpa/334 °C).

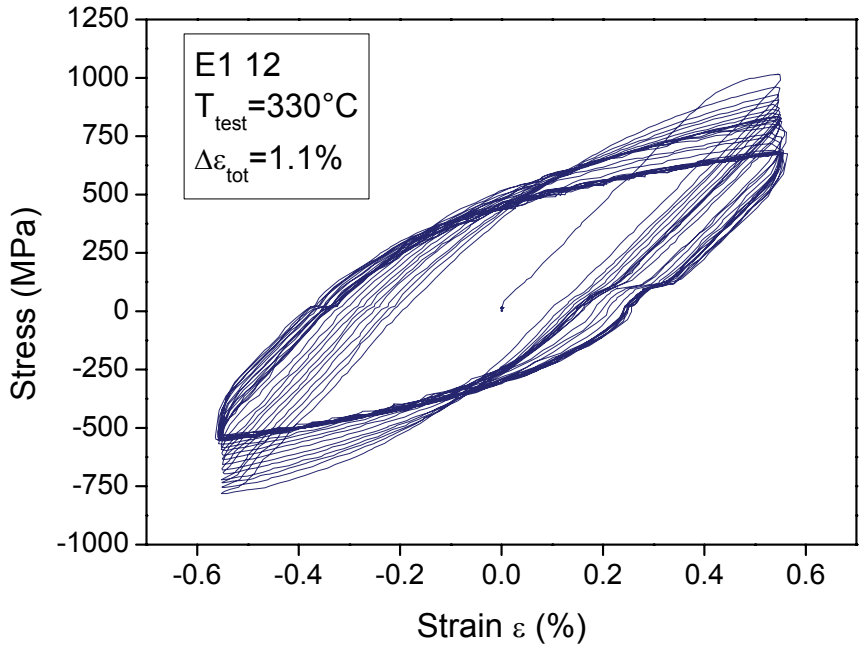

Fig. 11-5 Stress vs. strain for E1 12 (70.8 dpa/334 °C).

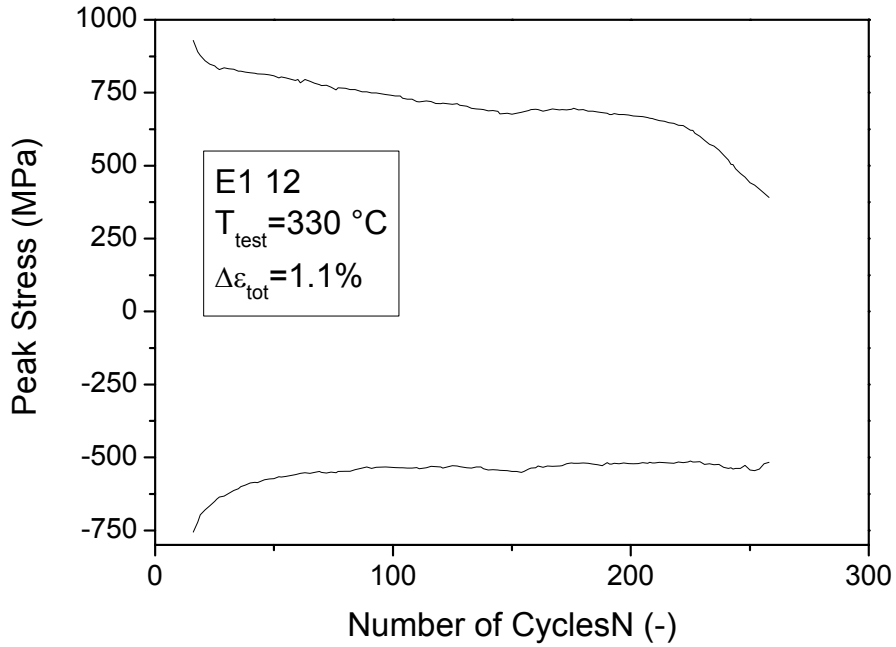

Fig. 11-6 Peak cyclic stresses vs. number of cycles for E1 12 (70.8 dpa/334 °C).

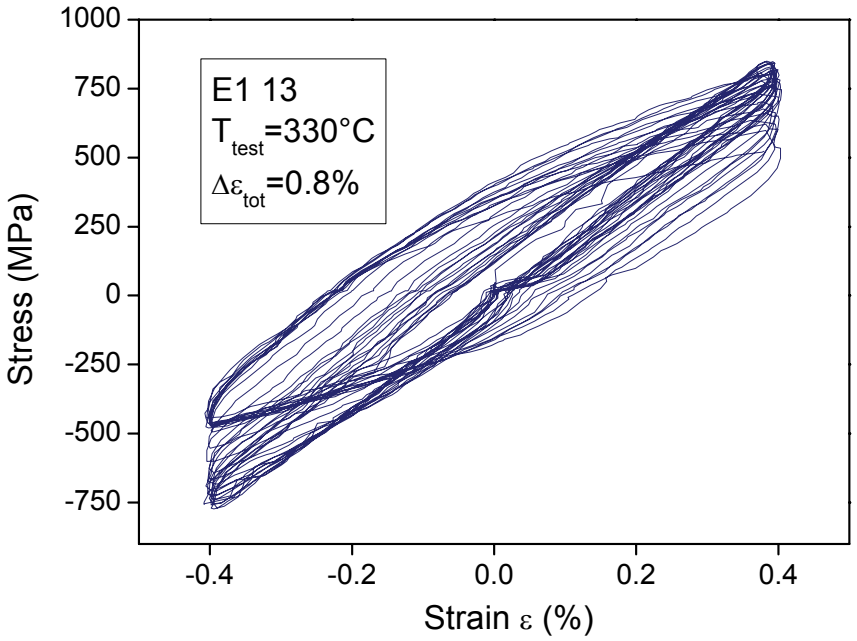

Fig. 11-7 Stress vs. strain for E1 13 (70.8 dpa/334 °C).

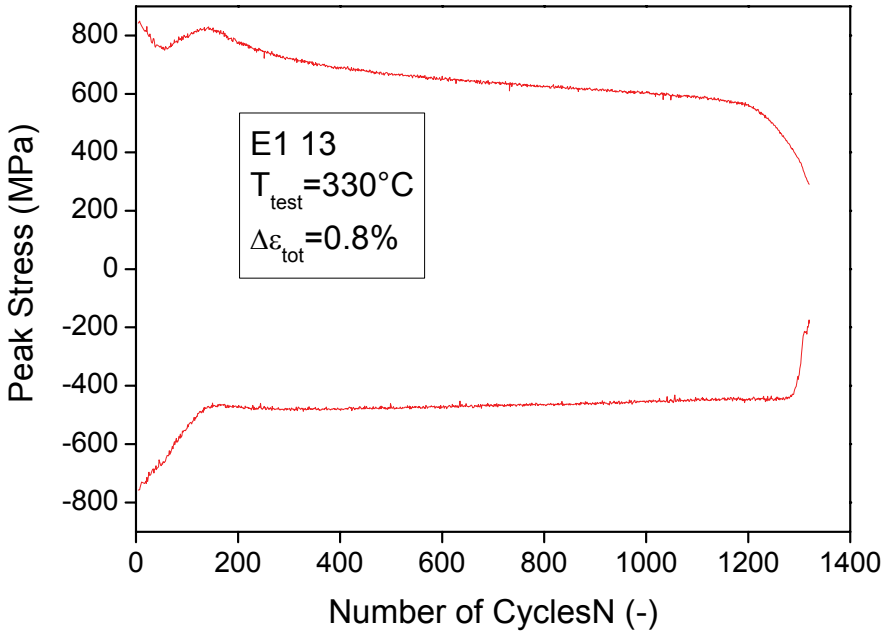

Fig. 11-8 Peak cyclic stresses vs. number of cycles for E1 13 (70.8 dpa/334 °C).

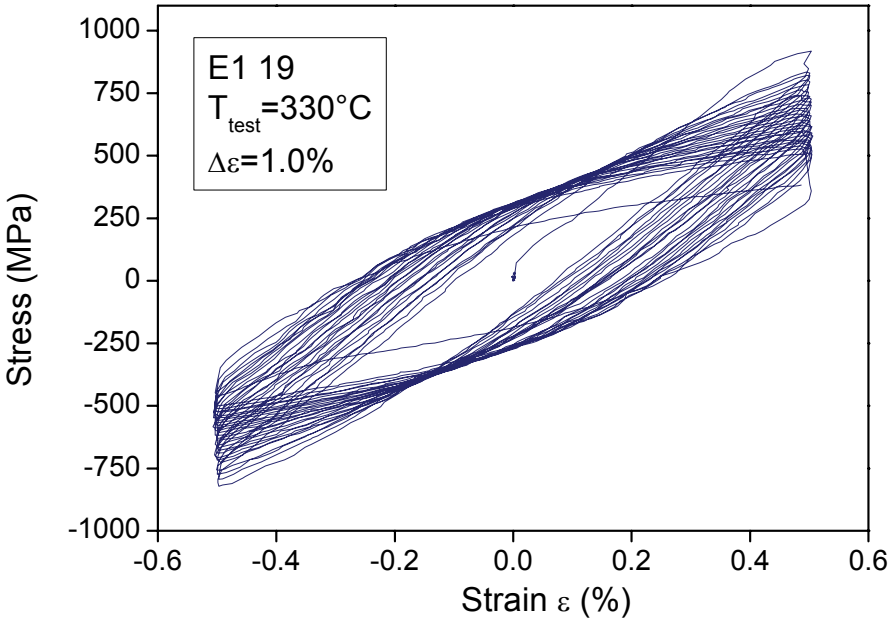

Fig. 11-9 Stress vs. strain for E1 19 (46.8 dpa/337.5 °C).

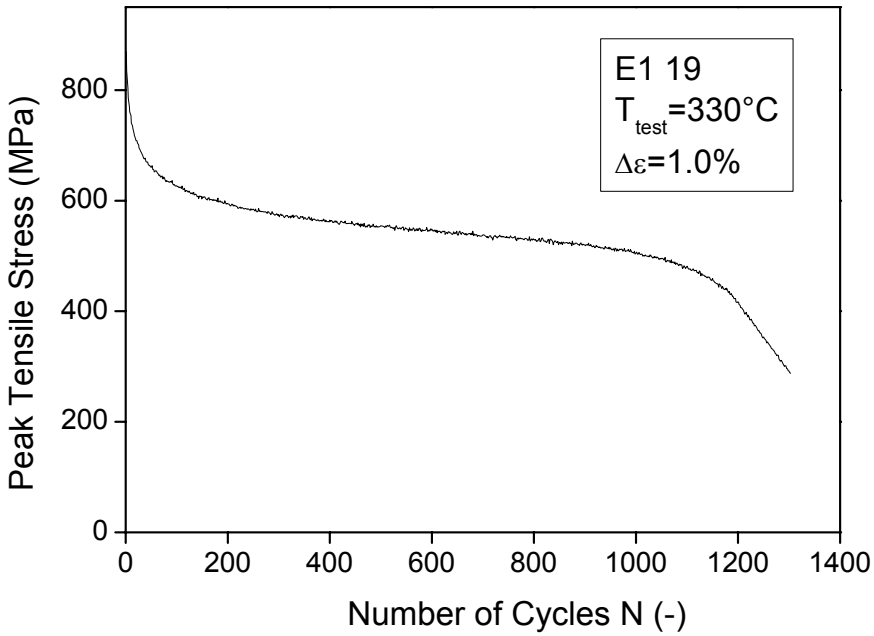

Fig. 11-10 Peak tensile stress vs. number of cycles for E1 19 (46.8 dpa/337.5 °C).

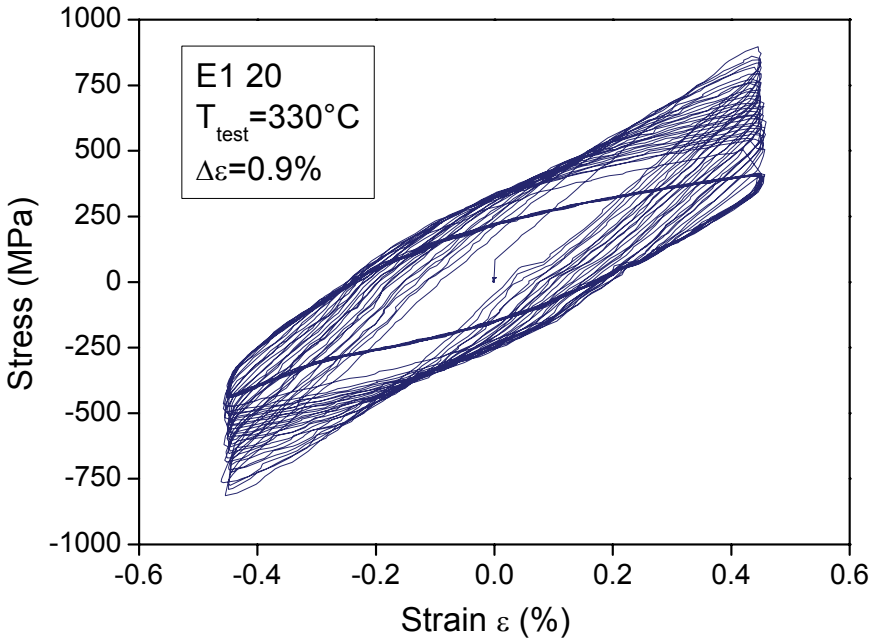

Fig. 11-11 Stress vs. strain for E1 20 (46.8 dpa/337.5 °C).

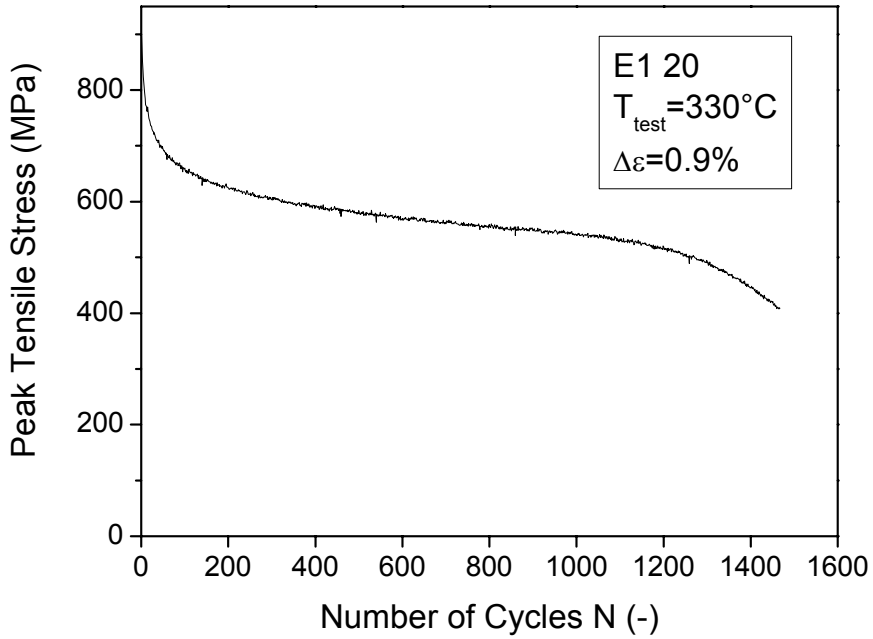

Fig. 11-12 Peak tensile stress vs. number of cycles for E1 20 (46.8 dpa/337.5 °C).

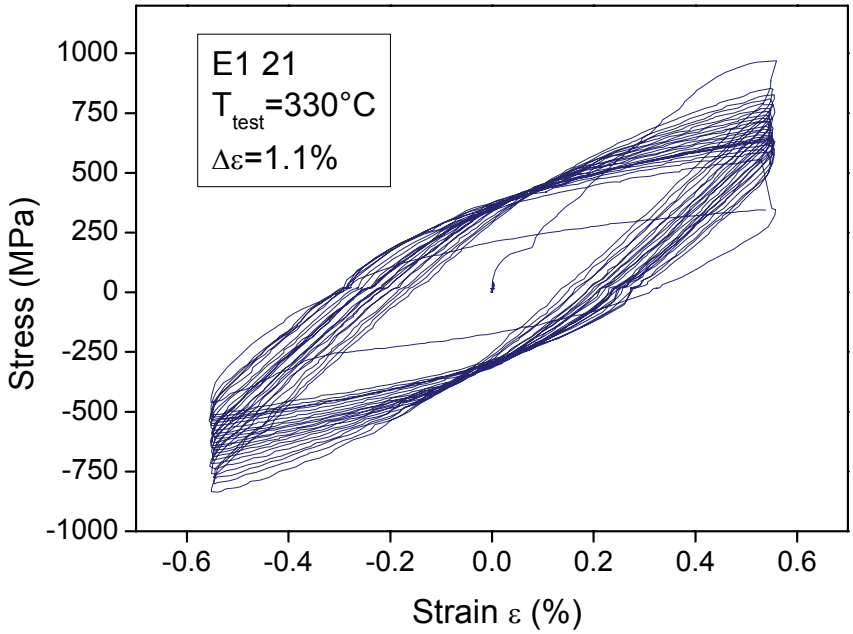

Fig. 11-13 Stress vs. strain for E1 21 (46.8 dpa/337.5 °C).

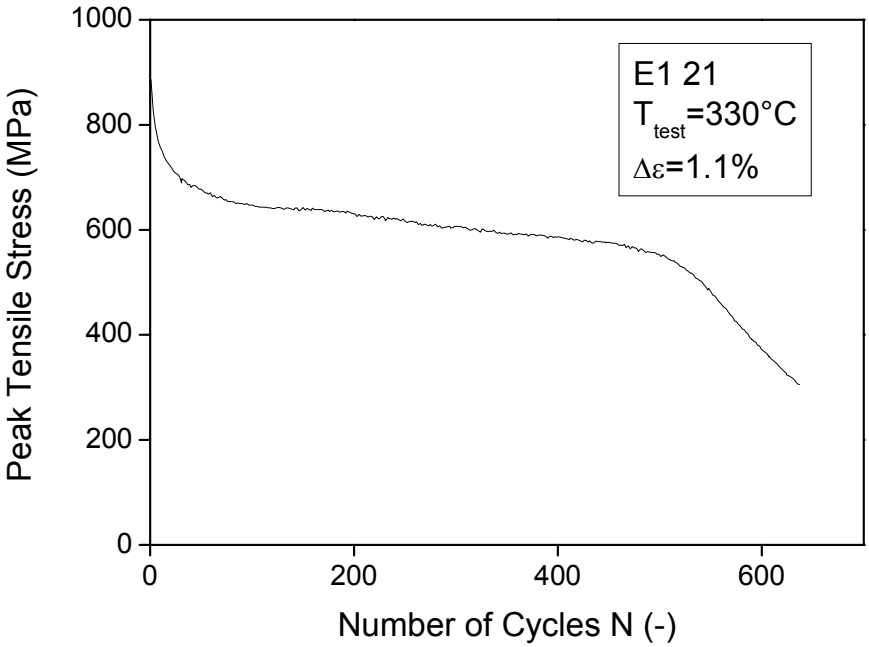

Fig. 11-14 Peak tensile stress vs. number of cycles for E1 21 (46.8 dpa/337.5 °C).

11.2 EUROFER 97 HT

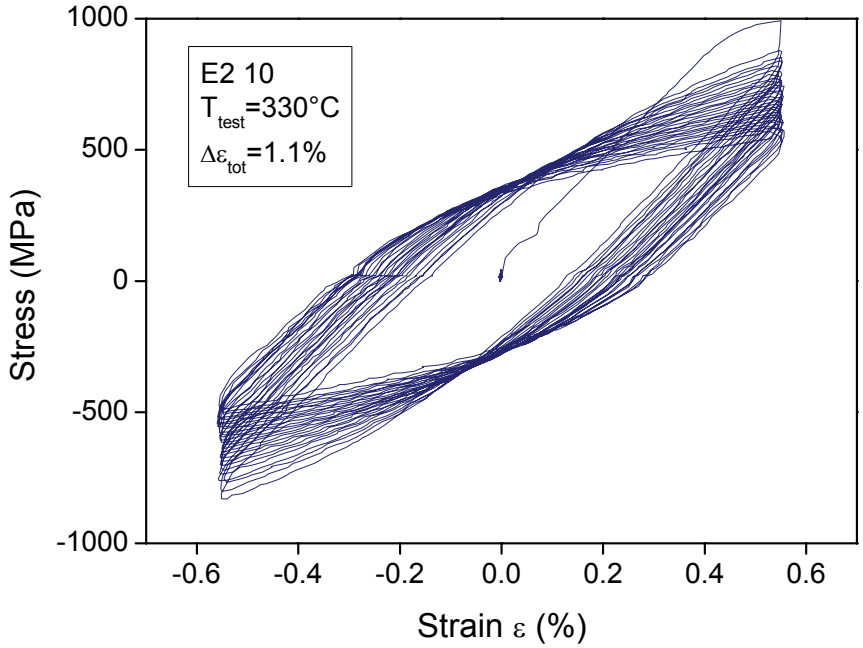

Fig. 11-15 Stress vs. strain for E2 10 (70.8 dpa/334.0 °C).

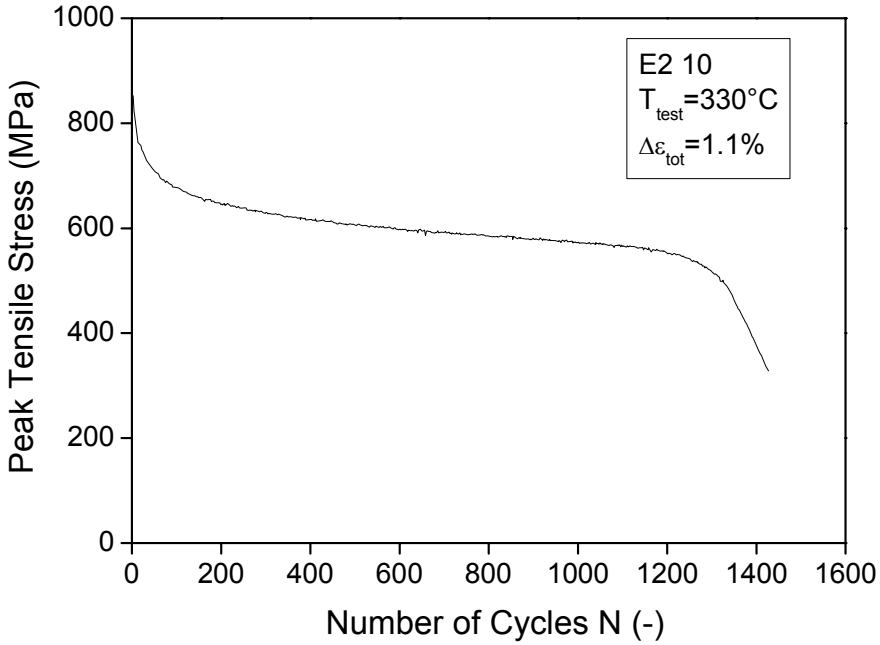

Fig. 11-16 Peak tensile stress vs. number of cycles for E2 10 (70.8 dpa/334.0 °C).

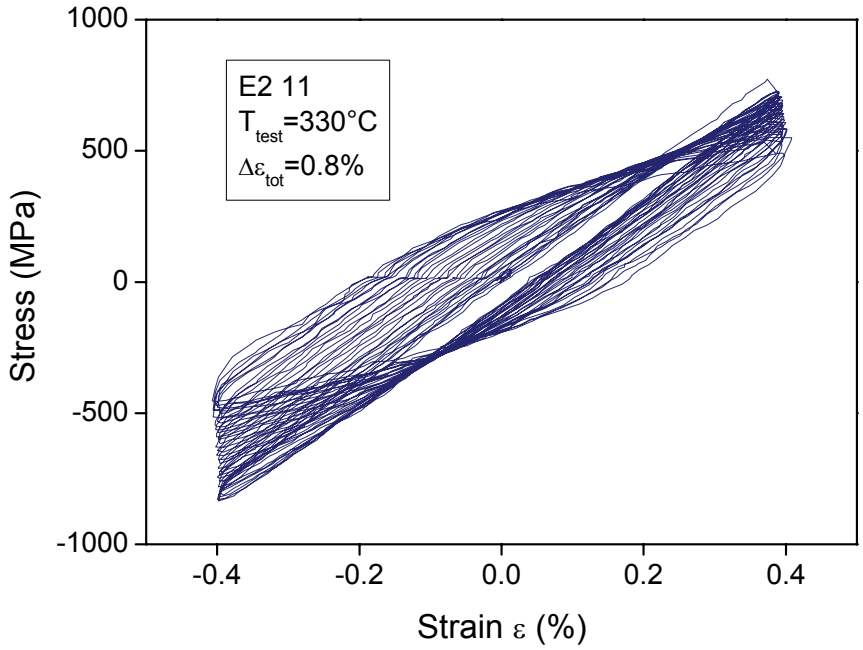

Fig. 11-17 Stress vs. strain for E2 11 (70.8 dpa/334.0 °C).

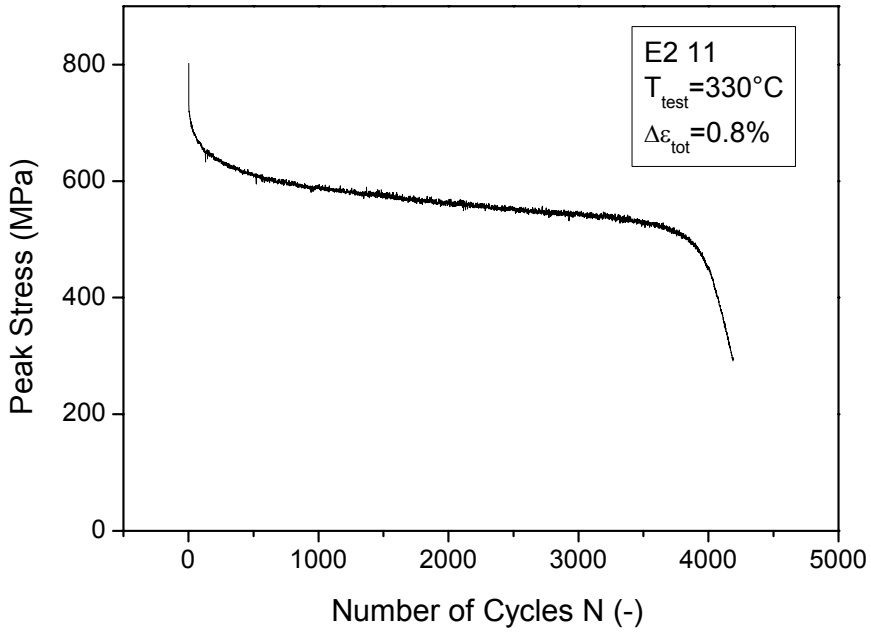

Fig. 11-18 Peak tensile stress vs. number of cycles for E2 11 (70.8 dpa/334.0 °C).

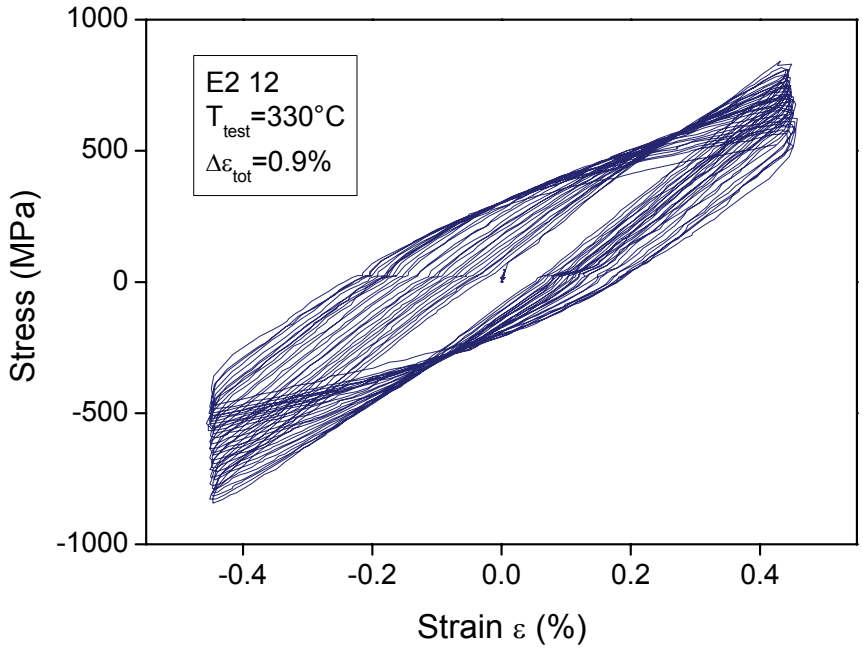

Fig. 11-19 Stress vs. strain for E2 12 (70.8 dpa/334.0 °C).

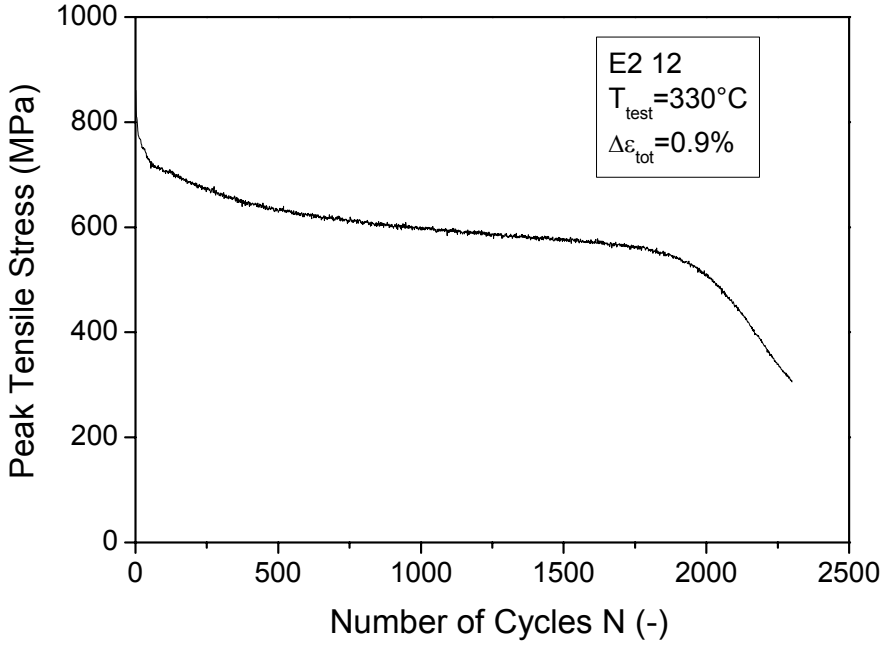

Fig. 11-20 Peak tensile stress vs. number of cycles for E2 12 (70.8 dpa/334.0 °C).

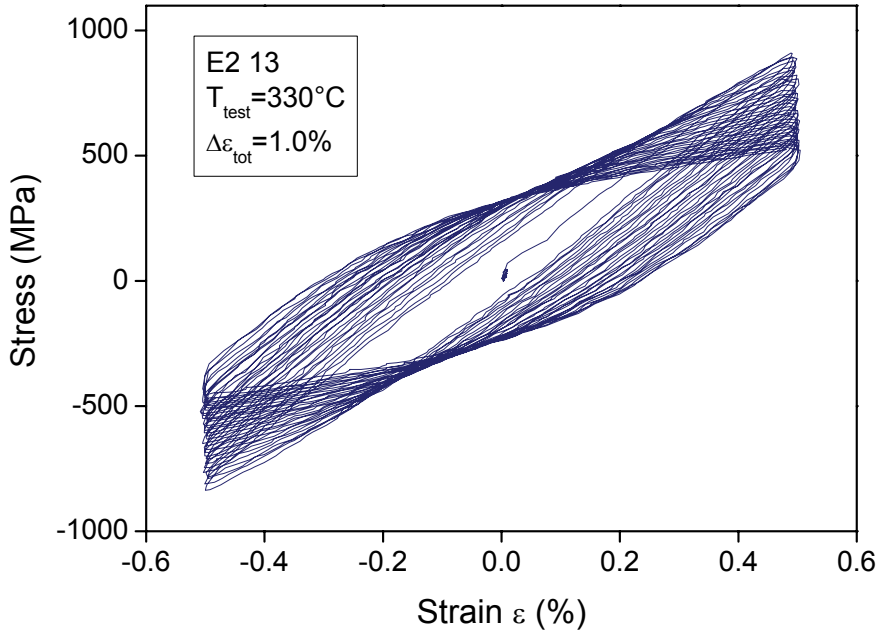

Fig. 11-21 Stress vs. strain for E2 13 (70.8 dpa/334.0 °C).

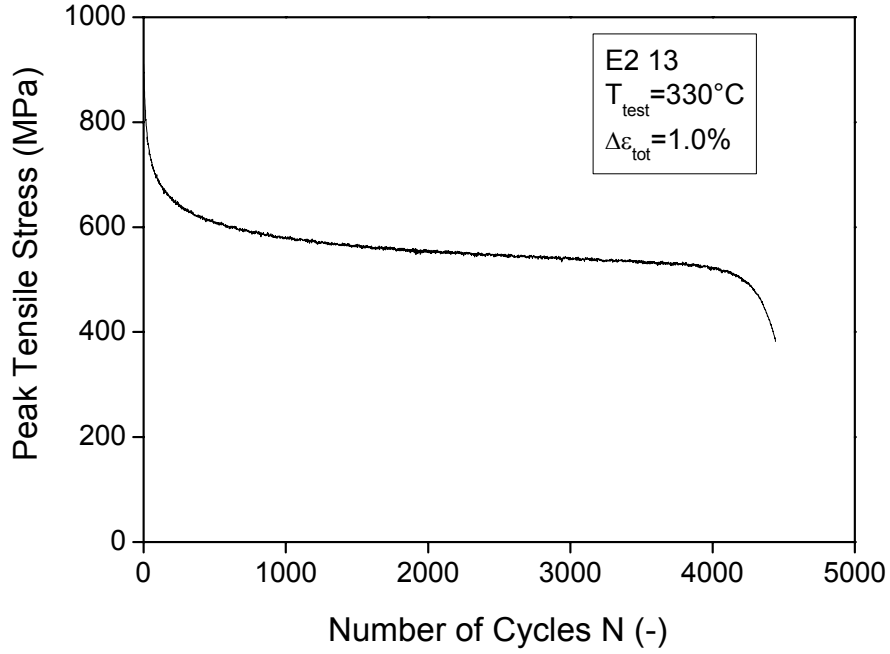

Fig. 11-22 Peak tensile stress vs. number of cycles for E2 13 (70.8 dpa/334.0 °C).

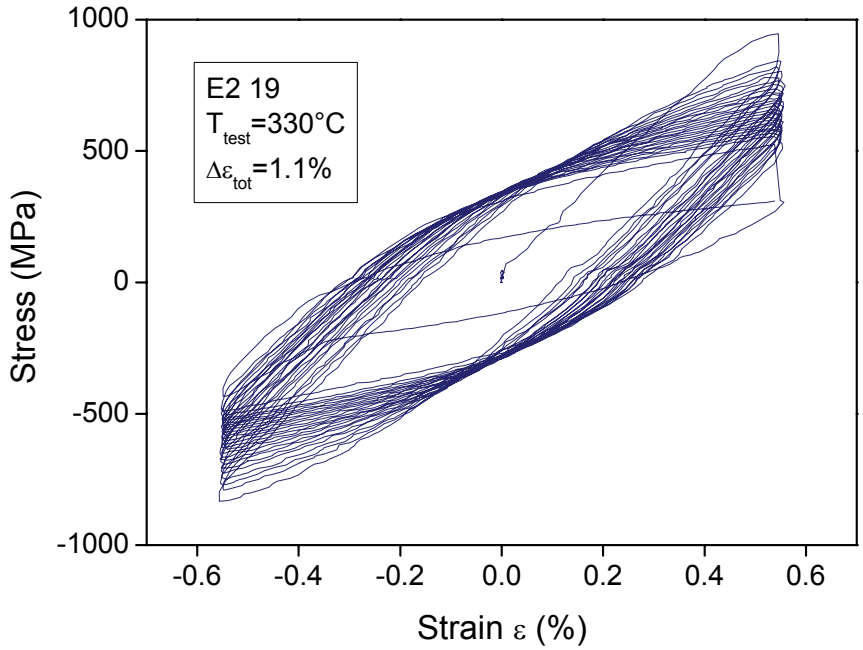

Fig. 11-23 Stress vs. strain for E2 19 (46.8 dpa/337.5 °C).

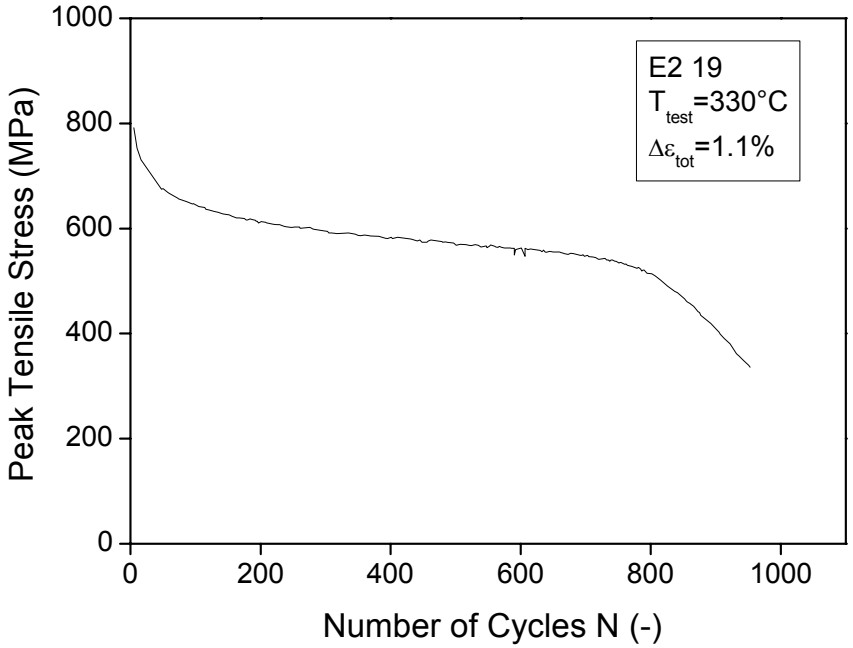

Fig. 11-24 Peak tensile stress vs. number of cycles for E2 19 (46.8 dpa/337.5 °C).

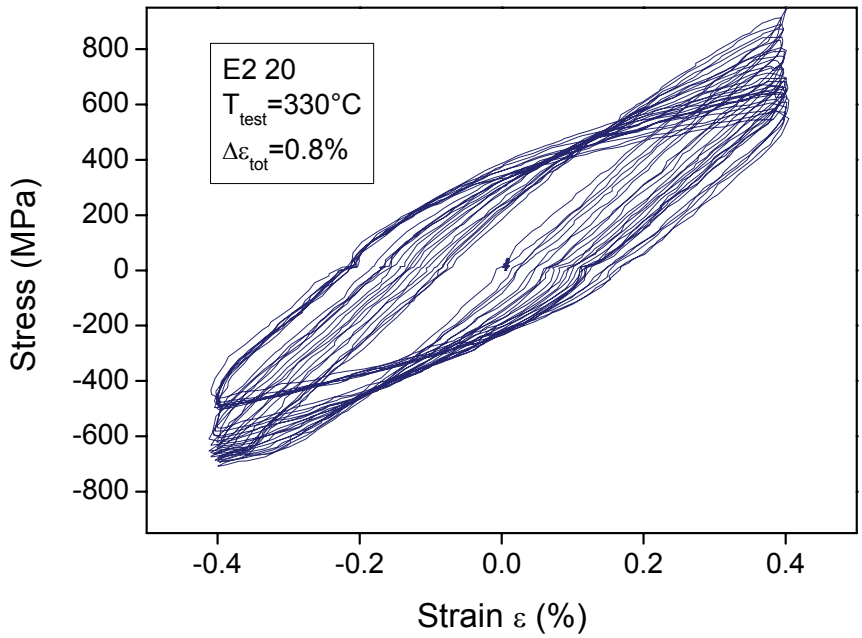

Fig. 11-25 Stress vs. strain for E2 20 (46.8 dpa/337.5 °C).

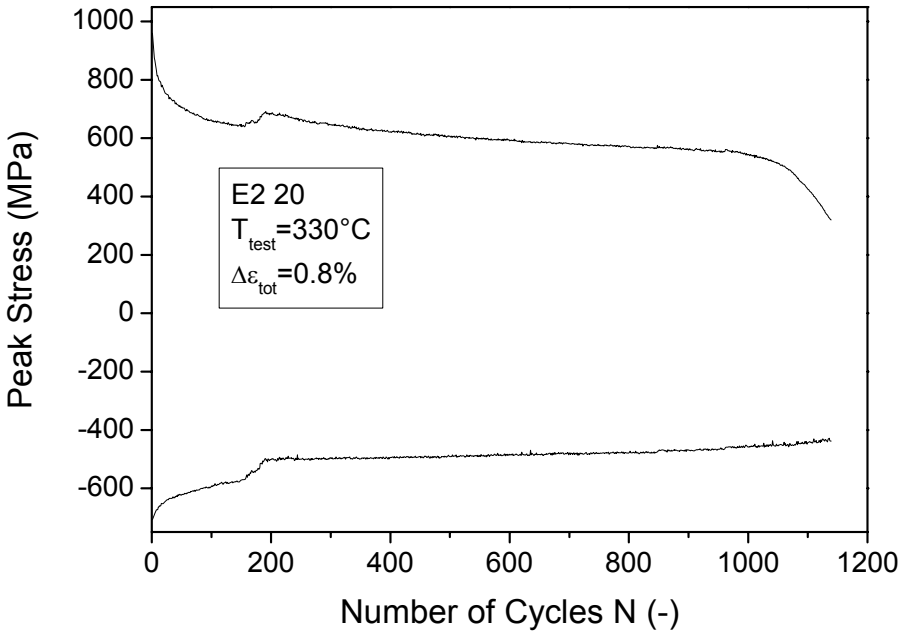

Fig. 11-26 Peak stress vs. number of cycles for E2 20 (46.8 dpa/337.5 °C).

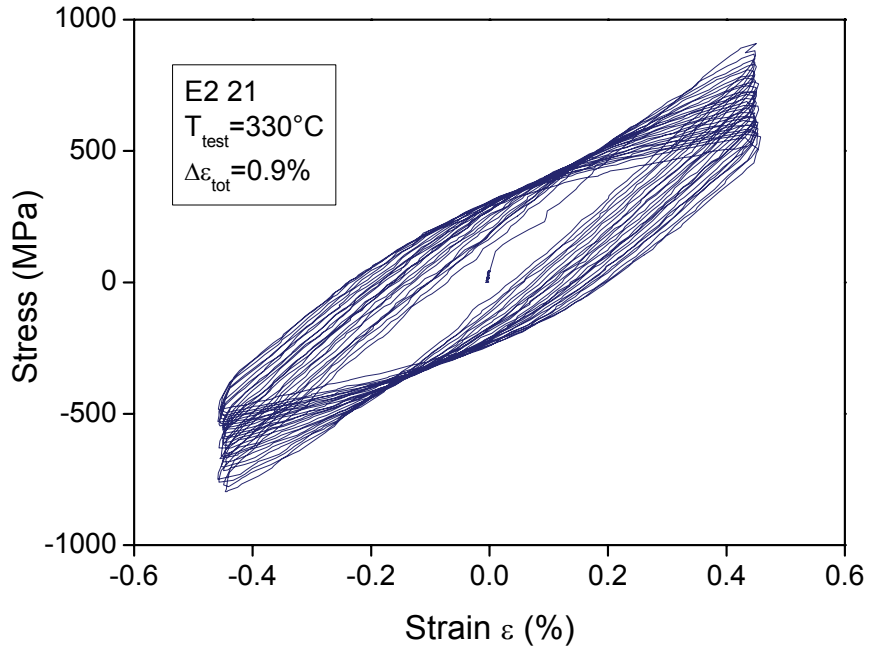

Fig. 11-27 Stress vs. strain for E2 21 (46.8 dpa/337.5 °C).

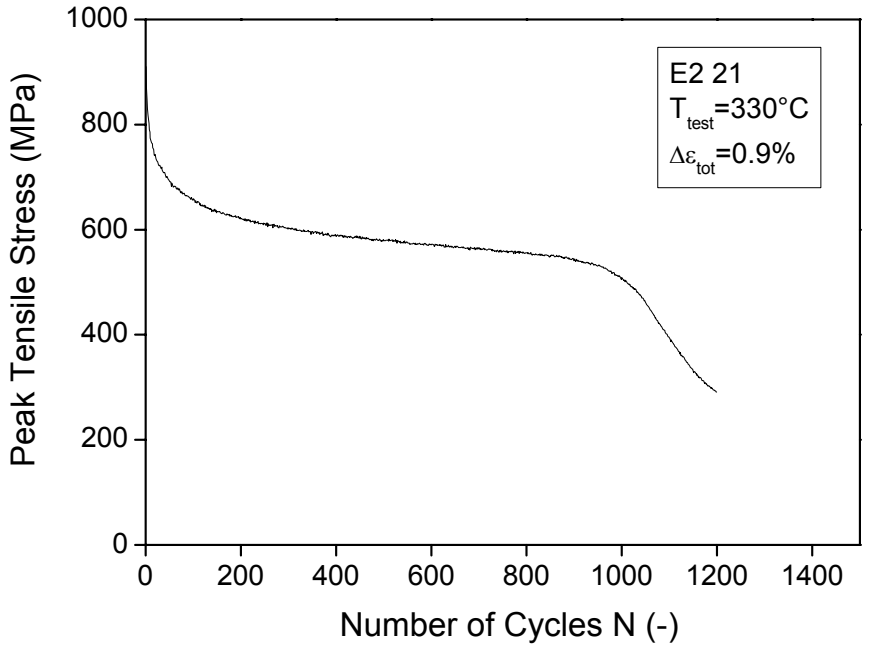

Fig. 11-28 Peak stress vs. number of cycles for E2 21 (46.8 dpa/337.5 °C).

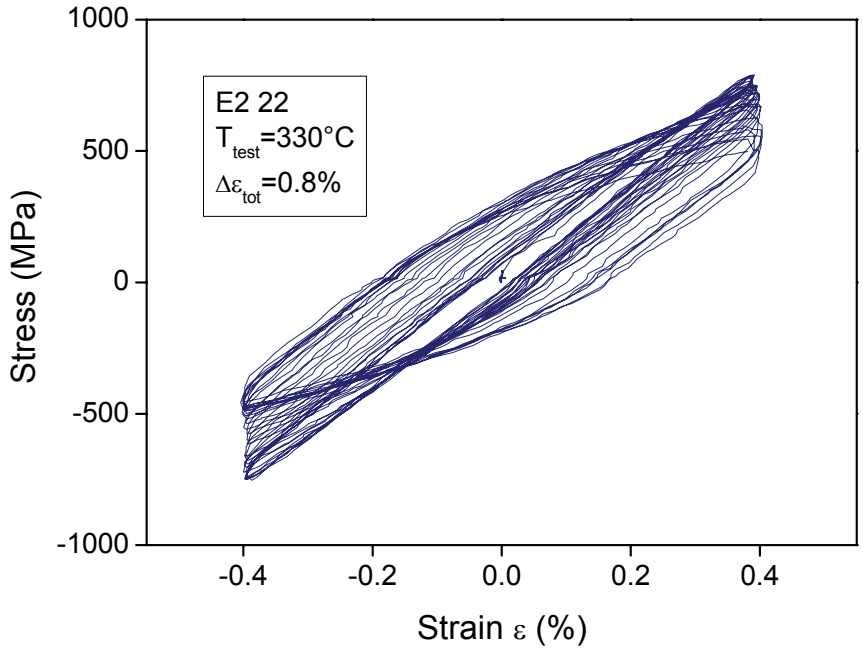

Fig. 11-29 Stress vs. strain for E2 22 (46.8 dpa/337.5 °C).

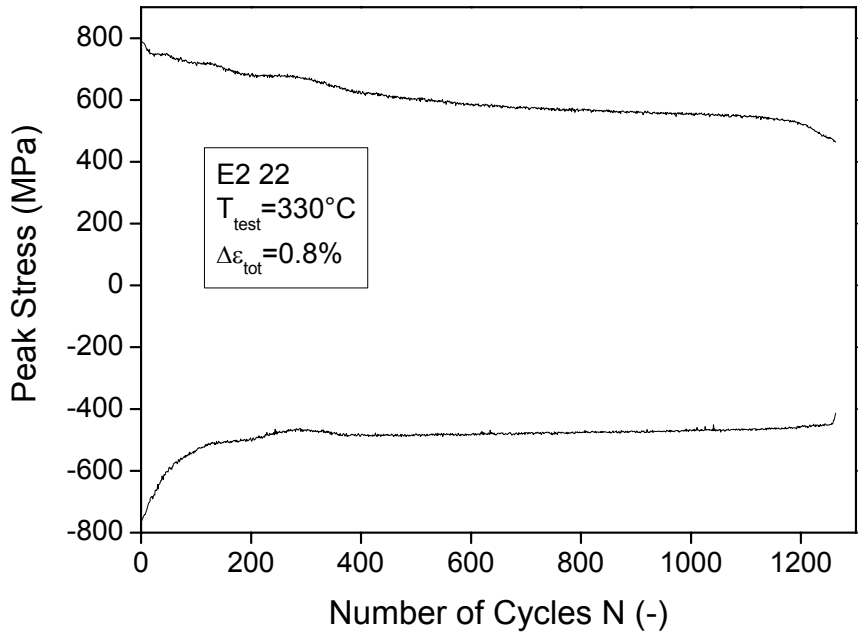

Fig. 11-30 Peak stress vs. number of cycles for E2 22 (46.8 dpa/337.5 °C).

11.3 F82H-mod.

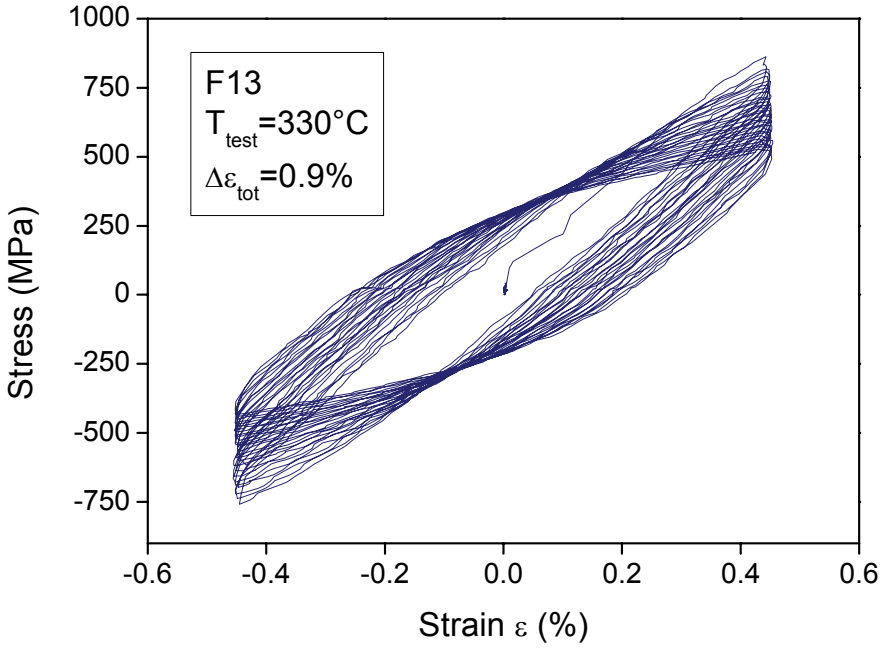

Fig. 11-31 Stress vs. strain for F13 (46.8 dpa/337.5 °C).

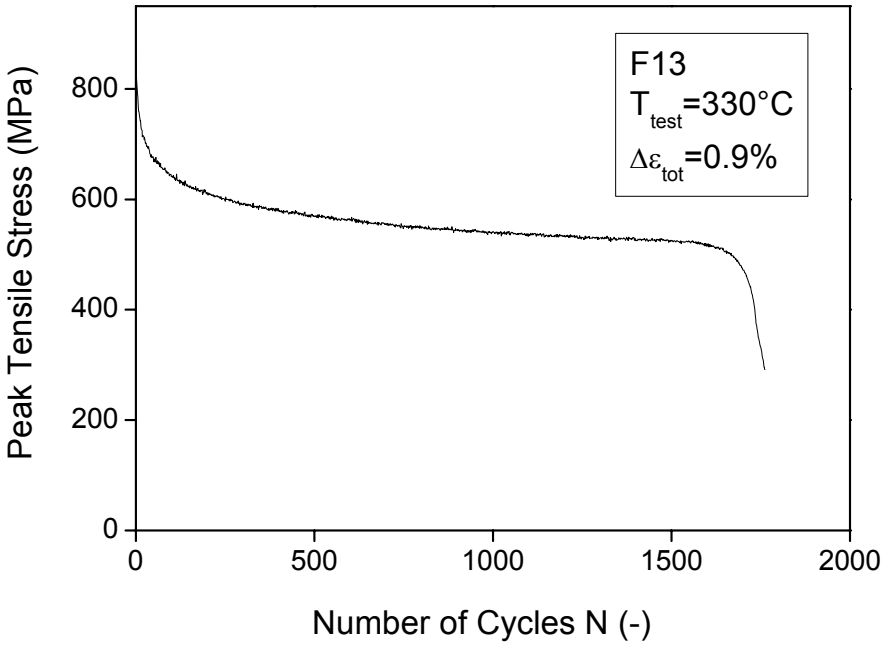

Fig. 11-32 Peak stress vs. number of cycles for F13 (46.8 dpa/337.5 °C).

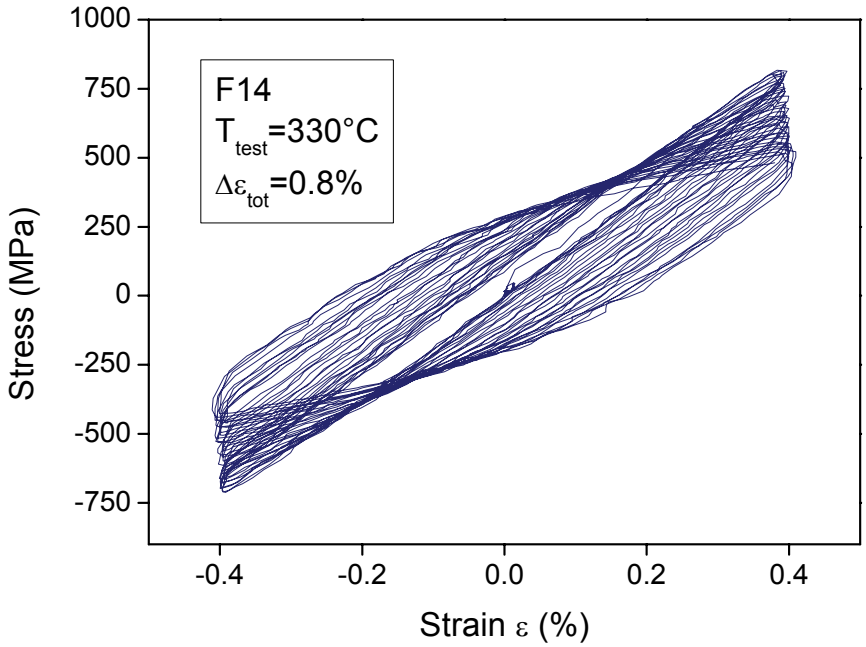

Fig. 11-33 Stress vs. strain for F14 (46.8 dpa/337.5 °C).

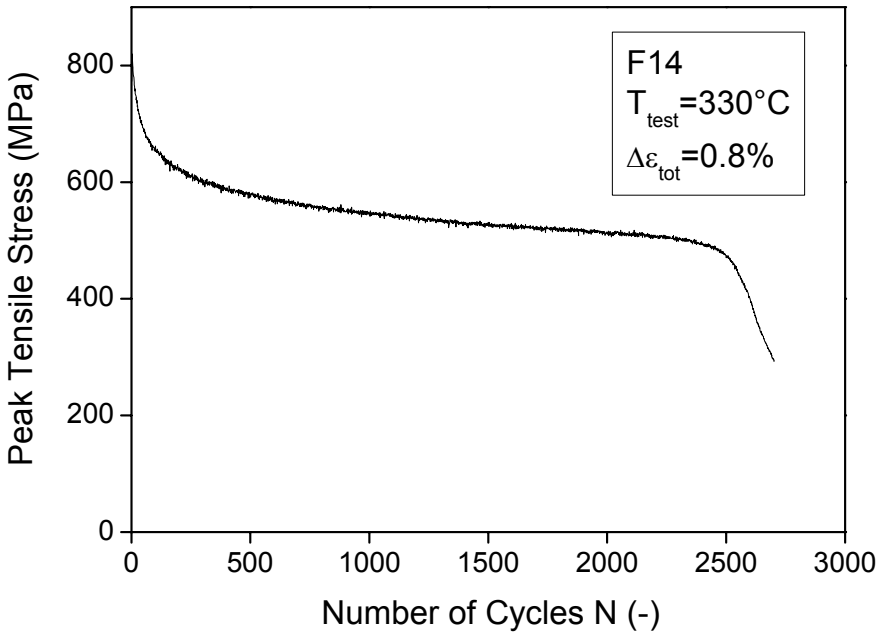

Fig. 11-34 Peak stress vs. number of cycles for F14 (46.8 dpa/337.5 °C).

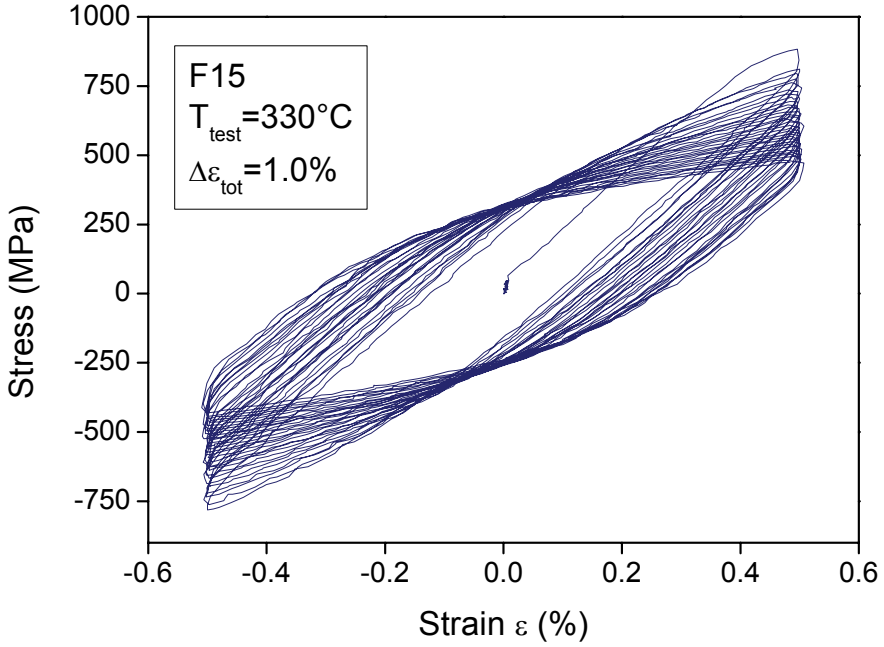

Fig. 11-35 Stress vs. strain for F15 (46.8 dpa/337.5 °C).

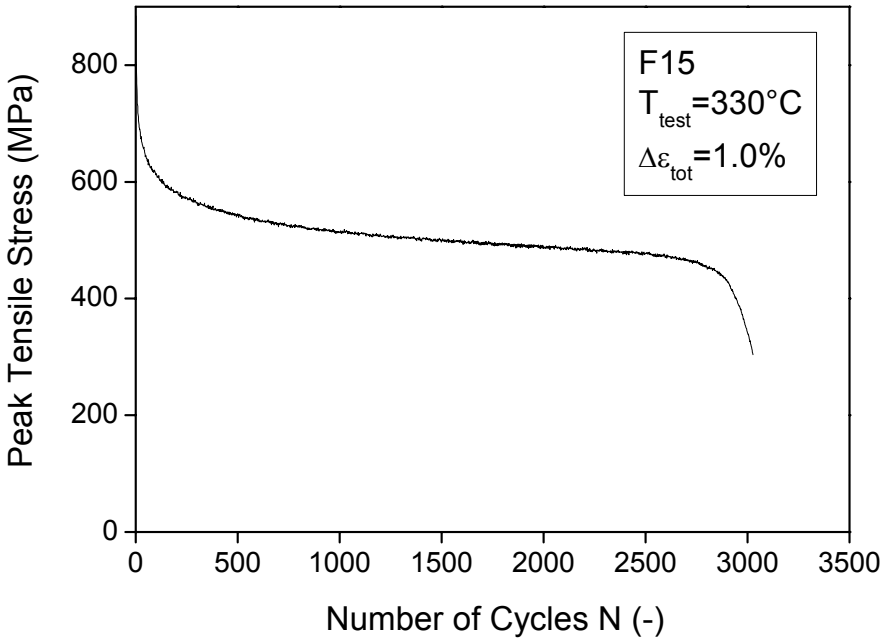

Fig. 11-36 Peak stress vs. number of cycles for F15 (46.8 dpa/337.5 °C).

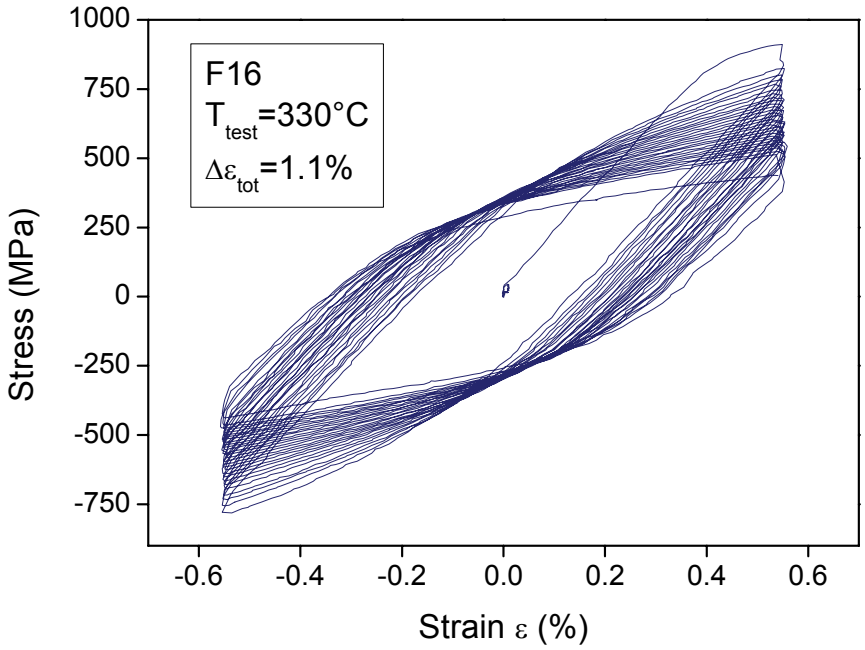

Fig. 11-37 Stress vs. strain for F16 (46.8 dpa/337.5 °C).

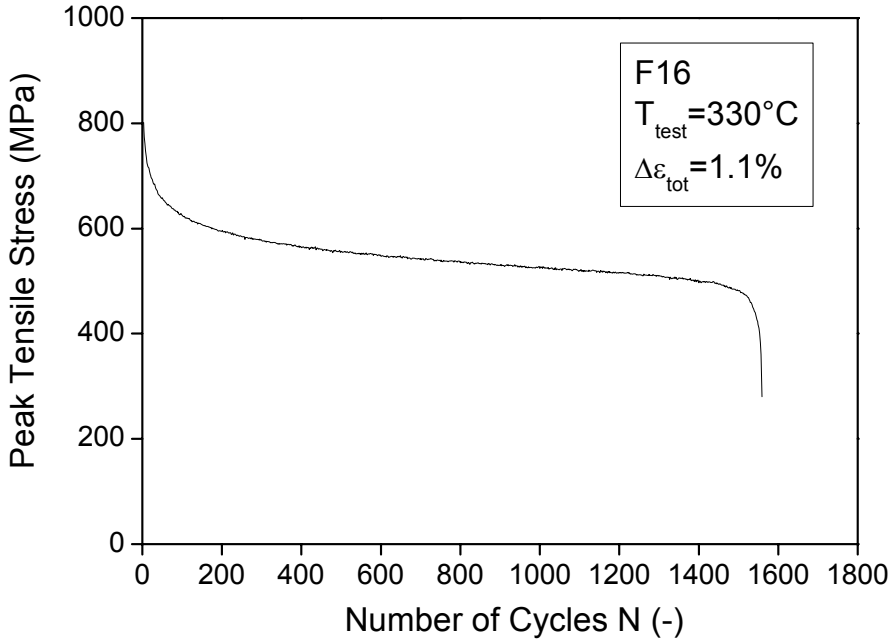

Fig. 11-38 Peak stress vs. number of cycles for F15 (46.8 dpa/337.5 °C).

11.4 OPTIFER IVc

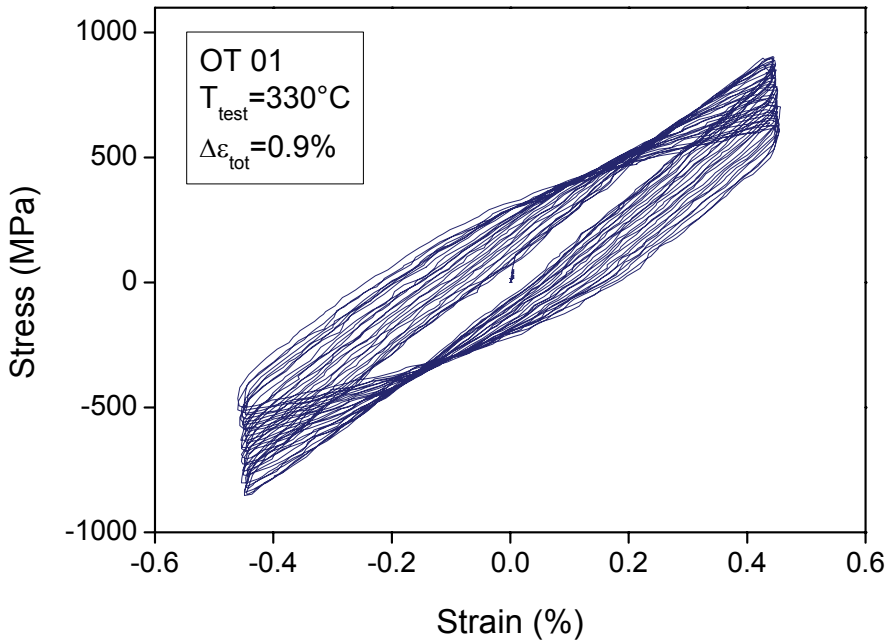

Fig. 11-39 Stress vs. strain for OT 01 (70.8 dpa/334.0 °C).

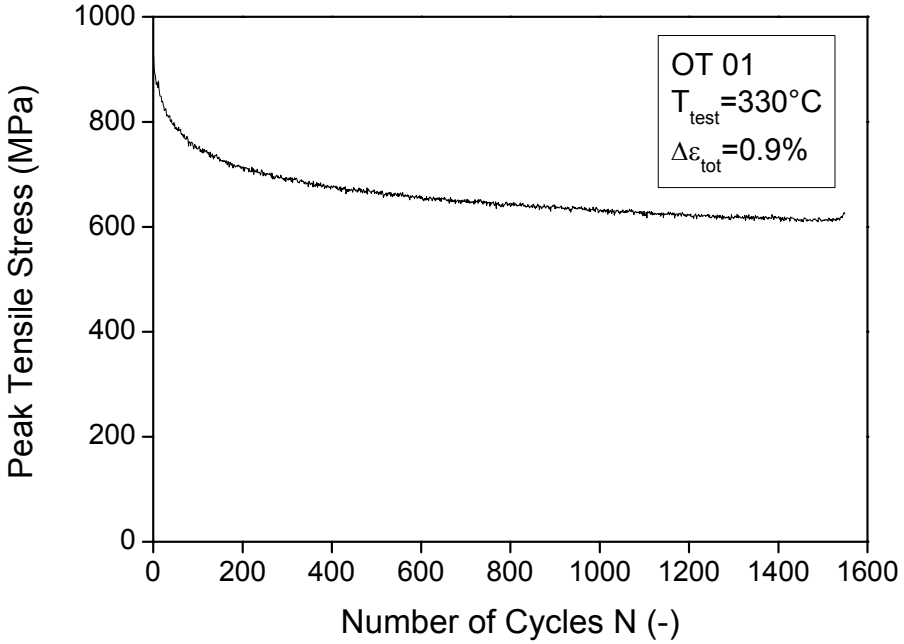

Fig. 11-40 Peak stress vs. number of cycles for OT 01 (70.8 dpa/334.0 °C).

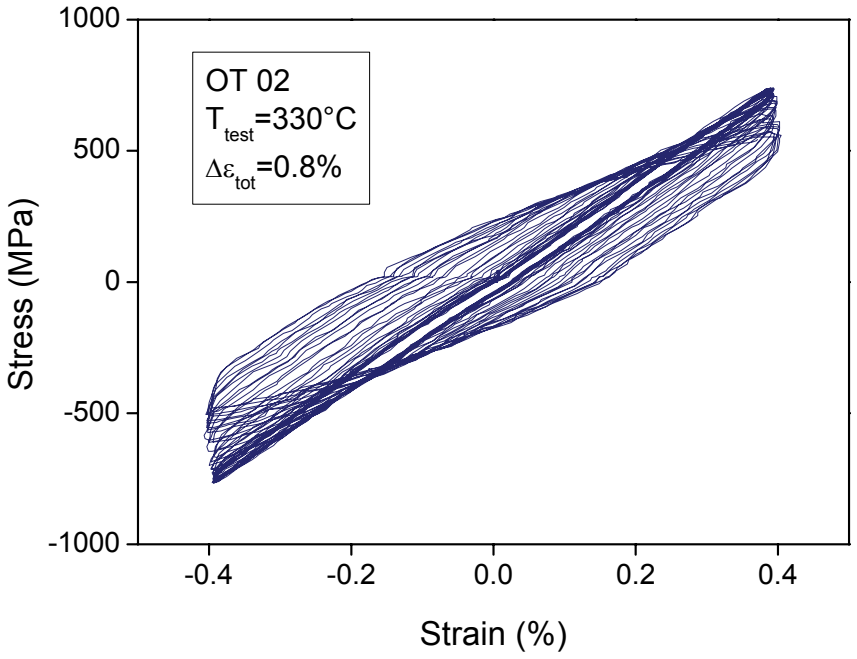

Fig. 11-41 Stress vs. strain for OT 02 (70.8 dpa/334.0 °C).

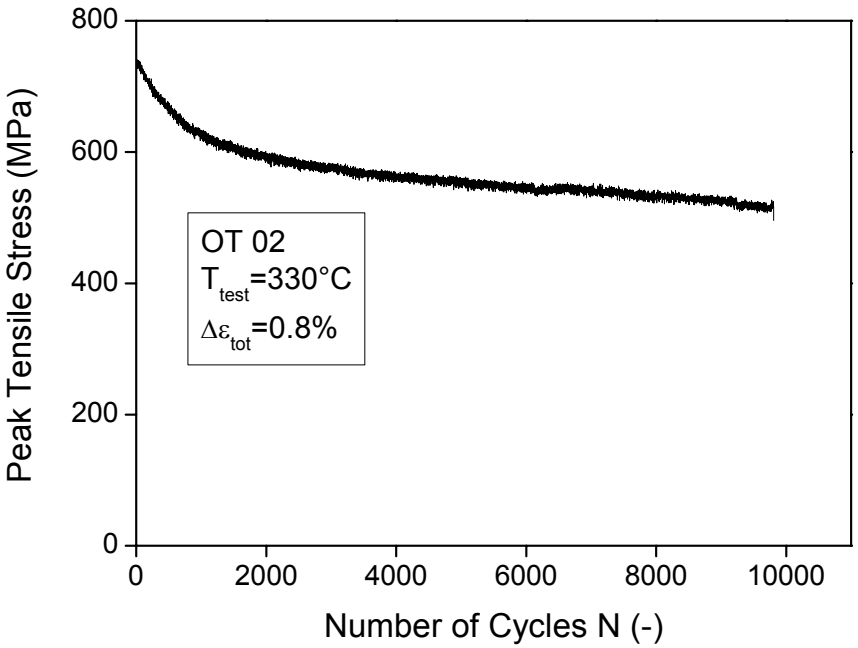

Fig. 11-42 Peak stress vs. number of cycles for OT 02 (70.8 dpa/334.0 °C).

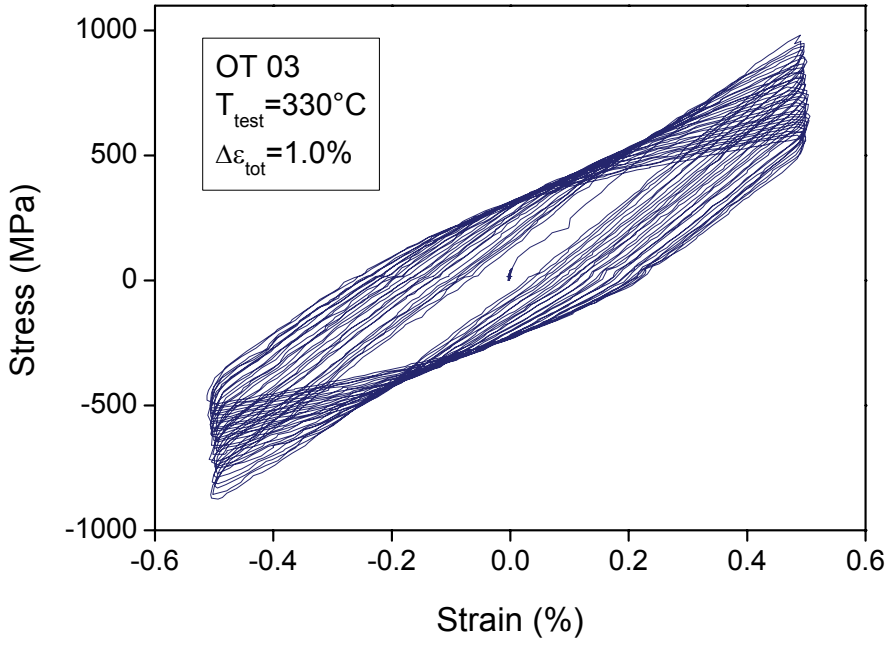

Fig. 11-43 Stress vs. strain for OT 03 (70.8 dpa/334.0 °C).

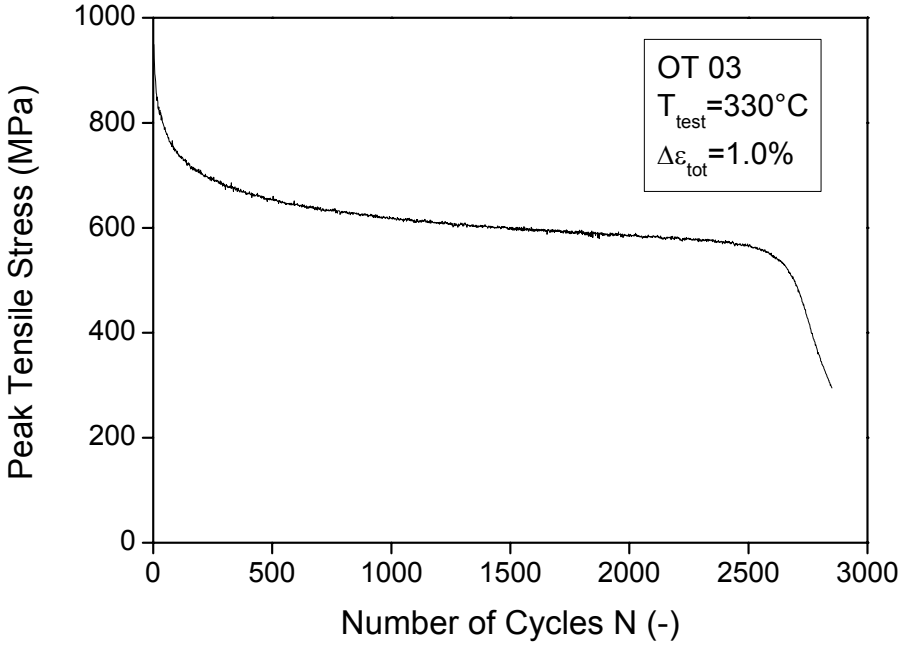

Fig. 11-44 Peak stress vs. number of cycles for OT 03 (70.8 dpa/334.0 °C).

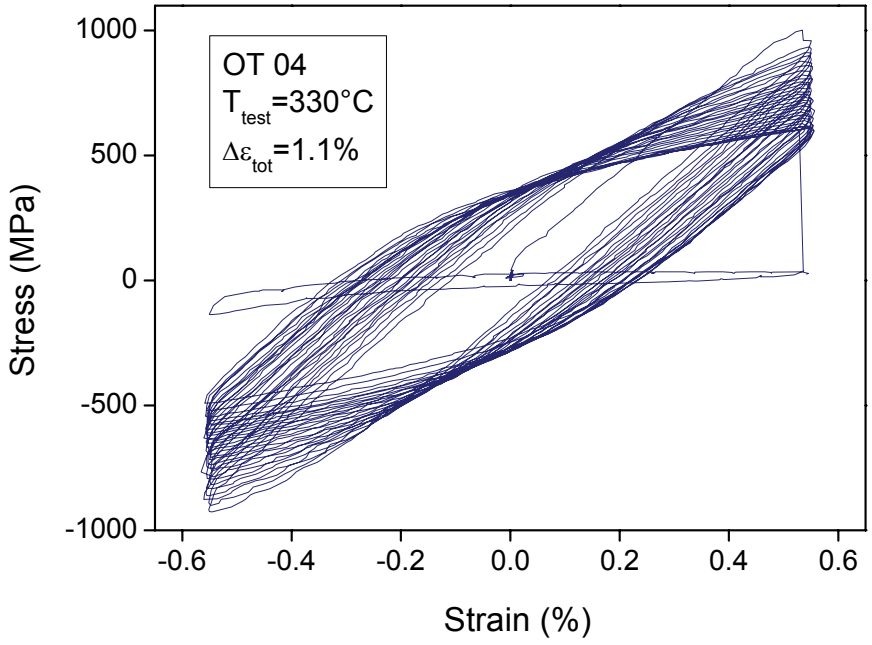

Fig. 11-45 Stress vs. strain for OT 04 (70.8 dpa/334.0 °C).

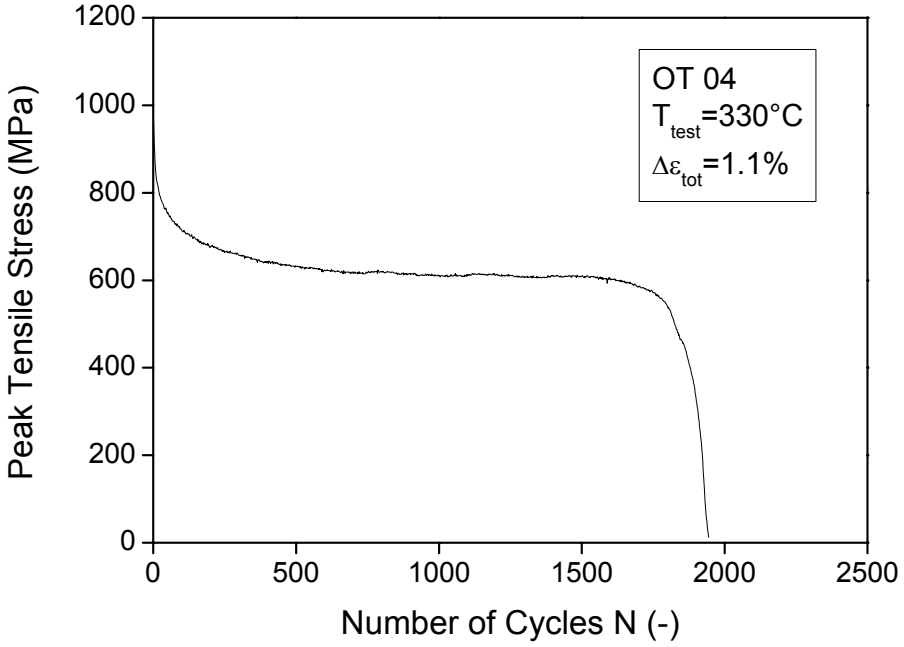

Fig. 11-46 Peak stress vs. number of cycles for OT 04 (70.8 dpa/334.0 °C).

11.5 BS-EUROFER

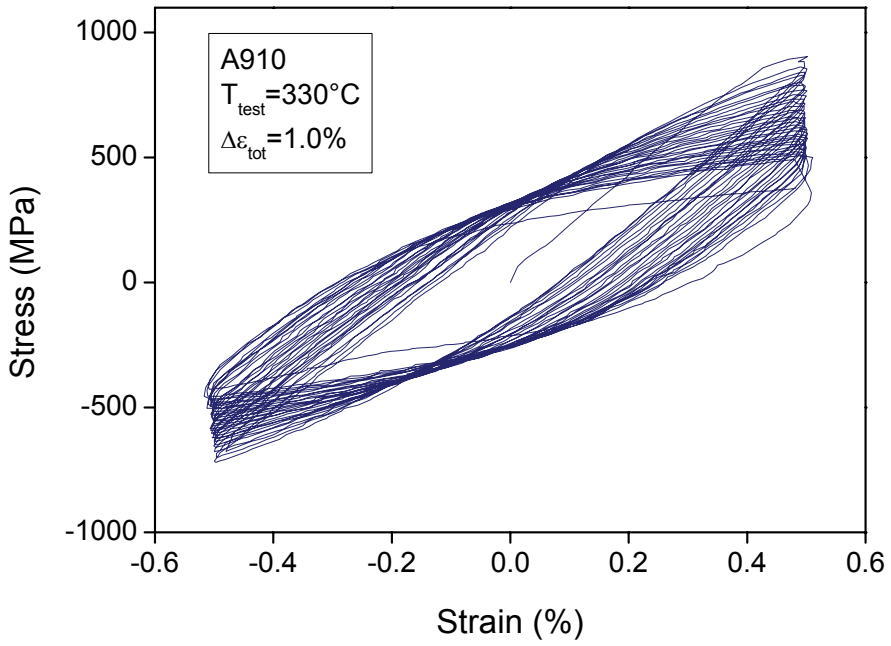

Fig. 11-47 Stress vs. strain for A910 (46.8 dpa/337.5 °C).

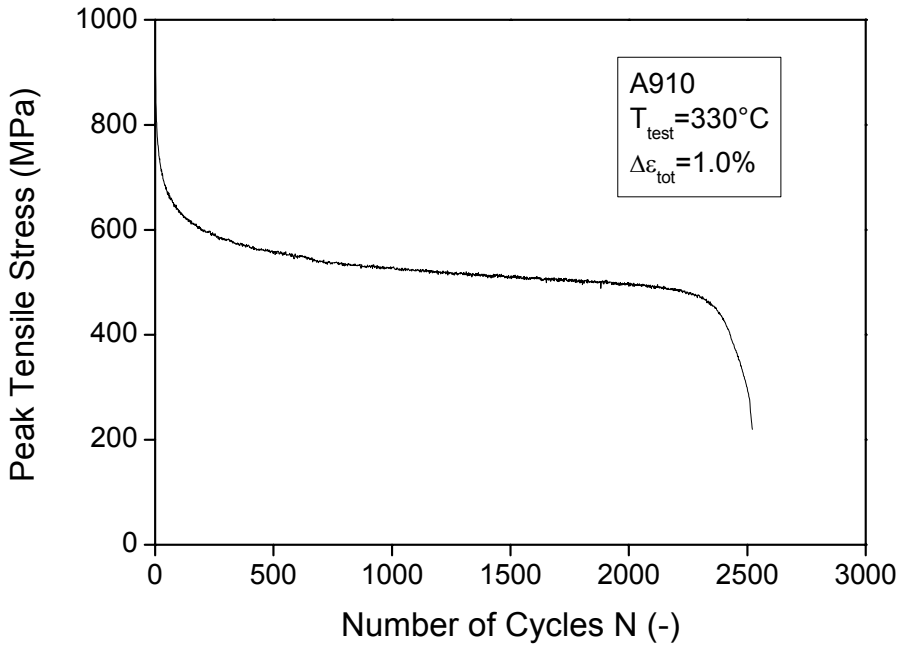

Fig. 11-48 Peak stress vs. number of cycles for A910 (46.8 dpa/337.5 °C).

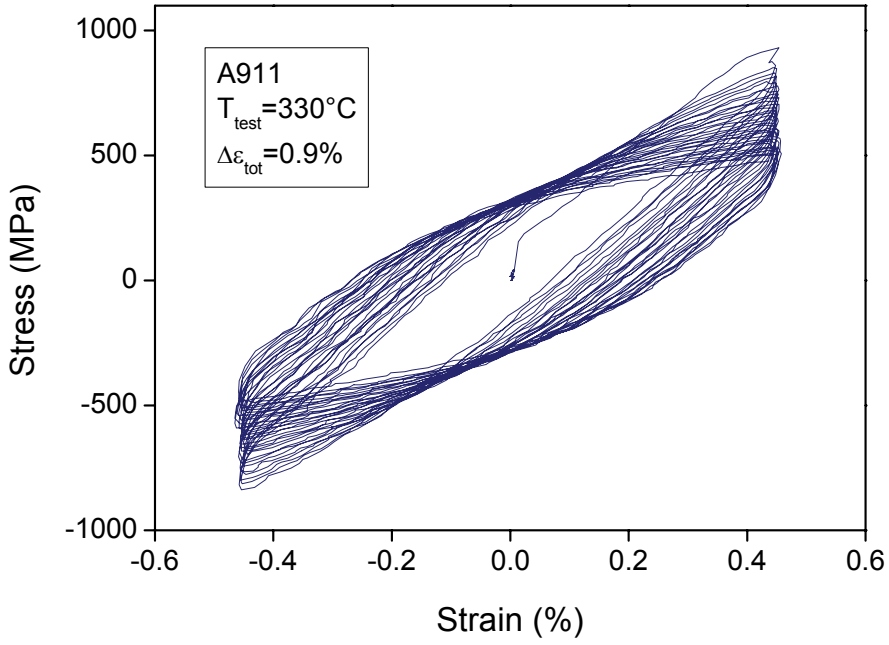

Fig. 11-49 Stress vs. strain for A911 (46.8 dpa/337.5 °C).

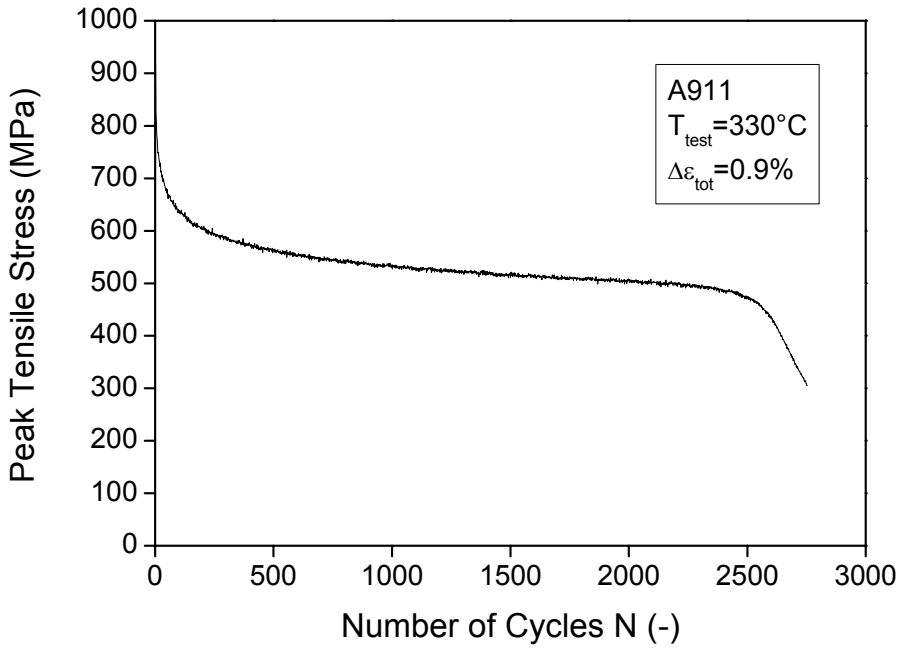

Fig. 11-50 Peak stress vs. number of cycles for A911 (46.8 dpa/337.5 °C).

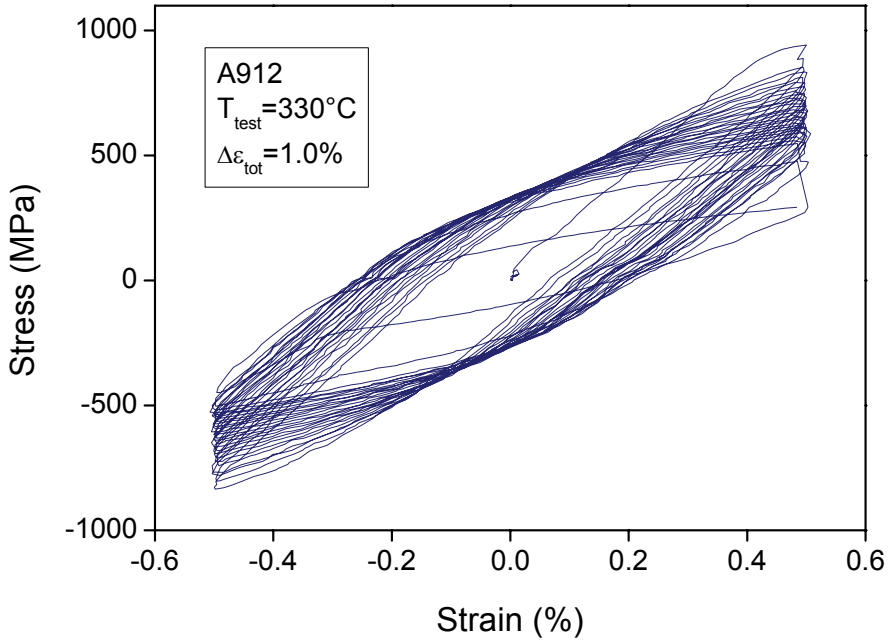

Fig. 11-51 Stress vs. strain for A912 (46.8 dpa/337.5 °C).

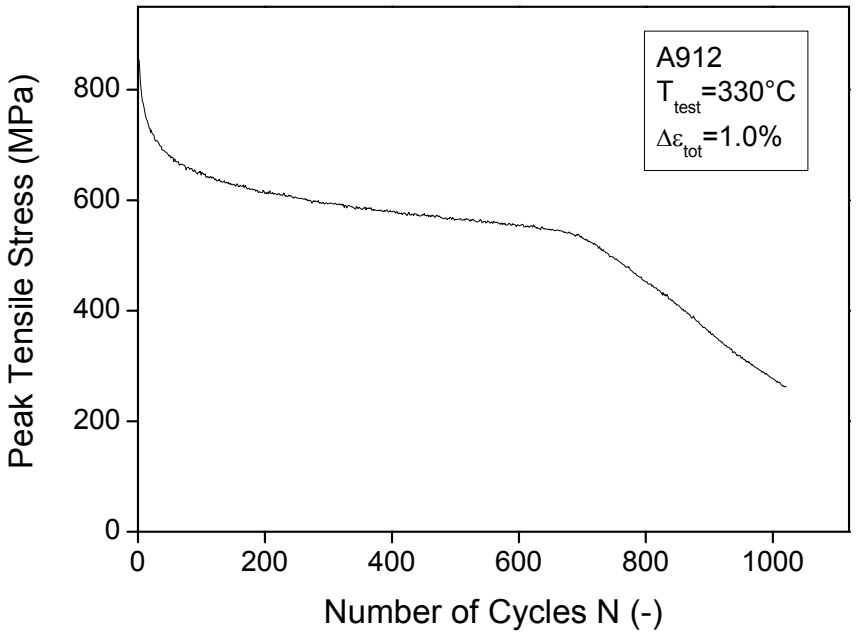

Fig. 11-52 Peak stress vs. number of cycles for A912 (46.8 dpa/337.5 °C).

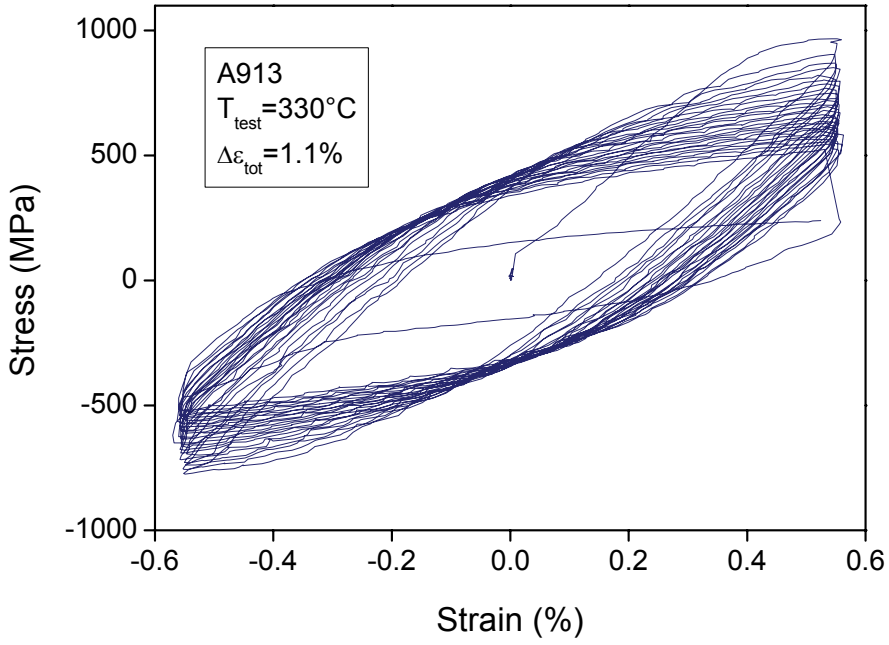

Fig. 11-53 Stress vs. strain for A913 (46.8 dpa/337.5 °C).

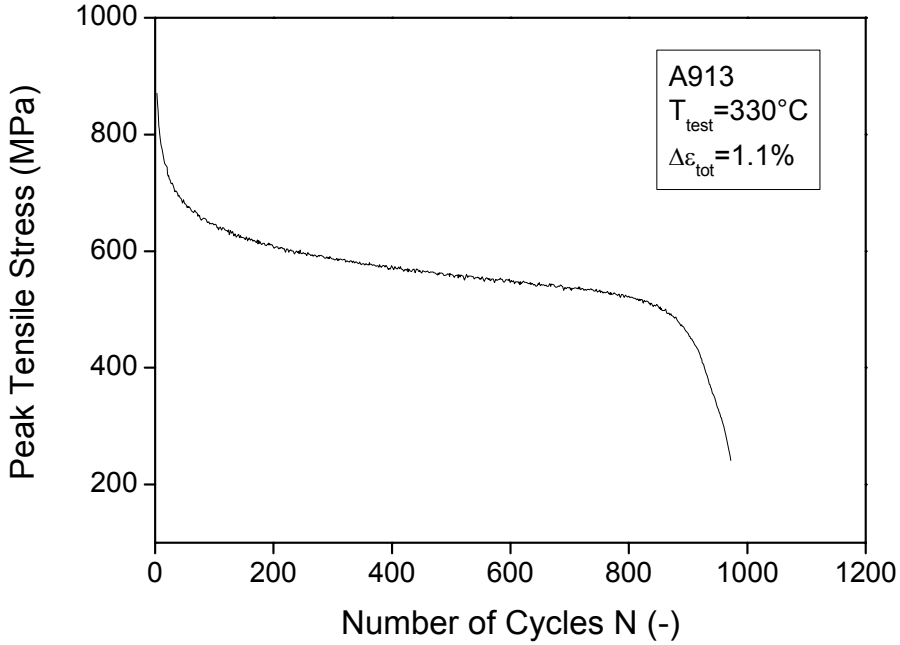

Fig. 11-54 Peak stress vs. number of cycles for A913 (46.8 dpa/337.5 °C).

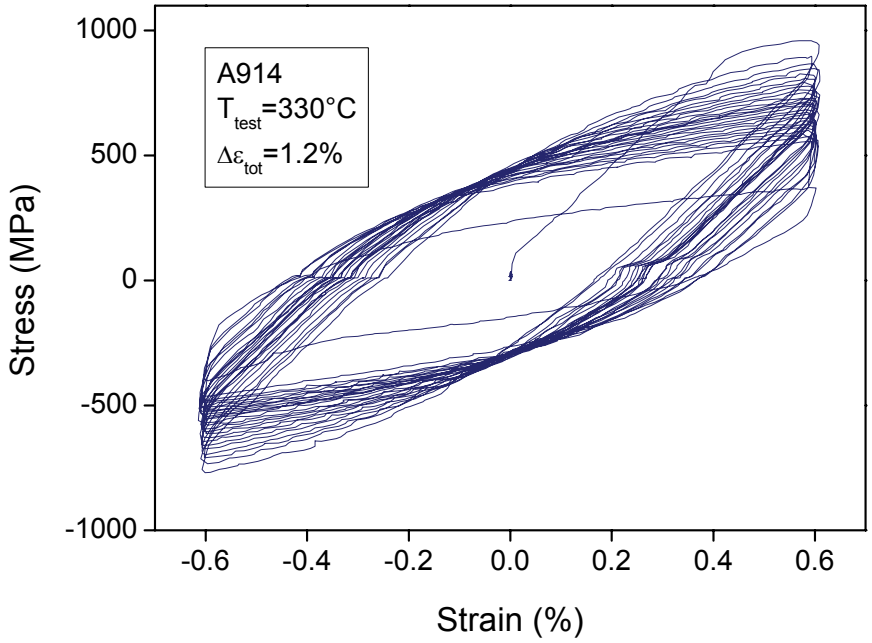

Fig. 11-55 Stress vs. strain for A913 (46.8 dpa/337.5 °C).

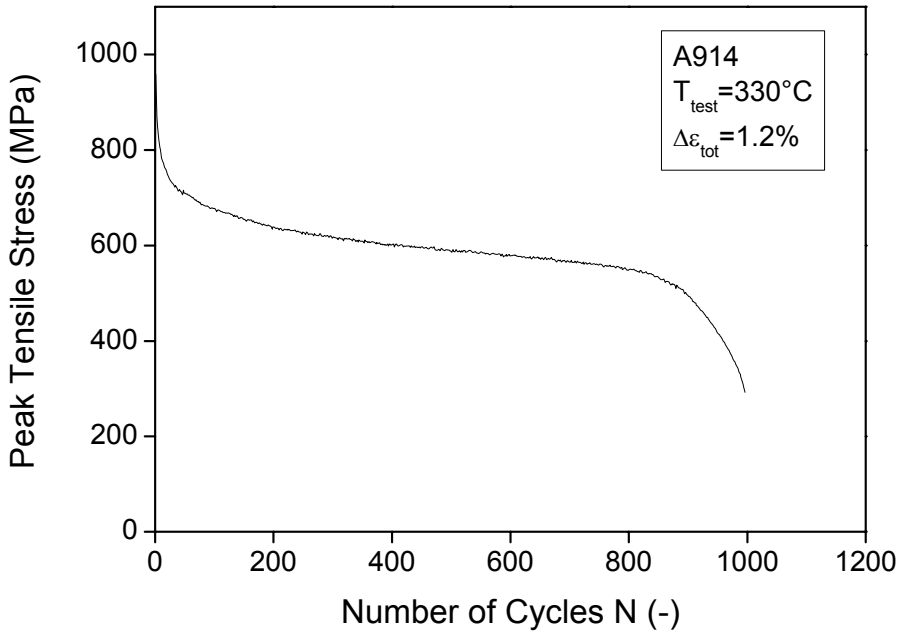

Fig. 11-56 Peak stress vs. number of cycles for A914 (46.8 dpa/337.5 °C).

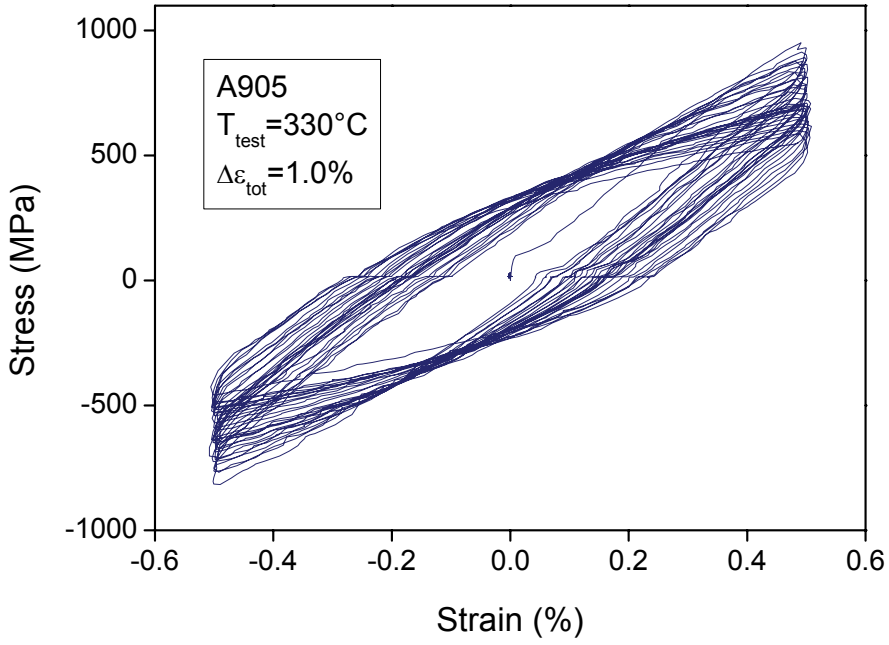

Fig. 11-57 Stress vs. strain for A905 (70.8 dpa/334.0 °C).

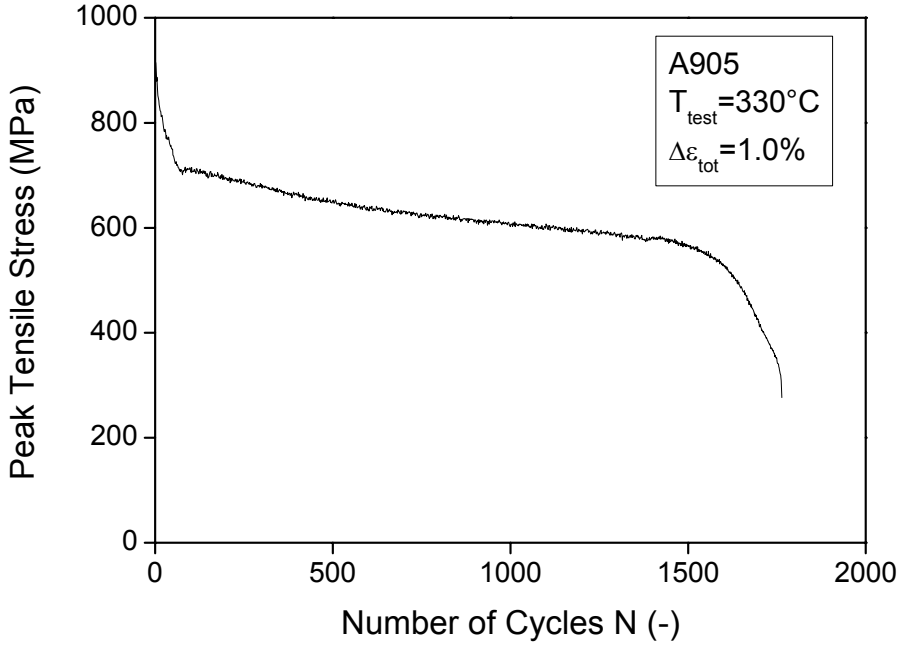

Fig. 11-58 Peak stress vs. number of cycles for A905 (70.8 dpa/334.0 °C).

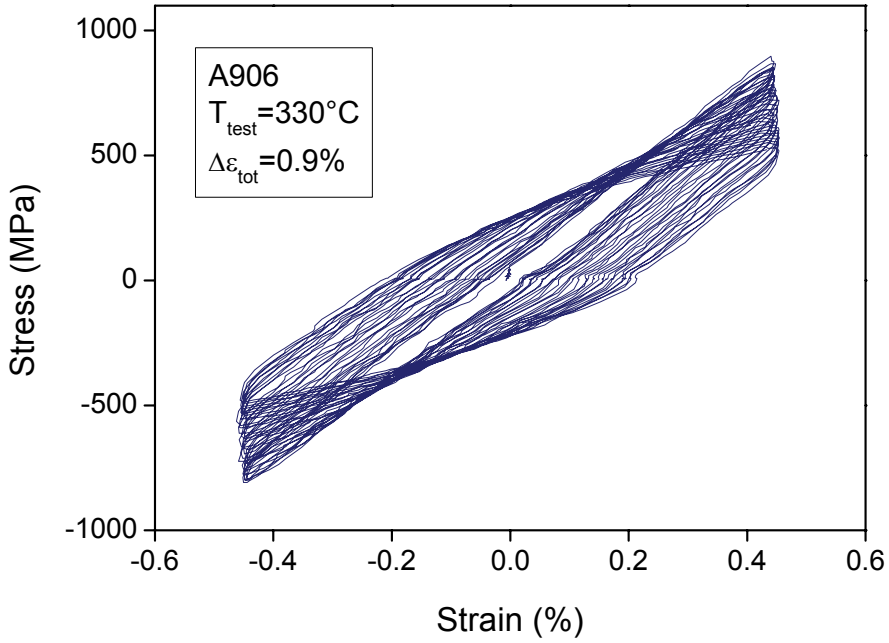

Fig. 11-59 Stress vs. strain for A906 (70.8 dpa/334.0 °C).

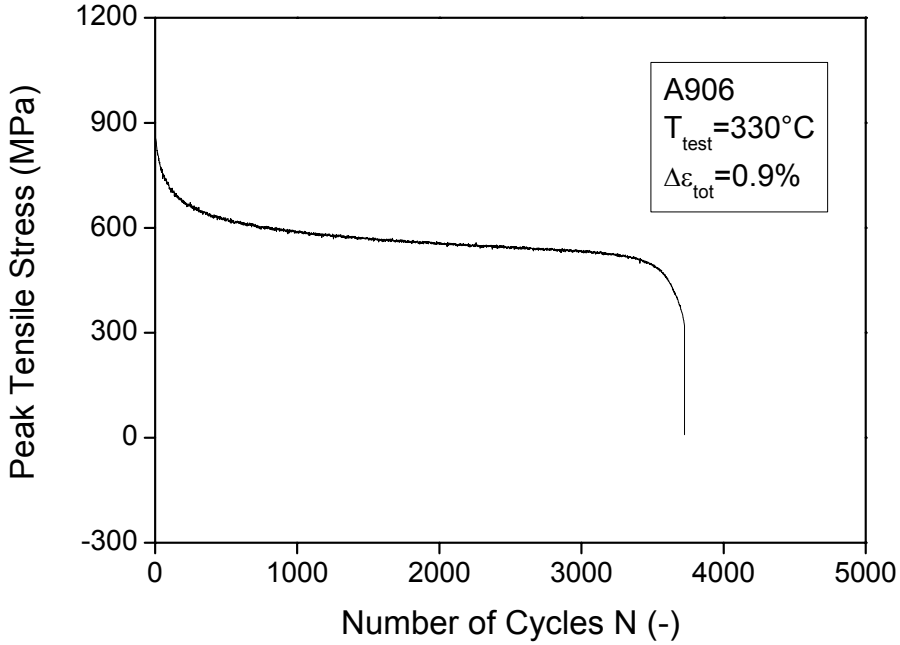

Fig. 11-60 Peak stress vs. number of cycles for A906 (70.8 dpa/334.0 °C).

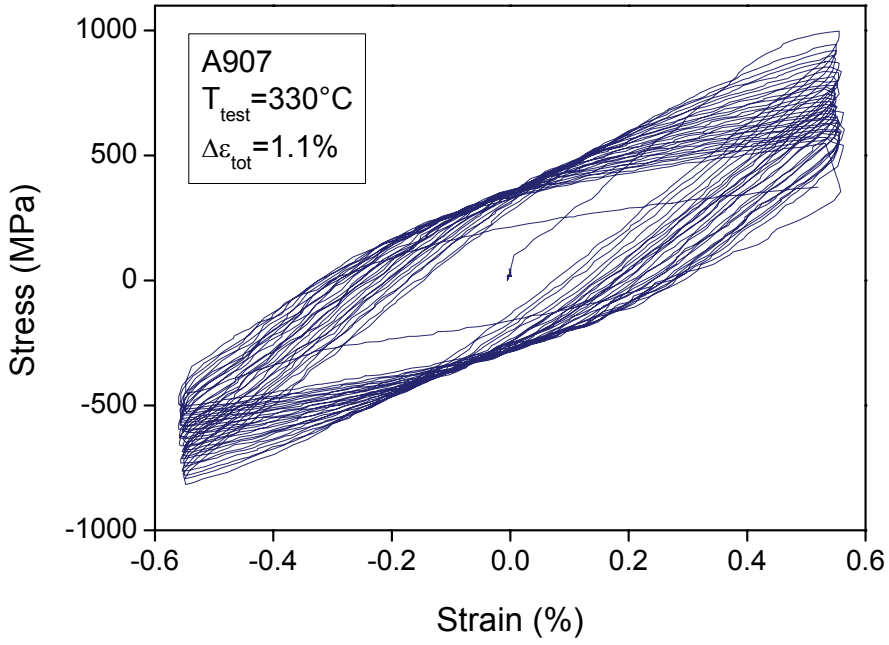

Fig. 11-61 Stress vs. strain for A907 (70.8 dpa/334.0 °C).

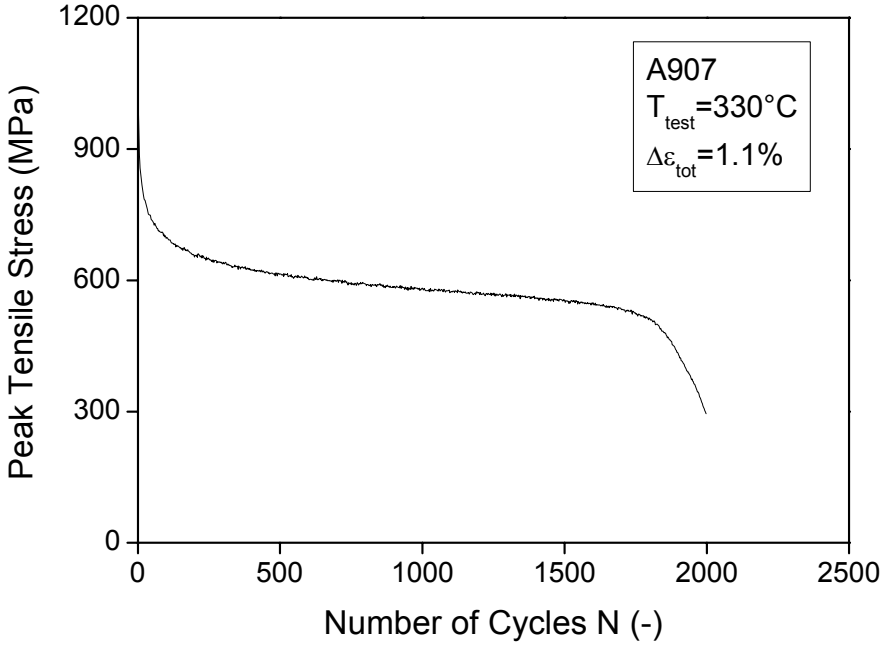

Fig. 11-62 Peak stress vs. number of cycles for A907 (70.8 dpa/334.0 °C).

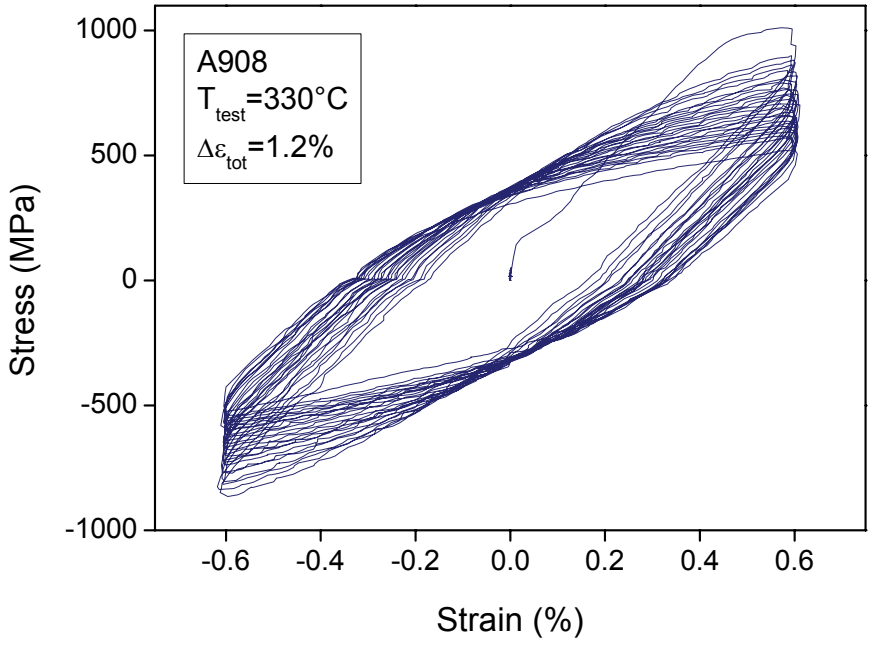

Fig. 11-63 Stress vs. strain for A908 (70.8 dpa/334.0 °C).

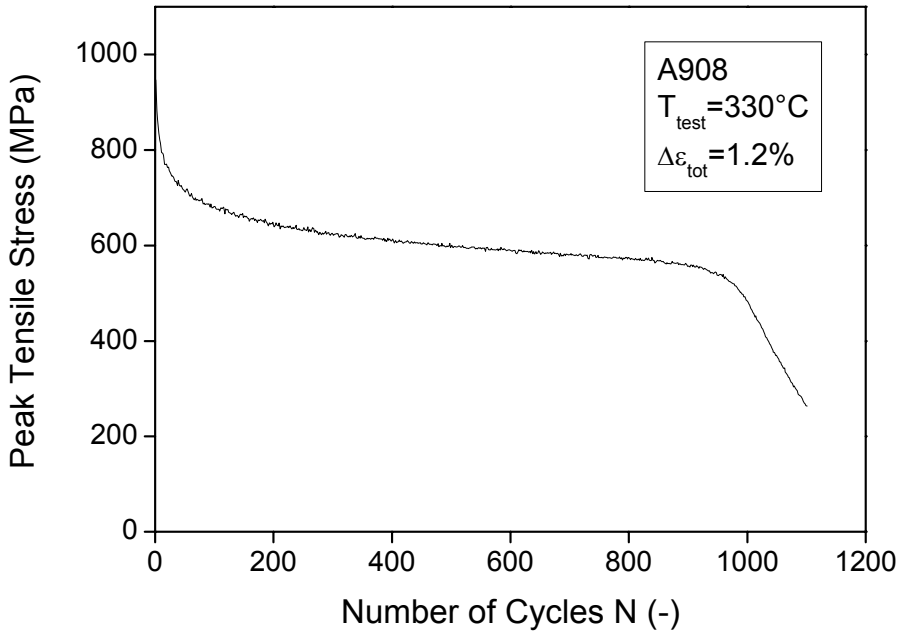

Fig. 11-64 Peak stress vs. number of cycles for A908 (70.8 dpa/334.0 °C).

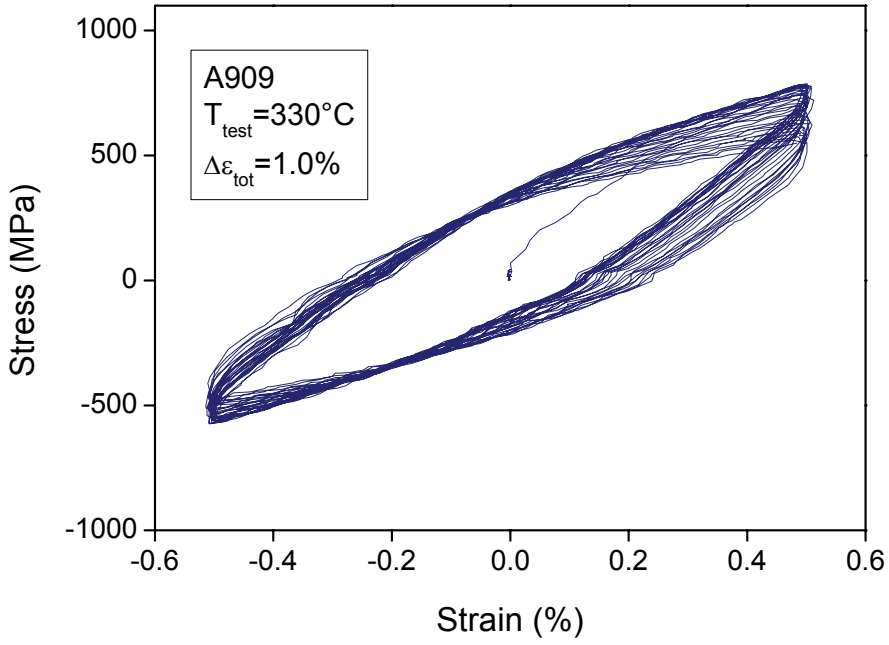

Fig. 11-65 Stress vs. strain for A909 (70.8 dpa/334.0 °C).

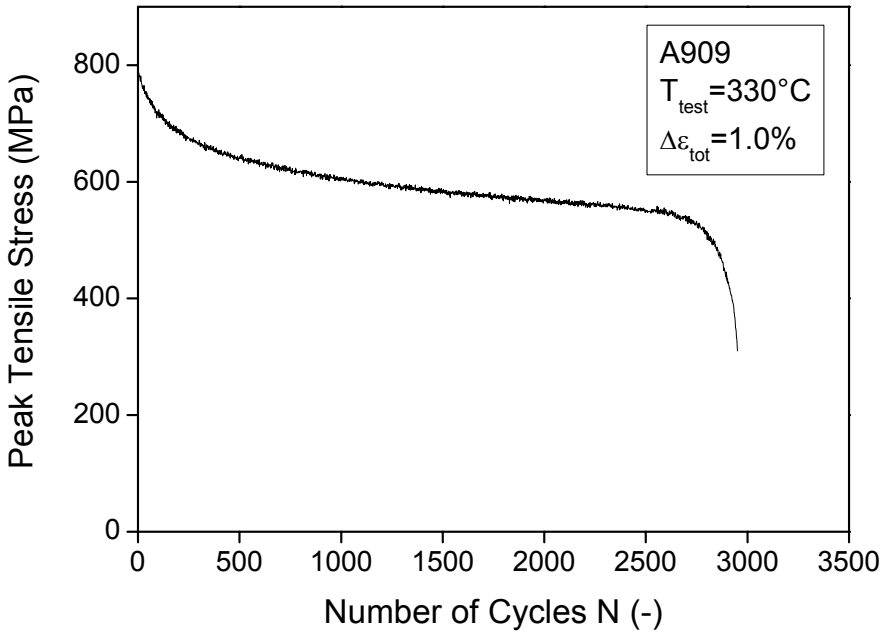

Fig. 11-66 Peak stress vs. number of cycles for A909 (70.8 dpa/334.0 °C).

11.6 EURODShip (EUROFER 97 with 0.5 wt.% Y_2O_3)

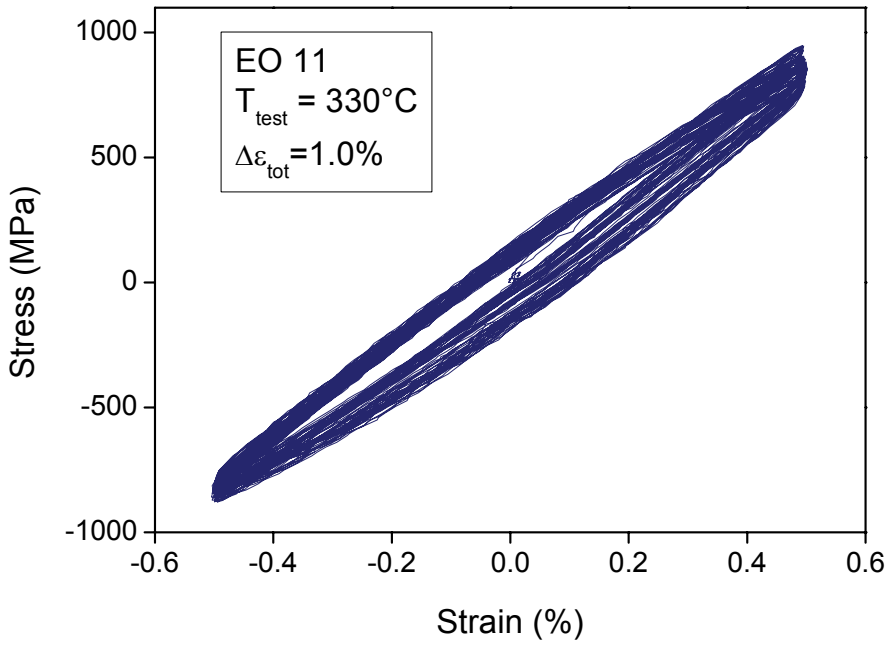

Fig. 11-67 Stress vs. strain for EO 11 (46.8 dpa/337.5 °C).

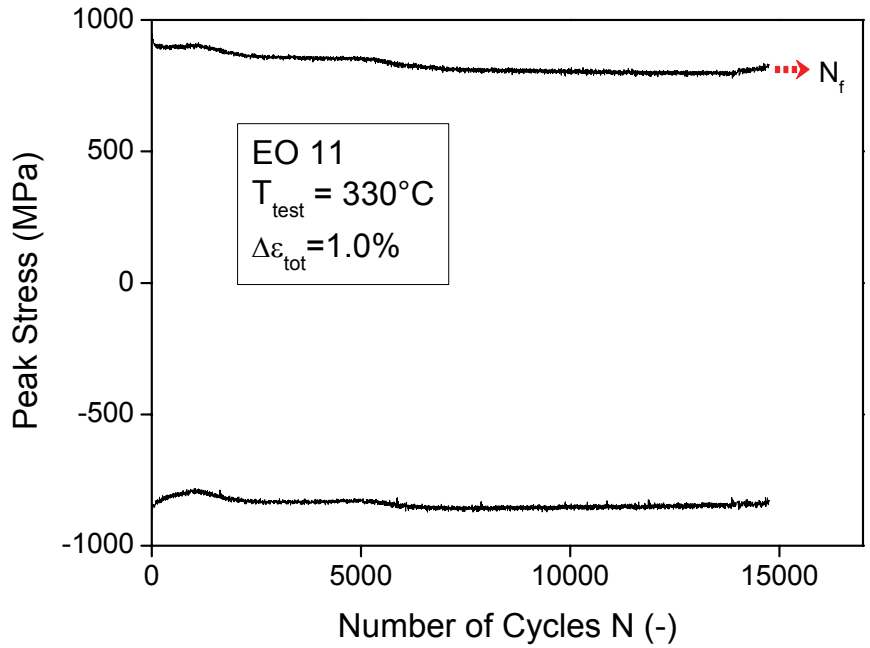

Fig. 11-68 Peak stress vs. number of cycles for EO 11 (46.8 dpa/337.5 °C).

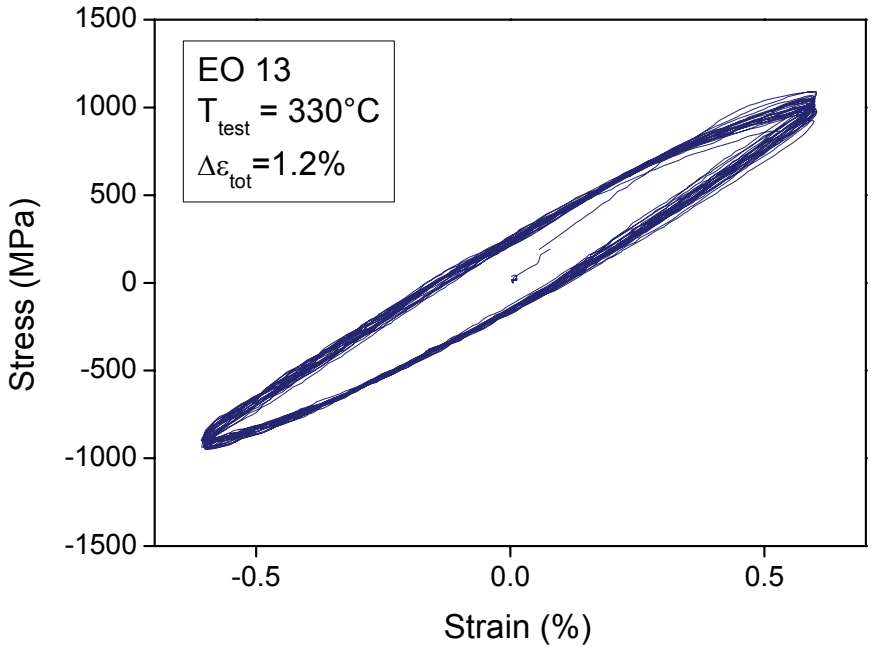

Fig. 11-69 Stress vs. strain for EO 13 (46.8 dpa/337.5 °C).

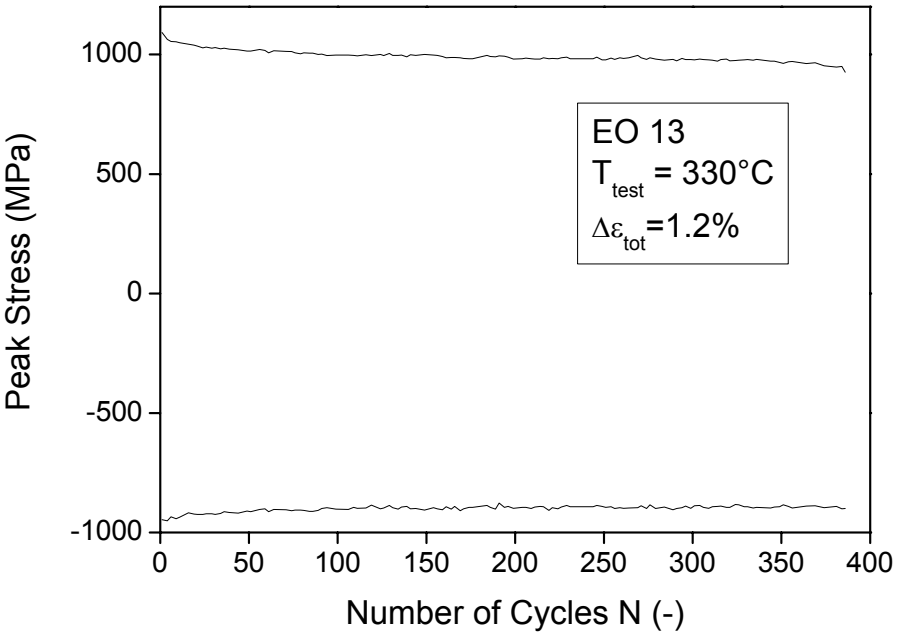

Fig. 11-70 Peak stress vs. number of cycles for EO 13 (46.8 dpa/337.5 °C).

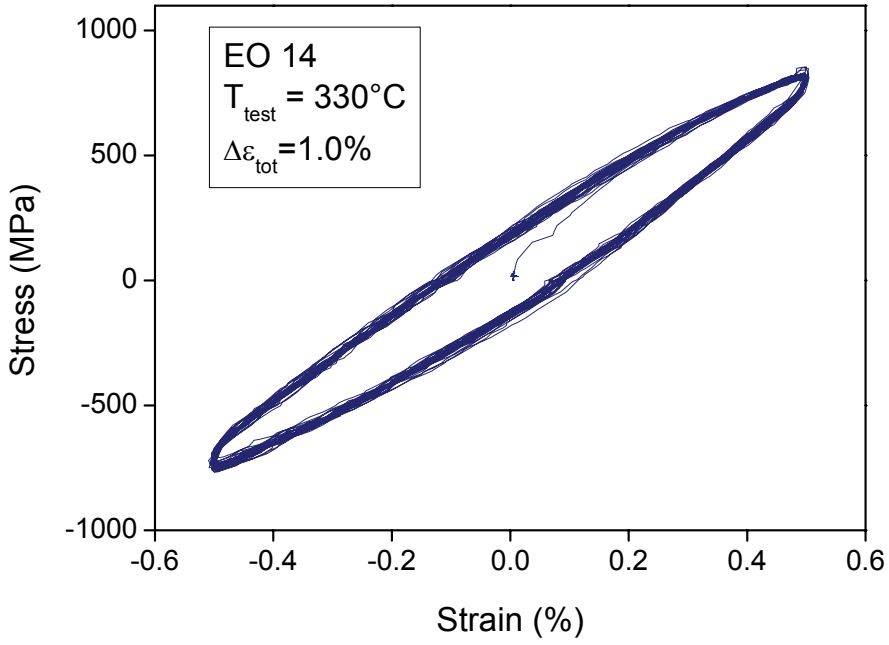

Fig. 11-71 Stress vs. strain for EO 14 (46.8 dpa/337.5 °C + 550 °C/3 h).

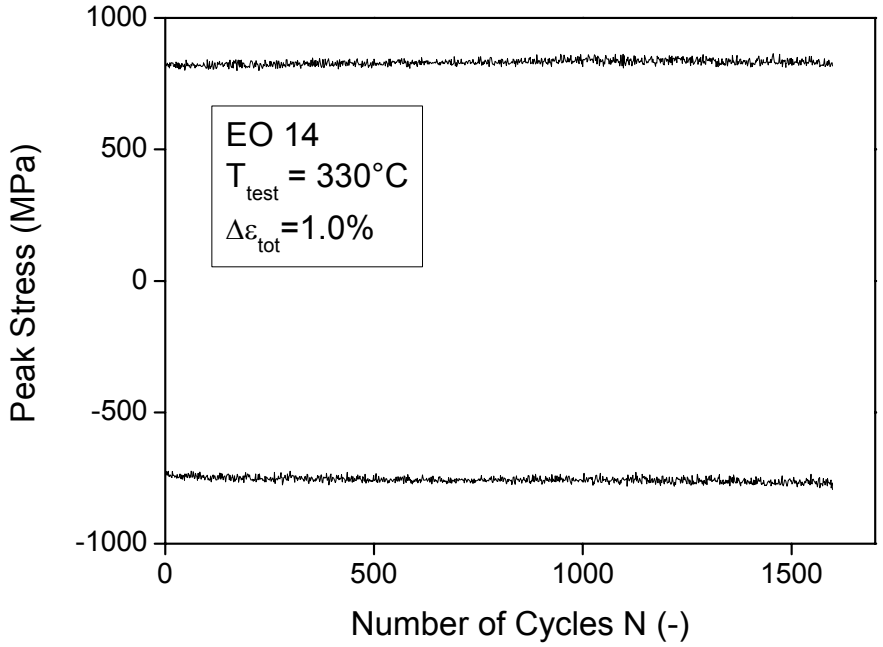

Fig. 11-72 Peak stress vs. number of cycles for EO 14 (46.8 dpa/337.5 °C + 550 °C/3 h).

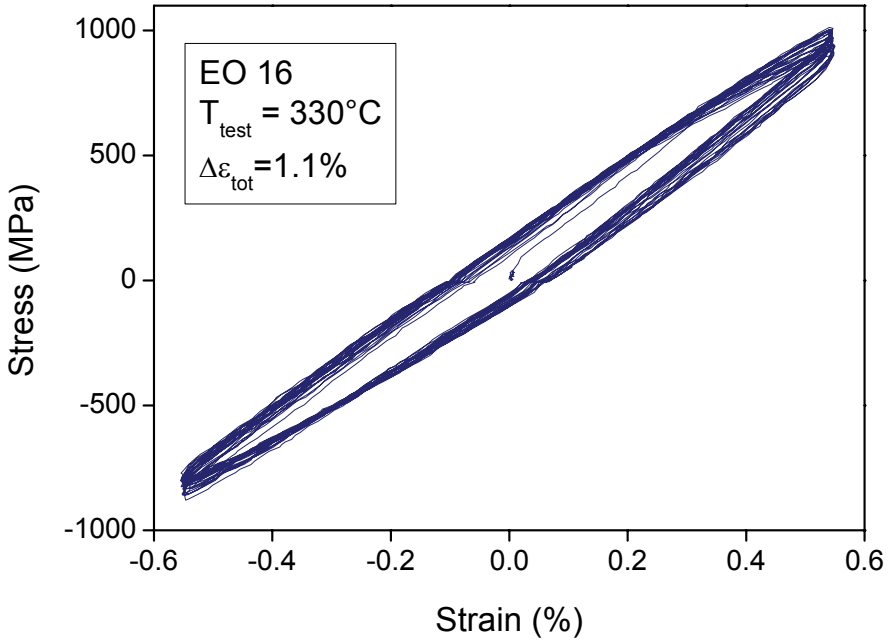

Fig. 11-73 Stress vs. strain for EO 16 (46.8 dpa/337.5 °C).

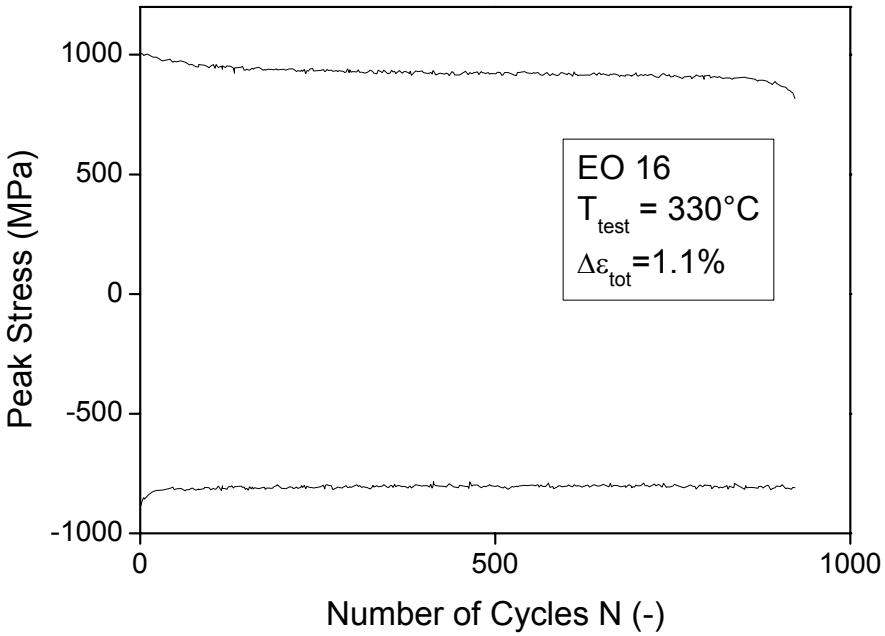

Fig. 11-74 Peak stress vs. number of cycles for EO 16 (46.8 dpa/337.5 °C).

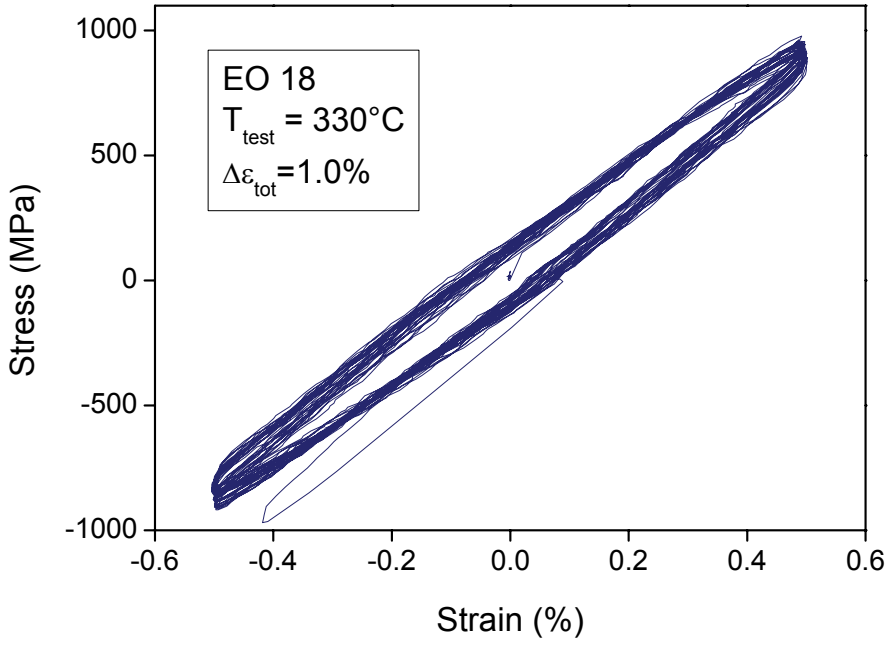

Fig. 11-75 Stress vs. strain for EO 18 (46.8 dpa/337.5 °C).

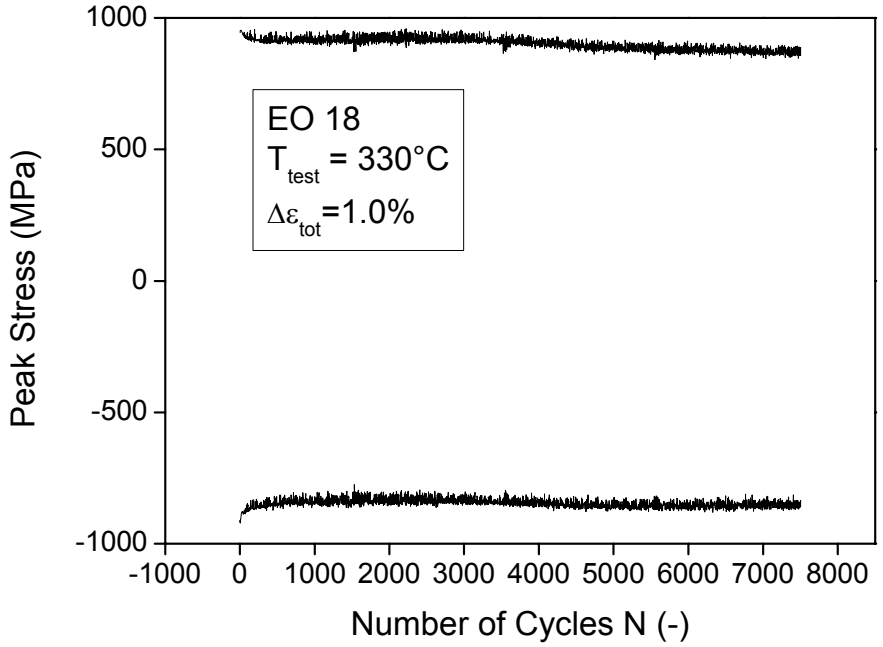

Fig. 11-76 Peak stress vs. number of cycles for EO 18 (46.8 dpa/337.5 °C).

11.7 ADS 2

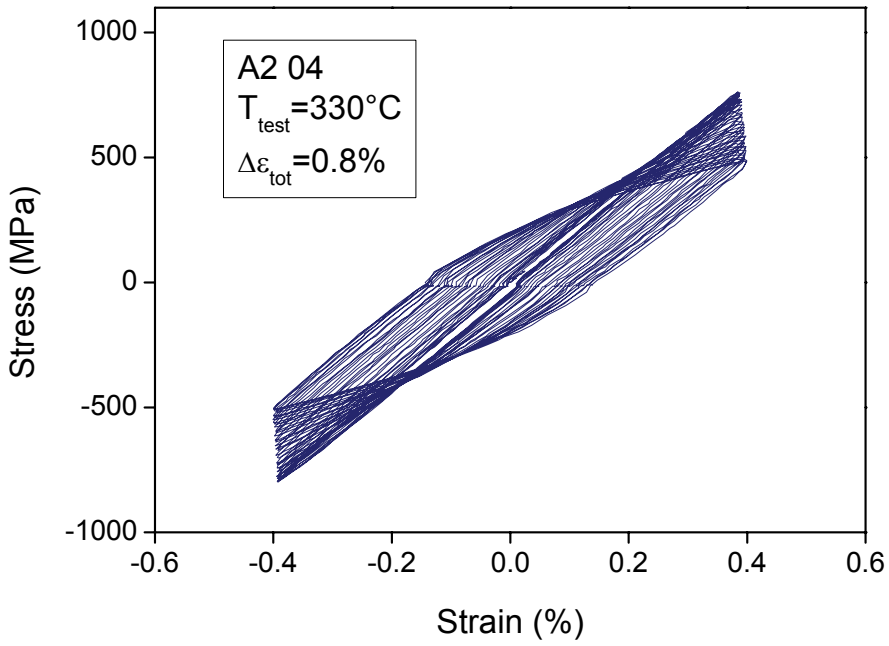

Fig. 11-77 Stress vs. strain for A2 04 (70.8 dpa/334.0 °C).

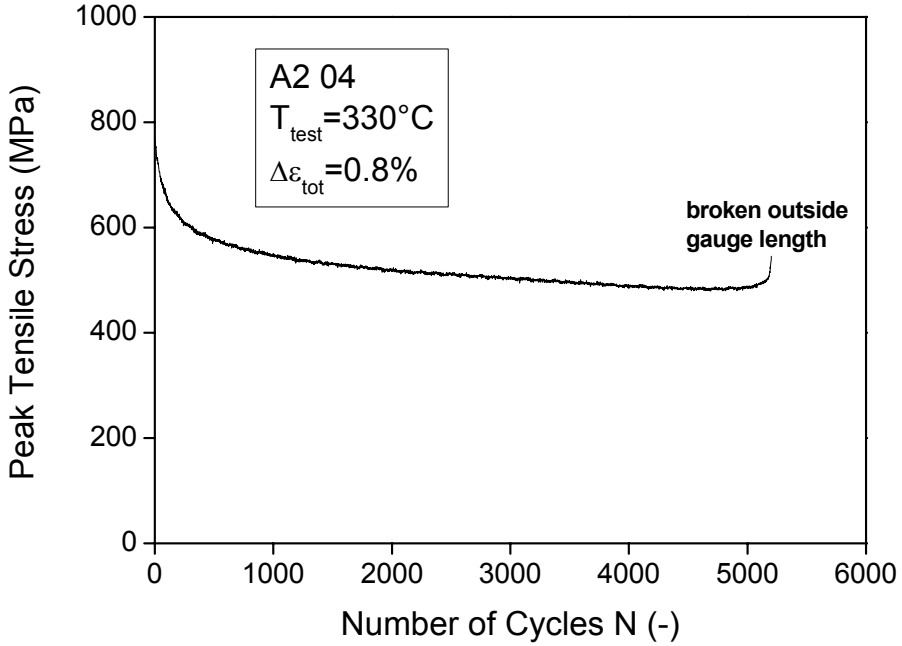

Fig. 11-78 Peak tensile stress vs. number of cycles for A2 04 (70.8 dpa/334.0 °C).

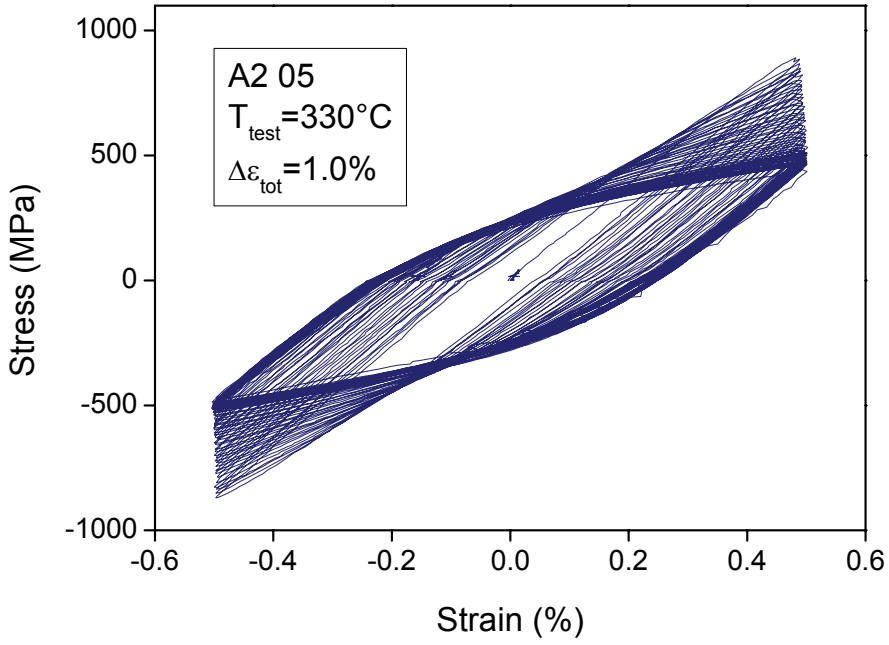

Fig. 11-79 Stress vs. strain for A2 05 (70.8 dpa/334.0 °C).

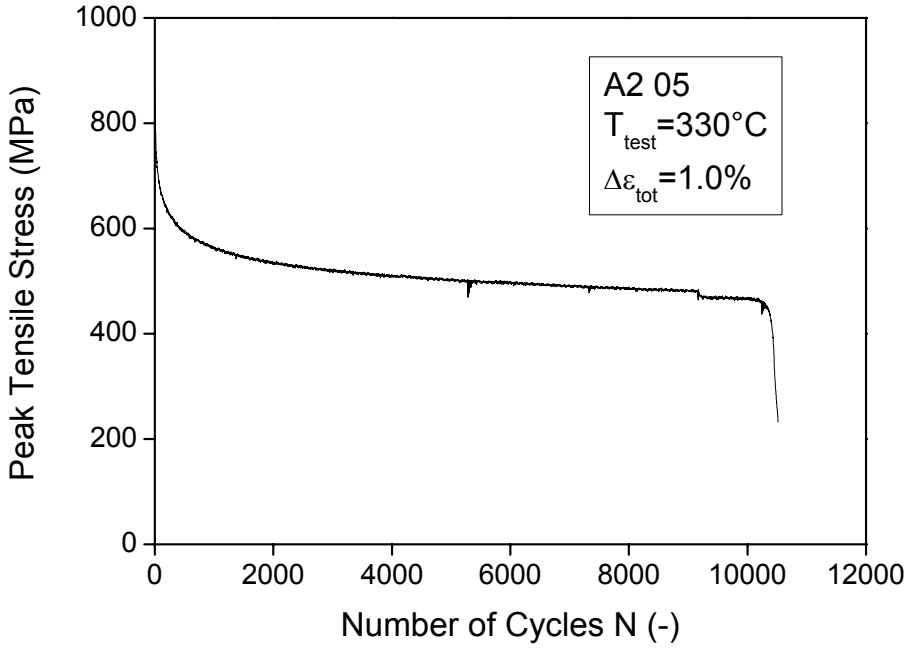

Fig. 11-80 Peak tensile stress vs. number of cycles for A2 05 (70.8 dpa/334.0 °C).

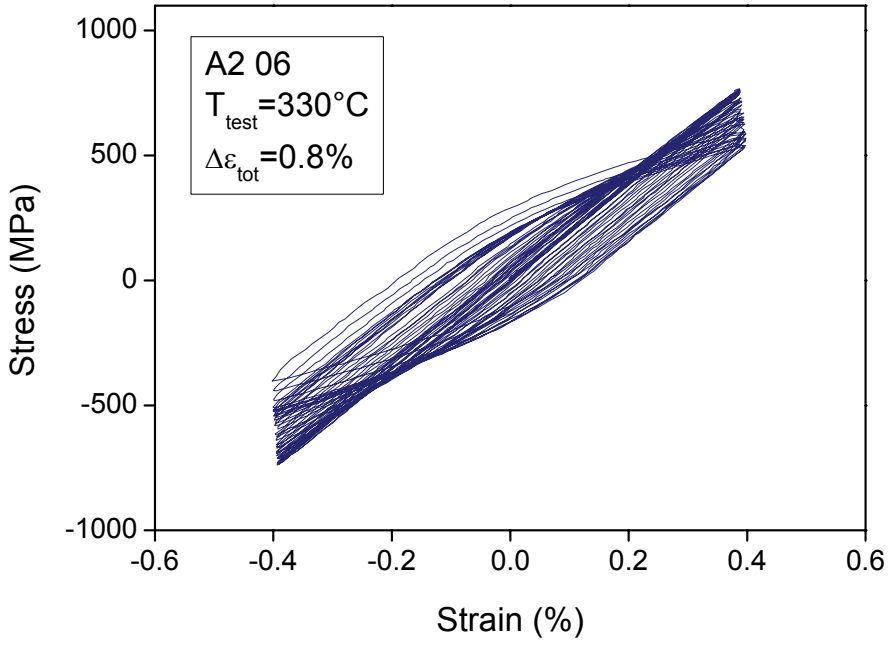

Fig. 11-81 Stress vs. strain for A2 06 (70.8 dpa/334.0 °C).

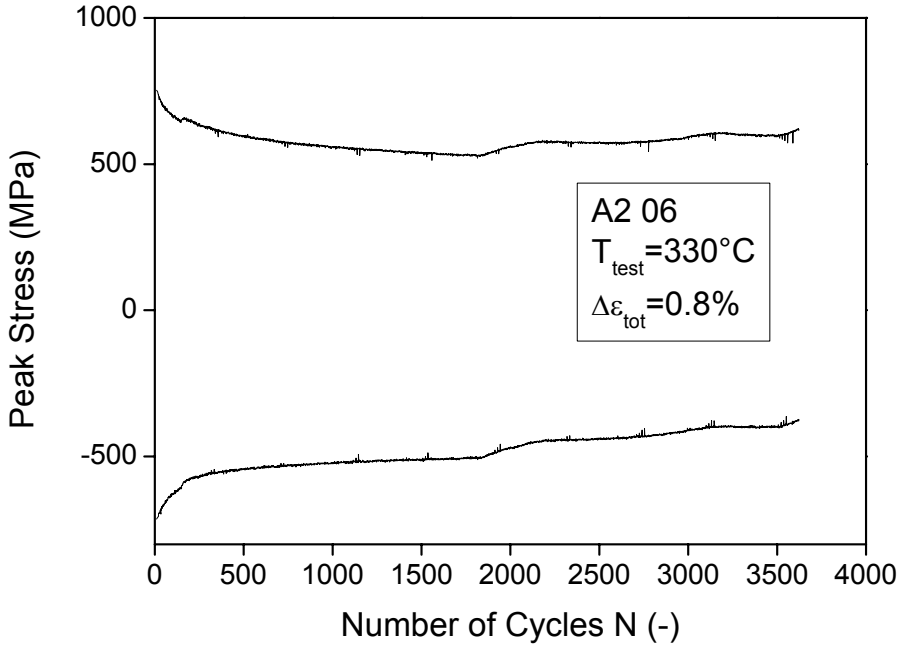

Fig. 11-82 Peak stresses vs. number of cycles for A2 06 (70.8 dpa/334.0 °C).

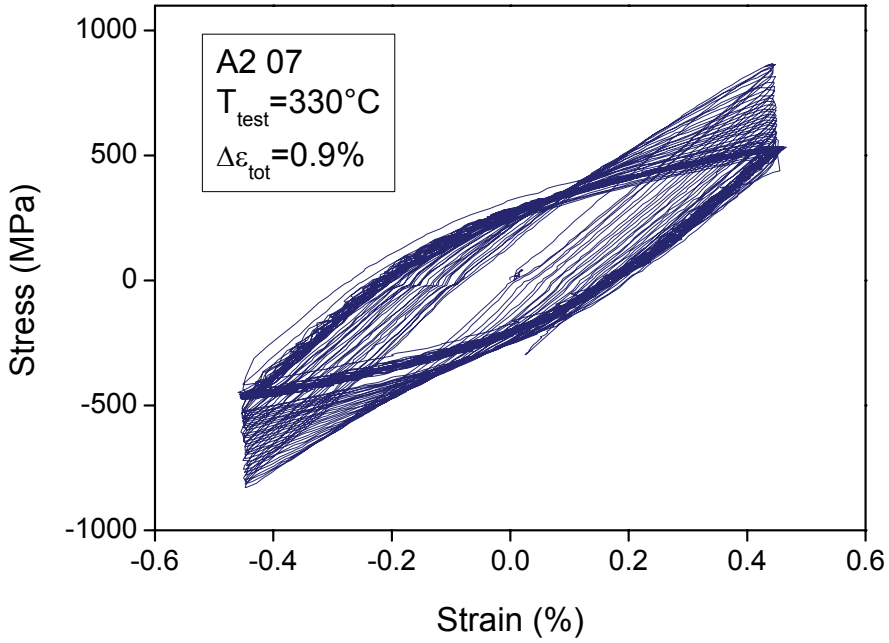

Fig. 11-83 Stress vs. strain for A2 07 (70.8 dpa/334.0 °C).

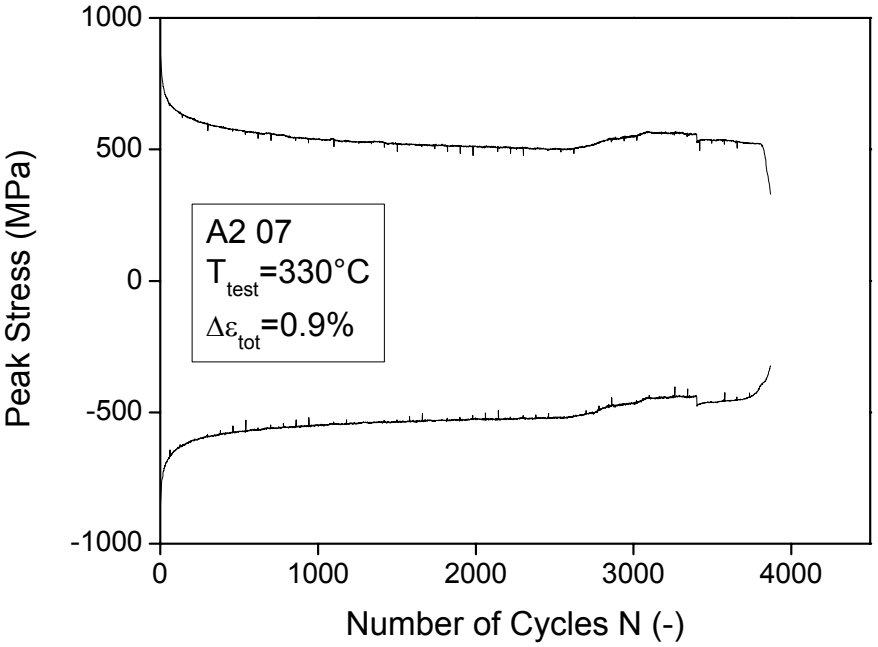

Fig. 11-84 Peak stresses vs. number of cycles for A2 07 (70.8 dpa/334.0 °C).

11.8 ADS 3

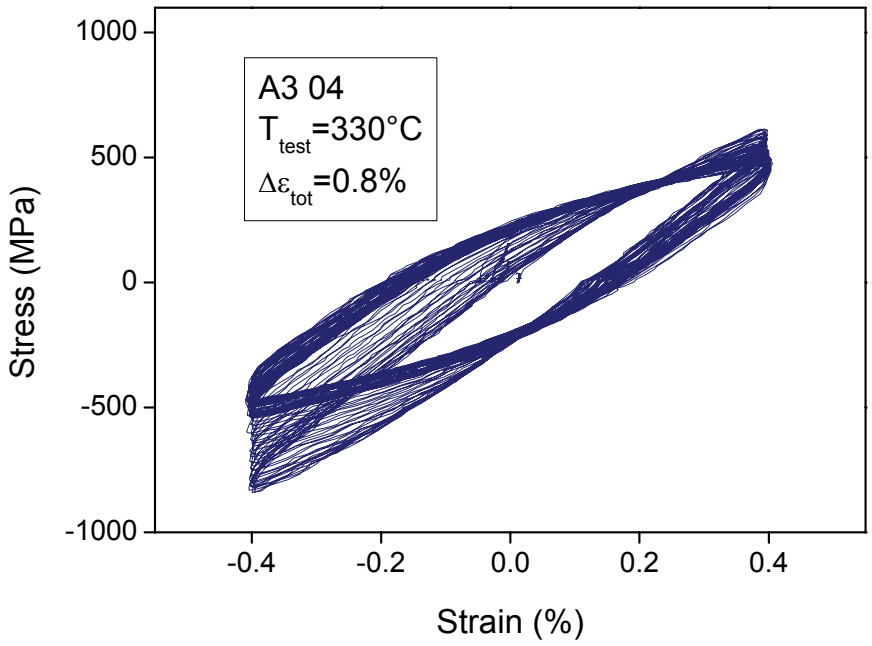

Fig. 11-85 Stress vs. strain for A3 04 (70.8 dpa/334.0 °C).

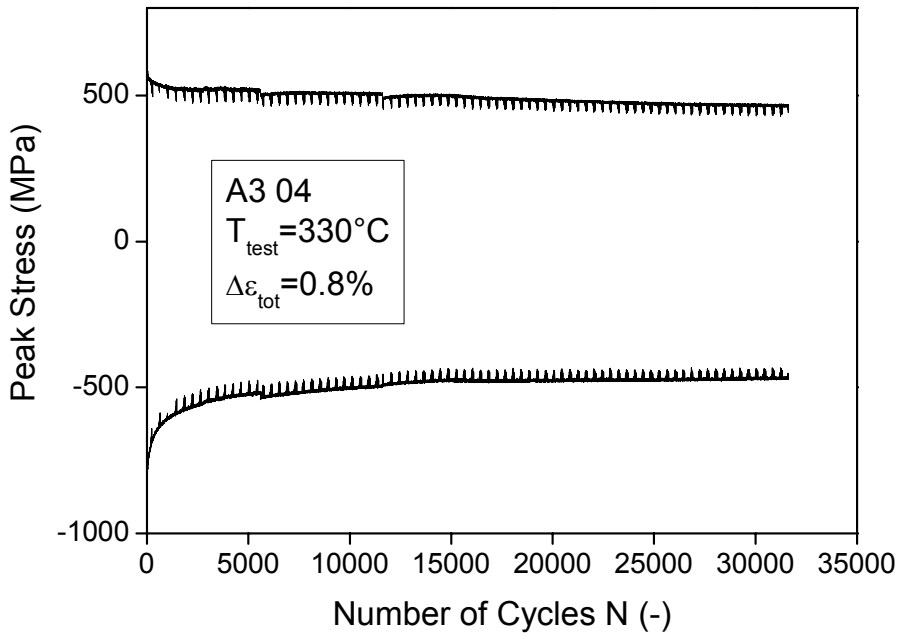

Fig. 11-86 Peak stresses vs. number of cycles for A3 04 (70.8 dpa/334.0 °C).

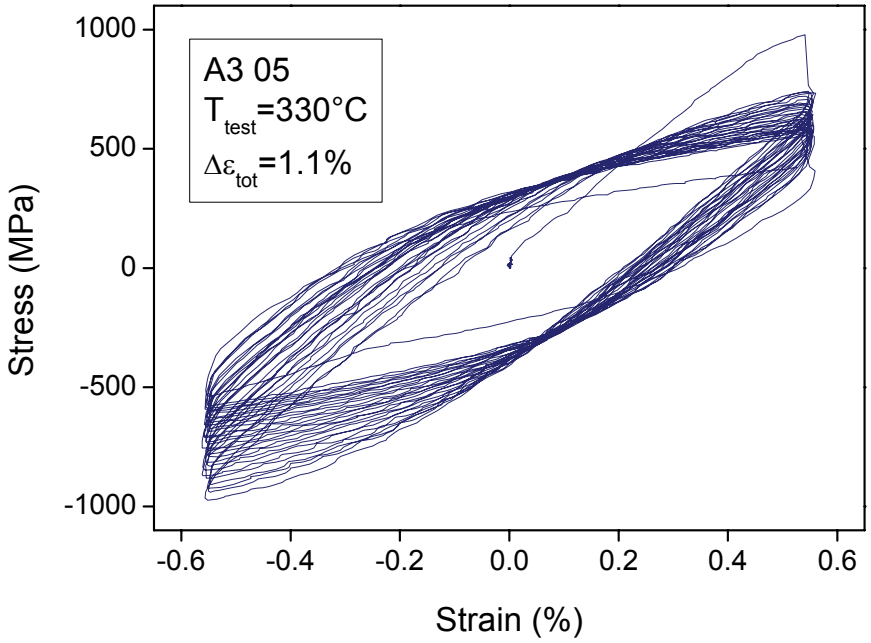

Fig. 11-87 Stress vs. strain for A3 05 (70.8 dpa/334.0 °C).

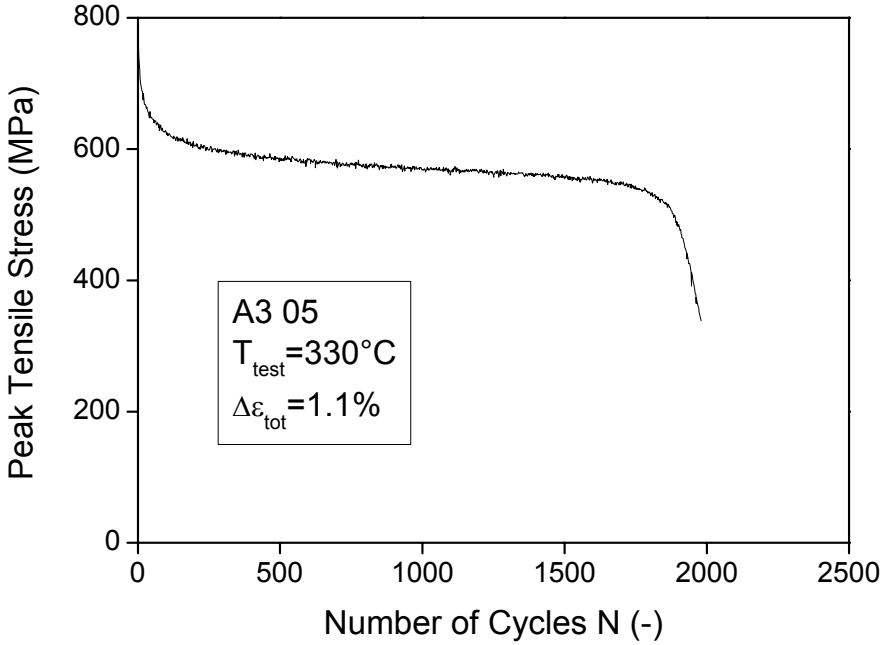

Fig. 11-88 Peak tensile stress vs. number of cycles for A3 05 (70.8 dpa/334.0 °C).

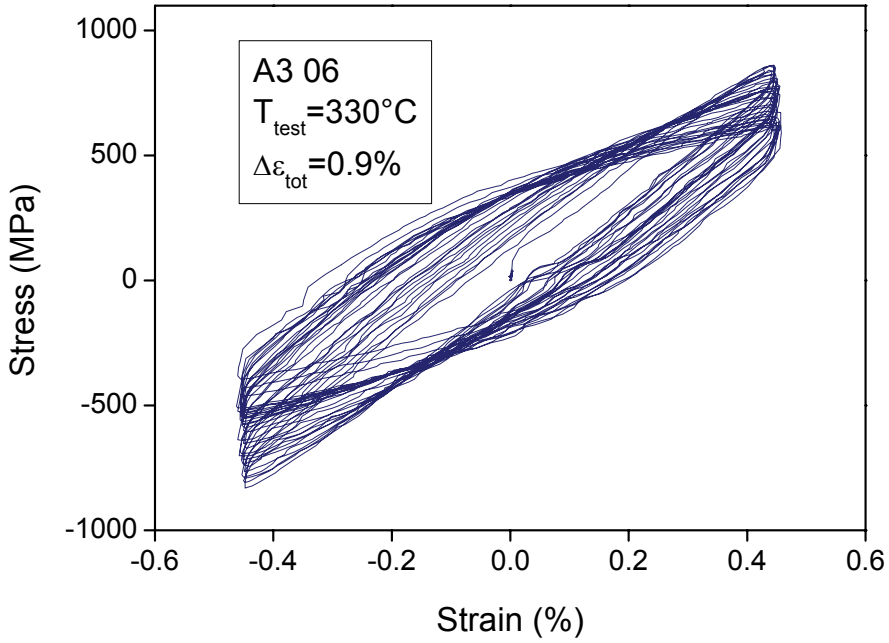

Fig. 11-89 Stress vs. strain for A3 06 (70.8 dpa/334.0 °C).

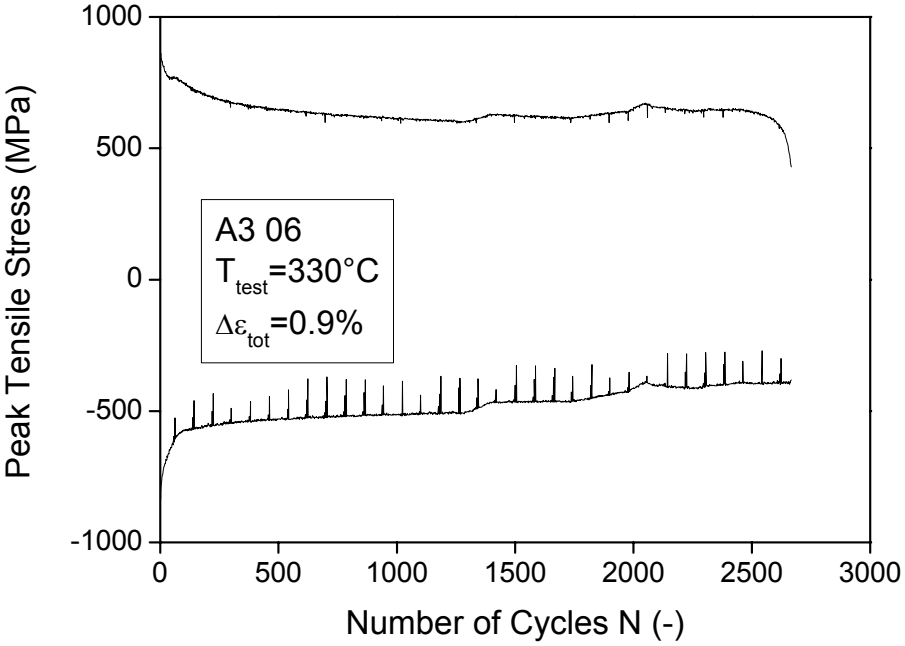

Fig. 11-90 Peak stresses vs. number of cycles for A3 06 (70.8 dpa/334.0 °C).

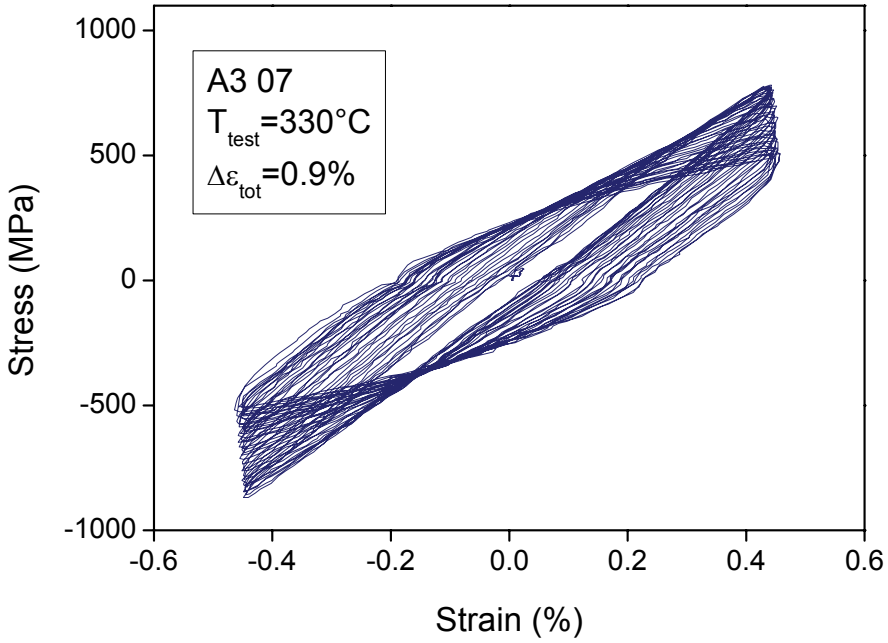

Fig. 11-91 Stress vs. strain for A3 07 (70.8 dpa/334.0 °C).

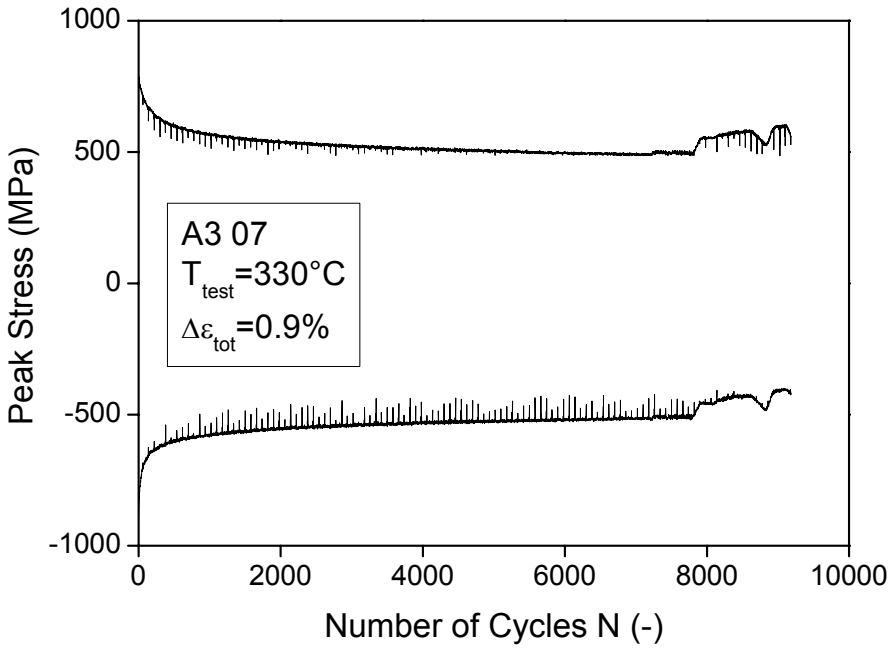

Fig. 11-92 Peak stresses vs. number of cycles for A3 07 (70.8 dpa/334.0 °C).

11.9 ADS 4

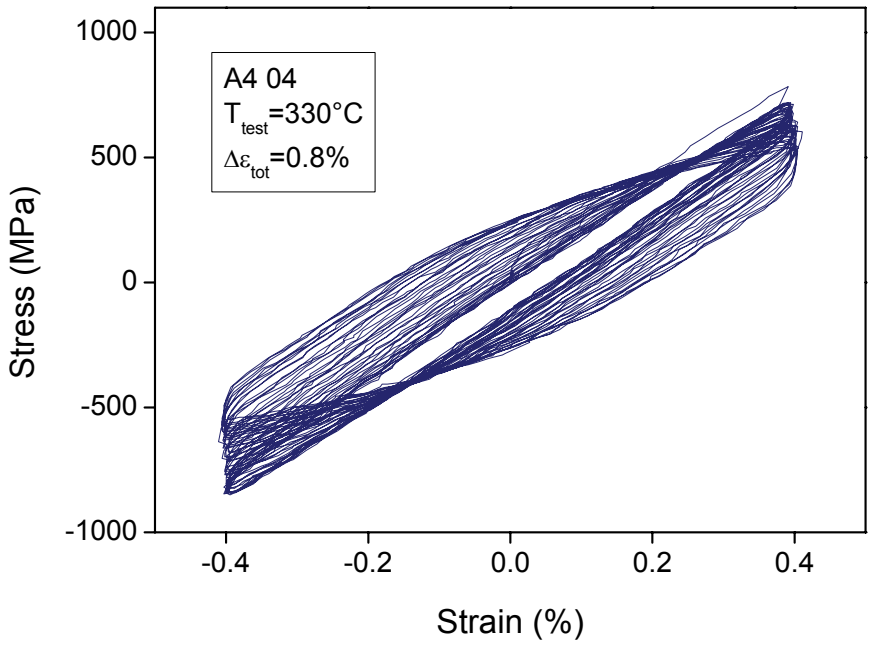

Fig. 11-93 Stress vs. strain for A4 04 (46.8 dpa/337.5 °C).

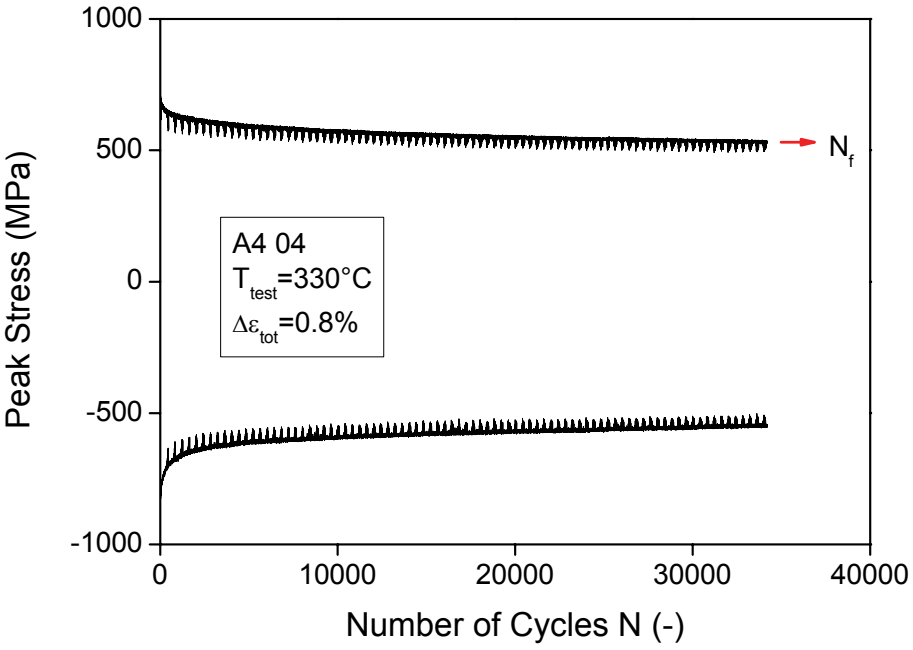

Fig. 11-94 Peak stresses vs. number of cycles for A4 04 (46.8 dpa/337.5 °C).

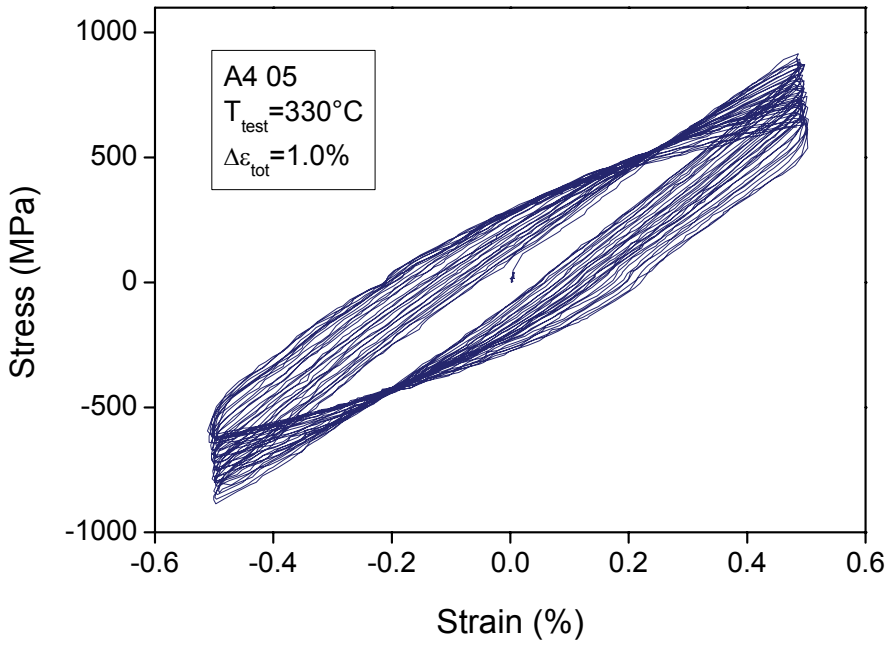

Fig. 11-95 Stress vs. strain for A4 05 (46.8 dpa/337.5 °C).

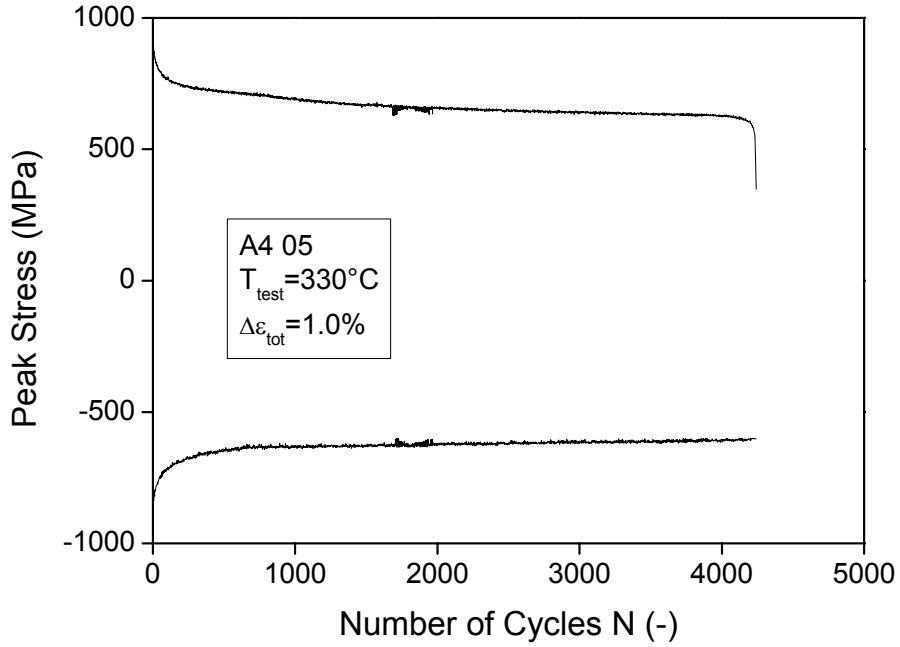

Fig. 11-96 Peak stresses vs. number of cycles for A4 05 (46.8 dpa/337.5 °C).

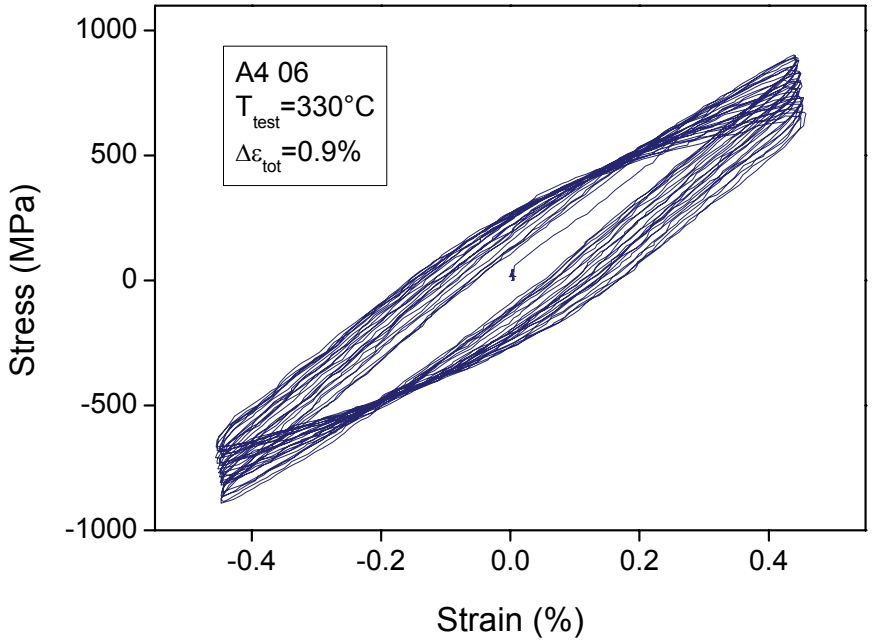

Fig. 11-97 Stress vs. strain for A4 06 (46.8 dpa/337.5 °C).

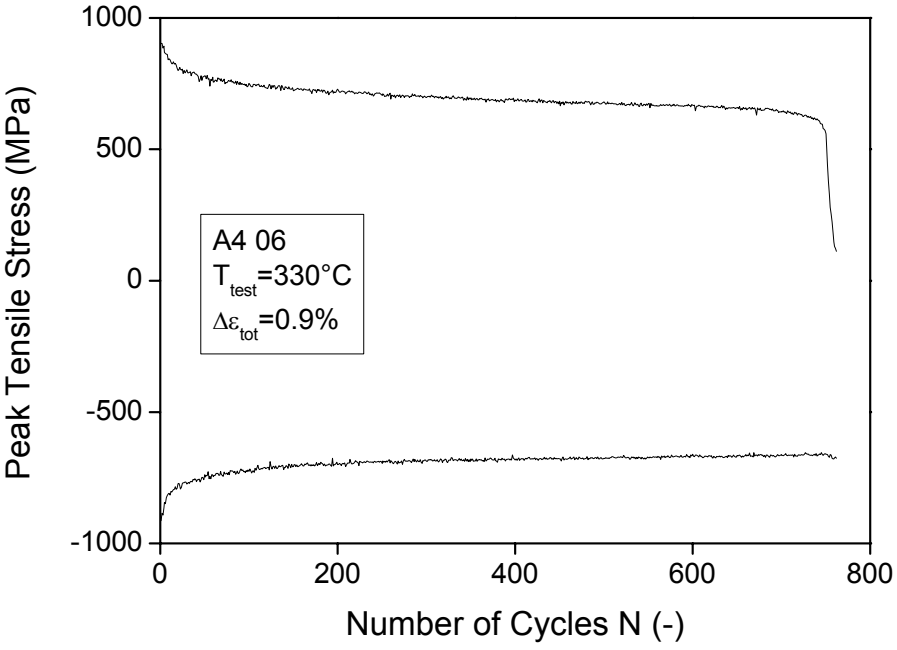

Fig. 11-98 Peak stresses vs. number of cycles for A4 06 (46.8 dpa/337.5 °C).

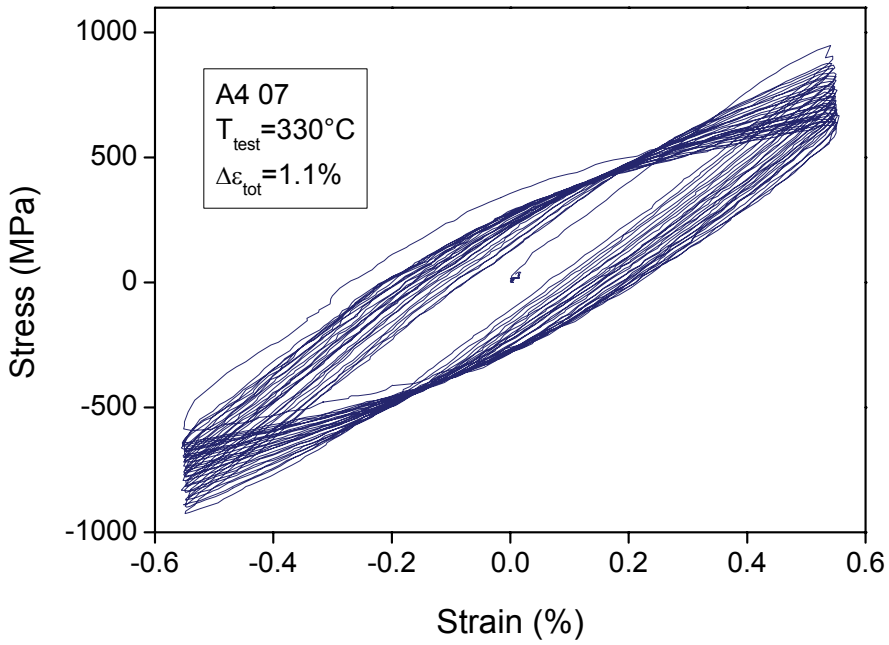

Fig. 11-99 Stress vs. strain for A4 07 (46.8 dpa/337.5 °C).

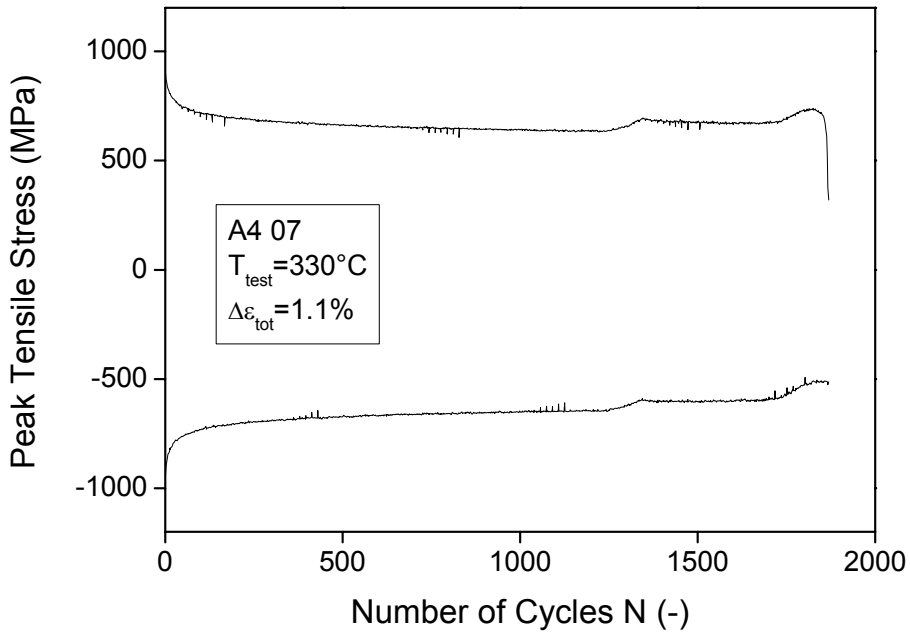

Fig. 11-100 Peak stresses vs. number of cycles for A4 07 (46.8 dpa/337.5 °C).

11.10 EUROF-EB

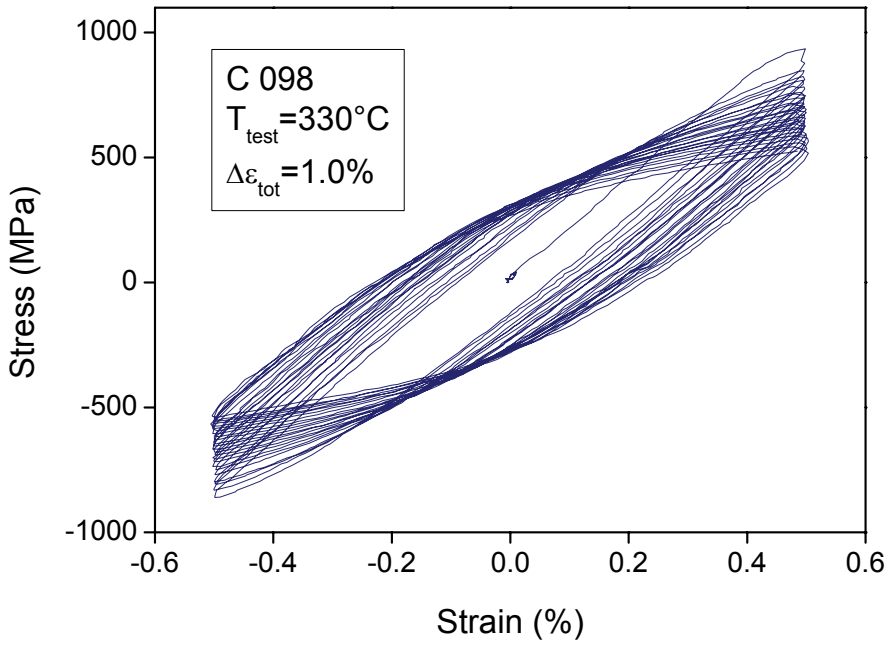

Fig. 11-101 Stress vs. strain for C 098 (70.1 dpa/331.5 °C).

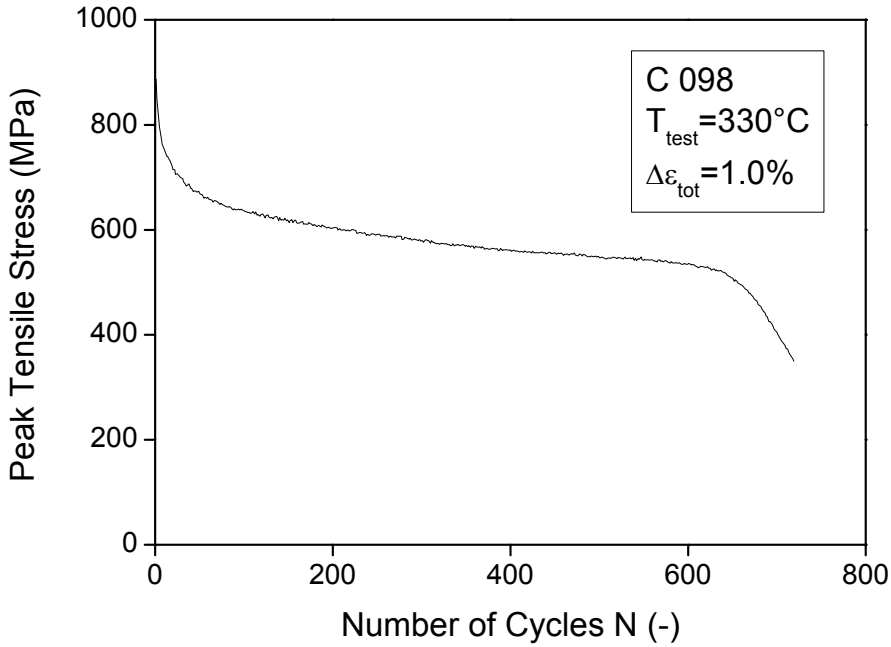

Fig. 11-102 Peak tensile stress vs. number of cycles for C 098 (70.1 dpa/331.5 °C).

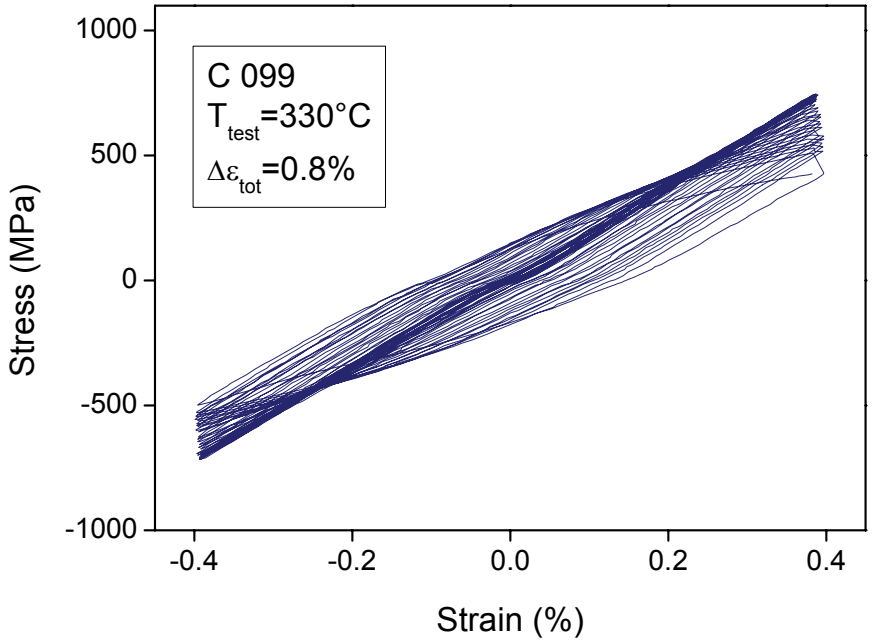

Fig. 11-103 Stress vs. strain for C 099 (70.1 dpa/331.5 °C).

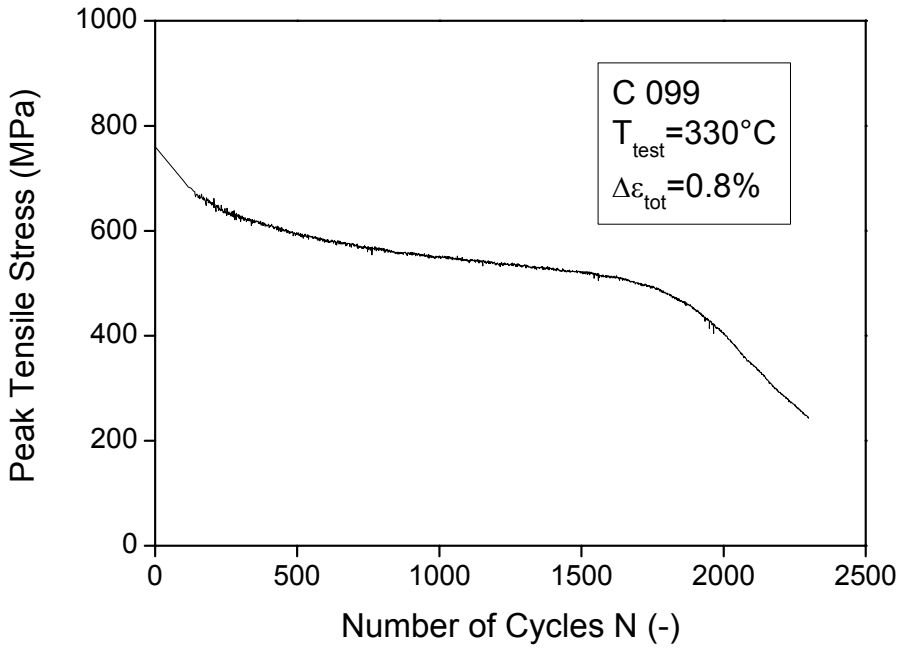

Fig. 11-104 Peak tensile stress vs. number of cycles for C 099 (70.1 dpa/331.5 °C).

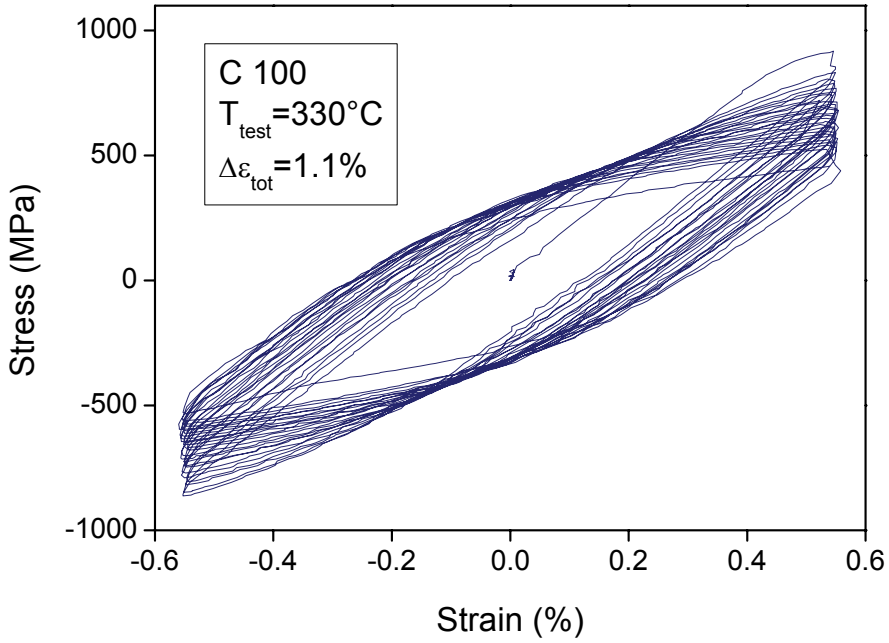

Fig. 11-105 Stress vs. strain for C 100 (70.1 dpa/331.5 °C).

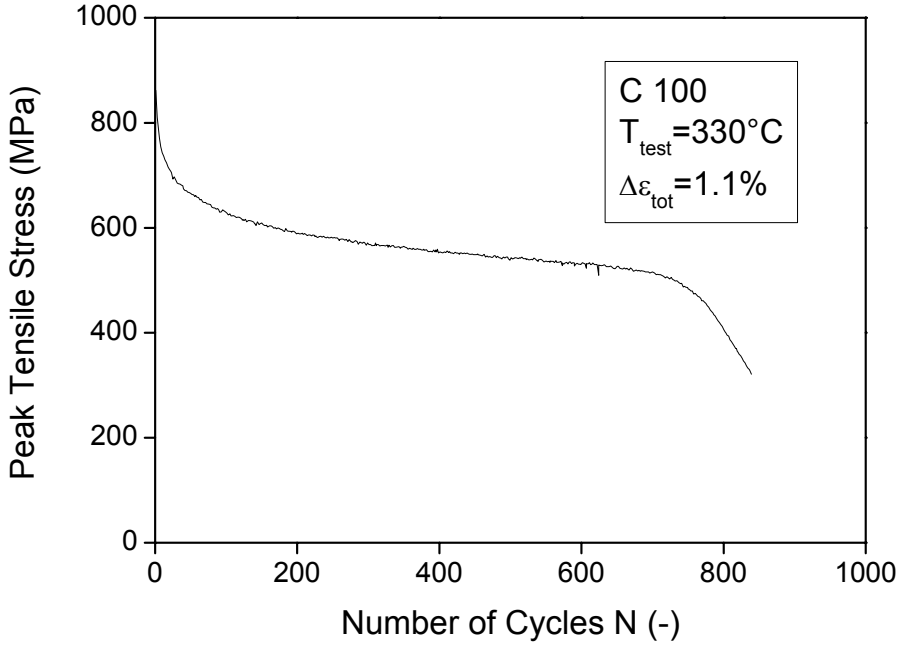

Fig. 11-106 Peak tensile stress vs. number of cycles for C 100 (70.1 dpa/331.5 °C).

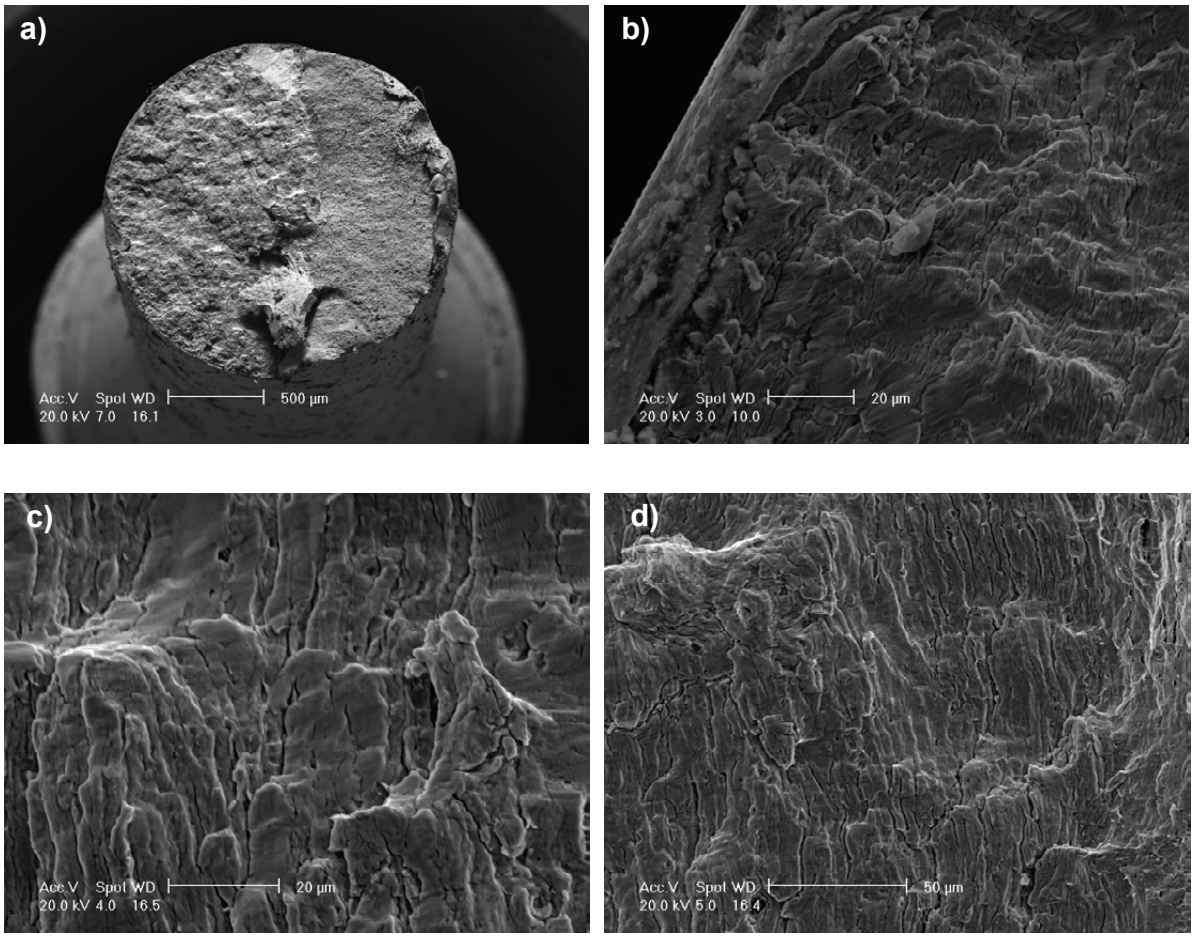

Fig. 11-107 SEM micrographs of E1 21 (47 dpa/337 °C) after LCF test at $\Delta\varepsilon_{tot}$ = 1.1% at 330 °C: a) an overall view; b) fracture appearances close to the specimen surface; c) fracture appearances in the middle area of the fatigue crack propagation; d) fracture appearances close to the end the fatigue crack propagation.

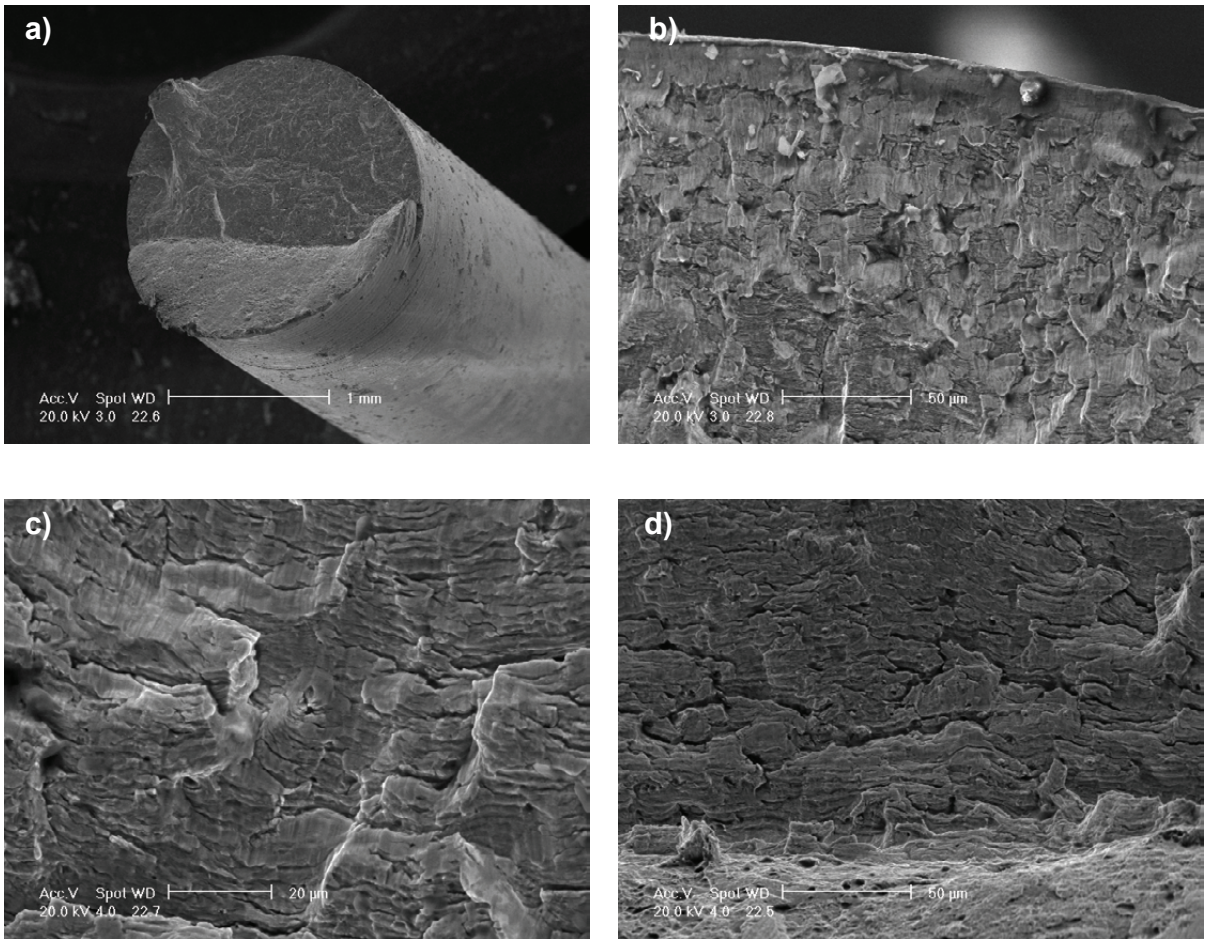

Fig. 11-108 SEM micrographs of E1 10 (71 dpa/334 °C) after LCF test at $\Delta\varepsilon_{tot}$=1.0% at 330 °C: a) an overall view; b) fracture appearances close to the specimen surface; c) fracture appearances in the middle area of the fatigue crack propagation; d) fracture appearances close to the end the fatigue crack propagation.

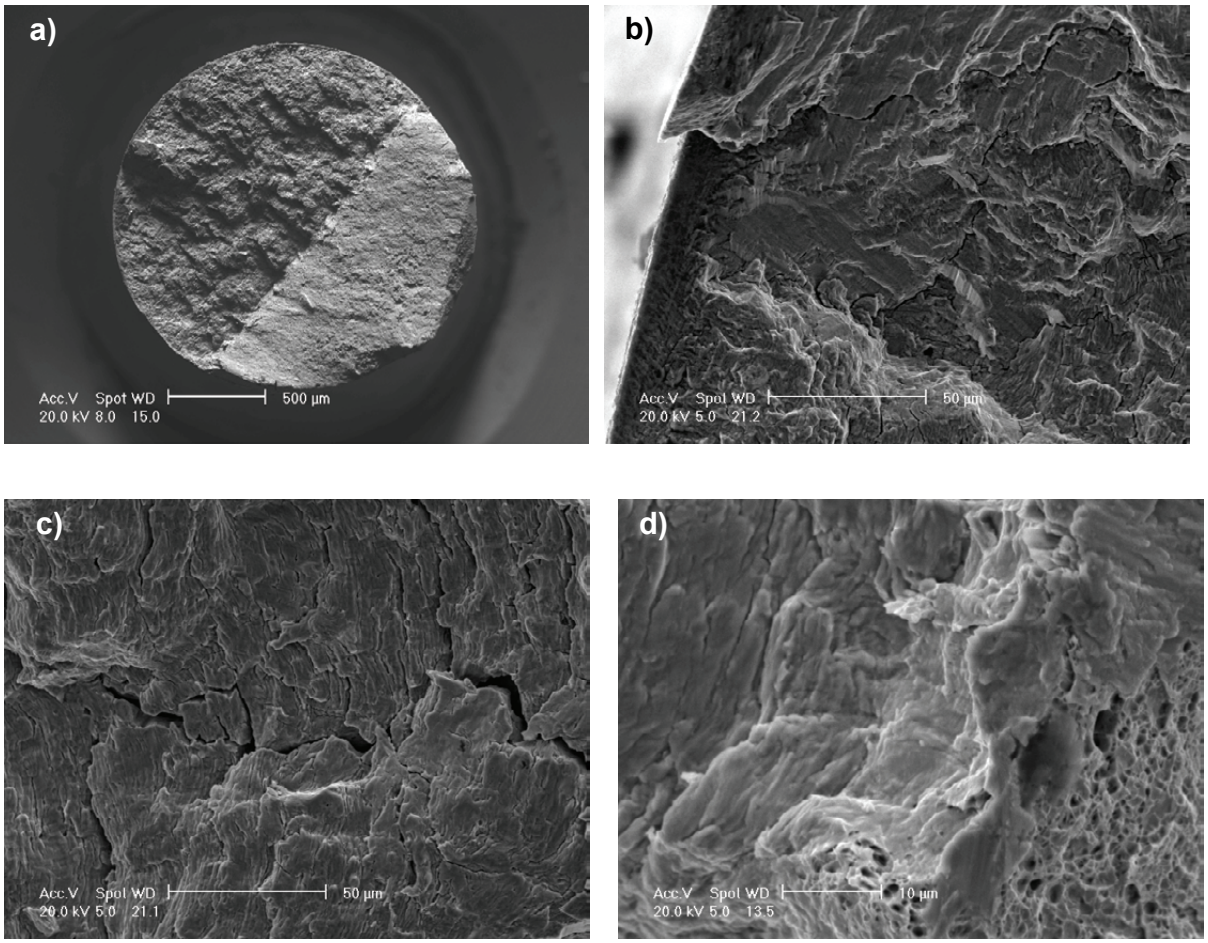

Fig. 11-109 SEM micrographs of E2 12 (71 dpa/334 °C) after LCF test at $\Delta\varepsilon_{tot}$ = 0.9% at 330 °C: a) an overall view; b) fracture appearances close to the specimen surface; c) fracture appearances in the middle area of the fatigue crack propagation; d) fracture appearances close to the end the fatigue crack propagation.

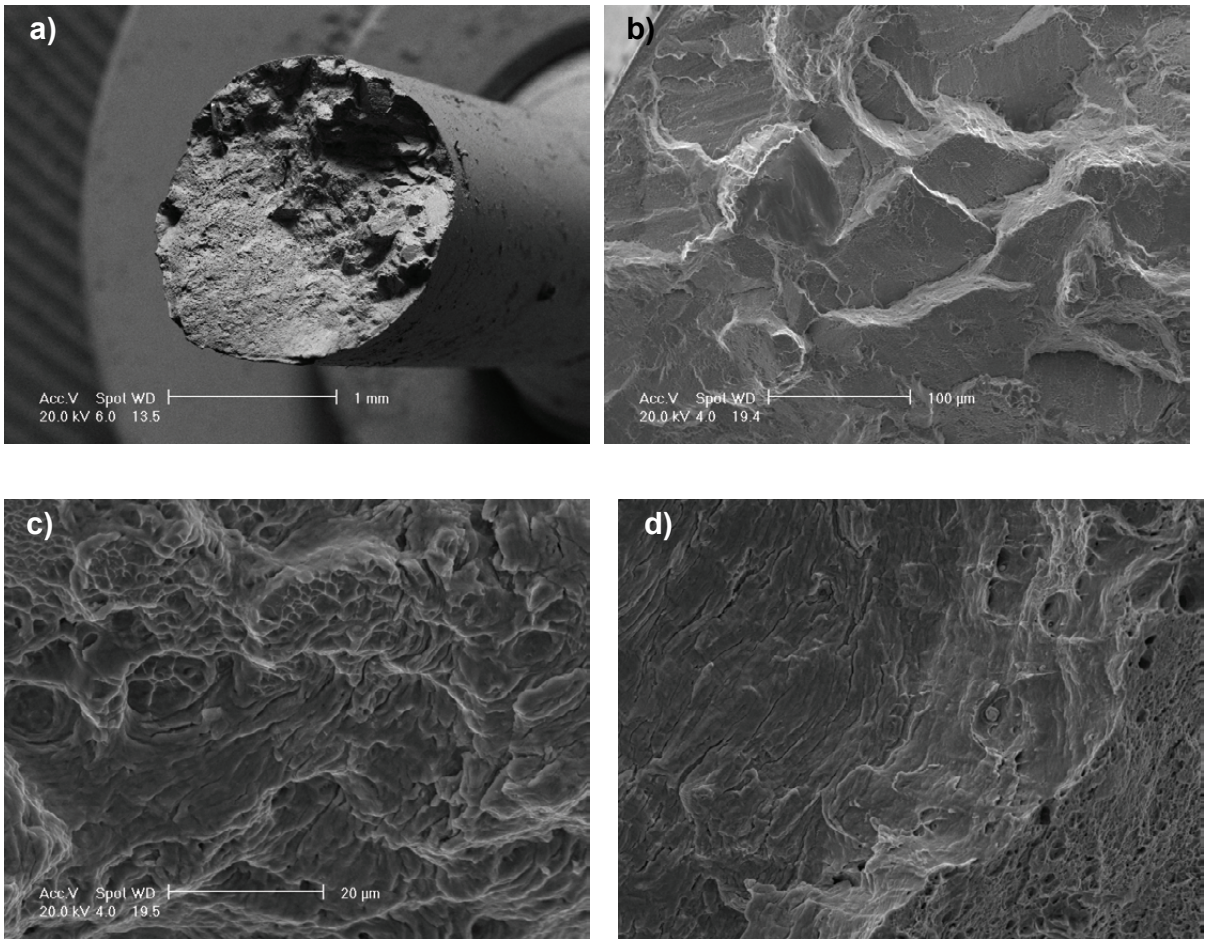

Fig. 11-110 SEM micrographs of F 13 (47 dpa/ 337 °C) after LCF test at $\Delta\varepsilon_{tot}$ = 0.9% at 330 °C: a) an overall view; b) fracture appearances close to the specimen surface; c) fracture appearances in the middle area of the fatigue crack propagation; d) fracture appearances close to the end the fatigue crack propagation.

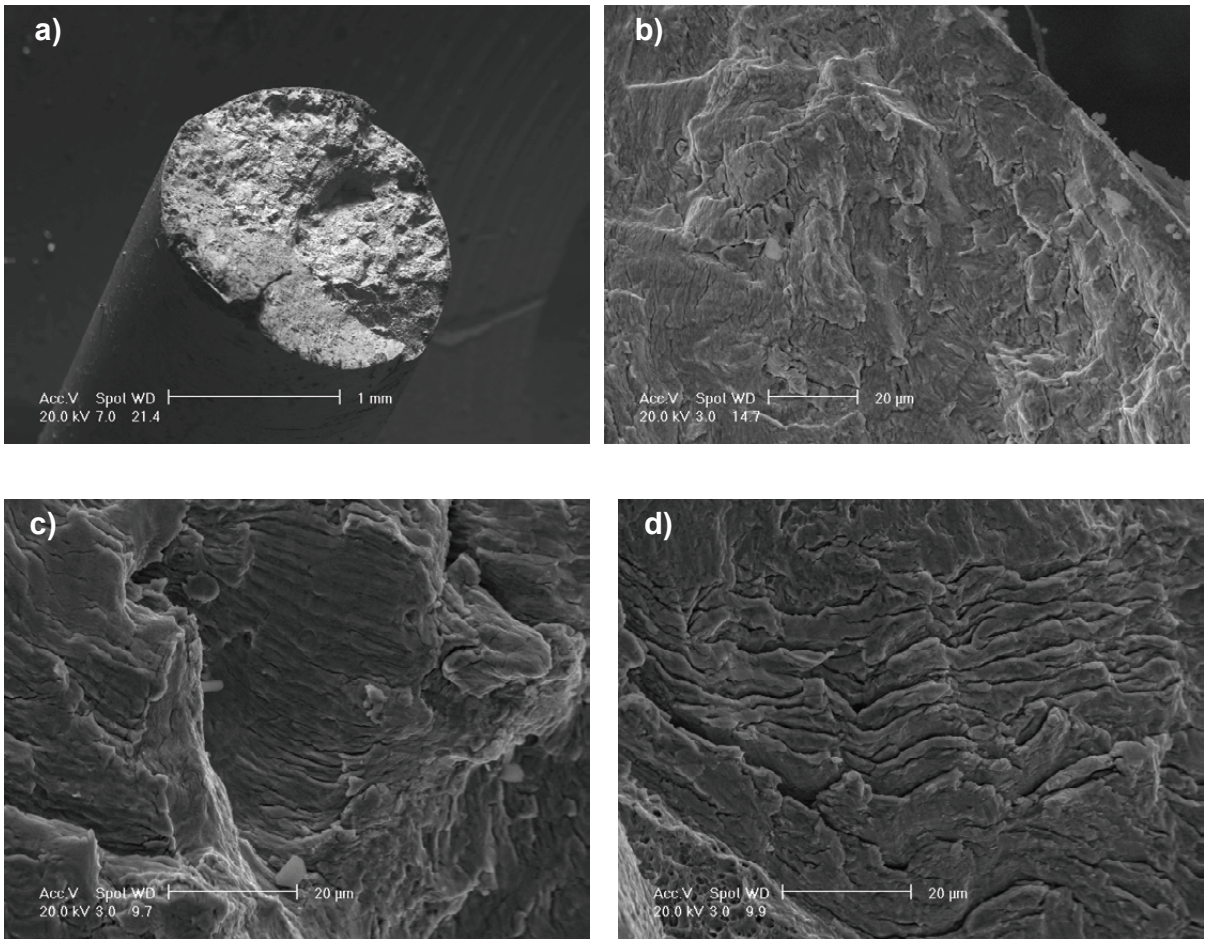

Fig. 11-111 SEM micrographs of F 15 (47 dpa/ 337 °C) after LCF test at $\Delta\varepsilon_{tot}$ = 1.0% at 330 °C: a) an overall view; b) fracture appearances close to the specimen surface; c) fracture appearances in the middle area of the fatigue crack propagation; d) fracture appearances close to the end the fatigue crack propagation.

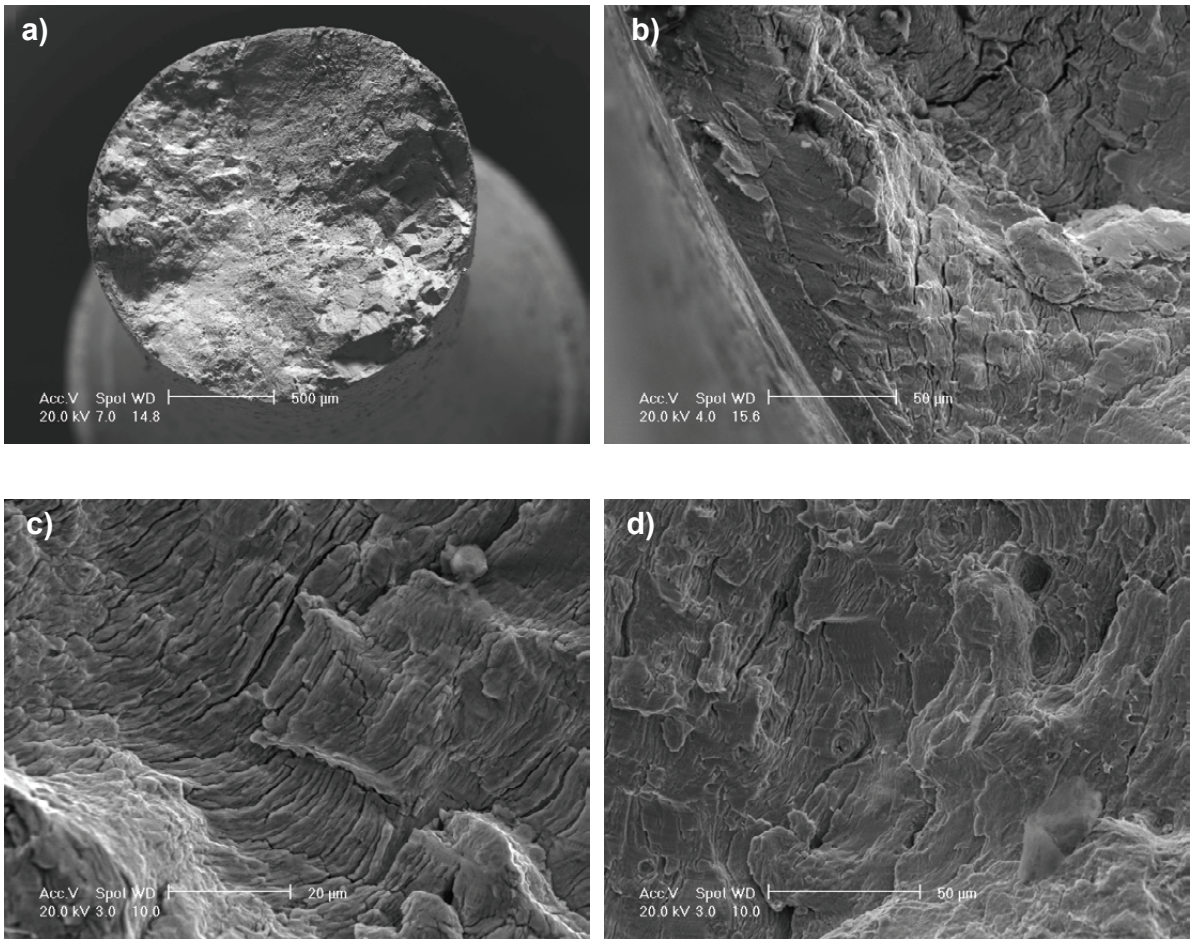

Fig. 11-112 SEM micrographs of F 16 (47 dpa/ 337 °C) after LCF test at $\Delta\varepsilon_{tot}$ = 1.1% at 330 °C: a) an overall view; b) fracture appearances close to the specimen surface; c) fracture appearances in the middle area of the fatigue crack propagation; d) fracture appearances close to the end the fatigue crack propagation.

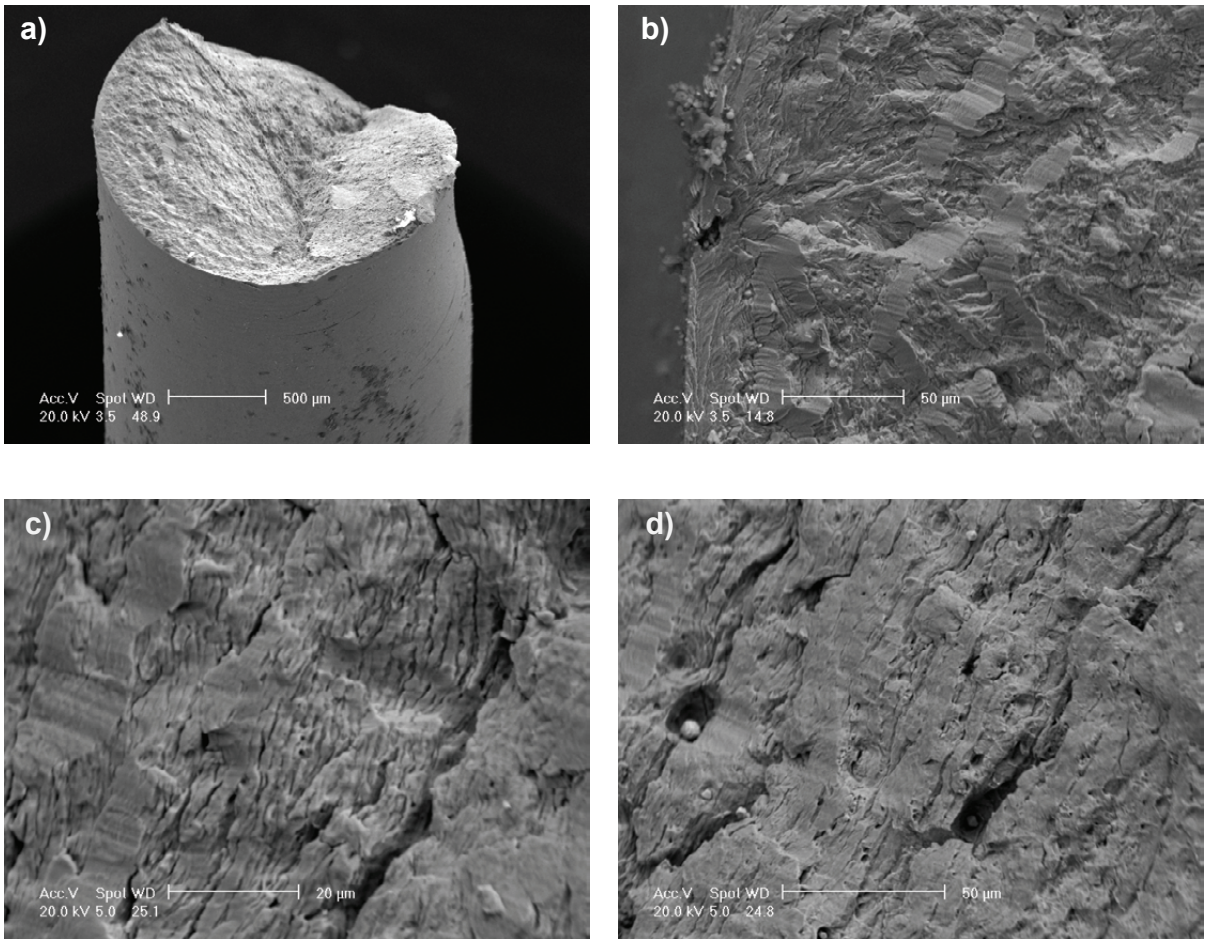

Fig. 11-113 SEM micrographs of OT 02 (71 dpa/ 334 °C) after LCF test at $\Delta\varepsilon_{tot}$ = 0.8% at 330 °C: a) an overall view; b) fracture appearances close to the specimen surface; c) fracture appearances in the middle area of the fatigue crack propagation; d) fracture appearances close to the end the fatigue crack propagation.

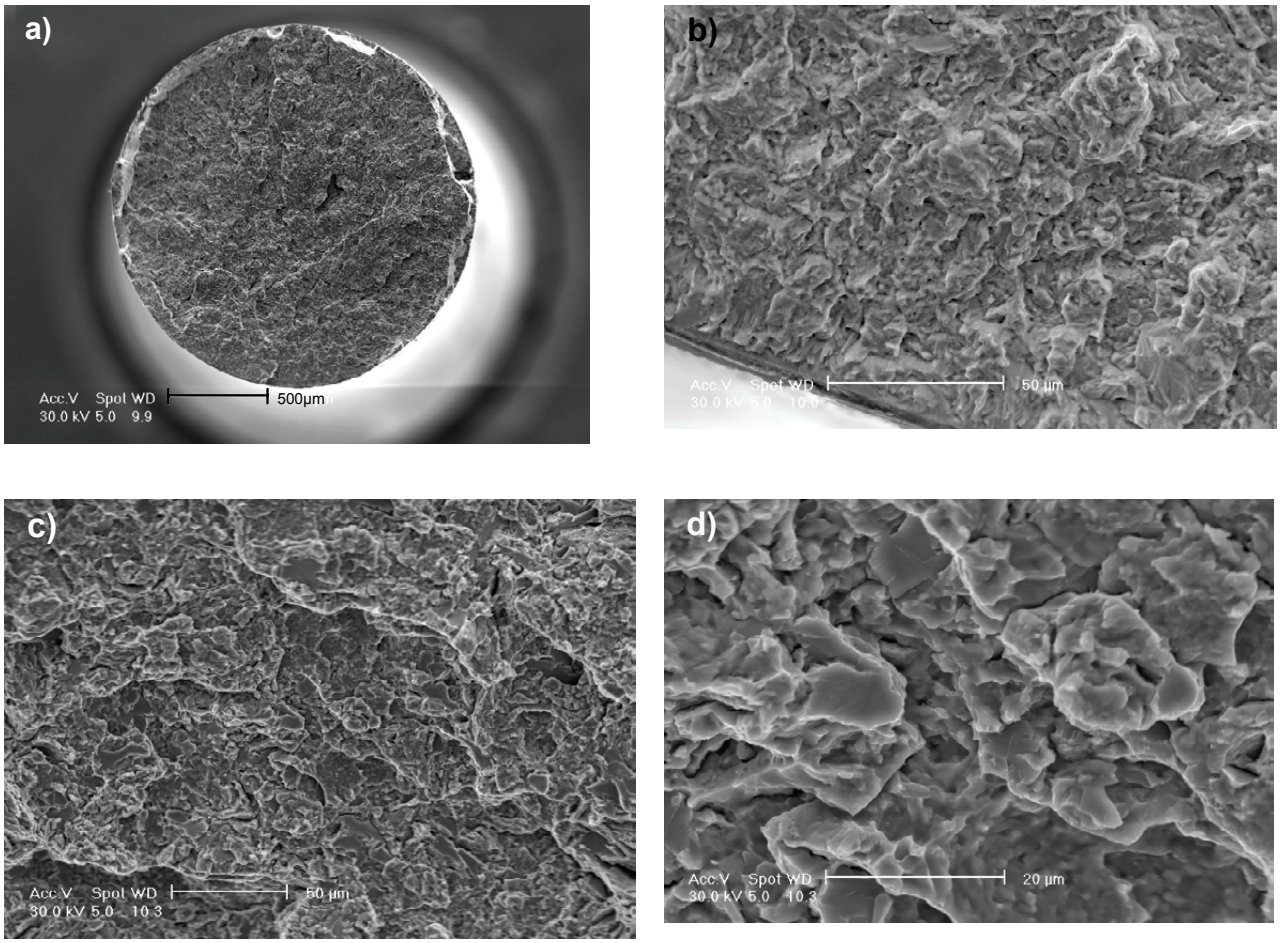

Fig. 11-114 SEM micrographs of EO 13 (47 dpa/ 337 °C) after LCF test at $\Delta\varepsilon_{tot}$ = 1.2% at 330 °C: a) an overall view; b) fracture appearances close to the specimen surface; c) and d) fracture appearances in the middle area of the fatigue crack propagation.

12 Annex: Intellectual Property Right

The results obtained within the studies performed under this task did not yield any specific innovation or intellectual property.

ISSN 1869-9669
ISBN 978-3-86644-703-5